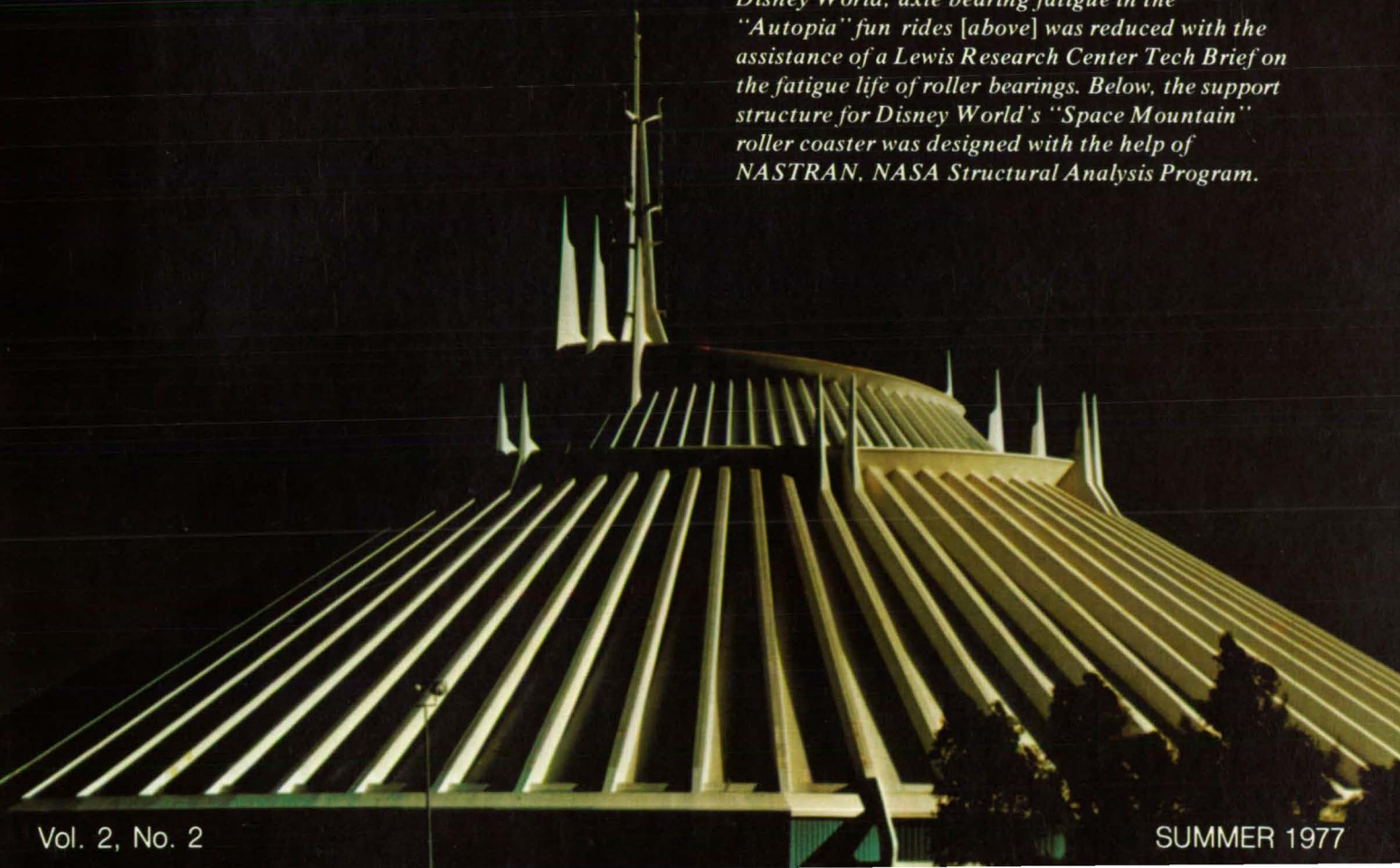


NASA Tech Briefs

National
Aeronautics and
Space
Administration



Aerospace spinoffs improve safety and save costs in the entertainment industry. At Disneyland and Disney World, axle bearing fatigue in the "Autopia" fun rides [above] was reduced with the assistance of a Lewis Research Center Tech Brief on the fatigue life of roller bearings. Below, the support structure for Disney World's "Space Mountain" roller coaster was designed with the help of NASTRAN, NASA Structural Analysis Program.



About the NASA Technology Utilization Program

The National Aeronautics and Space Act of 1958, which established NASA and the United States civilian space program, requires that "The Administration shall provide for the widest practicable and appropriate dissemination of information concerning its activities and the results thereof."

To help carry out this objective the NASA Technology Utilization (TU) Program was established in 1962. It offers a variety of valuable services to facilitate the transfer of aerospace technology to nonaerospace applications, thus assuring American taxpayers maximum return on their investment in space research; thousands of spinoffs of NASA research have already occurred in virtually every area of our economy.

The TU Program has worked for engineers, scientists, technicians, and businessmen. And it can work for you.

NASA Tech Briefs

Tech Briefs is published quarterly and is free to any U.S. citizen or organization. It is both a current-awareness medium and a problem-solving tool. Potential products ... industrial processes ... basic and applied research ... shop and lab techniques ... computer software ... new sources of technical data ... concepts ... you will find them all in NASA Tech Briefs. The first section highlights a few of the potential new products contained in Tech Briefs. The remainder of the volume is organized by technical category to help you quickly review new developments in your areas of interest. Finally, a subject index makes each issue a convenient permanent reference file.

Further Information on Innovations

Although many articles are complete in themselves, others are backed up by Technical Support Packages (TSP's). TSP's are available without charge and may be ordered by simply completing the enclosed TSP Request Card. Further information on some innovations is available for a nominal fee from other sources, as indicated at the ends of the articles. In addition, Technology Utilization Officers at NASA Field Centers will assist you directly when necessary. (See page A4.)

Patent Licenses

Many of the inventions described are under consideration for patents or have been patented by NASA. Unless NASA has decided not to apply for a patent, the patent status is described at the end of each article. For further information about the Patent Program see page A8.

Other Technology Utilization Services












To assist engineers, industrial researchers, business executives, city officials, and other potential users in applying space technology to their problems, NASA sponsors six Industrial Applications Centers. Their services are described on page A6. In addition, an extensive library of computer programs is available through COSMIC, the Technology Utilization Program's outlet for NASA-developed software. (See page A5.)

Applications Program

To help solve public-sector problems in such areas as safety, health, transportation, and environmental protection, NASA TU Applications Teams, staffed by professionals from a variety of disciplines, work with Federal agencies, local governments, and health organizations to identify critical problems amenable to technical solutions. Among their many significant contributions are a rechargeable heart pacemaker, a lightweight fireman's breathing apparatus, aids for the handicapped, and safer highways.

Reader Feedback

We hope you find the information in NASA Tech Briefs useful. A reader feedback card has been included because we want your comments and suggestions on how we can further help you apply NASA innovations and technology to your needs. Please use it, or if you need more space, write us a letter.

NASA TU Services	A3	Technology Utilization services that can assist you in learning about and applying NASA technology.	
New Product Ideas	A9	A summary of selected innovations of value to manufacturers for the development of new products.	
Tech Briefs	173	Electronic Components and Circuits	
	187	Electronic Systems	
	197	Physical Sciences	
	219	Materials	
	237	Life Sciences	
	249	Mechanics	
	265	Machinery	
	273	Fabrication Technology	
	283	Mathematics and Information Sciences	
	Subject Index	287	Items in this issue are indexed by subject; a cumulative index will be published yearly.

COVERS: The photographs on the front and back covers illustrate recent developments by NASA and its contractors that have resulted in commercial and nonaerospace spinoffs. You can use the TSP Request Card at the end of this issue to find out more about the "fatigue life of roller bearings" [Circle 58], the "air-pressure sensor for medical diagnosis" [Circle 59], the "solar-powered refrigerator" [Circle 60], the "copy frame" [Circle 61], and "NASTRAN" [Circle H]. [NASTRAN is available from COSMIC, described on page A5.]

**About This
NASA Publication**

NASA Tech Briefs, a quarterly publication, is distributed free to U.S. citizens to encourage commercial application of U.S. space technology. For information on publications and services available through the NASA Technology Utilization Program, write to the Director, Technology Utilization Office, P. O. Box 8756, Baltimore/Washington International Airport, Maryland 21240.

"The Administrator of National Aeronautics and Space Administration has determined that the publication of this periodical is necessary in the transaction of the public business required by law of this Agency. Use of funds for printing this periodical has been approved by the Director of the Office of Management and Budget through August 31, 1977."

This document was prepared under the sponsorship of the National Aeronautics and Space Administration. Neither the United States Government nor any person acting on behalf of the United States Government assumes any liability resulting from the use of the information contained in this document, or warrants that such use will be free from privately owned rights.

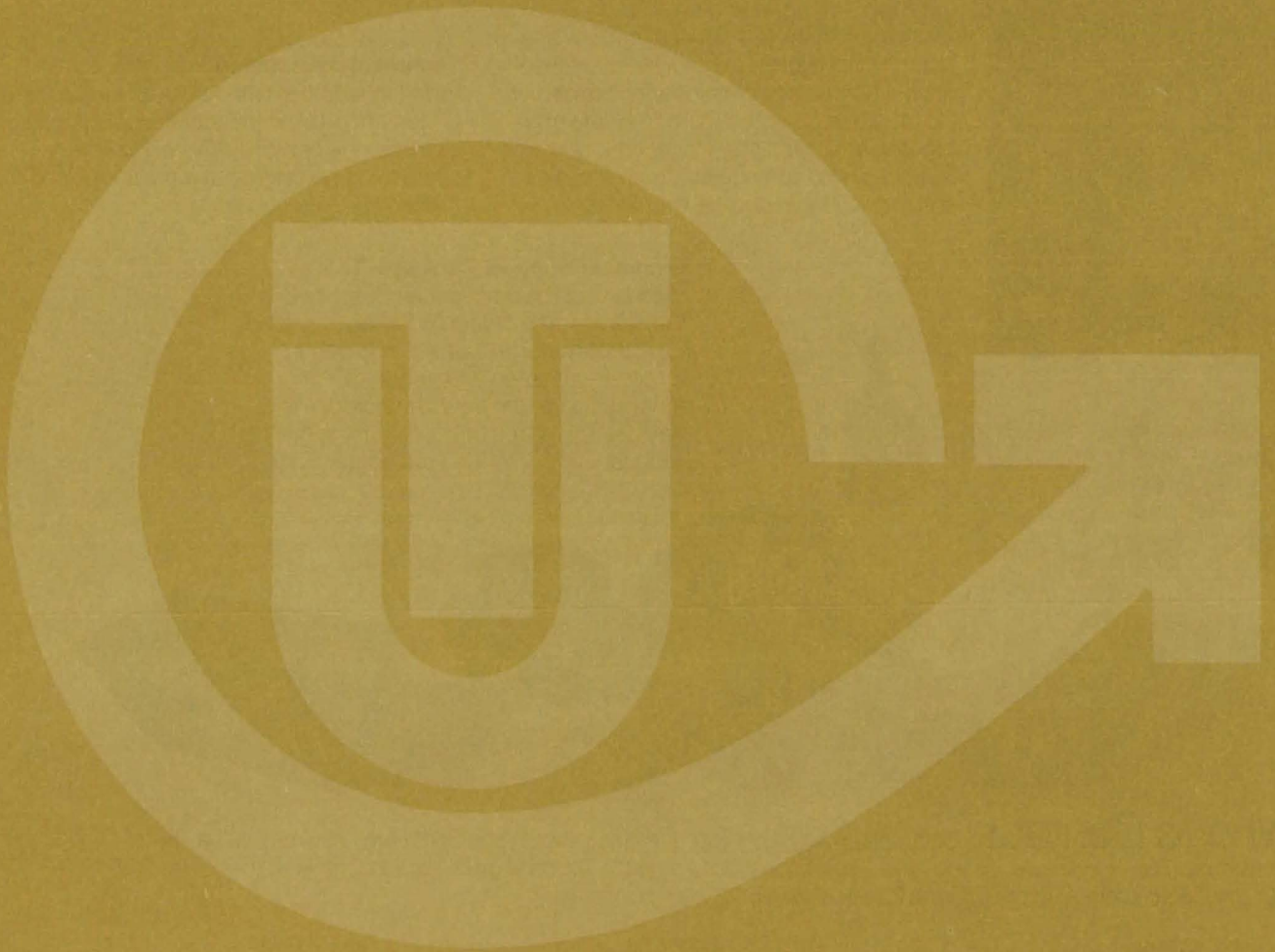
Change of Address

Change of Address: If you wish to have NASA Tech Briefs forwarded to your new address, use one of the Subscriptions cards enclosed in the back of this volume of NASA Tech Briefs. Be sure to check the appropriate box indicating change of address.

**Communication Concerning
Editorial Matter**

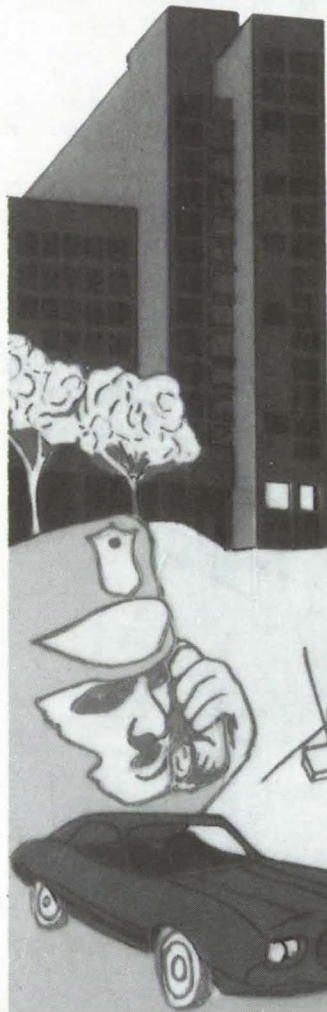
For editorial comments or general communications about NASA Tech Briefs, you may use the self-addressed Feedback card in the back of NASA Tech Briefs, or write to: The Publications Manager, Technology Utilization Office (Code KT), NASA Headquarters, Washington, DC 20546. Technical questions concening specific articles should be directed to the Technology Utilization Officer of the sponsoring NASA Center (addresses listed on page A4.)

NASA TU SERVICES



THE NASA TECHNOLOGY UTILIZATION OFFICERS

They will help you apply the innovations described in Tech Briefs.



The Technology Utilization Officer (TUO)

Each NASA Center has a Technology Utilization Officer — An applications engineer whose job is to help you make use of new technology developed at his center. He brings you the NASA Tech Briefs and other special publications, sponsors conferences, and arranges for expert assistance in solving technical problems.

Technical Assistance

Working together with NASA Scientists and Engineers and the Industrial Applications Centers, the center TUO's can answer specific questions about innovations and related NASA technology.

Technical Support Package (TSP's)

For many of the innovations described in Tech Briefs, the center TUO has prepared additional material that will help you in detailed evaluation and actual use or construction of the new technology. You may get TSP's free of cost by using the TSP Request Card or writing the center TUO.

Who to Contact. Of course, many technical questions about Tech Briefs are answered in the TSP's, but when no TSP is available, or you have further questions, write the Technology Utilization Officer at the center that sponsored the research at the address listed below.

Charles K. Kubokawa
Ames Research Center
Code AU: 230-2
Moffett Field, CA 94035
(415) 965-5554

Clinton T. Johnson
Hugh L. Dryden Flight Research Center
P. O. Box 273
Edwards, CA 93523
(805) 258-3311, Ext. 568

Donald S. Friedman
Goddard Space Flight Center
Code 704.1
Greenbelt, MD 20771
(301) 982-6242

John T. Wheeler
Johnson Space Center
Code AT3
Houston, TX 77058
(713) 483-3809

Raymond J. Cerrato
John F. Kennedy Space Center
Code SA-RTP
Kennedy Space Center, FL 32899
(305) 867-2780

John Samos
Langley Research Center
Mail Stop 139A
Hampton, VA 23665
(804) 827-3281

Paul Foster
Lewis Research Center
21000 Brookpark Rd.
Cleveland, OH 44135
(216) 433-4000, Ext. 6832

Aubrey D. Smith
Marshall Space Flight Center
Code AT01
Marshall Space Flight Center, AL 35812
(205) 453-2224

John C. Drane
NASA Resident Legal Office-JPL
4800 Oak Grove Drive
Pasadena, CA 91103
(213) 354-6420

Gilmore H. Trafford
Wallops Flight Center
Wallops Island, VA 23337
(804) 824-3411, Ext 201

Louis Mogavero, Director
Technology Utilization Office
Code KT
NASA Headquarters
Washington, DC 20546
(202) 755-3103

COSMIC

(Computer Software Management & Information Center)

AN ECONOMICAL SOURCE OF COMPUTER PROGRAMS DEVELOPED BY THE GOVERNMENT.

COSMIC is sponsored by NASA to give you access to over 1400 computer programs developed by NASA and the Department of Defense, and selected programs from other government agencies. It is one of the Nation's largest software libraries.

COSMIC charges very reasonable fees for programs to help cover part of their expenses—and NASA pays for the remainder. Programs generally cost from \$500 to \$1000, but a few are more expensive and many are less. Documentation is available separately and very inexpensively.

COSMIC collects and stores software packages, insures that they are complete, prepares special announcements (such as Tech Briefs), publishes an indexed software catalog, and reproduces programs for distribution. **COSMIC** helps customers to identify their software needs, follows up to determine the successes and problems, and provides updates and error corrections. In some cases, NASA engineers can offer guidance to users in installing or running a program.

COSMIC programs range from management (pert scheduling) to information science (retrieval systems) and computer operations (hardware and software). Hundreds of engineering programs perform such tasks as structural analysis, electronic circuit design, chemical analysis, and design of fluid systems. Others determine building energy requirements, optimize mineral exploration, and draw maps of water-covered areas using NASA satellite data. In fact, the chances are, if you use a computer, you can use **COSMIC**.

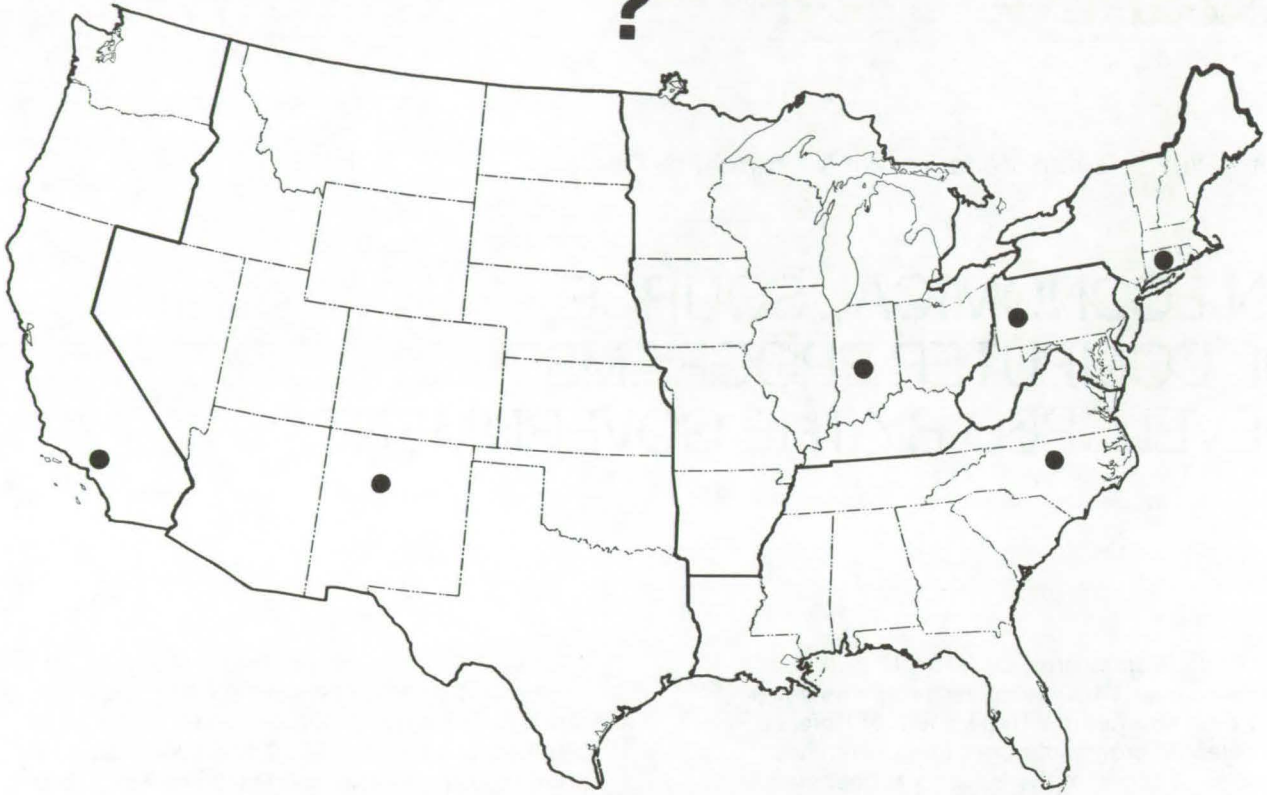
***COSMIC** is eager to help you get the programs you need. For more information about services or software available from **COSMIC**, fill out and mail the **COSMIC** Request Card in this issue.*

COSMIC: Computer Software Management and Information Center

Suite 112, Barrow Hall, Athens, Georgia 30602 Phone: (404) 542-3265

WHERE IS THE WORLD'S LARGEST BANK OF TECHNICAL DATA

?



It's in Bloomington and Pittsburgh, it's in Storrs, Connecticut and Research Triangle Park, North Carolina; and it's in Albuquerque and Los Angeles.

NASA IAC's — INDUSTRIAL

You can get more information and more data on more technical subjects through NASA's network of IAC's than anywhere else in the world. About 8,000,000 documents and growing at the rate of 50,000 more each month!

Major sources include:

- 750,000 NASA Technical Reports
- Selected Water Resources Abstracts
- NASA Scientific and Technical Aerospace Reports
- Air Pollution Technical Information Center
- NASA International Aerospace Abstracts
- Chem Abstracts Condensates
- Engineering Index
- Nuclear Science Abstracts
- NASA Tech Briefs
- Government Reports Announcements

and many other specialized files on food technology, textile technology, metallurgy, medicine, business, economics, social sciences, and physical science.

The IAC's are one of the most economical ways of staying competitive in today's world of exploding technology. The help available from the network ranges from literature searches through expert technical assistance.

Literature Searches

Help in designing your search, typically from 30 to 300 abstracts in as narrow or broad an area as you need, and complete reports when you need them. The most complete "search before research" available!

Current Awareness

Consult with our applications engineers to design your personal program — selected monthly or quarterly abstracts on new developments in your speciality. It's like having your own journal!

Technical Assistance

Our applications engineers will help you evaluate and apply your literature-search results. They can help find answers to your technical problems and put you in touch with scientists and engineers at NASA Field Centers.

To obtain more information about how NASA's IAC's can help you — Check the IAC box on the TSP Request Card in this issue, Or write or call the IAC nearest you.

APPLICATIONS CENTERS

How to get reports and other documents discussed in this issue of Tech Briefs

Many of the innovations in Tech Briefs are described in detail in reports available at a reasonable cost through one or more of the IAC's. To order a report, call or write the IAC referenced at the end of the Tech Brief article at the address below. Be sure to list the titles and accession numbers (N76-..., N75-..., etc.) of those you wish to purchase.

Aerospace Research Application Center (ARAC)
Indiana University-Purdue University at Indianapolis
1201 E. 38th St.
Indianapolis, IN 46205
E. Guy Buck, Director
(317) 264-4644

Knowledge Availability Systems Center (KASC)
University of Pittsburgh
Pittsburgh, PA 15260
Edmond Howie, Director
(412) 624-5211

New England Research Application Center (NERAC)
Mansfield Professional Park
Storrs, CT 06268
Dr. Daniel U. Wilde, Director
(203) 486-4533

North Carolina Science & Technology
Research Center (NC/STRC)
P. O. Box 12235
Research Triangle Park, NC 27709
Peter J. Chenery, Director
(919) 549-0671

Technology Application Center (TAC)
University of New Mexico
Albuquerque, NM 87131
Stanley A. Morain, Director
(505) 277-4000

Western Research Application Center (WESRAC)
University of Southern California
University Park
Los Angeles, CA 90007
Radford King, Director
(213) 746-6132

NASA INVENTIONS AVAILABLE FOR LICENSING

Over 3,500 NASA inventions are available for licensing in the United States - both exclusive and nonexclusive.

Nonexclusive Licenses

Nonexclusive licenses for commercial use are encouraged to promote competition and to achieve the widest use of inventions. They must be used by a negotiated target date but are usually royalty free.

Exclusive Licenses

An exclusive license may be granted to encourage early commercial development of NASA inventions, especially when considerable private investment is required. These are generally for 5 to 10 years and usually require royalties based on sales or use.

The NASA patent licensing program also provides for licensing of NASA-owned foreign patents. In addition to inventions described in Tech Briefs, "NASA Patent Abstract Bibliography," containing abstracts of all NASA inventions, can be purchased from: National Technical Information Service, Springfield, Va., 22161. This document is updated semi-annually.

Patent Licenses and the NASA Tech Brief

Many of the inventions reported in Tech Briefs are patented or are under consideration for a patent at the time they are published. When this is the case, the current patent status is described at the end of the article; otherwise, there is no statement about patents. **If you want to know more about the patent program or are interested in license for a particular invention, write the Patent Counsel at the NASA Field Center that sponsored the research. Be sure to refer to the NASA reference number in parenthesis at the end of the Tech Brief.**

Robert F. Kempf
NASA Headquarters, Code GP
400 Maryland Ave., S.W.
Washington, DC 20546
(202) 755-3932

Darrell G. Brekke
Ames Research Center
Mail Code: 200-11A
Moffett Field, CA 94035
(415) 965-5104

John O. Tresansky
Goddard Space Flight Center
Mail Code: 204
Greenbelt, MD 20771
(301) 982-2351

Marvin F. Matthews
Lyndon B. Johnson Space Center
Mail Code: AM
Houston, TX 77058
(713) 483-4871

James O. Harrell
John F. Kennedy Space Center
Mail Code: SA-PAT
Kennedy Space Center, FL 32899
(305) 867-2544

Howard J. Osborn
Langley Research Center
Mail Code: 313
Hampton, VA 23665
(804) 827-3725

Norman T. Musial
Lewis Research Center
Mail Code: 500-113
21000 Brookpark Road
Cleveland, OH 44135
(216) 433-4000

Leon D. Wofford, Jr.
Marshall Space Flight Center
Mail Code: CC01
Marshall Space Flight Center, AL 35812
(205) 453-0020

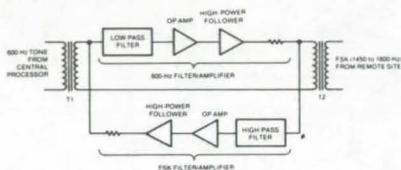
Monte F. Mott
NASA Resident Legal Office-JPL
4800 Oak Grove Drive
Pasadena, CA 91103
(213) 354-2700

NEW PRODUCT IDEAS



NEW PRODUCT IDEAS are just a few of the many innovations described in this issue of NASA Tech Briefs and having promising commercial applications. Each is discussed further on the referenced page in the appropriate section in this issue. If you are interested in developing a product from these or other NASA innovations, you can receive further technical information by requesting the TSP referenced at the end of the full-length article or by writing the Technology Utilization Office of the sponsoring NASA center (see page A4). NASA's patent-licensing program to encourage commercial development is described on page A8.

Bidirectional Amplifier



A "bidirectional" amplifier, originally designed to improve a lightning-warning electric-field-meter system at Kennedy Space Center, could be used to improve signal-to-noise ratios in other applications. The amplifier is inserted into a single transmission line and can amplify signals of different frequencies traveling in both directions, a situation that leads to signal blocking and continuous feedback problems if conventional amplifiers are used. The bidirectional amplifier uses low- and high-pass filters to amplify signals entering either of its two input terminals and has been prototyped and tested under field conditions.

(See page 175.)

Heat Pipe Controls Bearing Temperature

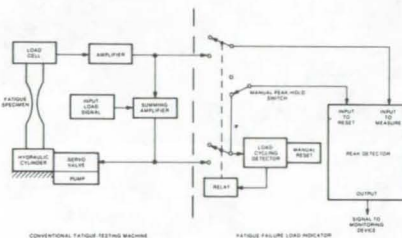
A new application of heat-pipe technology can reduce bearing temperatures and temperature differentials in rotating assemblies. A heat pipe that was mounted along the centerline of an assembly used to store energy in an electrically-driven rotating flywheel was found to be the most efficient technique for transporting heat from the bearing inner race and for limiting temperature gradients. In this application, water was used as the working fluid, and the pipe could be operated either with or without an internal wick. Tests showed that the heat-pipe technique is clearly superior to the use of a solid high-conduction rod, such as copper, at the shaft center. (See page 267.)

Improved Alloy for Catalytic Reactors

An improved Ni-Cu-Zr alloy is a potentially superior material for use in catalytic reactors. The new material is a minor alloy modification of Monel alloy 400, a known catalyst, but has better mechanical properties at high operating temperatures from 1,300° to 1,700° F and may give the long-term durability required for use with internal-combustion engines. These better characteristics, including higher tensile strength and ductility, longer stress-rupture life, and superior grain-boundary strength, are obtained by adding 0.2 percent Zr to the base alloy and applying the appropriate thermal mechanical processing. The resulting material, though improved mechanically, shows identical oxidation behavior and catalytic properties as Monel alloy 400.

(See page 225.)

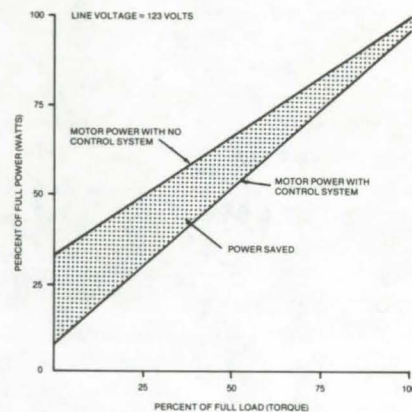
Fatigue-Failure Load Indicator



A new indicator that can be used with conventional fatigue-testing machines can easily and economically record the load at the instant of material failure. Previously, machine test loads, rather than specimen breaking loads, were determined because of the considerable auxiliary equipment and extra expense required to record the actual loads. The new indicator uses a commercially-available peak detector to monitor the load carried by the

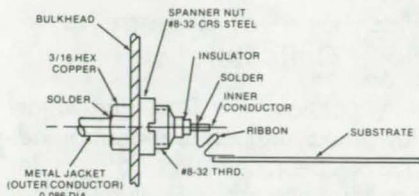
specimen during each cycle of the test and to retain the exact load that causes the specimen to break. The detector also has a switch setting that lets the operator check the value of the applied load at any time. (See page 251.)

Power Saver for AC Induction Motors



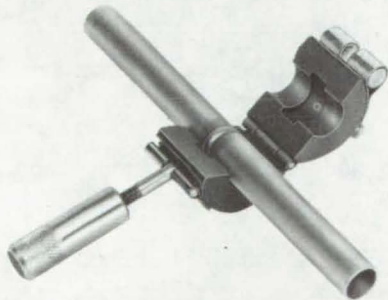
Relatively simple and inexpensive circuitry will improve the power factor and reduce power dissipation in induction motors operating below full load. An electronic control system has proved capable of raising power factors from 0.2 to 0.8 and reducing no-load power by a factor of 5 or 6. It consists of a typical phase-control circuit and a new circuit that senses the voltage/current phase lag in the induction motor and develops a control pulse that regulates the motor voltage in response to changing loads. The circuit has been tested on a 1/3-hp split-phase motor and 1/4- and 3/4-hp capacitor-start motors. In all three cases, the slowdown due to reducing the applied voltage was less than 2 percent. (See page 179.)

Vibration-Resistant PC Board Feedthrough



An inexpensive ribbon interface can reduce vibration-induced failures of connections between coaxial cables and printed-wiring boards. The method can also be used to link wiring boards on either side of a coaxial feedthrough. The interface, which uses a simple annealed-nickel ribbon loop soldered to the inner conductor and to the board, can lower fabrication costs by reducing the number of parts needed, a primary goal of electronics equipment designers. The ribbon has a hole drilled in one end for insertion of the inner conductor of a cable or feedthrough and a blank end that is soldered to the appropriate point on the circuit board. Whereas previous cable connectors have required the use of high-temperature solders to connect the ground-plane conductor to the bulkhead, only low-temperature solder is needed for both the inner and outer conductors with the new interface. (See page 276.)

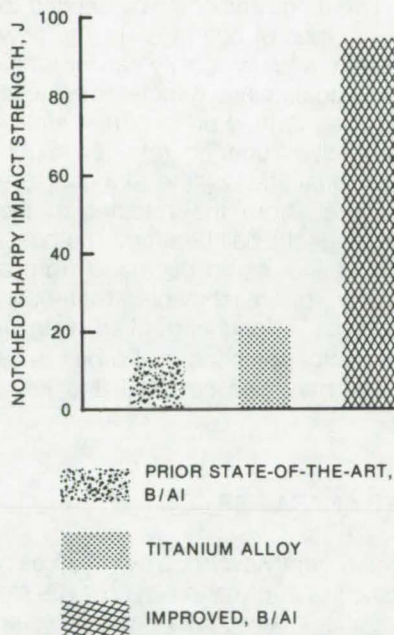
Inspection Tool for Butt-Welded Tubing



An inspection tool tests the cohesion of butt-welded joints that are difficult to reach with conventional weld-seam testers. The tool can detect fluid leakage as well as gas leaks and is particularly useful in

detecting leakage in joints that are close to one another. It consists of a small elastic collar surrounded by a metal casing held tightly about the weld via a screw clamp. Any leakage through the weld is contained in the collar; then it is bled to a suitable detection device. As originally designed, the tool is slipped over tubing typically having an outside diameter of 3/16 to 1/2 in. (See page 277.)

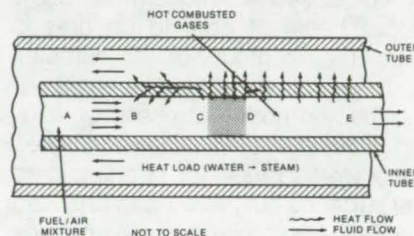
Impact-Resistant Boron/Aluminum Composites



Boron/aluminum (B/Al) composites with impact strengths up to 10 times greater than titanium alloys can be fabricated, using the proper materials and processing conditions. Previous B/Al composites have exhibited good tensile strength, but have lacked the impact strength needed for applications such as fan blades in aircraft-turbine engines. For fan blades, the possibility of bird strikes requires that strong impact-resistant materials be utilized. The new composites obtain their improved properties from ductile base materials, larger boron fibers and interfiber spacings, and by proper choice of fabrication temperatures. They may be useful in other aerospace applications, such as compressor blades and guide vanes, and in nonaerospace applications,

such as sports equipment, high-performance automobile wheels, and prosthetic devices. (See page 221.)

Fuel Burner With Low Nitrogen Oxide Formation



A new fuel burner can maintain efficient combustion while reducing the formation of polluting nitrogen oxides. The burner, which is presently being tested, is well suited for use in utility boilers, water and space heaters, and other combustors. The new approach uses a furnace in which a working fluid, such as water or steam, shares a common wall with the combustion zone. This close coupling transfers heat more efficiently so that the burning gases never reach free-flame temperatures. The low temperature prevents the formation of appreciable amounts of nitrogen oxides, thus limiting pollution. The key features of the system have been independently tested and verified, and tests of the entire system are underway. (See page 257.)

Aspirin/Metiamide Reduces Stomach Ulceration

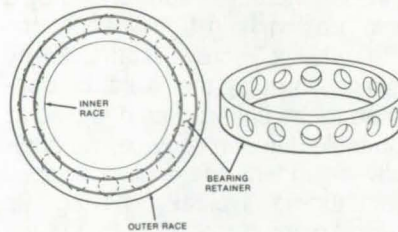
A combination of aspirin and metiamide has been found to reduce gastric erosion or ulceration that can occur under stress when aspirin is taken alone. The new formulation could help relieve gastric distress in patients who take large doses of aspirin for diseases such as rheumatoid arthritis. Metiamide, a recently synthesized antihistamine, has been tested on rats and shown effective in inhibiting stress-induced ulceration, with and without aspirin. Ulcer sizes (lengths) were reduced by up to 90 percent from the no-drug

or aspirin-only condition, and the fraction of animals that developed no ulcers at all was increased. (See page 242.)

Molding Cork Sheets to Complex Shapes

A proposed technique would allow large sheets of cork to be draped over the contour of a complex surface and bonded in place without introducing undue stresses or folding in the sheet. Existing techniques have worked well for bonding onto flat surfaces but have led to cracking and breaking problems with complex shapes. The new process involves interrupting the curing cycle before final polymerization and completing the cure under heat and pressure with the material draped over its supporting surface. Depending on the particular application, the sheet could be bonded to the surface during final cure, or it could be first-formed in a mold and bonded to the surface in a separate step. (See page 278.)

Magnetically-Controlled Bearing Lubrication



Magnetic force is used to retain and supply a lubricant in a bearing system under development. The easily fabricated technique works for ball bearings and could be applied to other types of bearings. In the new system, a low-viscosity carrier lubricant containing minute magnetic particles is held on a permanently-magnetized bearing retainer. Sufficient quantities of the lubricant are delivered from the retainer to the nonmagnetic ball bearing. The bearing retainer could be made from a variety of machinable materials, such as a phenolic filled with a magnetic component. Porous materials may also be used and have

the added feature of acting as a lubricant reservoir. (See page 271.)

Modular Test System for Solar Collectors

A portable, recirculating-water-flow, and temperature-control device has been used with both a solar simulator and actual Sunlight to test and evaluate several solar-collector panel coatings, panel designs, and scaled-down collector subsystems. The system has been used to test a vacuum-insulated collector and an insulated-box configuration in direct Sunlight; other tests were made to study the effect of vacuum insulation on stagnation temperature and heat gain, the effects of flow rate and inlet temperature on heat gain, and the effect of reflectors on heat gain. Preliminary data that were gathered with the test system indicate that an insulated-box (flat-plate) collector with an inexpensive nonselective coating would be satisfactory for residential and commercial space-heating and service hot-water systems. (See page 207.)

PATENT LICENSES RECENTLY GRANTED BY NASA FOR COMMERCIAL USE OF NASA-OWNED INVENTIONS

The patent licenses listed below have been recently awarded by NASA as part of its program to encourage the commercial application of its new technology. For information on how you may obtain nonexclusive or exclusive license for the commercial use of NASA inventions, see page A8 of this issue.

A nonexclusive license to Pyramid Plastics, Meriden, Connecticut, for U.S. Patent No. 3,814,083, covering an invention entitled "Apparatus and Method for Processing Korotkov Sounds."

A nonexclusive license to Sila-King, Incorporated, Bellaire, Texas, for U.S. Patent No. 3,856,534, covering an invention entitled "Anti-Fog Composition."

A nonexclusive license to Hohman Plating and Manufacturing, Incorporated, Dayton, Ohio, for U.S. Patent No. 3,953,343, covering an invention entitled "Bearing Material."

A nonexclusive license to R. B. Johnson, Indianapolis, Indiana, for U.S. Patent No. 3,964,928, covering an invention entitled "Lead-Oxygen Closed-Loop Battery System."

A nonexclusive license to Horace Moore, Plant City, Florida, for U.S. Patent Nos. 3,632,242 and 3,714,332, covering inventions entitled "Apparatus for Making Diamonds" and "Process for Making Diamonds."

A nonexclusive license to Turtle Mountain Corporation, St. Paul, Minnesota, for U.S. Patent No. 3,719,891, covering an invention entitled "Intruder Detection System."

A nonexclusive license to North American Manufacturing Company, Cleveland, Ohio, for U.S. Patent Nos. 3,869,676 and 3,883,812, covering inventions entitled "Diode-Quad Bridge" and "Diode-Quad Bridge Transducer and Discriminator Circuit."

A nonexclusive license to GEE Electronics, Belmont, California, for U.S. Patent No. 3,719,891, covering an invention entitled "Intruder Detection System."

Electronic Components and Circuits



**Hardware,
Techniques, and
Processes**

- 175 Bidirectional Amplifier
- 175 Wide-Dynamic-Range Detector
- 177 Digital Frequency-Offset Detector
- 178 Thermal-Impedance Test for Hybrid Power Devices
- 179 Save Power in AC Induction Motors
- 181 Power Switch/Filter for Digital Circuits
- 181 "Exclusive-OR" Frequency Multiplier
- 182 Three-Level Signal Sampler Has Automatic Threshold
- 184 Pulse-Width-Modulated High-Current Power Supply
- 185 MIS Diode Structure in As⁺-Implanted CdS
- 186 Noise Reduction in Photomultiplier Circuits

Bidirectional Amplifier

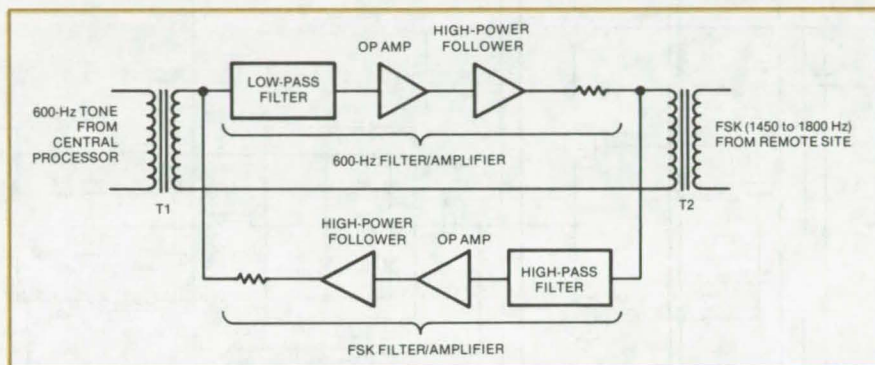
Amplification of two signals of different frequencies being propagated in both directions along a single line

John F. Kennedy Space Center, Florida

A "bidirectional" amplifier has helped to improve a lightning-warning electric-field-meter system at Kennedy Space Center. In this system, long signal lines connect a central processor to each of 25 remote sites. A poor signal-to-noise ratio had been experienced for interrogate signals from the processor to the remote stations and for the frequency-shift-keyed (FSK) data signals back to the processor.

Conventional signal amplification could not solve the problem. The signals to be amplified are sent in both directions along a single pair of telephone lines. Amplification of the FSK signal would interfere with reception of the interrogate signal, and inversely, amplification of the interrogate signal would block the FSK signal. As a result, the system had to operate on a marginal basis, and the distance of remote stations has been limited. In this situation, simple back-to-back amplifiers would not work because of continuous feedback that would cause an "infinite" gain situation.

The bidirectional amplifier, which has been prototyped and tested under field conditions, uses filters to solve these problems. It is a two-stage transformer-coupled device that amplifies both the incoming



The **Bidirectional Amplifier** uses filters to selectively amplify signals falling into two frequency bands. The solid state filters are built using two operational amplifiers with selected resistors and capacitors to provide the correct cutoff frequencies.

600-Hz signal and the outgoing FSK signals, 1,450-Hz to 1,800-Hz (see figure). The transformers are used to convert the differential line inputs to single-ended amplifier signal inputs.

One of the stages, the 600-Hz filter/amplifier circuit, amplifies only the 600-Hz interrogate signal transmitted from the central processor to each remote site. This stage contains a 600-Hz low-pass five-pole Chebyshev filter that prevents amplification of the higher-frequency FSK signals. It is followed by an operational amplifier and a high-power follower with 600 ohms output impedance.

The other stage, the FSK filter/amplifier circuit, amplifies only the 1,450-Hz to 1,800-Hz FSK data signals. This stage contains a 1,450-Hz high-pass five-pole Chebyshev filter that prevents amplification of the 600-Hz interrogate signal. The filter is followed by an operational amplifier and a high-power follower with 600 ohms output impedance.

This work was done by Larry D. Holley of Kennedy Space Center and John W. Caldwell and David R. Ingalls of Federal Electric Corp. For further information, Circle 1 on the TSP Request Card. KSC-10856

Wide-Dynamic-Range Detector

A 40-dB linear detector is driven by a high-impedance current source.

Goddard Space Flight Center, Greenbelt, Maryland

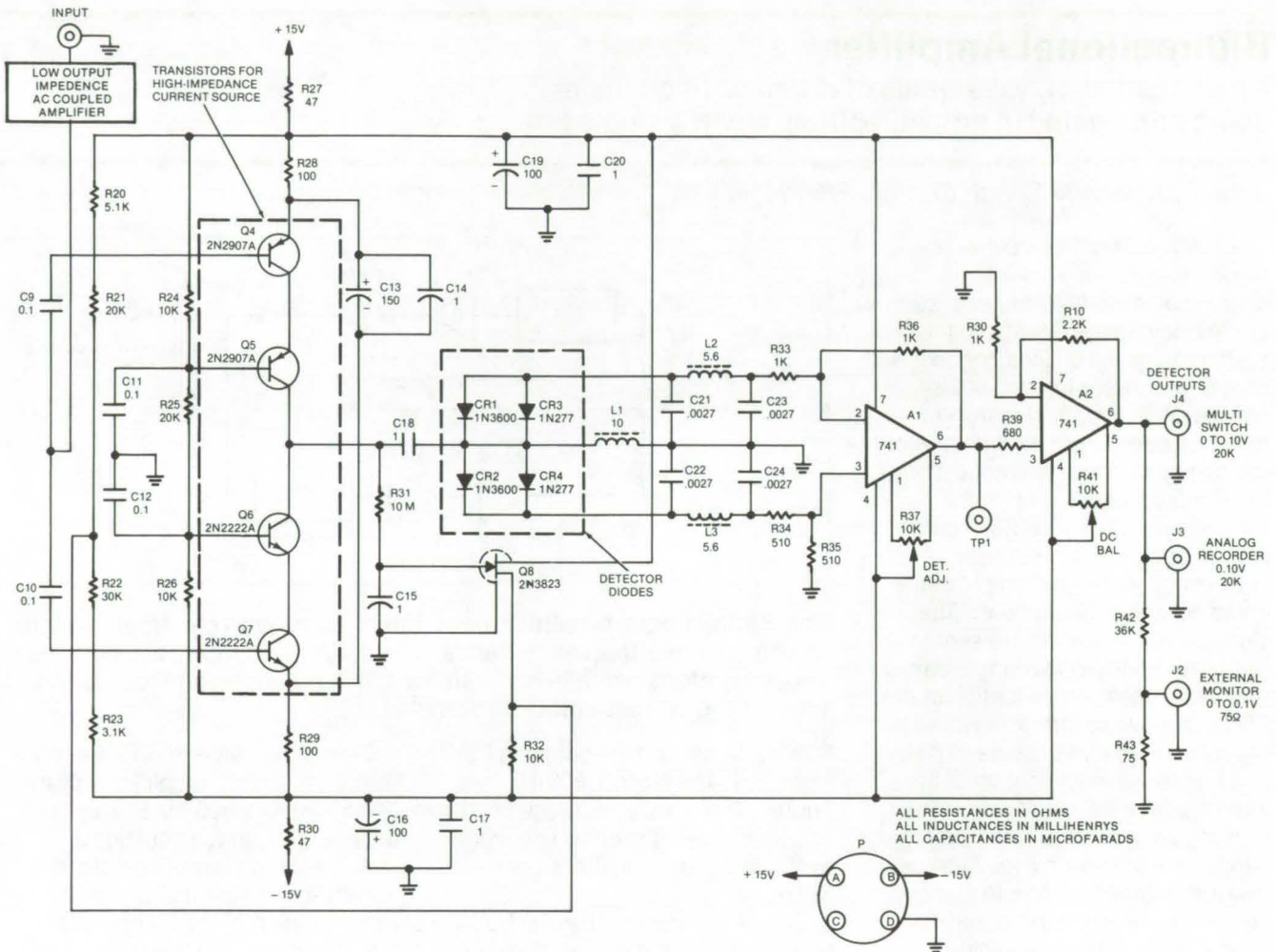
When signals vary rapidly over a wide dynamic range, detection can be a problem. Conventional semiconductor diode detectors cannot be used when the signal drops below about $0.6 V_{RMS}$ because they become nonlinear at such low

levels. Even if automatic gain control is used to keep the minimum level above 0.6 V, the maximum signal level would be 60 V, impractically high for solid-state circuitry. It is possible to switch in successively larger attenuation as the signal in-

creases, but this range switching is often inconvenient, especially for unpredictably varying signals.

A new circuit solves the dynamic-range problem by driving the diode detector with an amplifier having a

(continued on next page)



The **Linear Detector Circuit** has a high-impedance current source ensuring that the detector-diode output stays linear over a 40-dB range of input. Best operation is over the range of 3 to 300 mV.

high and constant output impedance. Originally developed for measuring electromagnetic interference, the basic circuit could also be used in high-performance AM radios, tape players, and phonographs.

The nonlinearity of diode detectors at low voltages results from their change in forward resistance. At high signal levels (greater than 1 V_{rms}), the forward resistance is usually several hundred ohms, but it increases rapidly as the signal level drops. However, the resistance change can be minimized by driving

the detector from a current source. If the current can be made independent of the detector-circuit resistance, then the voltage drop across the load resistor is unaffected by changes in the detector-diode resistance. Both low-level and high-level signals can thus be detected linearly.

A circuit that produces the requisite resistance-independent current is shown in the figure. Transistors Q_4 through Q_7 are part of a complementary amplifier circuit with an output impedance of about 2 M Ω . The average direct-current level at the

collectors of Q_5 and Q_6 is held at zero by Q_8 . The detector is a full-wave type consisting of two half-wave rectifiers connected differentially to dc amplifier A_1 . Filters in the rectifier circuits remove carrier ripple. The overall circuit has good linearity down to a few millivolts. The 40-dB range with best linearity is between 3 and 300 mV.

*This work was done by Robert J. Matheson of The U.S. Department of Commerce and by Fred W. Field and Samuel Sabaroff of Hughes Aircraft Corp. for **Goddard Space Flight Center**. No further documentation is available. GSC-12149*

Digital Frequency-Offset Detector

A simple, low-cost detector with designer-selectable tolerances compares two or more input frequencies.

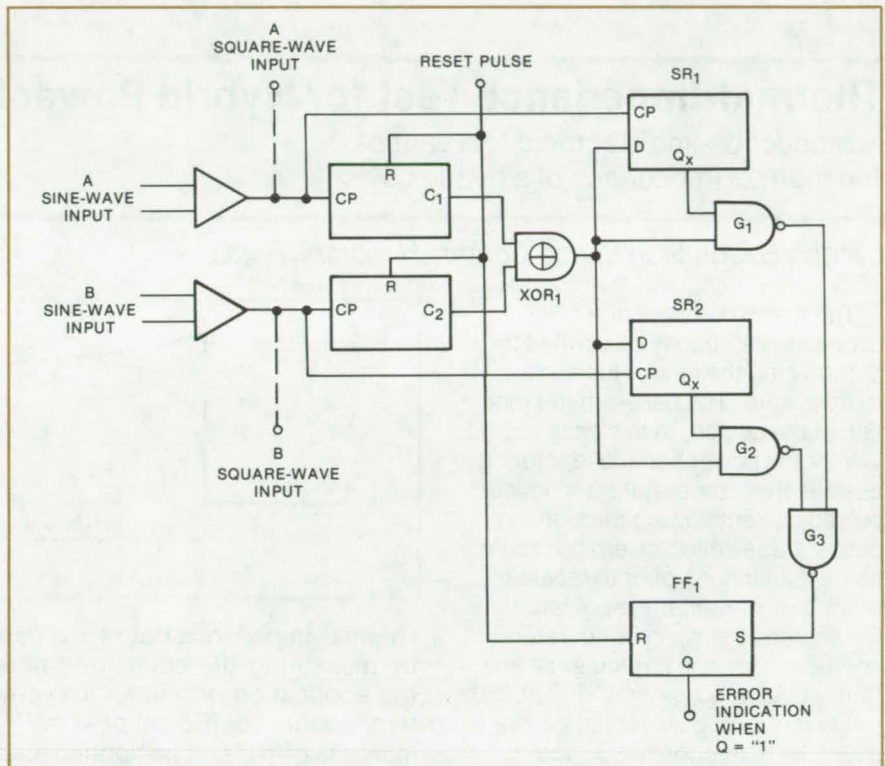
Lyndon B. Johnson Space Center, Houston, Texas

An increasing number of electronic systems utilize precision frequency sources for timekeeping, navigation, radar, ECM, and collision avoidance, among other applications. In order to ensure proper operation of these systems, it is necessary to verify the accuracy of the frequency source. Conventional laboratory test equipment, however, is too heavy and complex for onboard measurement of the accuracy of precision frequency sources. A new detector provides extremely-accurate frequency comparison, with minimal circuitry and with extreme ease of adjustment.

The detector compares two input frequencies and indicates whether they are further apart than a desired tolerance. Thus frequency measurement is relative rather than absolute, unless one of the inputs is a known accurate frequency standard or source.

Since many high-accuracy oscillators have sine-wave outputs, the detector circuit initially converts the sine-wave inputs into square waves. If either or both of the inputs are square waves, they would be connected directly to the indicated terminal for square waves (see figure).

The square waves are then divided down independently by counters C_1 and C_2 . The counter outputs are fed to an "exclusive or" (XOR_1), and the output goes to the data inputs of two shift registers, SR_1 and SR_2 . Shift register SR_1 is clocked by the A square wave, and shift register SR_2 is clocked by the B square wave. The output of XOR_1 is also connected to two NAND gates, G_1 and G_2 . The second input to the G_1 gate comes from one of the shifted outputs of SR_1 (SR_1, Q_x). Similarly the second input to G_2 comes from SR_2, Q_x . The outputs of G_1 and G_2 are connected to NAND gate G_3 , where the output is connected to the



The **Digital Frequency-Offset Detector** has application to any electronic system where accurate timing or frequency control is important. The detector is fairly simple and low cost and will provide a warning if the frequencies being compared fall outside the selected tolerance. Some variation in tolerance is possible through control of the reset pulse.

set input of an R-S flip-flop, F/F_1 . If the true (Q) output of F/F_1 is a "1", this indicates that the A and B frequency inputs are further apart than the circuit tolerance.

At a periodic interval an externally-generated reset pulse is used to clear counters C_1 and C_2 and F/F_1 . This reset pulse determines the interval during which frequency shifts are allowed to accumulate in the counters, and it also clears transient errors out of the circuit.

Three parameters determine the frequency offset beyond which the circuit will alarm:

1. The period of the reset pulse,
2. The number of shift registers used in SR_1 and SR_2 , and

3. The number of counting stages in C_1 and C_2 .

These parameters are all inter-related according to

$$\frac{S}{F_i P_r} = E_t$$

where

E_t = error threshold

S = number of shift-register stages

F_i = nominal input frequency

P_r = reset-pulse period

Using two shift registers and a 40-second reset period, two 5-MHz sources can be compared within 10^{-8} of a pulse period. The number of shift registers can be increased to reduce the likelihood of quantization

(continued on next page)

errors; a corresponding increase in reset period is required to maintain the same error threshold.

The number of counter stages required in C_1 and C_2 depends on the width of the XOR pulse that is required to trigger the circuit, which

in turn is dependent on the number of shift-register stages. For most applications a 4-bit counter is adequate.

This work was done by Robert W. Bogart and Michael J. Juengst of Westinghouse Electric Corp. for

Johnson Space Center. For further information, Circle 2 on the TSP Request Card.

Inquiries concerning rights for the commercial use of this invention should be addressed to the Patent Counsel, Johnson Space Center [see page A8]. Refer to MSC-16358.

Thermal-Impedance Test for Hybrid Power Devices

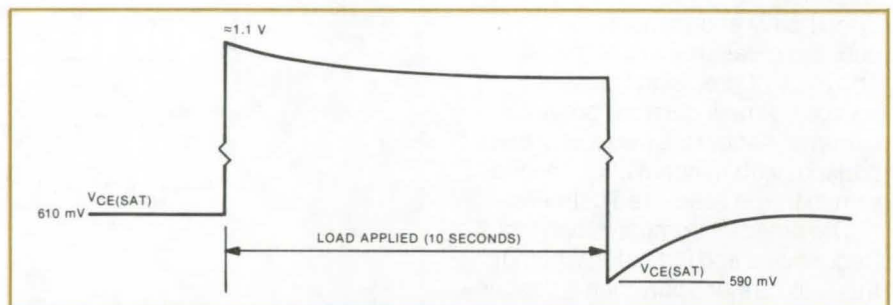
A production-line electrical test verifies the thermal impedance of a hybrid device.

Lyndon B. Johnson Space Center, Houston, Texas

The thermal impedance of a hybrid structure may be verified by determining the device junction temperature. The base-emitter junction of the device, in this case a Darlington power semiconductor, is used as the temperature transducer; pulsed current flowing through the output stage collector-emitter zone heats the junction prior to measurement. For instance, the power Darlington $V_{CE(SAT)}$ temperature coefficient for one particular device family evaluated is $-2 \text{ mV}/^\circ\text{C}$ at 150 mA bias. Pulsing current at a 5-watt power level through the device makes the temperature rise: in this instance, a $V_{CE(SAT)}$ change of -40 mV indicates a junction-temperature rise of 20°C .

The test itself is part of an in-process electrical screen to verify the eutectic bond quality between the BeO substrate and the Kovar case. Since the method can be integrated into the existing electrical test program, the time and the number of steps required to evaluate the Darlington performance are reduced.

The results of a typical test are shown in the figure. A Darlington was first prebiased with 150 mA, and the collector-emitter saturation voltage was measured. (Under this



Thermal-Impedance Data for a Darlington power device may be obtained by measuring the collector-emitter saturation voltage before and after the application of a load. The device producing the curve above had a temperature coefficient of $-2 \text{ mV}/^\circ\text{C}$; the -20-mV drop corresponds to an increase of 10°C . The applied load was 5 A, raising the output voltage to 1.1 V. Thus the power dissipated was 5.5 W, corresponding to a thermal impedance of $1.8^\circ\text{C}/\text{W}$.

condition, the device dissipates about 120 mW.) The Darlington is then loaded to 5 A (at 5.5 watts) for about 10 seconds. (The load could be applied for up to 30 seconds as a test margin.)

When thermal equilibrium results, the load is switched back to 150 mA, and the instantaneous $V_{CE(SAT)}$ is recorded a second time. The difference between the prepower and postpower $V_{CE(SAT)}$ is proportional to the junction temperature rise. The thermal impedance can then be calculated from the voltage change, the power change, and the known temperature coefficient.

For test purposes, a maximum acceptable change in $V_{CE(SAT)}$ can be established as a screening criterion. For instance, in one Darlington test, -50 mV , corresponding to a 25°C temperature rise, was set. It should be noted that the 50-mV measurement will reflect the temperature rise of the case as well as that of the case-to-junction interface.

This work was done by Ralph E. Gardner, Robert L. Jones, and Leslie H. Seymour of Rockwell International Corp. for Johnson Space Center. No further documentation is available. MSC-16643

Save Power in AC Induction Motors

Electronic control loop conserves energy by reducing the voltage applied to lightly loaded motor.

Marshall Space Flight Center, Alabama

Relatively simple and inexpensive circuitry will improve the power factor and reduce power dissipation in induction motors operating below full load. Power factors as low as 0.1 or 0.2 can exist when such motors are partially loaded or unloaded. When this is the case, relatively large currents flow, and little work is being performed. Hence, I^2R losses will occur at all points in the distribution system, including the motor windings, even though no mechanical power is delivered.

An electronic control system has proved, under tests, capable of raising power factors from 0.2 to 0.8 and resulting in energy savings as shown in Figure 1. The power losses are reduced by sensing the phase lag between the voltage and current. This information is fed to the electronic controller shown in Figure 2. This circuit forces the motor to run at a constant predetermined optimum power factor, regardless of load or line voltage variations (within the limits of the motor).

Voltage is varied by using a solid-state switch (such as a Triac or equivalent), which blocks current in either direction until a gate voltage is applied, at which point it will conduct in either direction. When the gate voltage is removed, the Triac remains on until the current goes through zero. Current does not flow again until the gate voltage is applied again. To vary the RMS voltage applied to a motor, the gate is triggered at a given point during the cycle, and the device switches off as the current goes through zero.

The circuitry in the top half of Figure 2 is a typical phase-control and firing-angle circuit. Voltage V_1

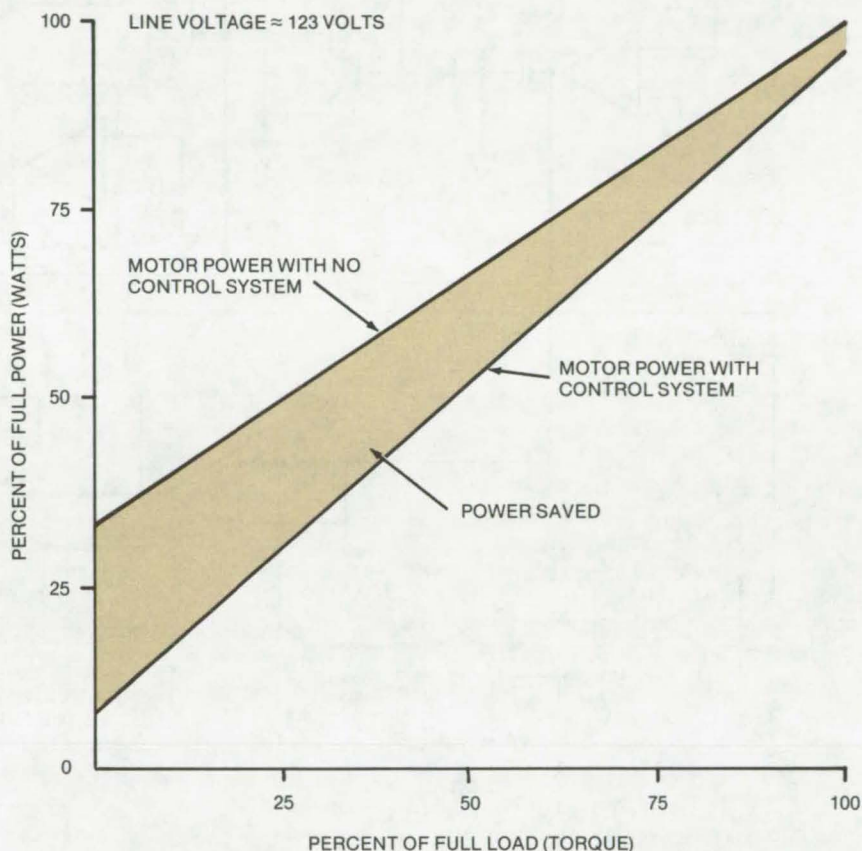


Figure 1. **Power Saved** is shown as averaged from tests made on a 1/3-hp split-phase motor and 1/4- and 3/4-hp capacitor-start motors. The top curve is the total power taken as a function of load with no control system. The bottom curve represents the total power with the voltage controlled by the circuit in Figure 2. Curves are plotted as percent of full power versus percent of full load. The circuit reduced the no-load power by a factor of 5 or 6 and increased the power factor from 0.2 to 0.8. In all three motors, the slowdown due to reducing the applied voltage was less than 2 percent.

is a ramp waveform with its vertical portion synchronized with the zero crossings of the sinusoidal load voltage; V_2 is a dc error signal; and V_3 is a train of pulses that become wider as the error signal increases.

When the pulse is positive, a voltage will be applied to the gate of the Triac.

The error signal is derived in the circuitry in the lower half of Figure 2.

(continued on next page)

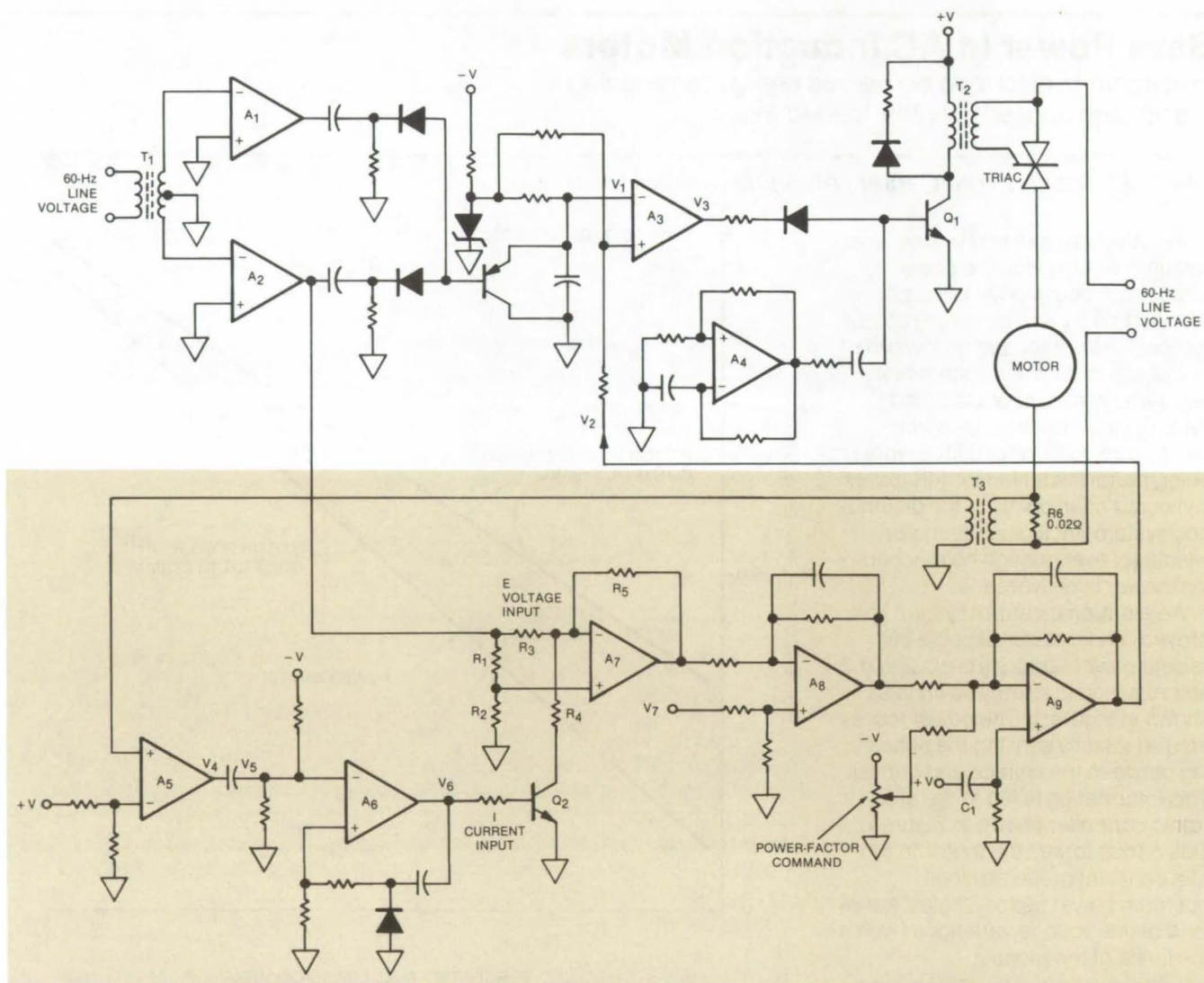


Figure 2. The **Electronic Control Circuit** consists of a typical phase-control circuit (top half) and a new circuit that senses the voltage/current phase lag in an ac inductor motor. This phase lag is used to produce an error signal (V_2) for the phase-control circuit, where a control pulse is developed to switch a Triac that regulates the motor voltage in response to loads.

The phase lag between the voltage and current in the motor is sensed and is used to produce a dc voltage proportional to phase lag. This signal is fed back and summed with a power factor command signal. The difference between these two

voltages is an error signal (V_2) that drives amplifier A_3 and controls the voltage to the motor.

This work was done by Frank J. Nola of **Marshall Space Flight Center**. For further information, Circle 3 on the TSP Request Card.

This invention is owned by NASA, and a patent application has been filed. Inquiries concerning license for its commercial development should be addressed to the Patent Counsel, Marshall Space Flight Center [see page A8]. Refer to MFS-23280.

Power Switch/Filter for Digital Circuits

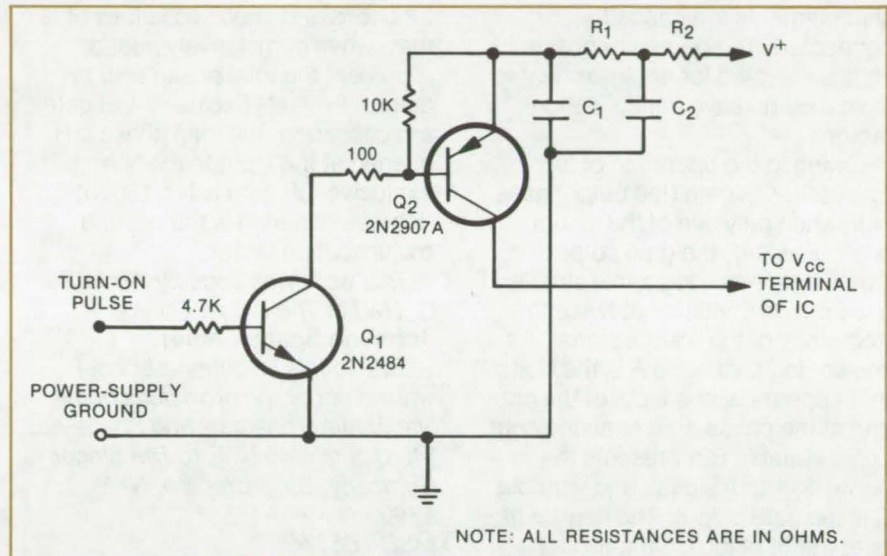
Power consumption is reduced by clocking on active components only as needed.

Lyndon B. Johnson Space Center, Houston, Texas

One inexpensive and practical method of reducing dissipation in a digital circuit is to power the active components only as they perform a function, as for instance when operating briefly during a low duty cycle. Power is saved by clocking on the power for the IC's only when necessary, so that the IC's draw no energy during periods of inactivity.

A solid-state switch/low-pass filter has been designed to source these components. The filter employs a storage capacitor that is trickle-charged to present a constant load to the main power supply. Other filter components are used to smooth transients as the IC's are switched on. Although the circuit is used in spacecraft electronics where power drain is of utmost importance, it may be useful in other battery-powered equipment (such as a ground-based remote pollution monitor incorporating a microprocessor for data analysis).

A schematic of the switch/filter is shown. Power is supplied to the switching transistors Q_1 and Q_2 via the filter network comprised of C_1 , C_2 , R_1 , and R_2 . As Q_1 and Q_2 turn on, current is drawn from C_1 , a capacitor that is charged to a voltage equal to the IC supply voltage (V_{CC}) and the collector-emitter drop across Q_2 .



The **Power Switch/Low-Pass Filter** reduces power consumption in digital circuits that are switched on for comparatively short periods of time and that might otherwise "idle" for the remainder of the cycle. Current flows through R_2 and R_1 to trickle-charge capacitor C_1 . When Q_1 and Q_2 are turned on, the capacitor discharges through the load via Q_2 . The technique may not work in high-speed circuits; in other circuits the power savings are proportional to the complement of the duty cycle.

The V^+ supply therefore is slightly greater than 5 volts for TTL devices but is less than 5.5 volts (the design maximum specified for these devices). The values of R_1 and R_2 are chosen to permit C_1 to charge to the required voltage during the off

cycle. Components C_2 and R_2 are optional; they provide additional circuit filtering.

*This work was done by Harold R. McHugh of Ball Brothers Research Corp. for Johnson Space Center. No further documentation is available.
MSC-16442*

"Exclusive-OR" Frequency Multiplier

Degree of signal phase shift determines the desired multiplication factor.

Lyndon B. Johnson Space Center, Houston, Texas

An Exclusive-OR logic element and a phase-shift network may be combined to perform frequency multiplication in a digital logic circuit. The Exclusive-OR gate

structure uses both input terminals connected in parallel to receive signals from the same source. Prior to injection into the gates, the input signal is split: Half passes through

the phase shifter and then into one gate, while the remainder is directly introduced to the other gate input. Assuming a phase shift of 90° , the output frequency of the Exclusive-

(continued on next page)

OR is twice the frequency of the source.

The degree of output signal symmetry (and therefore the multiplication factor) depends on the amount of phase shift employed. For multiplication factors other than 2, a series of gate circuits and phase-shift elements are cascade-connected. The degree of phase shift is selected for each element to yield a cumulative multiplication factor.

Owing to the operation of an Exclusive-OR gate (the output goes high when only one of the inputs does likewise), the gate output varies between a logic-low state and a logic-high condition at twice the frequency of the source signal. As shown, logic variable A is the signal that appears at one input of the gate and at the phase-shift network input. Logic variable B represents the network output signal, and variable C is the gate output. The degree of phase shift of logic variable C

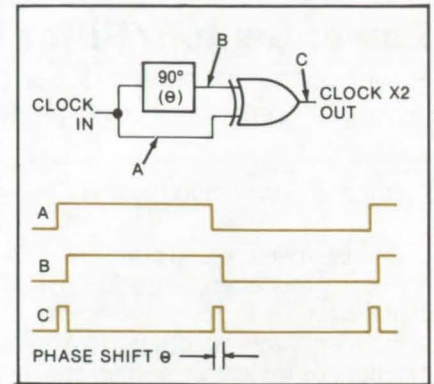
relative to A is a function of θ , about 10° in the example.

Although a single Exclusive-OR function is limited to frequency doubling when its common-source inputs are phase-shifted, it is possible to achieve an infinite variety of multiplying factors by cascading functions and choosing values of θ that, when cumulatively added, represent the total phase shift required. When N Exclusive-OR gates are cascaded, the total phase shift needed at the input to the Nth Exclusive-OR gate is $N/(180/n)$ degrees, where n is the desired multiplication factor.

This work was done by Kenneth G. Harf of The Singer Co. for Johnson Space Center.

Title to this invention has been waived under the provisions of the National Aeronautics and Space Act [42 U.S.C. 2457(f)], to The Singer Company, Binghamton, N. Y. 13902.

MSC-16677



The output of the **Exclusive-OR Frequency Multiplier**, logic variable C, is a signal having a frequency twice that of input variable A. Variable C results from the operating characteristics of the logic function that outputs a logic-high signal only when one or the other (but not both) of its inputs is high. The symmetry of C is a result of the choice of values used to create the phase shift θ . If, for instance, variable B is delayed about 10° with respect to A, C goes high for only about 10° in each period. A phase shift of 180° latches the output of the gate in the high state, thus preventing the Exclusive-OR multiplier from operating as such.

Three-Level Signal Sampler Has Automatic Threshold

Statistical errors introduced by D-to-A conversion are reduced.

Caltech/JPL, Pasadena, California

A newly-built three-level sampler has automatically controlled thresholds to track changes in the statistics of a sampled random process. The mean value of sampled data is removed, and the ratio of the standard deviation of the random process to the threshold is kept constant. Slow drifts in the level comparators and digital-to-analog converters are also removed. The ratio of the standard deviation to threshold level may be chosen within the constraints of the ratios of two integers N and M. These may be chosen to minimize the quantizing noise of the sampled process.

Computing autocorrelation functions from hard-clipped noise processes results in a degradation of the power spectra by a factor of $\pi/2$. This is usually offset by increasing the observation time by a factor of nearly 2.5. However, considerable improvement can be made by extending the number of quantizing levels. The approach described here employs a three-level sampler having automated dc removal and threshold tracking to remove amplifier gain variations in the receiver system and to establish optimum thresholds for minimizing the quantizing noise. The sampler uses

MECL logic and operates in excess of 100 MHz.

The effects of noise can be seen by describing the original data as $x(t)$: a stationary, zero-mean, Gaussian, random process having variance σ_x^2 . This process is assumed to be contaminated by drifts in the receivers and amplifiers such that a new time-varying process $y(t)$ is formed, where

$$y(t) = a(t)x(t) + b(t)$$

The functions $a(t)$ and $b(t)$ are slowly varying, and $a(t)$ is always assumed to be greater than zero. The process

$y(t)$ is to be sampled; however, the sampling thresholds may be chosen so as to remove the drifts $a(t)$ and $b(t)$ simultaneously. Figure 1 shows a simple three-level sampler that may be extended to operate for any number of levels. The reference voltages v_+ and v_- control the upper and lower thresholds of the comparators, respectively. The comparator C_1 gives a "1" state output when clocked if $y(t) > v_+$ and "zero" otherwise. The comparator C_2 gives a "1" state output if $y(t) < v_-$ and "zero" otherwise. Three sample levels result as shown in the truth table, and are called "1", "0", and "-1." The threshold voltages may be determined from certain running averages calculated from the

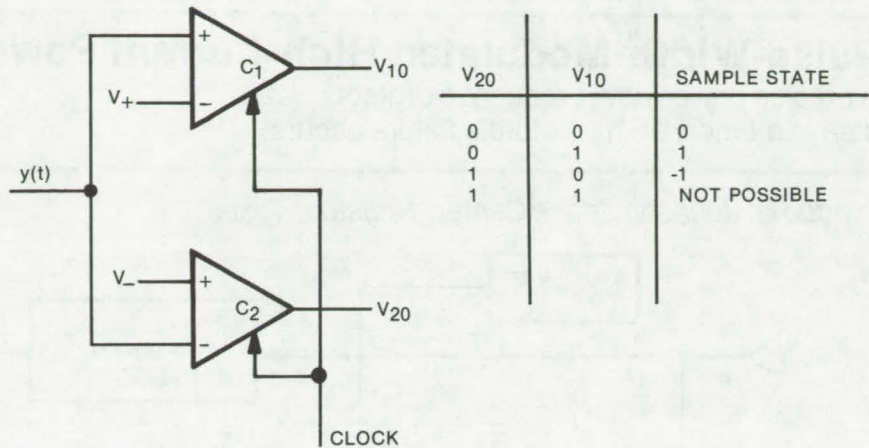


Figure 1. A **Simplified Three-Level Sampler** is shown with an output truth table defining the three states in terms of the comparator output signals v_{10} and v_{20} .

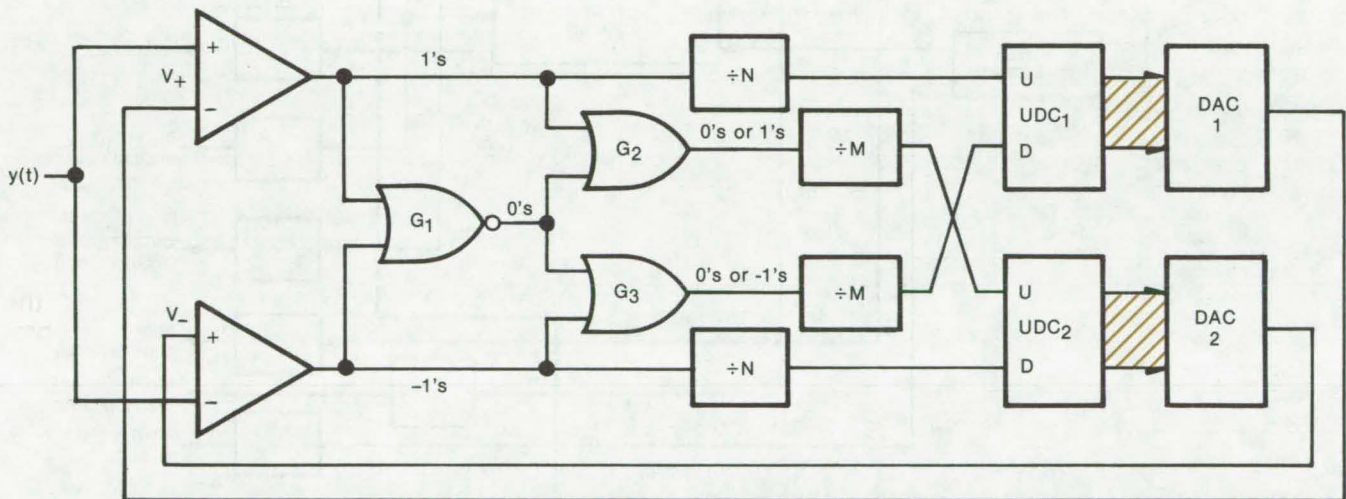


Figure 2. **Feedback Control** can be used to establish the threshold voltages v_+ and v_- so as to remove dc offsets and gain variations in the input signal.

comparator outputs v_{10} and v_{20} . The system then acts simultaneously as an automatic gain control and a dc removal control.

Any number of schemes can be used to establish the feedback signals v_+ and v_- ; one of the simplest is to force the average ratio "1's":("1's" + "0's") to be fixed while simultaneously forcing the ratio "-1's":("1's" + "0's") to equal published ratios for random Gaussian processing. Figure 2 shows a simple scheme to accomplish this.

The NOR gate, G_1 , yields a "1"

state for "0's" of the truth table of Figure 1. The "1's" and "0's" are merged by the OR gate G_2 , and likewise the "-1's" and "0's" by the gate G_3 . The divide-by-N and divide-by-M counters establish a proper balance between the "1's" and everything else and between the "-1's" and everything else. If the counts going into the up/down counters UD_1 and UD_2 are, on the average, equally up and down, the output count remains nearly constant; and the voltage at the output of the DAC's remains constant. If, for example, the rate of "1's"

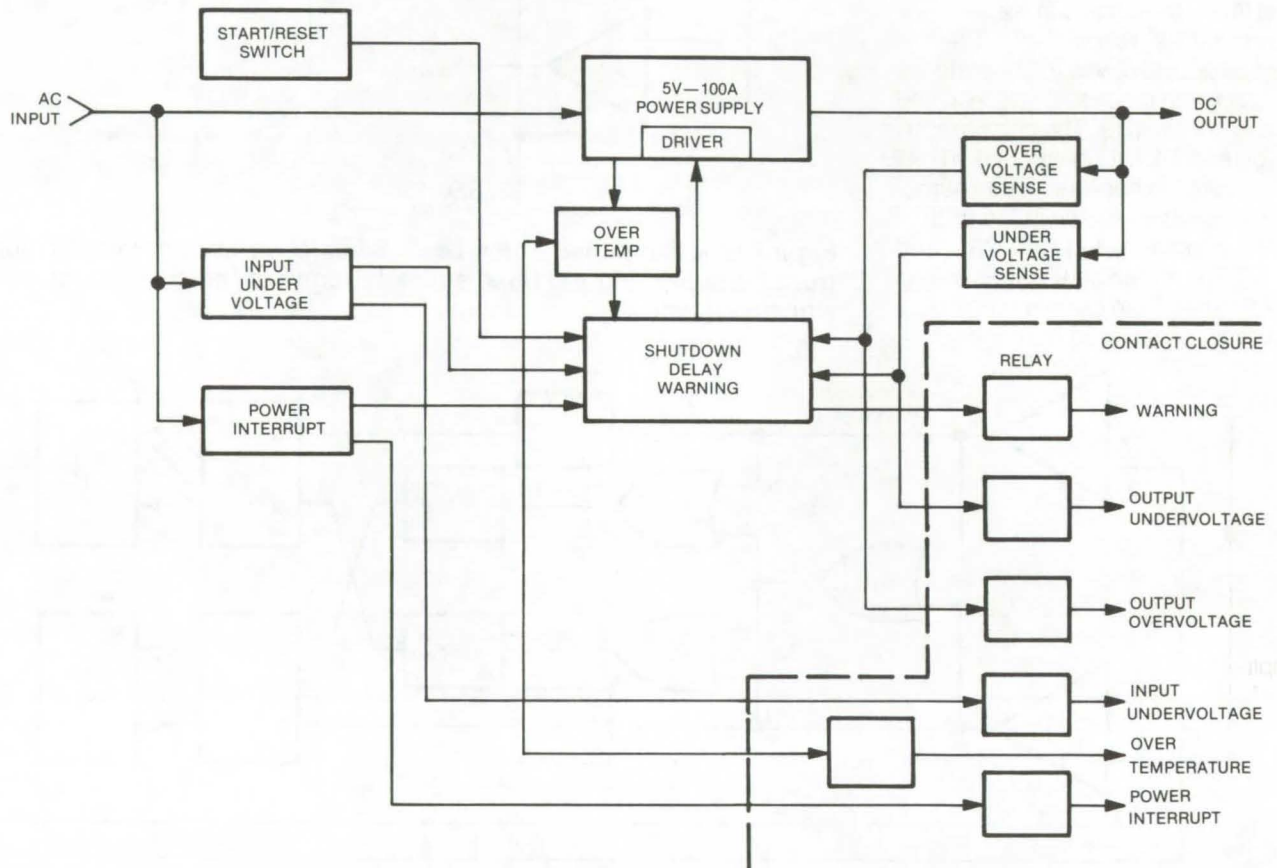
relative to the "0's" and "-1's" is too large, UD_1 will count upward, increasing the output of DAC_1 , which raises the threshold voltage v_+ and decreases the "1's" count rate. DAC_2 generates the lower reference voltage which is normally negative.

This work was done by Stanley S. Brokl, William J. Hurd, Raymond F. Jurgens, and Eugene R. Rodemich of Caltech/JPL. For further information, Circle 4 on the TSP Request Card. NPO-14042

Pulse-Width-Modulated High-Current Power Supply

A precise power-down sequence protects data in memory 15 ms before a failure occurs.

Lyndon B. Johnson Space Center, Houston, Texas



In the **High-Current Power Supply**, Schottky hot-carrier diodes are used to rectify the 20-kHz current input. This reduces power loss to 40 watts (at 100 A), as compared to a 100-watt loss, using conventional diodes. An external power-failure warning signal is detected by the control module which executes the power-down sequence. Protection from overcurrent failure also is built in via a sense circuit which trips a latch and terminates the power-up cycle when a preset current condition is exceeded in the switch. A sensed error initiates power supply shutdown in the following sequence: A 15-ms delay is initiated before the supply can shut down; relay contacts close in the failure indicator circuit; and relay contacts close in the failure warning circuit.

A 5-volt 100-ampere power supply occupying a volume of 600 in.³ (9,832 cm³) and operating at 20 kHz achieves an efficiency rating of approximately 80 percent at rated maximum output current. The pulse-width-type regulator supply incorporates a fail-safe circuit to prevent logic/memory loads from losing stored data if the supply protection circuit initiates power shut down.

The protection circuitry of the supply prevents damage caused by an overtemperature condition, and it will protect the logic/memory load from an undervoltage or overvoltage condition. A warning signal is sent to the control module (see the diagram) to warn of a power shut-down condition 15 ms in advance of actual turn off. This enables the command device to execute a

power-down sequence before power is lost.

The integrated-circuit (IC) logic control, consisting of a 20-kHz clock and a flip-flop, produces a clock drive signal and an inverted clock signal. Both the clock and inverted clock circuits are configured to terminate normal operation in the event an abnormal-condition signal is received. A latch circuit resets the

clock signal upon resumption of normal circuit operation.

The regulator resets the latch circuit when the supply is operating normally. The overcurrent sense circuit trips a latch and terminates

the power-up cycle when a preset current condition is exceeded in the switch. This allows the power supply to deliver power into a load without risk of damage to the load or to itself.

This work was done by Edward A. Messano and Herb E. Moore of General Electric Co., for Johnson Space Center. For further information, Circle 5 on the TSP Request Card.
MSC-14668

MIS Diode Structure in As⁺-Implanted CdS

Increased turnover voltage suggests metal-insulator-semiconductor structure.

Langley Research Center, Hampton, Virginia

Efficient light-emission processes found in some semiconductors have provided incentive in the past for attempting to fabricate green-light and blue-light emitting pn junctions from single-crystal structures of CdS, ZnSe, and ZnS. More recent work, including current-voltage (I-V) experiments involving N, P, As, Sb, and Bi ions, indicates As⁺ implants yield the best diode rectification properties. Preliminary evidence suggests that further work on As⁺ implants might yield a potentially-useful pn junction in CdS.

The implantation of As ions in samples sliced from undoped boules of CdS was accomplished at room temperature, using a mass-analyzed, electrostatically scanned, and offset beam to obtain a ± 1 -percent surface uniformity. Half of each CdS sample, excluding outer edges, was As⁺-implanted at various energies and fluences. Following sputter deposition of platinum electrodes to both the implanted and unimplanted surfaces, the samples were annealed in flowing nitrogen at 450° C. Finally, indium electrodes were evaporated to the front and back of the unimplanted region. An illumination mask was used, as shown in the illustration, to allow study of both illuminated and dark diodes.

Current-voltage characteristics for both dark and illuminated diodes on the implanted and unimplanted halves of CdS wafers were determined. Reverse bias data indicate a lower breakdown voltage for the implanted diodes (I diodes) than for the unimplanted diodes (U diodes).

These results have been attributed to a higher concentration of ionized defects in the depletion region of the I diodes.

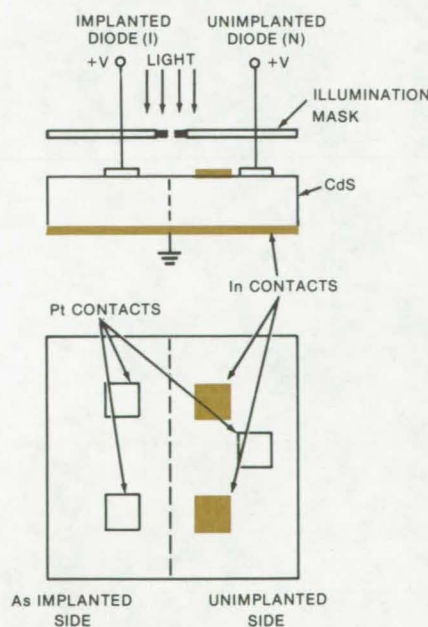
The forward bias I-V characteristics exhibit a contrasting behavior compared with the reverse bias results. For example, data indicate a forward turnover voltage of 1.15 V for the I diode compared with 0.65 V for the U diode. In darkness, the turnover voltages are 18 V for the I diode and 14 V for the U diode. These data indicate that the implanted layer has a substantial influence on the rectification properties. Furthermore, the turnover voltage for the I diode increases with increasing diode current, whereas

the turnover voltage for the U diode appears to remain relatively fixed.

Comprehensive analysis suggests that the model for the I diode should not include a pn junction as originally hypothesized, but rather, a metal-insulator-semiconductor (MIS) structure: in this case, a rectifying Pt-CdS potential barrier with turnover voltage that is increased by As⁺ implantation, in series with a nonlinear high-resistance layer. The increase in turnover voltage may be due to interface states modified by As⁺ implantation and/or to the presence of a thin insulating region between the CdS and the Pt electrode. Analysis further indicates that a decrease of the forward turnover voltages in going from dark to illuminated diodes is caused by optically-activated hole or electron tunneling processes through the MIS rectifying barrier.

Thus, the evidence suggests that the charge conduction in both the implanted and unimplanted structures is dominated by hole and/or electron tunneling through the Pt-CdS potential barrier. The difference in turnover voltages for the illuminated structures is believed to be caused by interface states modified by As⁺ implantation and/or the presence of a thin insulating layer between the Pt electrode and the implanted layer, thus suggesting a MIS structure.

This work was done by James A. Hutchby of Langley Research Center. For further information, Circle 6 on the TSP Request Card.
LAR-12156



CdS Diode Structure

Noise Reduction in Photomultiplier Circuits

Simple damping resistor added to cable acts as filter.

Langley Research Center, Hampton, Virginia

A source of noise in photomultiplier circuits has been identified and successfully eliminated by use of a simple resistor. The noise is generated as a result of pulses of cathode current exciting the cable, usually a coaxial cable, which supplies high voltage to the photomultiplier tube. The cable behaves essentially as a quarter (or odd multiple thereof)

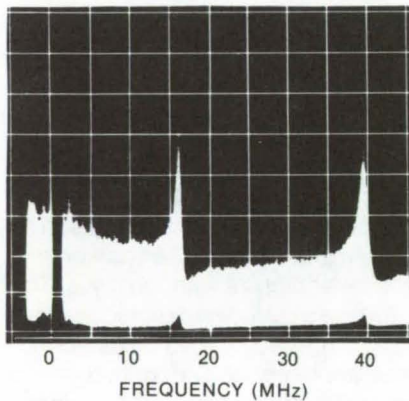


Figure 1. Without a Filter, the photomultiplier spectrum exhibits several noise peaks.

wavelength resonator with traveling waves reflected at the power supply. The resonator effect was verified by analysis of the spectrum (Figure 1) of resulting anode noise.

Altering the length of the cable merely shifts the positions of the peaks but does not eliminate the resonator effect. The insertion of a choke at the power supply has the primary effect of transforming the quarter-wave resonator to a half-wave resonator.

The noise pulses were eliminated very simply by the insertion of, in this case, a 0.1-watt resistor in the cable at the power supply. The resistor acts as a filter, damping out the traveling waves on the cable (Figure 2). The spectrum with the resistor in place shows the noise pulses effectively eliminated.

The resistor used should match the characteristic surge impedance of the cable. With this modification to the circuit, waves generated in the cable by high-frequency pulses and by fluctuations of cathode

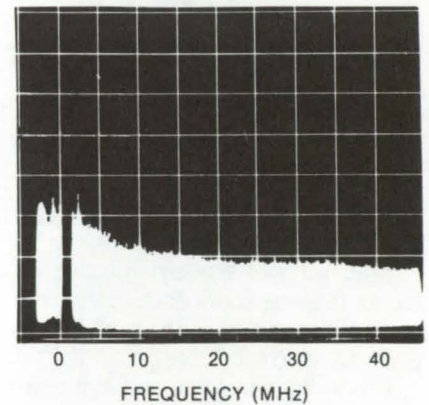


Figure 2. With a Filter resistor in place, the noise pulses in a photomultiplier tube are effectively eliminated.

current are no longer reflected at the power supply, but are successfully dissipated by the damping resistor.

This work was done by John M. Franke and Joseph H. Goad, Jr., of Langley Research Center. No further documentation is available. LAR-12091

Electronic Systems



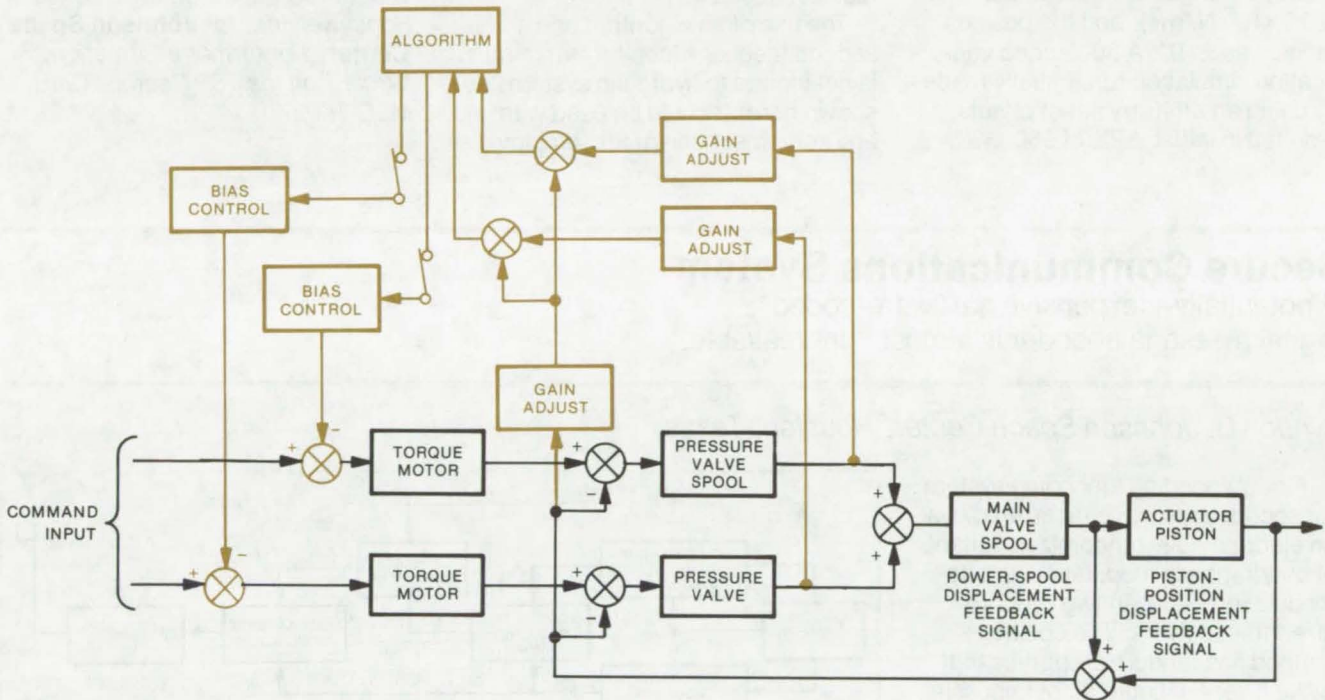
**Hardware,
Techniques, and
Processes**

- 189 Automatic Channel Trimming for Control Systems: A Concept
- 190 Secure Communications System
- 191 High Speed DAC
- 193 Multiplexed Fiber-Optic Transmission System
- 195 Advanced General-Purpose Computer

Automatic Channel Trimming for Control Systems: A Concept

Algorithm and second feedback loop compute trim biases for channels of multichannel servosystem.

Lyndon B. Johnson Space Center, Houston, Texas



Offset Is Automatically Trimmed in a two-channel electrohydraulic servosystem by using the second feedback circuit shown in color in this simplified diagram. The position command is set at zero so that the position feedback signal represents departure from the mechanical zero position. Channel-pressure output signals are summed with the position-error signal. The individual-channel offsets will be different and may be of either polarity. During a sampling period, the iterative algorithm computes biases for each channel, requiring a net bias of zero and a zero actuator position. These biases are then set and input as a constant to the system.

Differences between channels of a multichannel control system can be automatically normalized with a set of bias signals added to the channel inputs. The biases are computed by using a second feedback loop and an iterative algorithm. The technique was developed and tested on an analog simulator for the thrust-vector control system of the Space Shuttle. The concept could be applied to other automatic control systems, such as regulators and multichannel servosystems for remote manipulators in undersea mining and similar tasks.

The electrohydrodynamic servos for the Shuttle will have several redundant channels that are summed to control an actuator. The

output of each of these channels will have, in addition to the control pressure, a channel offset pressure, ΔP , due to channel variations. For a steady-state actuator position, these must sum to zero at the main power spool. In the untrimmed condition, the actuator will generally develop a position offset to bring the ΔP sum to zero. In addition, the ΔP 's are monitored to determine channel operation, and if they exceed a threshold value, the channel is bypassed. It is thus desirable to have the initial ΔP 's close to zero so the allowable variation will be the same for each channel.

Trimming the individual channels for steady-state error control requires the consideration of two types

of error signals. One is the conventional feedback error signal between the input command signal and the actuator piston as used in single-channel control systems. The other is the differential error signal between nominally identical channels and is peculiar to multichannel systems. The channels can be trimmed by setting up the second feedback circuit as shown in the illustration.

The feedback circuit uses an iterative algorithm to calculate a bias for each channel while the actuator-position command is at zero. Many different sets of biases will set the sum of the ΔP 's to zero, but only one set simultaneously adjusts the actuator position to zero.

(continued on next page)

Once calculated, the biases for each channel are used as a constant to be input during normal operation of the servomechanism.

Accuracy and convergence time of the algorithm are a function of the gain on the ΔP and position errors. For the design simulator, the maximum ΔP range was $\pm 3,000$ psi (20.7×10^6 N/m²), and the position range was $\pm 10^\circ$. A 30-second verification simulation run, initially made by using an arbitrary set of offsets, resulted in initial ΔP 's of 950, 330,

-780, and -500 psi (6.6×10^6 , 2.3×10^6 , -5.4×10^6 , and -3.5×10^6 N/m²) and a position offset of 0.12° . In this run, the position offset converged to 0.004° in 4 seconds and did not exceed 0.004° again. The ΔP 's converged to 40 psi (0.3×10^6 N/m²) in 5 seconds and did not exceed 40 psi again.

The use of an algorithm and a second feedback loop for trimming is not limited to hydraulic systems as shown here. It could be used with any servomechanism that employs

multiple input channels for purposes of redundancy. The concept could also be quite useful with regulators that employ several sensors; it could normalize differences between sensor placement and characteristics.

This work was done by Richard J. VanderVoort and Homer A. Sykes of Honeywell Inc. for Johnson Space Center. For further information, Circle 7 on the TSP Request Card. MSC-16027

Secure Communications System

A potentially-inexpensive hardware-coded digital message encoder is almost "unbreakable."

Lyndon B. Johnson Space Center, Houston, Texas

A new encoding/decoding system for secure communications employs an electronically randomized variant of quadrature phase modulation and demodulation between two synchronized transceivers. The coding method has random properties that make it very difficult, if not impossible, to decipher. The system is constructed from off-the-shelf components. Thus, it could be inexpensive enough for private and industrial use, as well as secure enough for national-security applications. It may be used with digital data, command signals, delta-modulated voice signals, digital TV signals, or any other data converted to digital form.

A typical transceiver for the encoder/decoder comprises three main units:

- a master timer,
 - a message encoder and transmitter, and
 - a message decoder and receiver.
- Messages are encoded by using the combined outputs of two pseudorandom-sequence generators as shown in Figure 1. These are 41-stage shift register devices, and the particular sequence obtained from each depends on which taps are used. With a clock rate of 250 kHz, a maximum-length sequence

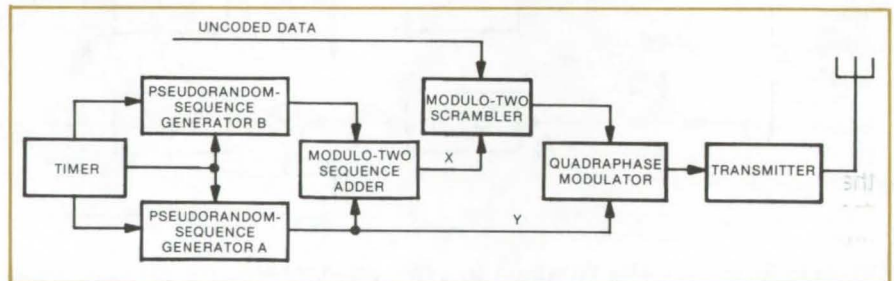


Figure 1. The **Encoder/Transmitter** is controlled by a timer that uses a very stable quartz-crystal oscillator as a reference. In addition to a clock signal, the timer produces two reset signals that are used to change the taps on the pseudorandom sequence generators and thus to change the coding (about once a month). The generators can be made from two off-the-shelf registers and an "exclusive OR" IC. The encoding sequence is produced by modulo-two addition of the two sequences, and the data are coded in another modulo-two adder (scrambler). One of the original sequences is transmitted along with the coded data for synchronization. Shift registers are placed at points X and Y to provide delays that match delays required in the receiver/decoder.

takes 102 days to repeat; when more than two taps are used, there are literally millions of different maximum-length sequences available. Each of the two sequence generators produces a different sequence, and the sequences have different lengths. These are combined in a modulo-two adder to form a new code, which is used to encode the transmitted data. The encoded data, along with one of the original pseudorandom sequences, are

transmitted via quadrature phase modulation or other suitable technique.

The timer is used to synchronize the encoding and decoding for the transmitter and receiver. Both generated sequences are reset periodically and at slightly different times. The key factors that must be known to decode the transmitted data are the two random sequences and the starting times for each. The number of possibilities are myriad. Thus at the receiver, one must know the

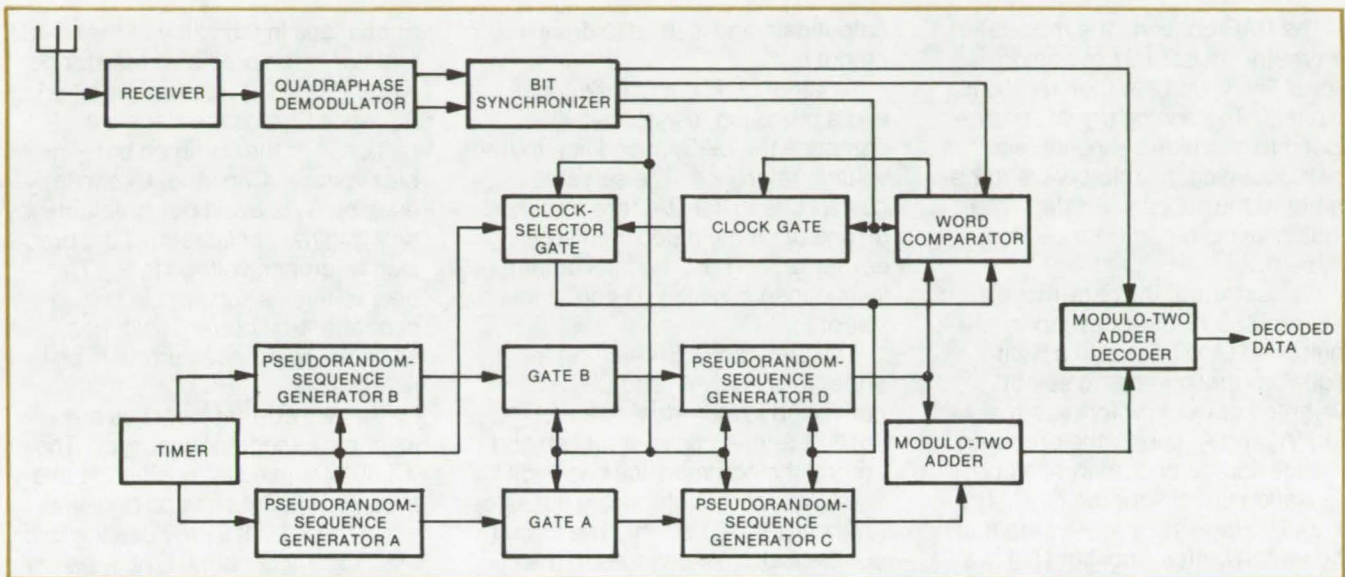


Figure 2. The **Receiver/Decoder** is controlled by a timer set identically to that in the transmitter/encoder, and it uses identical shift registers. Bit synchronization is achieved with the aid of the uncombined pseudorandom sequence transmitted with the coded data. The word comparator is, in essence, a frame synchronizer modified to operate with a continuous synchronizing bit stream. Generators A and B continuously generate the coding sequences; generators C and D are identical but are slightly delayed and are used for decoding and synchronization. Generator D produces the synchronization sequence for the word comparator, and C and D together produce the code for the decoder.

actual pin assignments for the shift register outputs and the program that is used to change tap assignments. If this information, the timing, and the wiring of the transceivers are kept secure, the code is virtually unbreakable.

The decoder/receiver is shown in Figure 2. The decoder produces the same two pseudorandom sequences as the transmitter/encoder. These are used to reproduce the encoding sequence, and the pseudorandom sequence that was transmitted with the encoded data is used in the

receiver for synchronization. The decoder also contains another pair of sequence generators that are identical to the first pair. When no message is being received, these act as shift registers. When a message is being received, the first pair of sequence generators continues to produce the timed coding sequence; the second pair is used to decode the received signal.

Before this system is initialized, the timers at all the stations must be synchronized. One way of doing this is to use a reference timer that is

connected to the system timer for startup. Finally, the coding parameters must be set in, either by switches or by using magnetic cards or similar devices.

*This work was done by George D. Doland of Lockheed Electronics Co., Inc., for **Johnson Space Center**. For further information, Circle 8 on the TSP Request Card.*

Inquiries concerning rights for the commercial use of this invention should be addressed to the Patent Counsel, Johnson Space Center [see page A8]. Refer to MSC-16462.

High Speed DAC

Modulated telemetry subcarriers are converted to 64 analog signal levels.

Caltech/JPL, Pasadena, California

A recently-developed high-switching-rate digital-to-analog converter (DAC) provides an effective means to convert a digitally-modulated data source to 64 analog levels. Minimum power dissipation is maintained while satisfying stringent requirements for rise and fall times,

settling time, overshoot, droop, final level, and symmetry. The high-speed ICL8018 (or equivalent) current switch is combined with the high-slew-rate HA2520 (or equivalent) operational amplifier to produce the multilevel output signal for telemetry. Typical switching

speed is 70 ns. The output signal level is determined by "AND'ing" the data-modulated subcarrier frequency (digital pulses) with a 6-bit digital control number to select the appropriate weighted current switches.

(continued on next page)

The DAC converts the modulated telemetry subcarriers to analog signal levels that are then routed to excitors. The analog signals correspond to modulation angles required for modulating the microwave transmitter at the subcarrier rates. The analog levels range from 350 to 1,750 mV.

As illustrated, the data-modulated source (360-kHz subcarrier) is multiplied (AND'ed) with a 6-bit digital control number to select weighted current switches. Amplifiers A₁ and A₂ supply the precision voltage source and reference compensation circuits for the DAC. The output voltage seen at the output of the switch buffer amplifier (A₃) is a reproduction of the modulated data with 64 possible (discrete) levels. The final amplifier (A₄) scales the

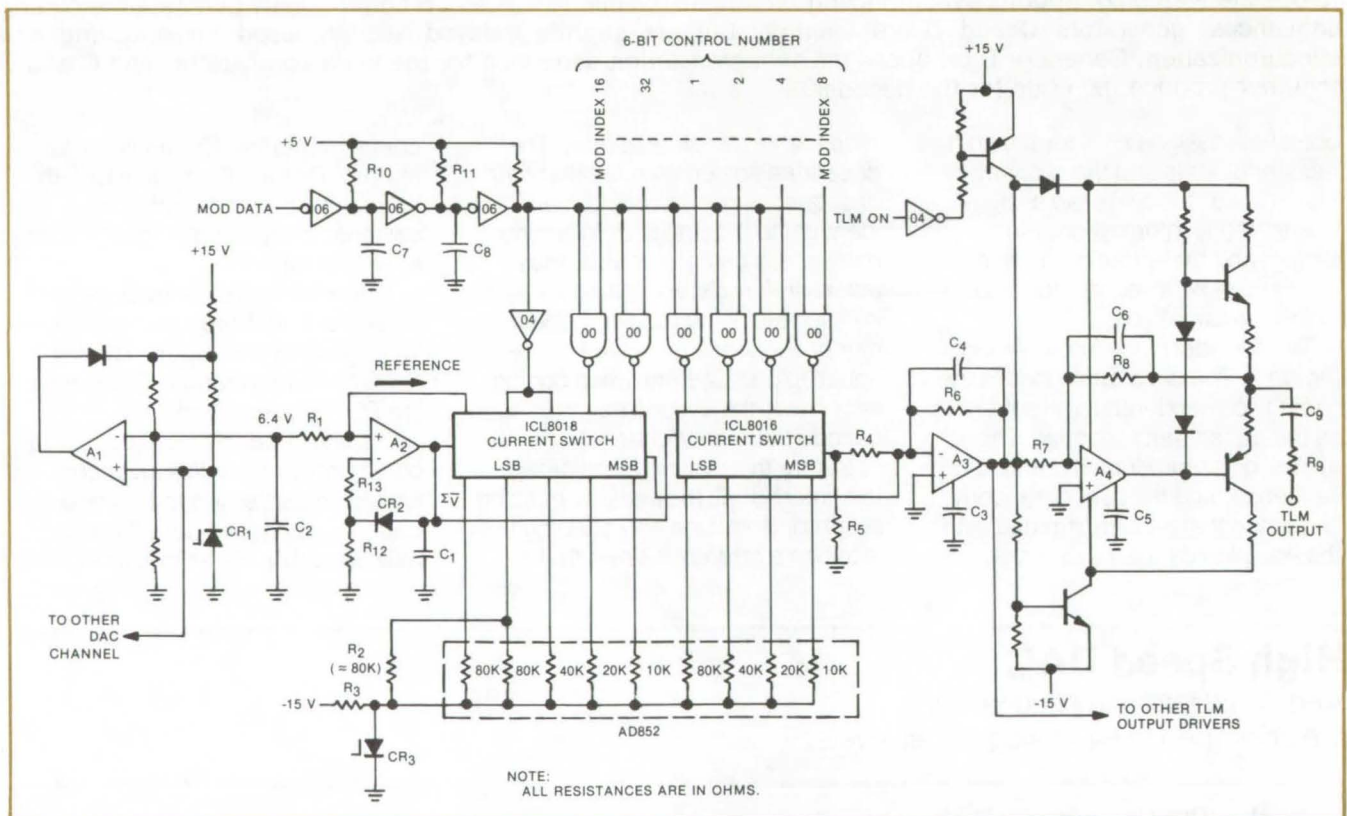
output gain and is used to drive the output line.

A pair of quad current switches and a precision resistor network comprise the DAC, in addition to the voltage reference. The selected control bits to the DAC are switched on and off at the modulated subcarrier rate. Thus, the final output level depends on the bit combination selected.

The precision +6.4-volt reference, formed by A₁ and CR₁, is converted to individual channel current references to establish and control the common line base voltage (bias) of the reference transistor (in the ICL8018 switch). The circuit compensates for changes in the emitter current resulting from changes in the base-to-emitter voltage of the switched semiconductor,

or changes in the value of the 80-kΩ resistor in the precision resistor network. Diode CR₂ prevents latchup of A₂, while C₁ aids the transient response of the common baseline bias voltage. Capacitor C₂ similarly enables A₂ to avoid power latchup by delaying the application of the precision reference voltage to R₁. This bias voltage is supplied to two separate 4-bit current switches, while the reference current is only used by one.

The two current switches are identical except for accuracy. The ICL8018 is used to provide the two most significant bits and pedestal, while the ICL8016 provides the four least significant bits. Since the same bias voltage is fed to both switches, the internal transistors must be matched and thus are replaced together.



A simplified schematic of one 6-bit channel in the **Data-Modulated DAC**: The precision current-setting and reference-setting resistors are provided in the AD852. The pedestal is formed by using the two least significant bits of the most significant current switch (ICL8018) in parallel with an additional external resistor (R₂). The voltage at the common point of the AD852 resistor network is stabilized for tighter control of the internal low-level-logic threshold voltage in the current switch. Changes in the current supplied to the precision resistor network result in changes in the bias voltage that directly affects the low-level-logic threshold voltage. Without tighter regulation of the -15-volt supply at this point, logic operation over the worst case extremes of temperature and voltage cannot be guaranteed. Therefore, a resistor and diode network, R₃ and CR₃, is used to stabilize the voltage (-11.7 volts) at this common point.

The outputs of the two current switches are added together to form the composite DAC output current. This is converted into a voltage source by A_3 , the current-to-voltage amplifier. Resistors R_4 and R_5 divide the four least significant bits of the output current by 4 for proper scaling. Resistor R_6 , in conjunction with amplifier A_3 , is used for voltage conversion and gain control. Capacitors C_3 and C_4 control the rise and fall times, overshoot, settling time, ripple, and generally stabilize the output-voltage waveform characteristics as the DAC is being switched at the subcarrier rate.

The DAC weighted-current switches are controlled by TTL-compatible logic elements that modulate the selected modulation index (output level) at the data-modulated subcarrier rate. The

current switches are capable of switching times less than 80 ns. However, due to the internal current-switch configuration and distributed external capacitance, the resulting waveform asymmetry at the output of amplifier A_3 is degraded (greater than 1 percent at the high subcarrier rate). In order to compensate for this, the data-modulated subcarrier (MOD DATA) signal-rising (and signal-falling) transitions are delayed until a minimum asymmetry is achieved at ambient temperature. The timing network (R_{10} , R_{11} , C_7 , and C_8) is used to control transition time.

The signal output of amplifier A_3 is supplied to two output line drivers in both the X-band and S-band DAC channels and also to a third (umbilical) amplifier in the X DAC channel. Each line driver is inde-

pendently power switched by command control for channel output redundancy with minimum system power drain. The dc offset in the output signal is removed by capacitor C_9 . Resistor R_9 enables load balancing, splitting the load into two precision 50-ohm components. Resistors R_7 and R_8 determine the gain scaling factor to adjust the final peak-to-peak output-signal level for the desired 0.35-V to 1.750-V range, while capacitors C_5 and C_6 are used to control channel bandwidth. The capacitors thus control the rise and fall times as well as the settling time and ripple level.

This work was done by James Durden of Motorola, Inc., for Caltech/JPL. For further information, Circle 9 on the TSP Request Card.
NPO-13805



Multiplexed Fiber-Optic Transmission System

Digital, audio, and video data channels spanning 100-MHz bandwidth are transmitted via a single fiber-optical link.

John F. Kennedy Space Center, Florida

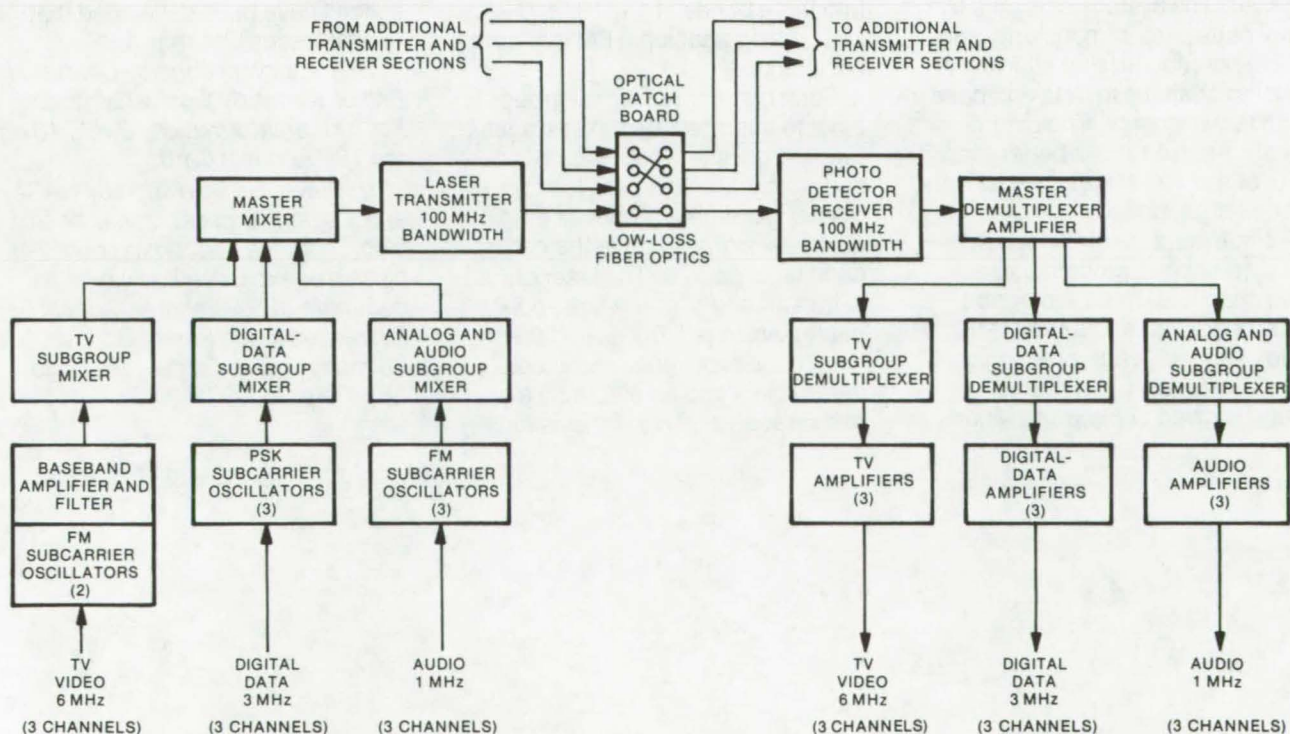


Figure 1. The **Fiber-Optic Transmission System** relays data channels over a 1,000-ft cable. A light-emitting diode (LED) has been used successfully in place of the helium-neon laser, and injection laser diodes are currently being evaluated as optical sources.

Low-loss optical fibers have been recognized as attractive alternatives to conventional copper cables for use in data transmission. Glass fibers offer significant reductions in size and weight, are immune to lightning, electromagnetic, and radio-frequency interference, and have a wide bandwidth characteristic. In addition, fiber optics are considerably simpler to install and maintain than copper, as they require none of the extensive shielding and conduit normally associated with conventional transmission lines.

A prototype 100-MHz bandwidth fiber-optic transmission system has been built and tested at the Kennedy Space Center in anticipation of an operational version which will replace the center's existing 13,000-mile (20,917-km) copper cable network. The prototype employs a frequency-deviation multiplexing (FDM) scheme to stack many analog, digital, audio, and video channels on a single optical fiber. An acoustically-modulated or electronically-modulated helium-neon laser has been used as the transmitting device, and an avalanche photodiode serves as the receiver. The system is flexible by virtue of its plug-in modularity and optical patchboard that allows it to adjust to changes in data and bandwidth requirements. The overall signal-to-noise ratio is better than 50 dB over the 100-MHz bandwidth and near 60 dB midband.

A block diagram of the system, which can accommodate three video channels, three 1-megabit digital channels, and three 1-MHz audio channels, each of which can accept up to 120 individual voice inputs, is given in Figure 1. Means

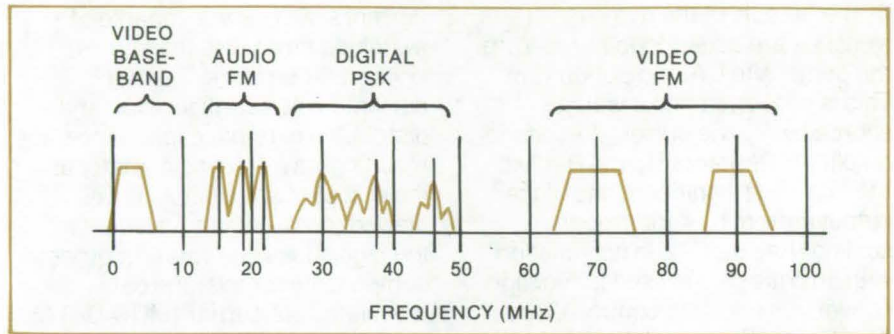


Figure 2. The **Multiplex Frequency Spectrum** accommodates nine data channels. The arrangement is not unique, and other blocking patterns have been utilized.

for blocking each of the nine channels into particular frequency ranges are provided, as indicated in Figure 2. One video channel occupies the 0- to 6-MHz baseband, while the other two are blocked into upper 6-MHz frequency bands centered at 70 and 90 MHz, using FM subcarrier oscillators (SCO). The digital data input signals are fed into phase-shift-keyed (PSK) subcarrier oscillators and are established into bands centered at 30, 38, and 50 MHz. The audio signals, which could also be analog data inputs with bandwidths that do not exceed the audio range, are blocked into three bands at 14, 18, and 22 MHz, using additional FM subcarrier oscillators.

Each of the three signal groups is input to intermediate mixer stages to form composite video, digital, and audio signals. These are fed to a master mixer that produces a final electrical signal to drive the helium-neon laser source. The laser output is transmitted over the fiber-optic cable, which is 1,000 feet (305 m) long in the prototype, and is converted back into an electrical signal at the receiver. This signal is fed

through master and subgroup demultiplexers to be reestablished into the nine original signal channels.

Two optical patchboards, as shown along the optical fiber in Figure 1, allow additional channel transmitters and receivers to be incorporated into the system, with the capability of selectively coupling these to one another. One or more of these could be devoted to wide-band analog data channels.

Additional work has been carried out to perfect single-fiber and multiple-fiber splicing techniques for use with the optical patchboard. Successful couplings for single-fiber splices have been developed that exhibit losses less than 1 dB.

This work was done by Charles H. Bell of Kennedy Space Center. For further information, Circle 10 on the TSP Request Card.

This invention is owned by NASA, and a patent application has been filed. Inquiries concerning nonexclusive or exclusive license for its commercial development should be addressed to the Patent Counsel, Kennedy Space Center [see page A8]. Refer to KSC-11047.

Advanced General-Purpose Computer

A low-power, 32K computer based on CMOS/SOS technology

Marshall Space Flight Center, Alabama

The latest member of the Space Ultrareliable Modular Computer (SUMC) family — SUMC-III-C — uses custom-designed complementary metal-oxide semiconductor/silicon-on-sapphire (CMOS/SOS) LSI arrays with critical computer paths packaged on thick-film hybrids. (Another version of SUMC-III-C, SUMC-III-B, uses standard CMOS manufacturing technology and is compatible with standard CMOS integrated circuits.)

In SUMC-III-C (see Figure 1), between 300 to 600 logic gates are provided per array with a typical stage delay of 3 to 5 ns. The computer is fully S/360-compatible at the user level and includes virtual memory. The CPU organization is based upon a multiplexed 32-bit data path, including floating-point hardware implemented with 8-bit building blocks. The flight unit dissipates less than 55 W (including power supply inefficiencies) for the CPU, the I/O processor, and for the 16K words of main memory. Typical I/O rate is 1×10^6 bytes/second per channel, with instruction times of $1.6 \mu\text{s}$ memory-to-register-add and $9.0 \mu\text{s}$ memory-to-register-multiply.

A new operating system operates in conjunction with the hardware to support virtual memory, fault-and-error recovery, and concurrent control of multiple real-time and batch applications. The system supports HAL/SM, FORTRAN IV, GOAL, and the S/360 assembler/user interfaces. Since the system is fully compatible with the S/360, considerable support software is available; program development and debugging on commercial computers aids in lowering system development costs.

The computer system (see Figure 1) employs two levels of address translation: one in the CPU, the other in each of the independent main memory unit (MMU) modules

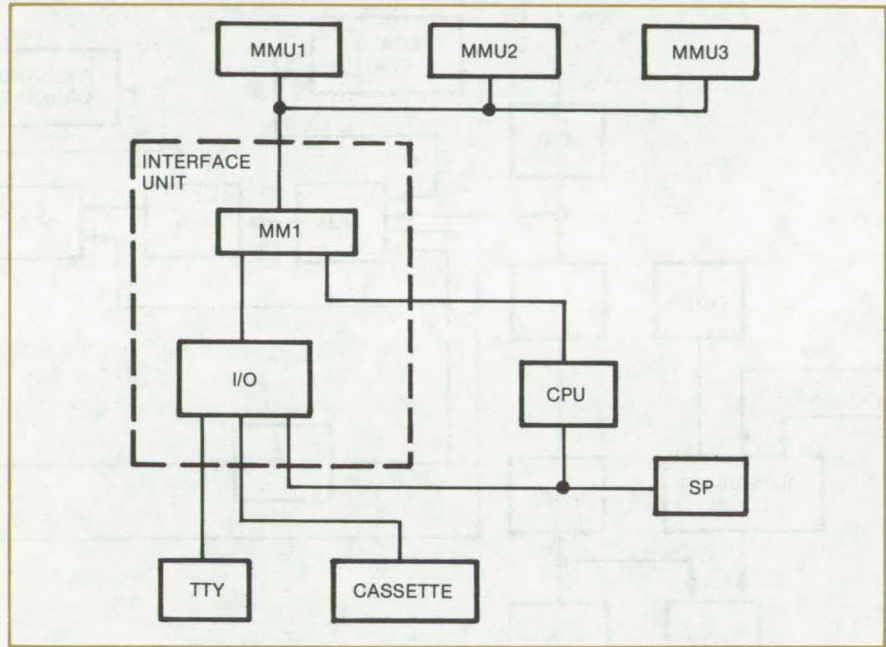


Figure 1. **SUMC-III-C** utilizes 74 custom CMOS LSI arrays with some commercial components. It is compatible with S/360 instructions and can execute an ADD (RR) instruction in $1.5 \mu\text{s}$. Both nonprivileged instructions and privileged instructions relating to I/O and system operations are executed. The 32-bit computer is comprised of three independent main memory units (MMU1 through MMU3) and a parallel I/O capability that is microprogramed. The parallel I/O provides a direct memory address capability. The CPU data path contains four substrates of two types: Each measures 4.2 by 1.8 in. (10.6 by 4.6 cm) and contains 11 CMOS/SOS custom arrays.

(of which there are three). Translation in the memory unit is performed in groups of 256 words by a content-addressable memory (CAM). The CAM can be loaded via the operating system and thus is used to perform memory management within the physical memory units. It can be used either to manage around a failure in the MMU or to reallocate address space to physical memory.

Main address translation for the virtual memory operation is performed by a CAM within the CPU. This CAM is also loaded and unloaded under operating-system control. Translation is performed on

pages variable in size from 1,024 to 4,096 bytes per page. In addition to the actual address translation, two usage checks are performed by the hardware: a check of the type of memory access (read, write, and execute) and memory interrupt, if access type is attempted that is not allowed for that page. A ring number check is also made on the degree of privilege needed to operate from that section of address space. The ring number indicates the level of privilege.

The central processor organization (see Figure 2) is based on a multiplexed 32-bit data path controlled with a microcode control

(continued on next page)

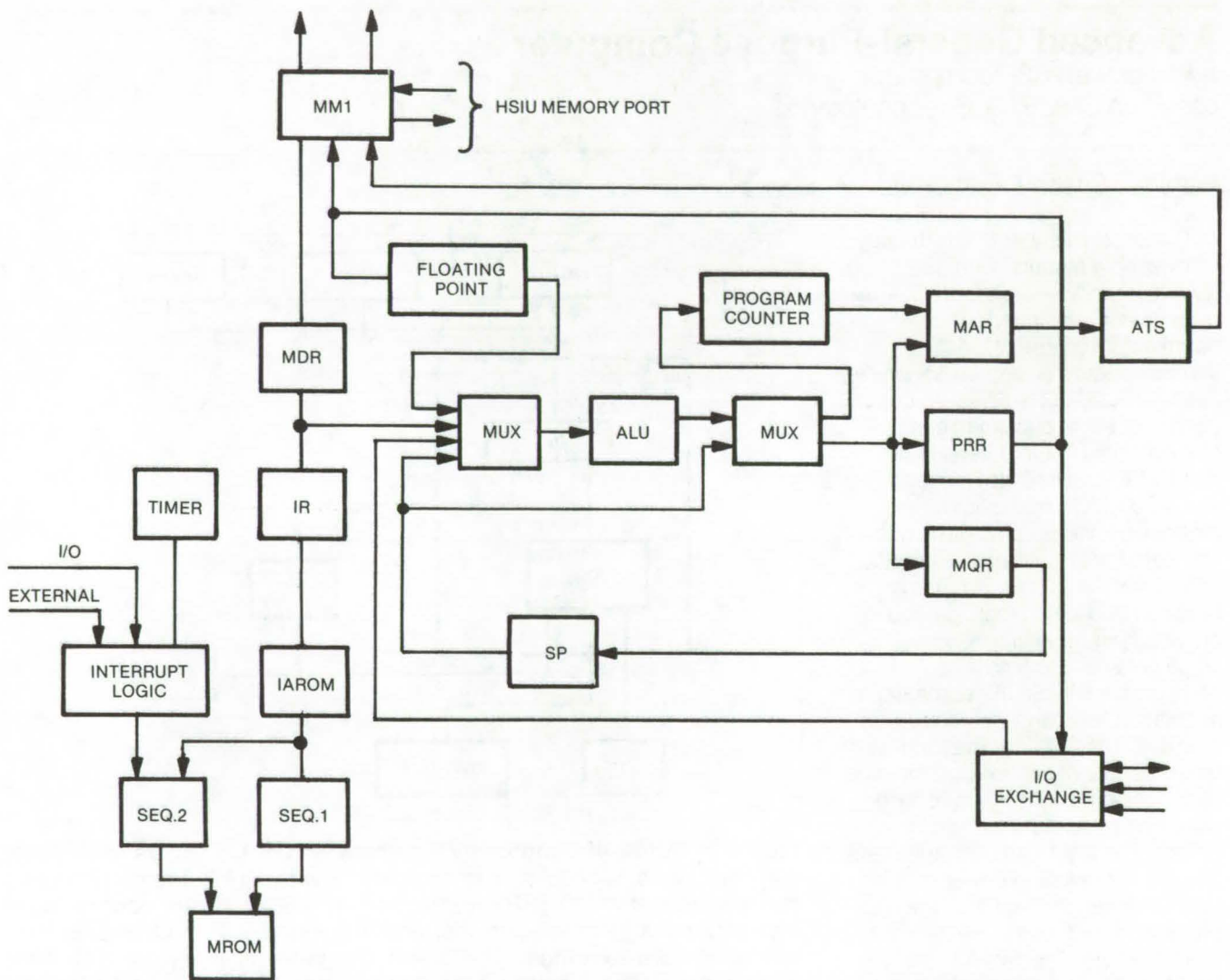


Figure 2. A **Block Diagram of the SUMC-III-C CPU**, showing how the computer is controlled via a two-level microprocessor: One read-only memory, the IAROM, is accessed with each new instruction to generate a starting address for the main microcode routine and to indicate conditions at the instruction level. The second-level microcode control (MROM) contains the sequence of microcode steps required to implement the macro instruction.

section. Floating-point arithmetic hardware is included. The computer is controlled via a two-level microprogram control. One read-only memory, the IAROM, is accessed with each new instruction to generate a starting address for the main microcode routine and to indicate conditions at the instruction level. The second-level microcode control, the MROM, contains the

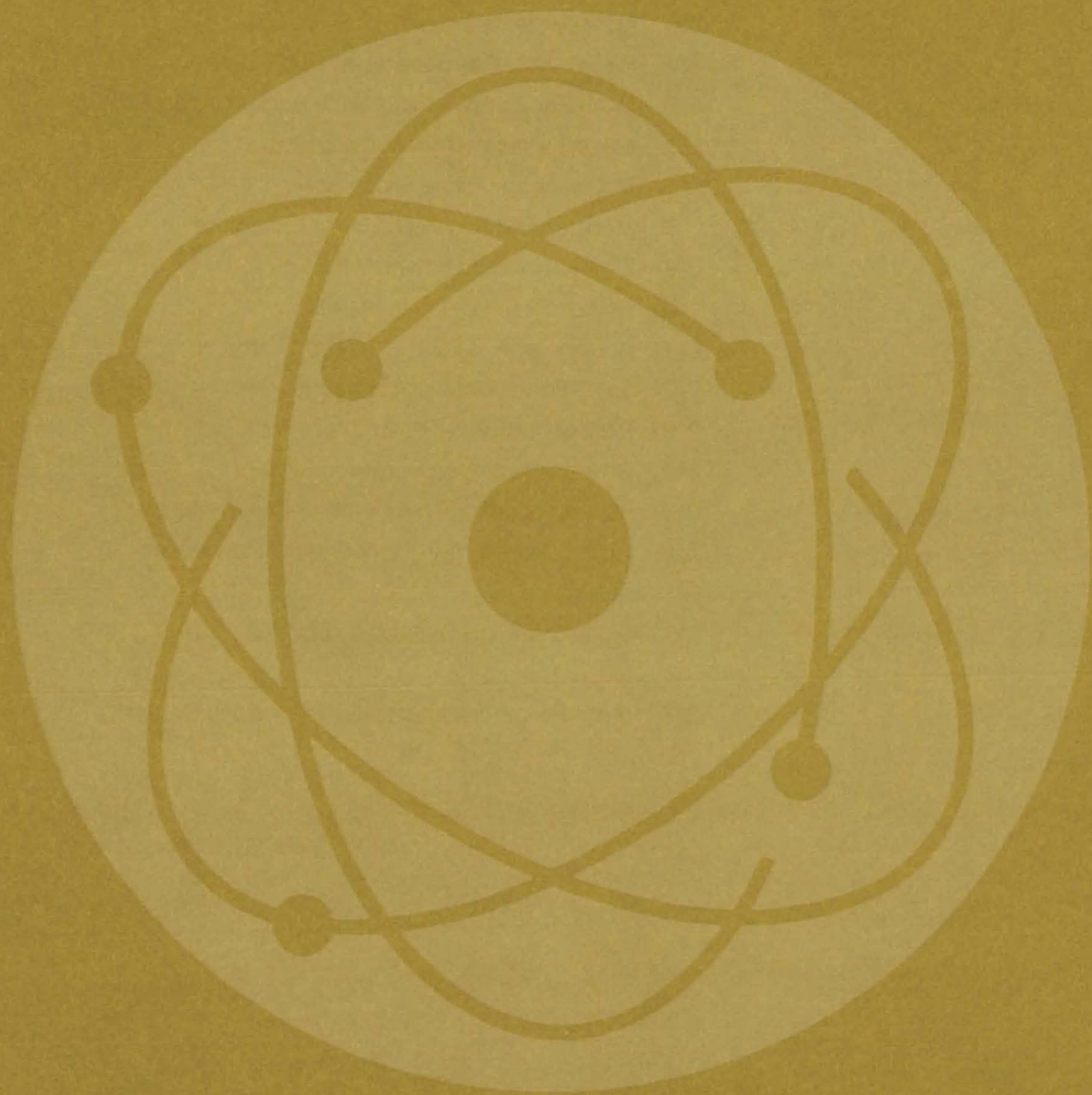
sequences of microcode steps required to implement the macro instruction.

The high-speed interface unit (HSIU) contains from one to seven independent channels. The total aggregate I/O rate for the HSIU is 4×10^6 bytes/second. Channel types are compatible with the S/360 selector channel capable of 10^6 byte/second throughput, the S/360 multiplexer channel capable of 250K

byte/second throughput, and a data bus controller with 1.6×10^6 byte/second throughput.

This work was done by W. A. Clapp, A. F. Cornish, R. B. Gordon, T. J. Lombardi, A. S. Merriam, C. L. Saxe, A. M. Smith, C. Strasberg, and D. R. Tryon of RCA Corp. for Marshall Space Flight Center. For further information, Circle 11 on the TSP Request Card. MFS-23531

Physical Sciences



Hardware, Techniques, and Processes

- 199 Low-Temperature Coal Desulfurization
- 200 Carbon-Chlorine-Carbon Sewage Treatment
- 201 Density Measurements of Trace Gases
- 202 Radioactive-Gas Separation Technique
- 203 Mass Spectrometer Has Wide Angular Acceptance
- 204 Mass Spectrometry Chemi-ionization
- 206 Multispectral Image Processor
- 207 Modular Test System for Solar Collectors
- 208 Electromagnetic Power Absorber
- 210 Hollow-Fiber H₂/O₂ Fuel Cell
- 211 Active-Cavity Radiometer/Pyrheliometer
- 212 Solar-Power Mountain Concept
- 213 Inexpensive High-Temperature Solar Collector
- 214 Alinement Tolerant Schlieren System
- 215 Superconducting Thermometer for Cryogenics
- 216 High-Pressure High-Temperature Transducer

Books and Reports

- 217 Solar-Cell Array Design Handbook

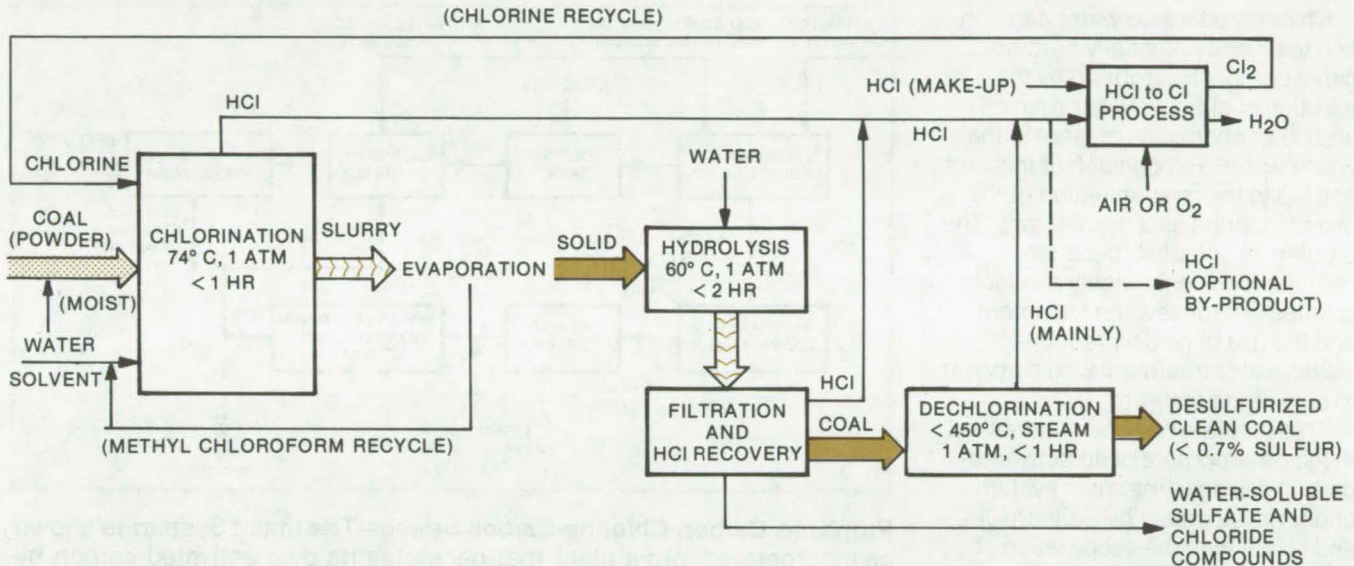
Computer Programs

- 218 Earth Resources Interactive Processing System

Low-Temperature Coal Desulfurization

Low-temperature chlorinolysis removes sulfur at a lower cost and higher efficiency.

Caltech/JPL, Pasadena, California



Low-Temperature Chlorinolysis is proposed as an economical method of removing sulfur from raw coal. Powdered coal is chlorinated in a slurry at 74° C. The chlorine converts sulfur in the raw coal, which occurs in pyrites and in organic compounds, to water-soluble sulfates. These are removed by washing. Subsequent steps dry the coal and remove the chlorine. Chlorine and solvents can be recovered for reuse.

Direct combustion of coal in coal-fired boilers has been limited in recent years, primarily because of the resultant SO₂ and particulate pollutants. Conventional gasification, liquefaction, and flue gas desulfurization for sulfur removal are expected to be costly, not very effective, and sometimes have sludge disposal problems.

In a proposed process, the low-temperature chlorinolysis of coal in an organic solvent would be used to remove both inorganic and organic sulfurs from coal. Chlorine is bubbled through a slurry of powdered moist coal in a solvent such as methyl chloroform for about 1 hour. The chlorinated slurry is filtered, and the remaining coal particles are leached with water for 1 to 2 hours to remove the sulfate compounds converted from the chlorinolysis of organic and pyritic sulfurs.

The coal is then placed in a dechlorinator where it is baked at approximately 300° to 500° C for

less than 1 hour. The organic solvent is recovered and recycled through low-temperature evaporation, and the sulfuric acid leached out in the filtrate of the hydrolysis washing step is also recovered from distillation.

Laboratory-scale experiments with a high-sulfur bituminous coal (4.77 percent S) have shown that up to 90 percent of the pyritic sulfur, 70 percent of the organic sulfur, and 76 percent of the total sulfur can be removed. In addition, toxic trace metal concentrations have been reduced significantly. The residual chlorine content in processed coal has been demonstrated to be lower through the dechlorination step than the chlorine content in the raw coal (e.g., 0.064 percent in processed coal versus 0.14 percent in the raw coal). Performance and process improvements are expected through further development now underway.

All the chlorine in this coal desulfurization process is recovered as hydrogen chloride, which can be

converted to chlorine for reuse by a commercial process. The overall costs should be relatively low, because the desulfurization occurs at ambient pressure and relatively low temperatures. Chlorinolysis also produces an improved feed stock for direct combustion and gasification, since the final product neither cakes nor swells. Preliminary cost estimates show that the overall cost of desulfurization by this process, taking into account all the costs including capital and operating costs, might be around \$9 to \$10 per ton of coal.

This work was done by Partha S. Ganguli, George R. Gavalas, George C. Hsu, and Sarkis H. Kalfayan of Caltech/JPL. For further information, Circle 12 on the TSP Request Card.

Inquiries concerning rights for the commercial use of this invention should be addressed to the Patent Counsel, NASA Resident Legal Office-JPL [see page A8]. Refer to NPO-13937.

Carbon-Chlorine-Carbon Sewage Treatment

Activated-carbon treatment following chlorination reduces concentration of potentially-dangerous chlorine derivatives.

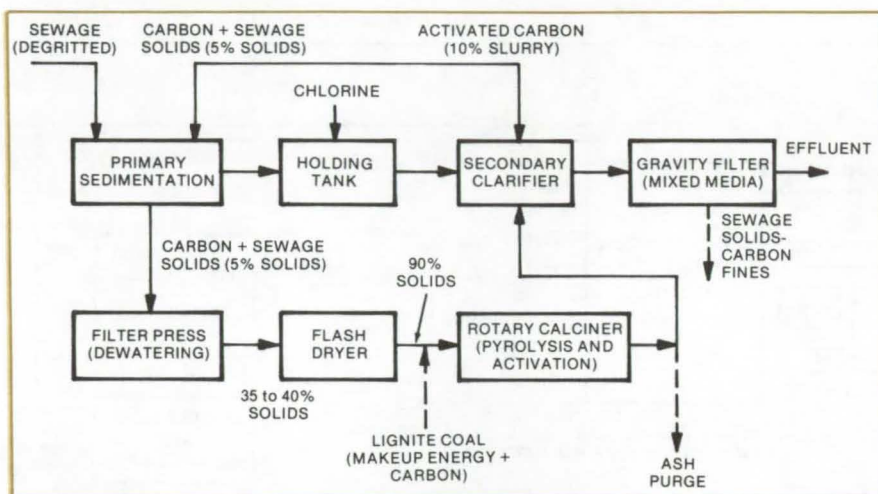
Caltech/JPL, Pasadena, California

Chlorinated waste water can contain toxic and potentially carcinogenic compounds formed by the reaction of chlorine with organics and other chemicals present in the waste water. Recognition of this fact has led to the reexamination of the use of chlorine as a disinfectant. The problem is complex, because chlorine is the only widely available disinfectant for sewage treatment, and the use of no disinfectant in waste-water treatment would appear to be a step backward.

This problem has been addressed in the development of an activated-carbon sewage-treatment system under development by Caltech/JPL and NASA with the cooperation of Orange County, California. The basic approach of NASA's treatment plan is to generate activated carbon at the treatment site to reduce the costs of operation (see "Less-Costly Activated Carbon for Sewage Treatment," NPO-13877, NASA Tech Briefs, Winter 1976, Vol. 1, No. 4, p. 573, for a description of this concept).

It has been suggested that the amount of chlorine and chlorinated compounds discharged from sewage plants can be reduced by incorporating chlorination intermediate to two separate treatments with activated carbon. The first activated-carbon treatment will remove much of the waste that might have otherwise been chlorinated, and the final activated-carbon treatment will remove most of the chlorinated compounds and residual chlorine.

Although somewhat similar approaches have been discussed in the past, they have not, for various reasons, been vigorously pursued. To determine the efficacy of this approach, laboratory studies have been conducted on the ability of



Proposed **Carbon-Chlorine-Carbon Sewage-Treatment System** is shown as incorporated into a plant that generates its own activated carbon by processing sewage solids. Carbon contact in the primary sedimentation basin removes a large amount of the contaminants; chlorination in the next step would require a residence time of 20 to 30 minutes. The second carbon treatment in the secondary clarifier would reduce the level of organics and destroy residual chlorine.

treatment with chlorine and activated carbon to remove potentially hazardous compounds, such as phenols, aliphatic amines, aromatic amines, and polychlorinated biphenyls. Further experiments were conducted using the final effluent from a waste-water plant in Orange County. These experiments showed that the proposed combined carbon-chlorination-carbon scheme could effectively disinfect the water while producing a final effluent low in chlorine and chlorine derivatives.

An important finding was that the conventional chlorination step greatly increases the concentration of the potentially-hazardous chlorinated substances, but this concentration is reduced if the chlorination is preceded by a first activated-carbon treatment. The final treatment with activated carbon then reduces chlorinated substances to a

level comparable with or lower than the original effluent. Furthermore, it removes any residual chlorine to prevent later formation of additional chlorinated organics.

The proposed scheme, as shown in the illustration, has an additional advantage. Activated carbon alone is not effective in removing ammonia from water. However, if sufficient chlorine is present, the ammonia is converted to chloramines, which are removed effectively by the subsequent activated-carbon treatment.

This work was done by Richard H. Green, Rebekah G. Howland, and Carl J. Wallace of Caltech/JPL. For further information, Circle 13 on the TSP Request Card.

Inquiries concerning rights for the commercial use of this invention should be addressed to the Patent Counsel, NASA Resident Legal Office-JPL [see page A8]. Refer to NPO-13972.

Density Measurements of Trace Gases

Nondispersive IR absorption apparatus uses feedback nulling to measure weak signals.

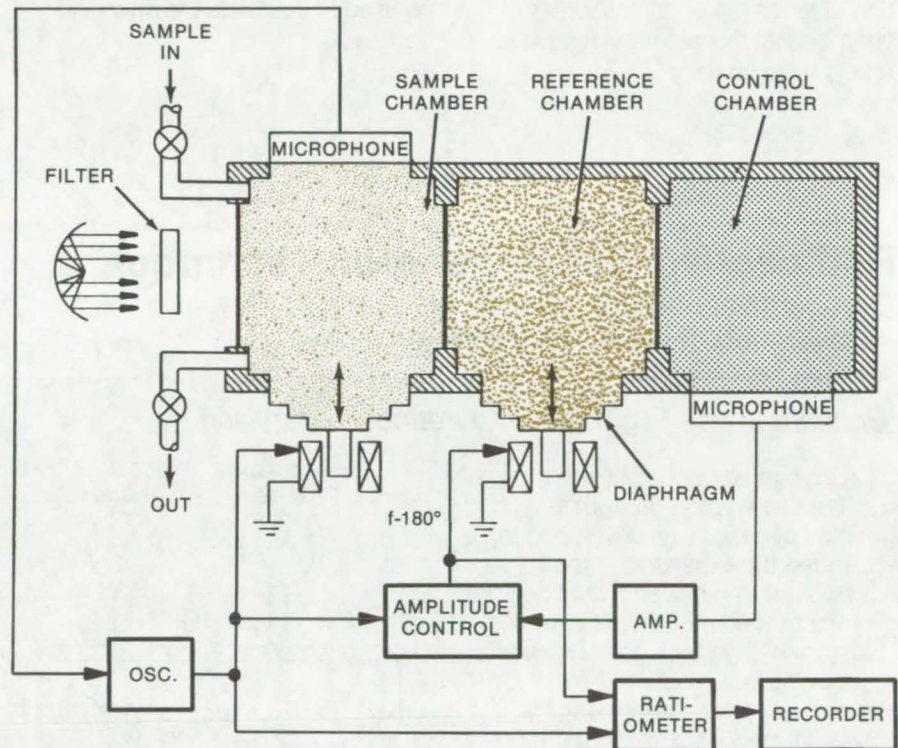
Ames Research Center, Moffett Field, California

The density, and thus the concentration, of trace components in a gas mixture can be measured using the nondispersive infrared absorption analyzer shown in the figure. This device accurately measures the absorption of radiation by a specific gas of interest, even though the gas is present only in a small amount and the absorption is weak.

In principle, the amount of absorption (peak amplitudes) by the gas being measured is made to vary by varying its pressure periodically. At the same time, another volume of gas, with a known amount of the gas of interest, absorbs radiation from the same source. This reference gas is subjected to controlled pressure variations at the same frequency as the test gas but out of phase 180° . When the absorptions, in the two chambers are made to "cancel" each other, the ratio of the densities of the particular gas in the two chambers is equal to the ratio of the relative pressure variations in the two chambers. The pressure ratio is monitored electronically, and the unknown gas density may be calculated readily.

The IR illumination is from a relatively broadband source that is filtered to transmit only frequencies absorbed uniquely by the gas of interest. This light is directed through three chambers:

- A sample chamber with an unknown quantity of the measured gas,
- A reference chamber with a known quantity of the measured gas, and
- A control chamber with an acoustical resonance frequency equal to the frequency used to modulate the pressure in the sample chamber.



A **Nondispersive IR Absorption Analyzer** measures trace amounts of a known component of a gas in a continuous-flow application or in measured batches. Pressure variations in a sample chamber and a reference chamber are 180° out of phase, producing out-of-phase variations in absorption-peak magnitudes. When these "cancel" as determined in a control chamber, the unknown density may be calculated from the ratio of the pressure-control signals. In another version, the intensity of the radiation source is varied to null the sample absorption, rather than using a reference chamber.

Pressures are monitored by microphones, and they are varied by solenoids that electromagnetically drive diaphragms in the chamber walls.

When the measurement begins, absorption occurs in the sample and reference chambers at a time-varying intensity; the frequency f_r is controlled by an oscillator. This dynamic component is amplified by resonance in the control chamber. A pressure-variation signal from the

control chamber (at the frequency f_r) is phase-reversed in an amplifier and is fed to an amplitude-control circuit. The product of the oscillator signal and the amplifier-chamber signal drives the solenoid in the reference chamber 180° out of phase with the solenoid connected to the sample chamber.

In this way, absorption peaks will occur in the reference chamber at the same instant absorption valleys occur in the sample chamber. This

tends to even out variations in absorption and thus eliminate variations in the radiation intensity received in the third chamber. A feedback-control system can be used so that the signal applied to the reference-chamber solenoid is just enough to cause a steady illumination to reach the amplification chamber. At this point the following relationship holds:

$$e_s = \frac{V_s}{V_r} e_r$$

where e_s and e_r are densities of the measured gas component in the sample and reference chambers and where V_s and V_r are the driving signals applied to the two solenoids ($\Delta P_x/P_x$ is proportional to V_x for each chamber). The ratio V_s/V_r is monitored by a ratiometer and can be used to calculate the unknown density.

This work was done by John Dimeff of Ames Research Center. For further information, Circle 14 on the TSP Request Card.

This invention has been patented by NASA [U.S. Patent No. 3,953,734]. Inquiries concerning nonexclusive or exclusive license for its commercial development should be addressed to the Patent Counsel, Ames Research Center [see page A8]. Refer to ARC-10760.

Radioactive-Gas Separation Technique

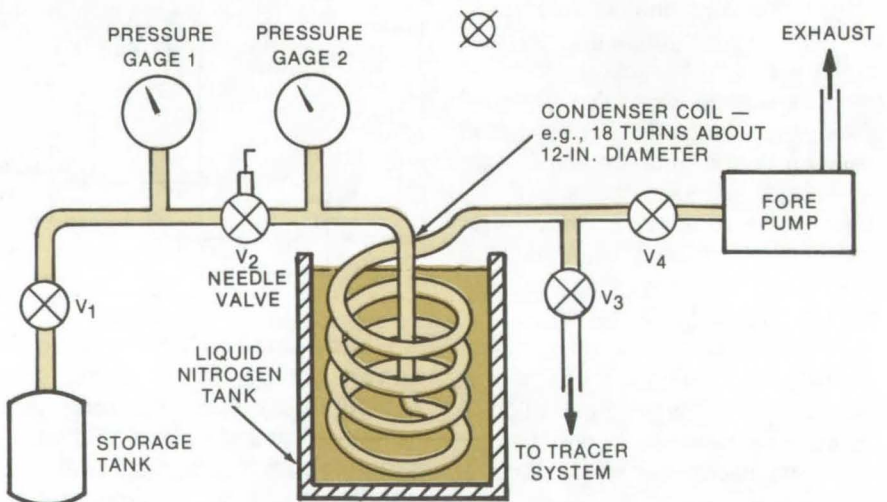
Cryogenic separation technique recovers radioactive gases inexpensively.

Goddard Space Flight Center, Greenbelt, Maryland

A cryogenic method of separating radioactive krypton-85 from a mixture of gases was developed to conserve the expensive krypton when used as a tracer in quality-control procedures. At the same time, recovery of the gas eliminates costly disposal problems. This modification of conventional refrigeration-and-cryogenic gas-separation techniques utilizes the differences in vapor pressures, melting points, and boiling points of components in a gaseous mixture. A series of temperature and pressure variations converts the gases independently to solid and liquid states, so they can be separated by simple means. A readily available cryogen (e.g., LN₂) is used, and no expensive refrigeration equipment is required.

The apparatus (see figure) consists of coiled copper tubing immersed in a container of liquid nitrogen at 77 K. Since krypton-85 has a normal boiling point of 119.8 K, and a melting point of 116.2 K, it freezes on the inner walls of the copper coil. At 77 K, the vapor pressure of krypton-85 is 2 to 3 mm Hg (0.25×10^3 to 0.4×10^3 N/m²).

Nitrogen has a normal boiling point of 77 K and a melting point of 63 K. With liquid nitrogen as the external cryogen, the nitrogen inside the copper tubing remains essen-



The Krypton Recovery Apparatus was developed to recover radioactive krypton from a gas mixture that had become too diluted with air for its intended use as a tracer gas. The diluted gas is kept in a storage tank. As tracer gas is required, the krypton is separated and later mixed with the proper amount of air for use as a tracer.

tially in the gaseous state. Its vapor pressure under these conditions is about 760 mm Hg (101×10^3 N/m²).

Oxygen has a normal boiling point of 90 K and a melting point of 54 K. As it passes through the copper coil, the oxygen gas liquifies. The vapor pressure of oxygen at 77 K is 130 mm Hg (17×10^3 N/m²).

Suitable valves, pressure gages, and adapters connect the external

storage tanks and the tracer-system tank and control the gas pressures and flow through the system. As the gases reach their respective phase-change temperatures and pressures, the valves in the system operate to pump the nitrogen and oxygen to the primary storage tank. The krypton-85 remains frozen to the walls of the condenser coil.

When separation is complete, the liquid nitrogen refrigerant is removed; the krypton in the coils then heats to a gas and is pumped into the tracer-system tank.

This approach can be used to recover other radioactive gases

from gas mixtures. The gas of interest should have a normal boiling point above the temperature of the cryogenic coolant, and its vapor pressure versus temperature curve should be significantly different than the same curves for other gases in the mixture.

This work was done by R. Haney, K. J. King, D. O. Nellis, R. S. Nisson, P. Robling, and W. Womack of **Goddard Space Flight Center**. For further information, Circle 15 on the TSP Request Card. GSC-12019

Mass Spectrometer Has Wide Angular Acceptance

Higher mass resolution is achieved by using an electrostatic analyzer of ac-modulated grids.

Caltech/JPL, Pasadena, California

Improved resolution in an ion mass and velocity spectrometer is achieved by replacing the electrostatic analyzer, used in conventional mass/velocity spectrometers, with a system of planar ac-modulated grids. The grids have a wide angular-acceptance cone, approaching a 90° half angle, and their angular response matches that of a sector magnetic analyzer. This gives focusing for all angles of incidence. Furthermore, the ac-modulation and detection scheme minimizes sensitivity to light and other types of radiation.

The principles of operation can be seen in Figure 1. The instrument consists of an electrostatic analyzer followed by a magnetic analyzer. The electrostatic analysis is performed by using a system of planar grids similar to those used in Faraday-cup plasma instruments. A modulation grid carries a voltage $V_0 \pm \Delta V$, where $\pm \Delta V$ is a square wave of amplitude ΔV . The detectors, D_1 and D_2 , are synchronously demodulated such that the grid-detector system acts as an $m(v_0 \cos \theta_0)^2/q$ filter,

where

m is the ion mass,
 v_0 is its incident velocity,
 θ_0 is its angle of incidence, and
 q is its charge.

The modulation grid and the grounded grids on either side are followed by a grid carrying an accelerating or decelerating potential V_a .

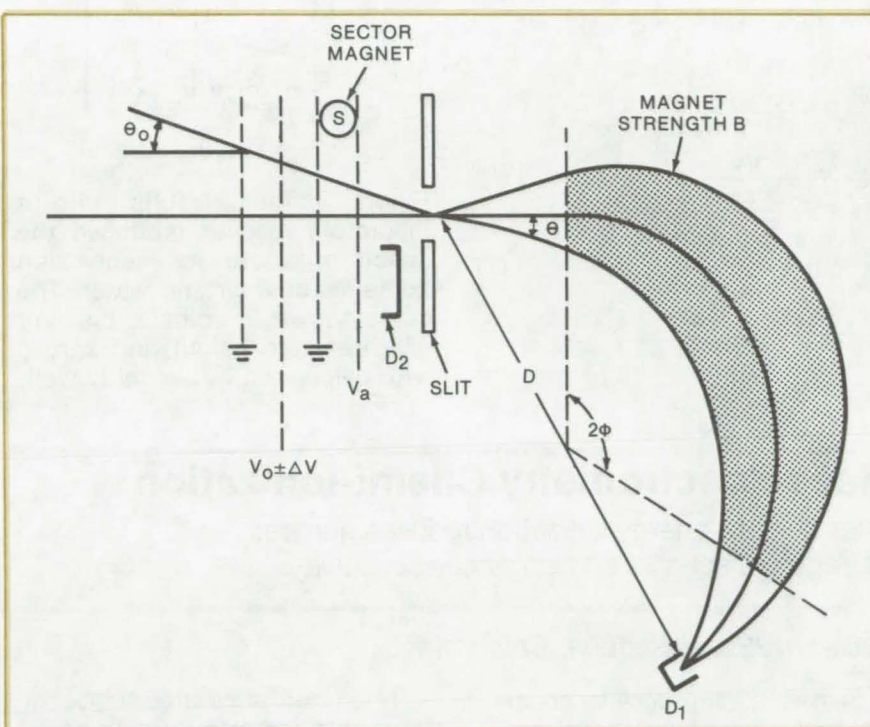


Figure 1. The **AC-Modulated Grid** used in the proposed mass/velocity spectrometer carries a voltage of $V_0 \pm \Delta V$. An additional grid carries an accelerating or decelerating potential of V_a .

This grid is followed by a sector magnet that sorts particles according to $mv \cos \theta/q$, where v and θ refer to the velocity and direction after acceleration or deceleration. The equations that describe this system are

$$\frac{1}{2}mv_0^2 \cos^2 \theta_0 = q(V_0 \pm \Delta V) \quad (1)$$

$$\text{Accelerator Grid:} \quad (2)$$

$$\frac{1}{2}mv^2 \cos^2 \theta = \frac{1}{2}mv_0^2 \cos^2 \theta_0 + qV_a$$

$$\text{Magnet:} \quad (3)$$

$$mv \cos \theta = \frac{1}{2} qBD \sin \phi$$

where

B is the field strength in the magnet gap,

Φ is the half angle of the magnet, and

D is the distance between slits.

Equations (1) through (3) can be combined to yield

$$\frac{m}{q} = \frac{B^2 D^2 \sin^2 \Phi}{8(V_0 + V_a)} \quad (4)$$

$$v_0 \cos \theta_0 = \left(\frac{2V_0}{m/q} \right)^{1/2} \quad (\text{when } \Delta V = 0) \quad (5)$$

$$\epsilon_0 \equiv \frac{1}{2} m v_0^2 \cos^2 \theta_0 = q V_0$$

In the proposed system, B , D , and Φ are fixed; V_0 and V_a are varied to obtain spectra of m/q and $v_0 \cos \theta_0$ or ϵ_0 . The resolution is found by differentiation of equations (4) and (5).

$$\frac{\Delta(m/q)}{m/q} = \frac{2\Delta D}{D} + \frac{\Delta V}{V_0 + V_a} =$$

$$\frac{2\Delta D}{D} + \frac{8m/q}{B^2 D^2 \sin^2 \Phi} \Delta V \quad (6)$$

$$\frac{\Delta \epsilon_0}{\epsilon_0} = \frac{\Delta V}{V_0} \quad (7)$$

ΔD in equation (6) is related to the aperture or slit width s by

$$\Delta D = s \frac{\cos \theta}{\sin(\Phi + \theta)} \quad (8)$$

This spectrometer has a wide acceptance angle, because all ions with the same $v_0 \cos \theta_0$ focus at the same place. Another useful feature is that the mass resolution $\Delta m/q$ can be controlled electronically by varying ΔV , the amplitude of the square wave on the modulation grid.

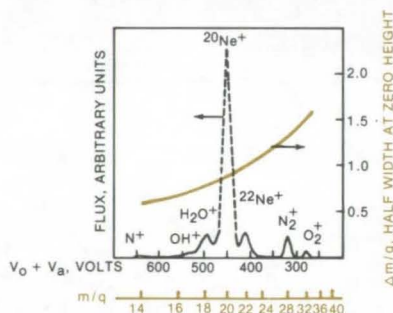


Figure 2. Test Results with a laboratory magnet produced the spectrum above for neon with some residual air and water. The curve shown in color is the half width at zero height and agrees with calculated values fairly well.

This concept for a mass-energy spectrometer has been tested with a laboratory magnet without any attempt to shape the field to reduce edge effects. Figure 2 shows the resulting spectrum of a wide-angle ion beam of neon with some residual air and water. The value of $\Delta m/q$ (= half width at zero height) calculated from equations (6) and (8) is also plotted in Figure 2; it is in reasonable agreement with the observed line widths.

This work was done by Marcia M. Neugebauer of Caltech/JPL. For further information, Circle 16 on the TSP Request Card. NPO-14111

Mass Spectrometry Chemi-ionization

Intermediate-energy ionization reduces number of fragment species and enhances sensitivity.

Caltech/JPL, Pasadena, California

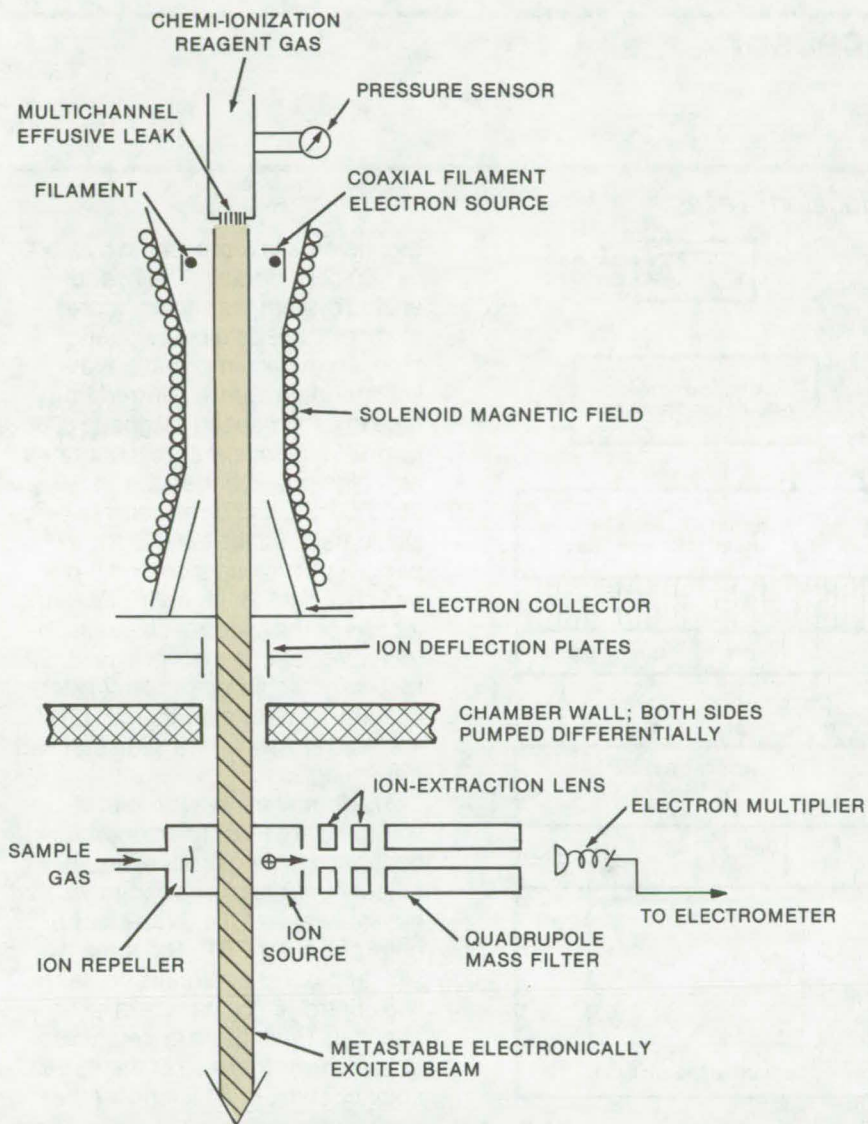
In mass spectroscopy for chemical analysis, the substance to be analyzed is usually fragmented and ionized by electron impact. The mass-to-charge ratios and the relative amounts of the various fragments, along with the energies of the impacting electrons, can be used to determine elemental composition, bond strengths, and other data useful in deducing the chemical compositions of specimens. Electron impact provides sufficient energy to break an analyzed molecule into almost all the possible ion species. Although this is often desirable, it can also be a drawback.

When there are a large number of fragments, the intensity of the peaks for each species will be small. This reduces the sensitivity of the analysis. The low intensity reduces sensitivity, and overlapping of the many peaks complicates interpretation of data. Alternative ionization techniques, photoionization and field ionization, are generally strong enough to produce only the parent molecular ion, sufficient for molecular-weight studies but not for structural or chemical analysis. Chemi-ionization has been discussed as an intermediate-energy source, but the technique has not

generally been reduced to practice for mass spectrometry.

Using the apparatus shown in the figure, chemi-ionization has now been applied successfully to mass spectrometry. This method results in simpler fragmentation and produces larger molecular ion peaks for compounds having stable parent ions. It therefore provides greater sensitivity than electron impact does for samples having lower energy ranges of ionization potentials.

A neutral chemi-ionization reagent feeds through a multi-channel effusive leak into and



The **Chemi-ionization Mass Spectrometer** produces and analyzes only relatively-large ionized fragments of the sample species. This reduces the number of peaks and increases their intensity, thereby increasing the sensitivity of the analysis. Ions of sample material formed are mass filtered and detected by standard methods. The sample to be analyzed is admitted to the mass-spectrometer source either as a gas from a standard vacuum inlet or as a solid sample. Solid samples are placed inside the source and heated to give a suitable vapor pressure. The results of experiments verified that simpler fragmentation patterns can be obtained using low-energy chemi-ionizing agents such as Ar, Kr, or Xe metastables. Structural differences between similar samples can be readily distinguished by this technique.

through an electron source contained in a first chamber. Electrons for bombarding the gas stream are emitted by a heated, coaxial filament supported within a cylindrical magnetic structure through which the gas passes under low pressure. The beam of electrons is magnetically merged and confined by the magnetic field and directed toward the gas stream. The stream emerges from the magnetic structure containing many electronically excited, long-lived (metastable) molecules.

Excess beam electrons are diverted and collected at the end of the magnetic structure, and any ion electrons or Rydberg highly-excited atoms are removed from the gas stream by the ion deflection plates at the outlet of the magnetic structure.

The neutral beam of metastable reagent gas molecules enters a quadrupole ion source in a sample chamber, which is differentially pumped to provide the necessary low-pressure environment. The electronically excited metastables ionize the sample gas in the chamber. The resulting ions are accelerated and focused in the quadrupole mass-spectrometer structure and then detected.

This work was done by James B. Laudenslager of Caltech/JPL. For further information, Circle 17 on the TSP Request Card. NPO-13857



Multispectral Image Processor

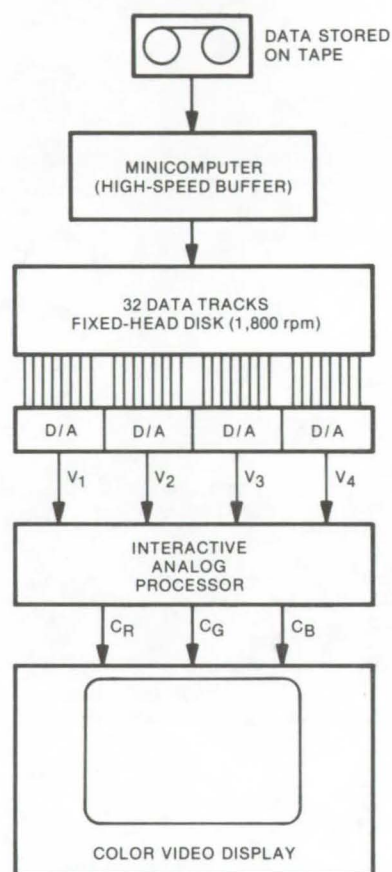
Correlation clustering of
250,000 pixels of data in real time

Lyndon B. Johnson Space Center, Houston, Texas

An interactive color display for multispectral imagery uses correlation clustering digitally to encode raw image data to develop a range of image information. The data, consisting of up to 250,000 pixels, are numerically classified in real time according to various image elements. Algorithmic signal manipulation is used to provide discrete control of individual image parameters. The system operator views a color classification map on a video display in which a given color represents a localized region in the multispectral feature space. Since the location and size of the regions are under operator control, the map can be changed from a broad level of classification to a narrower one at will.

Correlation-clustering techniques based on video data manipulation as presently used for land-use mapping is not, however, a flawless technique. A system that, for instance, uses a conventional three-color video display is severely limited, since each color represents the equivalent of one spectral channel of data. Clustering methods have been developed to overcome the three-channel limitation, but empirical data processing demanded by the methods requires considerable offline computer time. This iterative approach may take several days to produce the ideal color map of a given area.

In the new system, an operator controls a console in which the



The **Multispectral Image Processor** operates upon data supplied by an Earth Resources Technology Satellite (ERTS) in real time. Scanner data represented by an area of up to 500 by 500 pixels are stored on magnetic tape and then are transferred from the tape to a high-speed magnetic disk, using a minicomputer configured as a high-speed buffer. Up to 250,000 bits are stored in a track on the disk; eight parallel tracks store the 8-bit-per-pixel data for an entire TV frame for one of the spectral channels. The disk rotates at 1,800 rpm so that data for one frame are read every 1/30 second.

ground area is represented by a 500 by 500 pixel display. The hybrid analog system, as shown, stores scanner input data on magnetic tape. To extract information, the scanner data are transferred from tape to a high-speed magnetic disk, using a minicomputer that operates as a high-speed buffer. Up to 250,000 bits can be stored in a single track on the disk. Eight parallel tracks can store the 8-bit-per-pixel data for an entire TV frame for one of the spectral channels. If four spectral channels are used, 32 tracks (or 32 bits) representing the spectral signature for a given pixel are read in parallel via 32 fixed-head transducers.

The four channels (or four voltages) are fed into an operator-controlled analog processor. The output consists of three voltages that activate each of the three electron guns of a color CRT. The three similar processor circuits contain two control knobs per spectral channel. Thus, there are eight variable controls for each of the three color circuits, or 24 knobs for the analog processor.

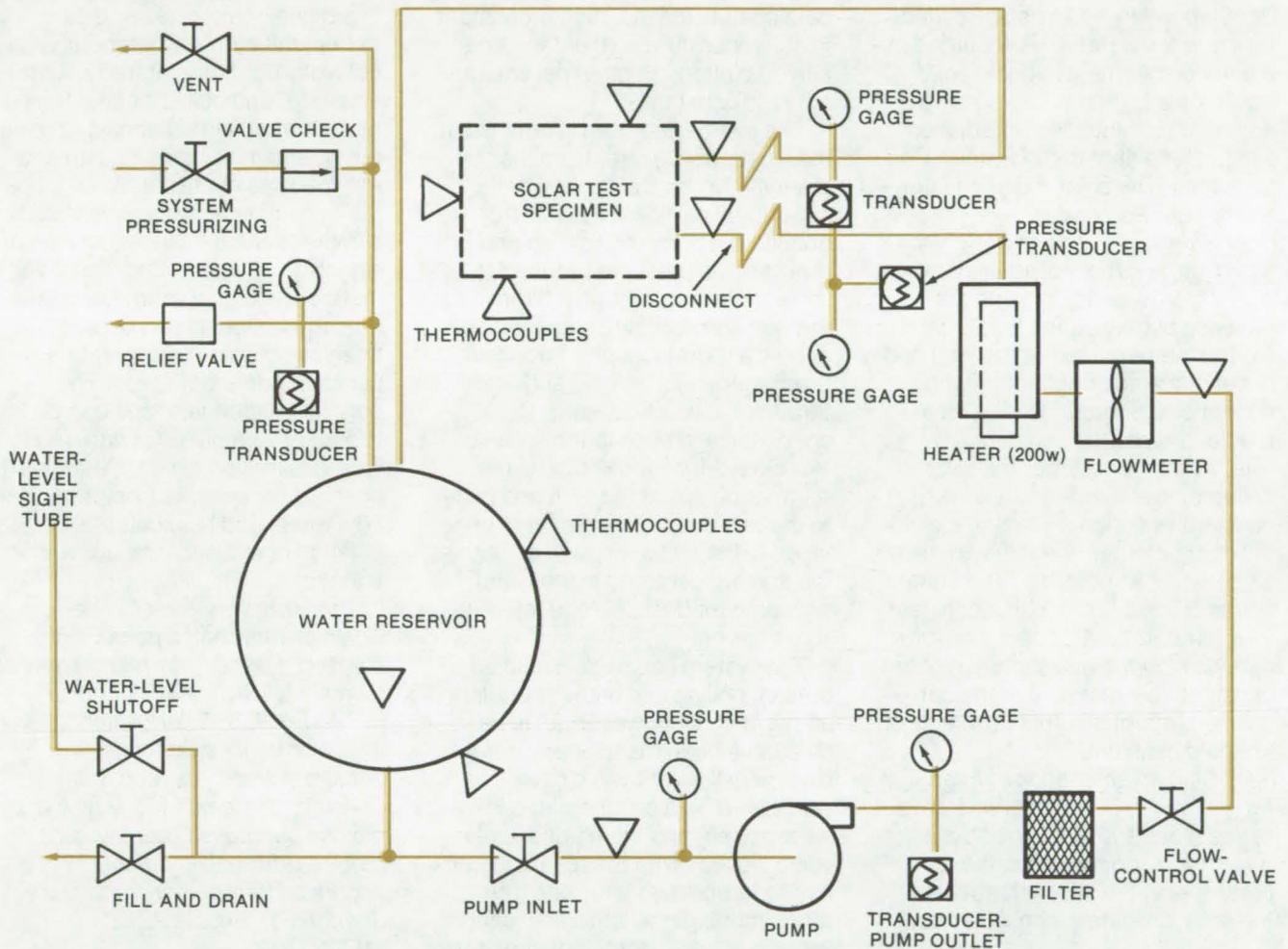
This work was done by Richard E. Haskell of Oakland University for Johnson Space Center. For further information, Circle 18 on the TSP Request Card.

Inquiries concerning rights for the commercial use of this invention should be addressed to the Patent Counsel, Johnson Space Center [see page A8]. Refer to MSC-16253.

Modular Test System for Solar Collectors

Test system has been used to evaluate coatings, substrates, and collectors.

Marshall Space Flight Center, Alabama



The **Solar-Collector Test System** shown above can be used with a solar simulator or Sunlight. When used with a simulator and data-acquisition and reduction systems, it is particularly useful for testing scaled-down systems.

A portable, recirculating-water-flow, and temperature-control device has been used with both a solar simulator and actual Sunlight to test and evaluate several solar-collector panel coatings, panel designs, and scaled-down collector subsystems. Tests were performed on two different sizes of vacuum-insulated solar collectors, including two different substrate materials and five different coating-and-substrate combinations. Tests were also

performed on nine different coating-and-panel designs utilizing an insulated-box (flat-plate) solar collector.

Tests were made primarily with a solar simulator; however, the larger of the two vacuum-insulated collectors and one of the insulated-box configurations were tested outside in direct Sunlight. In addition to tests in direct Sunlight, other tests were made to study the effect of vacuum insulation on stagnation temperature

and heat gain, the effects of flow rate and inlet temperature on heat gain, and the effect of reflectors on heat gain.

The test program is not complete, and additional tests are planned; but based on the data now available, it appears that an insulated-box (flat-plate) collector with an inexpensive nonselective coating would be satisfactory for residential and commercial space-heating and service hot-water systems. Test

data also indicate that optimized units with concentrating reflectors should permit operating temperatures high enough for use in absorption air-conditioning systems.

The test system was designed to make the following types of tests, with variations.

Dry Stagnation — The solar-collector-plate temperature is recorded as a function of time, while the solar-collector subsystem is exposed to actual or simulated solar radiation, without a coolant in the water passages. The solar radiation intensity is also recorded.

Heat Gain as a Function of Coolant Flow Rate — The individual data points from a series of tests are obtained by measuring and recording the temperatures at the inlet and outlet of the solar collector, with water flowing through it at a measured and recorded constant flow rate. At the same time, the solar collector is subjected to a known constant radiation. For each individual data point, all variables are held as constant as possible. The entire series of tests is run with a constant inlet temperature. Each successive data point is run at a slightly-higher constant flow rate so that the curve can be plotted; all other parameters are held constant.

Heat Gain as a Function of Inlet Temperature — Data points from a series of tests are obtained by measuring and recording the temperatures at the inlet and outlet of the solar collector, with water flow-

ing through it at a measured and recorded constant flow rate, and while the solar collector is subjected to a known constant radiation. For each individual data point, all variables (flow rate, inlet temperature, and solar intensity) are held as constant as possible. Each successive data point is run at a higher constant inlet temperature so that the curve can be plotted; all other parameters are held constant.

The test device used is outlined in the illustration. Water from the reservoir floods the suction of the centrifugal pump via the force of gravity; the pump picks it up and provides the pressure required to force the water through a filter, through a waterflow control valve, across a thermocouple, through a flowmeter and a heater, and then through the solar-collector test specimen and back to the reservoir in a closed-loop fashion. The two thermocouples at the inlet and outlet to the test collector are placed as close to the test specimen as possible and are centered in the water-flow path for best average temperature sensing.

The system can be pressurized to prevent boiling and allow operation above 100° C; however, all tests to date have been made unpressurized, with the vent valve open, the water level shut off, the pump inlet valves open, and the fill-and-drain valve closed. With the reservoir one-half to three-fourths full and the pump running, the waterflow control valve is adjusted for the desired flow

rate while observing the output of the water flowmeter as displayed on a digital counter.

The heater is used to control the water temperature at the inlet to the test collector. The solar simulator output is set, utilizing the pyrheliometer and a digital multimeter. The digital multimeter is used to read the pyrheliometer output in millivolts dc. Solar intensity, water-flow rate, and collector inlet temperature are monitored almost continuously, and minor trim adjustments are made as necessary.

A digital data-acquisition system samples sensor channels and feeds signals to an integrating digital voltmeter. The digital voltmeter measures these signals and causes a teletype machine to generate a punched paper data tape. The punched paper data tape can be fed to a small computer for data reduction, conversion of voltage signals to physical parameters (temperatures, flow rates, and heat gain), and calculation of statistical means and variations.

*This work was done by Fred J. Dolan of **Marshall Space Flight Center**. Further information may be found in NASA TM-X-73355 [N77-15489], "A Performance Evaluation of Various Coatings, Substrate Materials, and Solar Collector Systems" [\$5.00]. A copy may be purchased [prepayment required] from the National Technical Information Service, Springfield, Virginia 22151. MFS-23701*

Electromagnetic Power Absorber

Ridged tile is useful in high-power applications and serves as a blackbody radiometric standard.

Caltech/JPL, Pasadena, California

A new electromagnetic power absorber has a reflection coefficient of the order of a few tenths of a percent and is designed to maintain an isothermal temperature distribution in high-power microwave and laser applications. The composite, iron-filled, epoxy-and-aluminum

structure functions over a broad temperature range and has been utilized in satellite packages as a blackbody radiometric standard. The absorber is fabricated in tile modules that allow the assembly of compact and economical custom-design configurations.

The basic unit, as shown in Figure 1, is a 4- by 4-in. (10- by 10-cm) tile, formed by molding an iron-filled epoxy material in parallel ridges on an aluminum base. Aluminum fins extend into the epoxy and provide the required thermal conductivity to smooth out temperature gradients

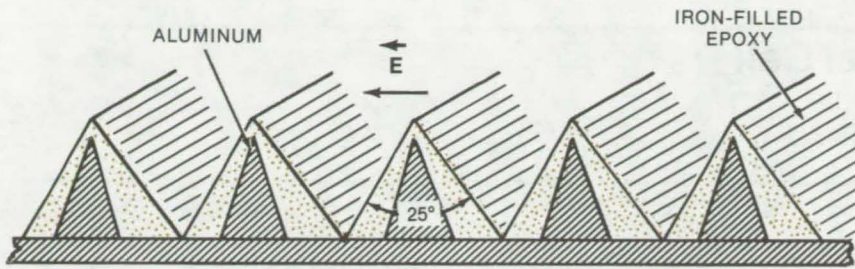


Figure 1. **Parallel Iron-Filled Epoxy Ridges** provide effective power absorption for radiation polarized in the direction of the electric field vector shown.

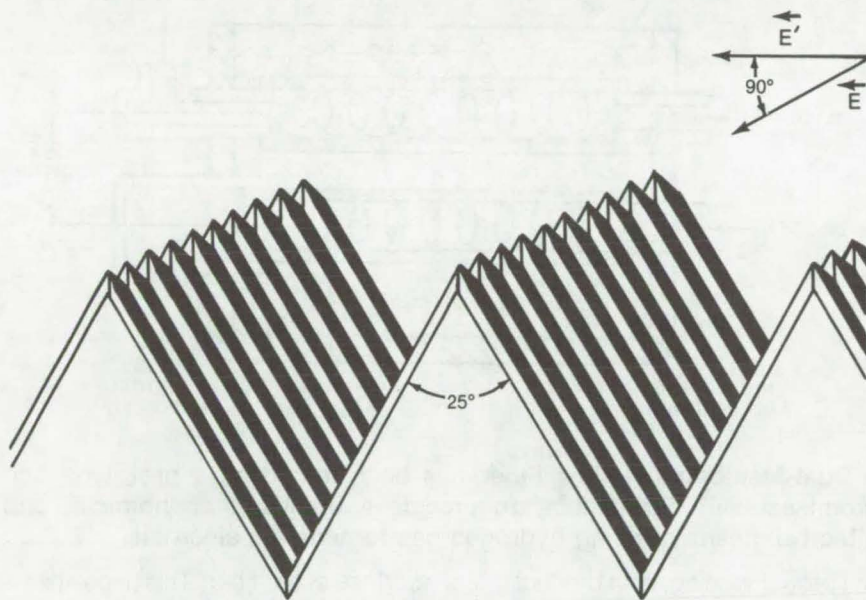


Figure 2. The **Array of Adjacent Absorber Tiles** absorbs both polarizations. The greater depth of this arrangement extends its operating range to longer wavelengths.

and to effect heat transfer between the absorber and a supporting heat sink.

Electromagnetic absorption occurs through two frequency-independent processes. First, there is an accumulation of absorption as a result of repeated scatterings

between adjacent wedges; and second, the wedge angle of 25° is chosen so that normally incident radiation satisfies Brewster's criterion for zero reflection. Brewster's law specifies that radiation polarized in the plane of incidence will be totally transmitted

without reflection at a dielectric interface provided the radiation is incident at an angle i , satisfying $\tan(i) = n$, where n is the index of refraction of the dielectric.

A multiple arrangement of adjacent tiles, oriented to form a wedge array as in Figure 2, may be used in setups that require both polarizations to be absorbed. Each individual slab absorbs one polarization as before, and the larger ridged structure, at the same wedge angle, is effective in absorbing the orthogonal component. In another application, a combination of tiles, shaped and assembled to form either a conical or a pyramidlike structure, provides a compact absorber, or blackbody radiator, which can be used in tight spaces.

An accurate microwave blackbody reference for radiometric calibrations over the temperature range 77 to 370 K has been built by coupling absorber tiles to a proportional gas-temperature controller in contact with the aluminum base. In addition, a cold reference standard at 77 K has been constructed with tiles immersed in a liquid nitrogen bath.

The absorber has been adapted for laboratory and field use by casting a styrofoam layer between the wedges and across the tile face. In this way, the epoxy surface is insulated against environmental changes and is not subject to convective heat loss. This technique also prevents the accumulation of moisture and serves as an effective infrared radiation shield.

This work was done by Richard Iwasaki of Caltech/JPL. For further information, Circle 19 on the TSP Request Card.

*Title to this invention has been waived under the provisions of the National Aeronautics and Space Act [42 U.S.C. 2457(f)], to the California Institute of Technology, Pasadena, California.
NPO-13830.*



Hollow-Fiber H₂/O₂ Fuel Cell

Dual-membrane hollow-fiber electrode increases reliability and reduces costs.

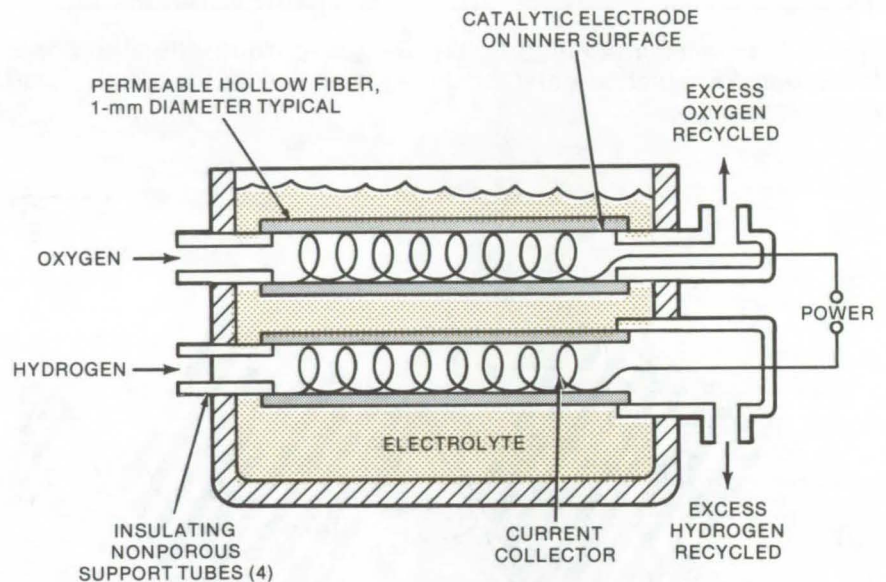
Caltech/JPL, Pasadena, California

Hydrogen/oxygen fuel cells use extremely complex flat-stack arrangements of membranes, gas-kets, channels, electrodes, and current collectors. They are difficult to fabricate and, in the case of solid-polymer electrolytes, are subject to catastrophic failure of the total system if there is one pinhole leak in the membrane between the oxygen and hydrogen sides.

Improved reliability and lowered costs could be achieved using a hollow-fiber electrode as shown in the illustration. A pair of hollow fibers are made from an ion-exchange material in the hydrogen-ion (H⁺) form (or of a hydrophilic permeable membrane material) and are immersed in an acid/water electrolyte. Each fiber contains a catalytic electrode deposited on its inner surface. A fuel such as hydrogen flows through one tube, and an oxidizer such as air flows through the other.

Because of the hollow-fiber configuration, a large electrode area can be obtained for a given cell volume. Since the fuel and oxidizer in each fiber are in intimate contact with the electrode-electrolyte interface and the electrolyte has a low internal resistance, high power densities can be obtained. Furthermore, a fuel cell of this type can be constructed relatively inexpensively because of the ease of fabrication of the hollow-fiber configuration compared with a flat membrane.

Leakage of fuel or oxidizer through the fiber does not result in a failure, as is the case for single-membrane solid-polymer-electrolyte



A Dual-Membrane Hollow Fiber has been tested as a prototype and promises, with refinement, to provide a practical, economical, and effective means of using hydrogen gas to generate electricity.

fuel cells. Flooding, with product water, cannot take place because the water that is formed migrates into the electrolyte where it can be easily removed by evaporation or distillation. Since the fiber is always exposed to electrolyte, the problems of drying and consequent failure are eliminated. Thermal control of the cell is simplified. By use of a reference electrode, the potential between it and each current collector can be monitored and cell performance maximized.

To prepare the fiber electrode, a current collector in the shape of a nonreactive wire spiral is inserted into the fiber. It is placed into the fuel cell, and a platinum catalyst is deposited electrically on the inner

surface of the fiber. This deposit is the electrode of the cell. A suitable electrolyte, such as a dilute aqueous solution of sulfuric acid or any other highly ionized acid, is added to the cell.

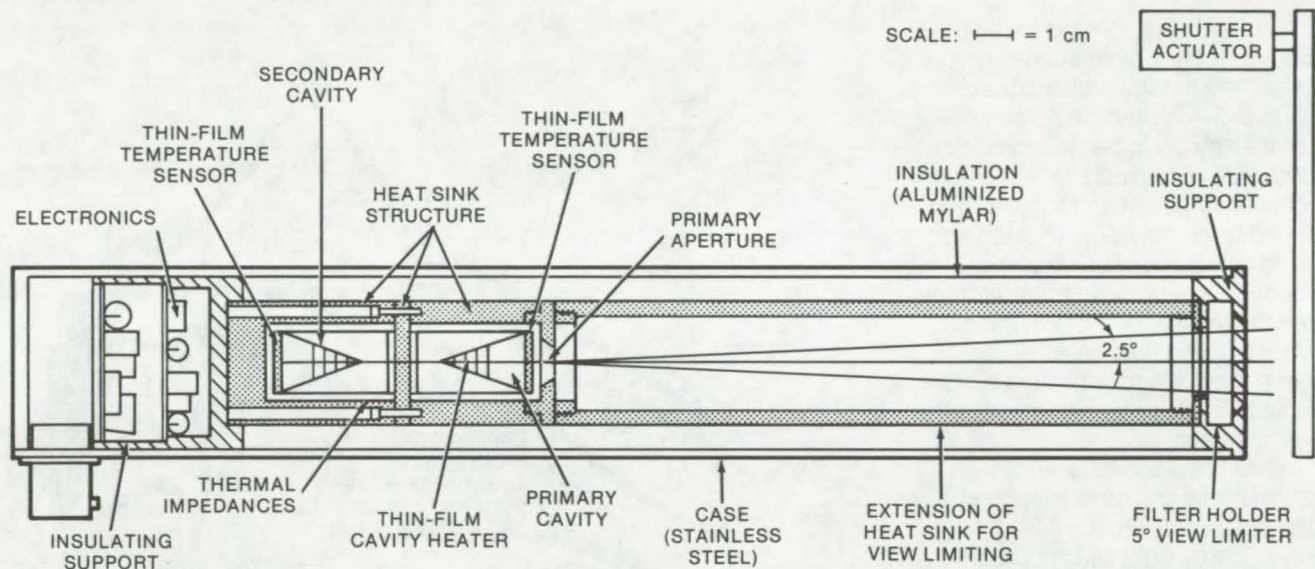
This work was done by John D. Ingham and Daniel D. Lawson of Caltech/JPL. For further information, Circle 20 on the TSP Request Card.

This invention is owned by NASA, and a patent application has been filed. Inquiries concerning nonexclusive or exclusive license for its commercial development should be addressed to the Patent Counsel, NASA Resident Legal Office-JPL [see page A8]. Refer to NPO-13732.

Active-Cavity Radiometer/Pyrheliometer

A long-term absolute uncertainty of ± 0.1 percent at the solar constant level

Caltech/JPL, Pasadena, California



The **Active-Cavity Radiometer/Pyrheliometer** uses thin-film-bonded heaters and temperature sensors. The electronic circuit uses a digital, power-bit design. An electrodeposited silver cavity and a thermal impedance structure aid in the mechanical and thermal homogeneity of the detectors.

A radiometer/pyrheliometer for measuring the Sun's radiant energy output combines improvements that enable it to achieve ± 0.1 percent long-term absolute uncertainty. The principal differences between this and earlier pyrheliometers are the use of a specular black cavity surface, a dual-cavity detector, an isothermally-confined 5° field-of-view, a thin-film cavity heater and temperature sensors, and new electronics and electrodeposited cavity/thermal impedance structures (see figure).

The black cavity, which incorporates a specular black paint absorption coating, is the most important contributor to the improved accuracy of the new instrument (a previous apparatus used a diffuse carbon black coating). The radiometer has a 30° cone angle, which causes an axial incident ray to undergo six internal interactions with the cavity walls, before reflection out of the

aperture. As a result, the uncertainty in effective cavity absorption can be less than $\pm 10^{-4}$ percent, compared to $\pm 10^{-1}$ percent when a diffuse coating is used. The overall size of the cavity is reduced by a factor of two, since it is no longer necessary to shade it. The smaller instrument mass also helps reduce the instrument time constant.

The dual-cavity configuration helps decrease sensitivity to heat-sink temperature drift. The secondary cavity views the heat sink and has thermal properties as nearly identical to the primary detecting cavity as possible. The temperature difference is monitored between the tops of both cavities. The primary cavity is in equilibrium with the incident radiant power; electrical heating power is provided by the instrument circuit and by the thermal environment of the heat sink. The secondary cavity is in equilibrium with the thermal environment of the

heat sink. It responds to heat-sink temperature drift and thus nulls the drift of the primary cavity. The active cavity mode is utilized in which the 0.5°C temperature difference between the cavity and heat sink is automatically maintained at a constant value. The active-cavity mode guarantees that the cavity is in the same thermodynamic state in both the shutter-closed (reference) and shutter-open (observation) phases of the measurement. This fact, in conjunction with the shuttered differential mode of measurement, significantly reduces the uncertainty of active-cavity radiometer observations relative to S. I. units.

This work was done by Richard C. Willson of Caltech/JPL. For further information, Circle 21 on the TSP Request Card.
NPO-13819

Solar-Power Mountain Concept

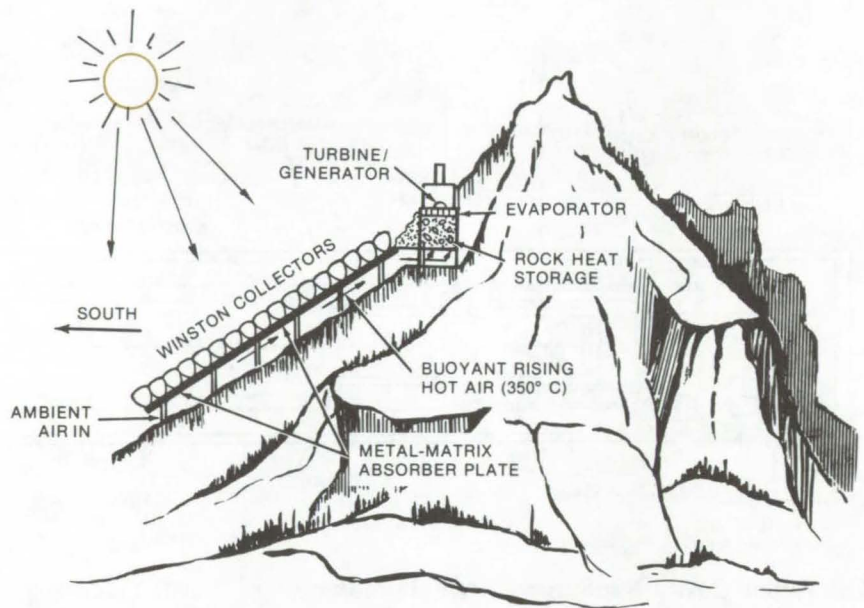
Solar collectors on a mountainside collect thermal energy for a mountaintop powerplant.

Caltech/JPL, Pasadena, California

An interesting scheme for large-scale collection of solar energy utilizes the natural advantages of a mountain. A closed single-unit collector array could be placed on the south side of the mountain where it would absorb heat and transfer it to air under the array. The heated air would rise along the side of the mountain to a bin of thermal-storage rocks at the top. A heat exchanger with a working fluid could extract energy from the rock bin and drive a Rankine-cycle turbine/generator to produce energy.

There is a basic difference between this and other proposed hillside solar-collection fields. A previously thought-out approach is to create buoyancy forces to generate and utilize kinetic energy in the rising heated air. In this concept, it is proposed to utilize the thermal energy of the heated air. It can be shown that the kinetic energy of the moving heated air is only a small percentage of the total energy absorbed from the Sun.

The collector array could consist of east-west rows of Winston concentrator troughs, butted together tightly to form a solid field. In the design concept, each row is about 2-1/2 meters wide and is covered with domed glass shells. The shells are provided with external antireflective coatings and semitransparent mirror coatings designed to reject infrared radiation emitted from the absorption surfaces of the troughs below. The space between the domes and absorption surfaces is on the order of 2 meters, and the enclosed volume between the domes and surfaces is evacuated to reduce convective and conductive heat losses. The absorption surfaces



The **Power-Mountain Concept** is a possible approach to economic collection of solar energy for large-scale use. It is estimated that, at a comparatively-reasonable construction cost, large quantities of air could be heated to around 350 °C to operate a Rankine-cycle turbine via a heat exchanger.

are treated with coatings having a high absorptivity-to-emittance ratio to reduce radiative heat loss.

A porous metallic matrix plate, attached to the undersides of the troughs, behaves as a large set of cavity radiators (blackbodies) with high absorptivity. Air flows through the matrix plate and exchanges heat with its thermally stratified layers. The surface of the mountain slope forms the lower boundary of a massive cavity that facilitates heating of the air.

This design concept offers significant cost advantages compared to other distributed-collection or power-tower proposals. The sloped arrangement made possible by mounting the collection field on the side of a mountain drastically reduces the heat-transport problem

of the level ground-based collector field. Air transports the collected heat energy without mechanical pumps, ducts, or pipes. The heated air rises in the atmosphere, and the buoyancy force supplies the pumping power without further cost. The butted-together Winston-type concentrator troughs eliminate the precision tracking requirement of the power towers.

In addition to the free air transport, the design is cost-effective in that it uses low-cost native rock for heat storage. Furthermore, it can utilize inexpensive real estate that is not suited for other uses because of the steepness of the slope.

This work was done by Victor C. Clarke, Jr., of Caltech/JPL. No further documentation is available. NPO-13861

Inexpensive High-Temperature Solar Collector

Similar to a flat-plate collector, a proposed concentrator uses water lenses to achieve temperatures near 200° C.

Caltech/JPL, Pasadena, California

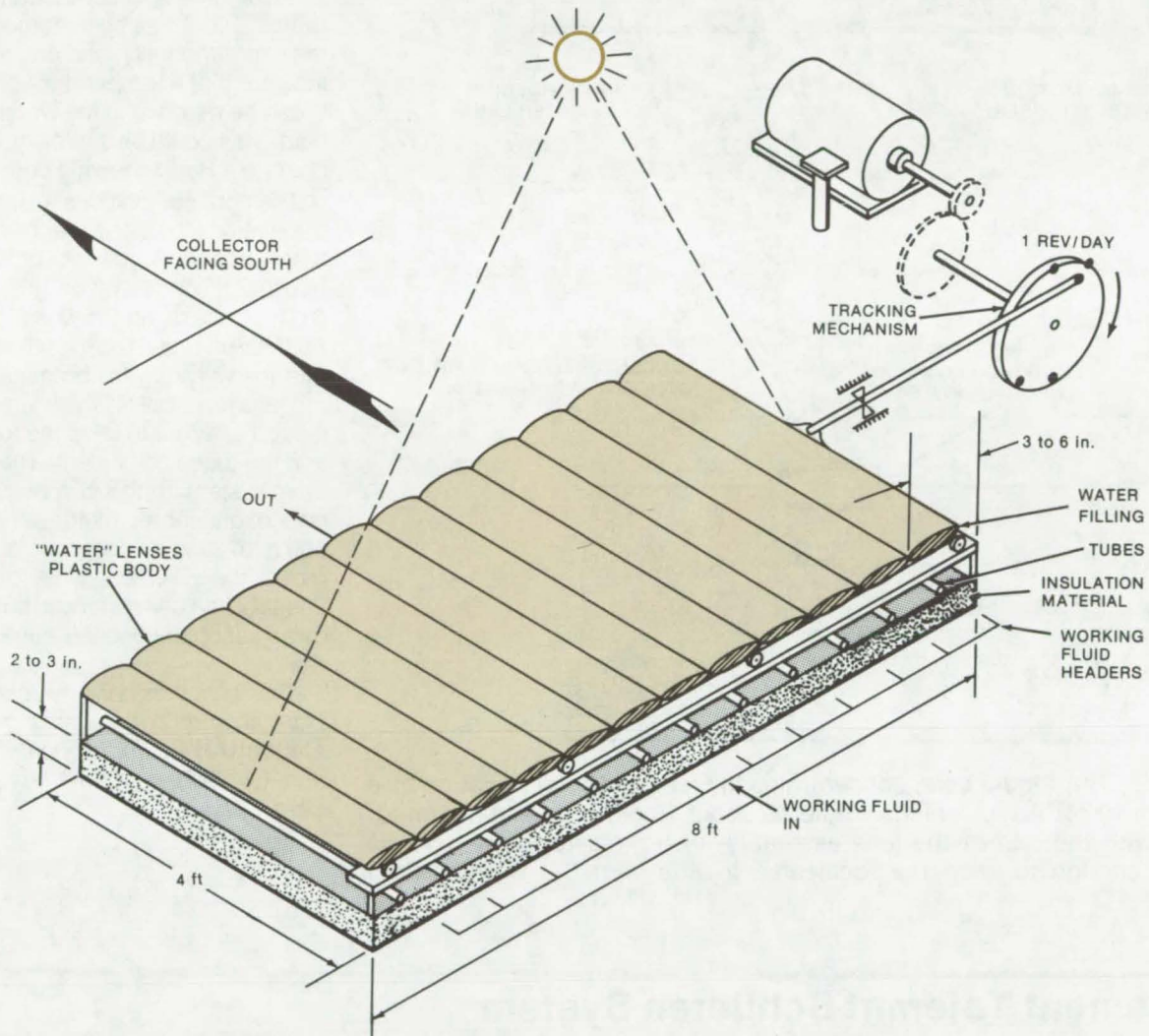


Figure 1. The **High-Temperature Solar Concentrator** is constructed similar to a flat-plate collector. The conventional glass cover plate is replaced with a series of lens-shaped shells that are filled with water. Although not shown in the illustration, the design includes compensation for expansion and contraction of the water and provisions for filling, draining, and cleaning the lens. The focal lines of the lenses are kept aligned with the working-fluid tubes by translational motion of the lenses in a daily cycle.

A new type of solar collector would use liquid lenses and simple translational tracking to concentrate solar radiation by a factor of 100:1. Shown in Figure 1, the proposed collector could be constructed much as flat-plate collectors are, at a cost of perhaps 25 percent more. Yet, preliminary experiments and calculations indicate that the new ar-

angement will be able to heat a working fluid to around 200° C, whereas conventional flat-plate collectors are limited to about 100° C.

The lens assembly (see Figure 2) is a series of parallel cylindrical lenses made of glass or plastic shells. The curvature of the lenses would be chosen for a high concentration ratio and a short focal length.

The space between the shells is filled with a liquid that has an index of refraction close to that of the lens shell. (For instance, the refractive index of water is 1.33 and that of glass is 1.5, close enough for the water-filled lens to approximate the performance of a solid lens.) The advantage of this approach over solid lenses is that the shells are less

(continued on next page)

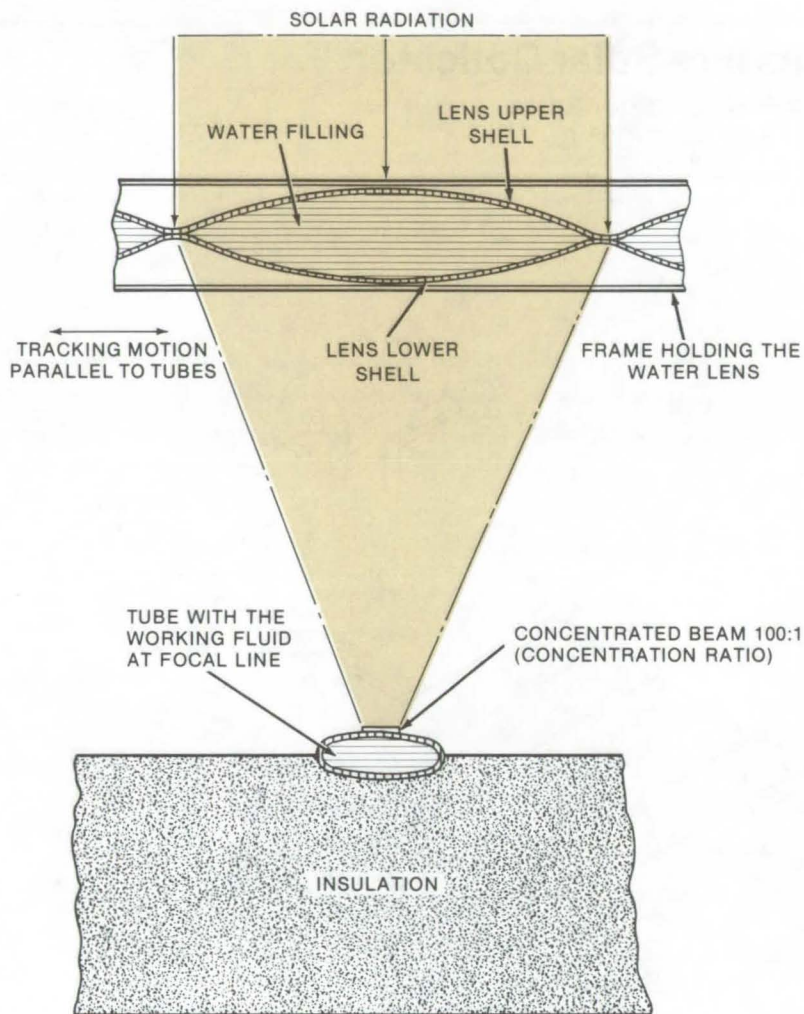


Figure 2. The **Liquid Lens** concentrates the received solar radiation by a factor of 100:1. A typical lens would be about 10 cm wide and mounted, along with the rest of the lens assembly, on rollers to allow it to be moved enough to keep the focal area in line with the working-fluid tubes.

expensive to manufacture and lighter and easier to handle.

The working-medium tubes are constructed as for a typical flat-plate collector, from copper, steel, or aluminum. They would be coated with a black paint and supported on a layer of thermal insulation. Using this type of lens, a concentration ratio of 100:1 has been demonstrated experimentally, and calculations indicate that a temperature of 200° C can be reached in the working fluid. This could be sufficient to operate a Rankine-cycle engine.

The concept includes a simple translational tracking mechanism that keeps the focus line, or line of maximum concentration, aligned with the tubes carrying the working fluid. As the Sun moves across the sky, this line will shift; to compensate, the lens assembly is cyclically moved at a rate to keep the focal line and the tubes coincident. The simple drive system for this purpose consists of an electric motor, a reduction gear, and an eccentric disk that moves the assembly on its rollers. Seasonal adjustments can be made by adjusting the eccentricity of the disk.

This work was done by Joseph Dorman and Fikry L. Lansing of Caltech/JPL. For further information, Circle 22 on the TSP Request Card. NPO-13979

Alignment Tolerant Schlieren System

Gas flows are effectively viewed with relaxed optical-precision requirements.

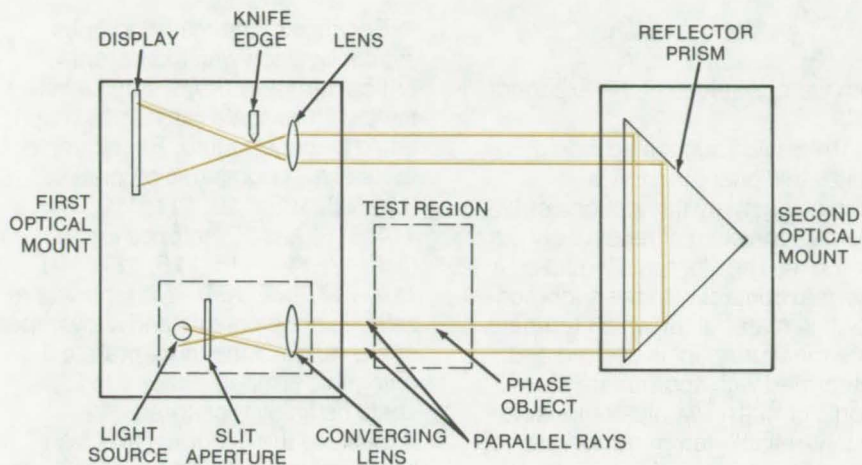
Ames Research Center, Moffett Field, California

Schlieren photography systems, used to view gas flows, normally require precise and stable placement of optical components located large distances from one another. These tolerance requirements are reduced by a modified arrangement in which the conventional optical path is folded at its center. A porro

prism is used to return and displace the light source.

The simplified schlieren system consists of two mountings on opposite sides of the test section that do not need to be rigidly fastened to each other. One mount carries a point light source (with collimating and focusing lenses and an adjust-

able knife edge) and a display screen; the other mount carries only a porro prism. Collimated light from the point source passes through the test section and then is returned by reflection from within the porro prism, where the beam is displaced laterally by approximately its diameter. The returned beam is passed



The **Schlieren System** consists of a small-area ("point") light source, a means of collimating the light, a means of focusing collimated light to a point, an adjustable knife edge, and a display screen, all mounted on a single mount, and a porro prism, mounted on a second mount.

through a focusing lens, is brought past the adjustable knife edge, and is displayed on the screen.

The operation of the folded schlieren, to the first order, is independent of relative motion between the optical mount and that carrying the porro prism. For linear motion of the porro prism in any direction, or for rotation about three perpendicular axes, any small motion taken

singly does not change the position of the focused spot of light on the knife edge (except perhaps parallel to it). Some motions and rotations change the location of the projected display on the screen, but a motion of perhaps a millimeter can be tolerated if there is a spatial resolution of several millimeters. However, since the diameter of the light spot may be only 50 μm , a 1- μm motion of the

spot may be read easily. Sensitivity of the system may be increased still further by making the system even more completely immune to flexure. Flexure of the components on the optical mounting may cause problems, but they are minimal compared with those created with a conventional schlieren system where optical components are mounted on opposite sides of the test section.

With a breadboard model, it was found possible to hold the prism in the hand while visually observing a schlieren picture. Thus, schlieren equipment could be built at less expense because of the relaxed requirements for rigidity; it possibly can be constructed as a portable model.

This work was done by William D. Gunter, Jr., of Ames Research Center. For further information, Circle 23 on the TSP Request Card.

This invention is owned by NASA, and a patent application has been filed. Inquiries concerning nonexclusive or exclusive license for its commercial development should be addressed to the Patent Counsel, Ames Research Center [see page A8]. Refer to ARC-10971.

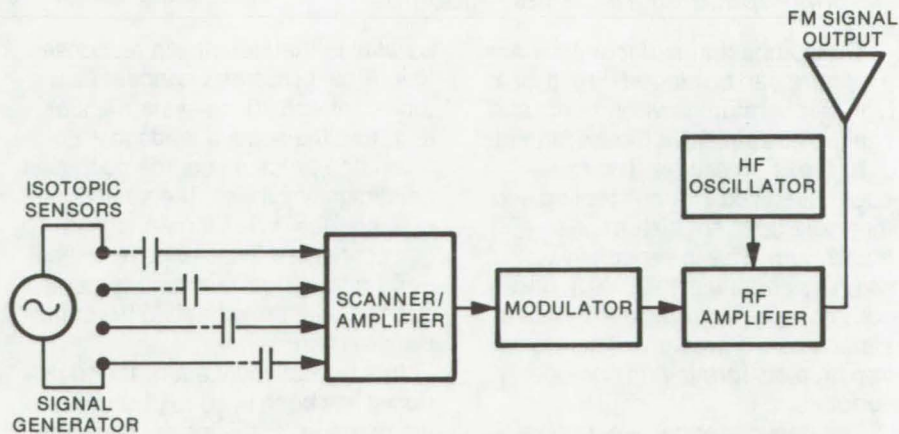
Superconducting Thermometer for Cryogenics

Digital electronic thermometer would use superconducting filaments as sensors.

Langley Research Center, Hampton, Virginia

There is a steadily increasing requirement in basic research and in engineering systems design for the employment of superconducting materials. Superconductors are being explored for space applications, for the establishment of strong magnetic fields in fusion and plasma research, and for possible application relating to the future transmission of electrical power throughout the United States. A new device, of great simplicity, is suggested for accurately monitoring the cryogenic temperatures at which superconductors operate.

The device suggested is essentially an "electronic thermometer"



An **Isotopic Temperature Monitor** is shown as it might be used with a remote-sensing system.

of high reliability that will monitor small temperature changes in the 4 to 20 K range. It has a basic "on/off" binary output making it readily adaptable to the generation of digital data.

The concept is based on the known phenomenon of superconductivity of isotopes of various elements occurring at predetermined critical temperatures. With certain metallic structures, the onset of superconductivity is dependent upon the isotopic mass that affects only the phonon spectrum of the lattice. For example, the critical temperature at which superconductivity occurs for mercury isotopes depends on the isotopic mass by the relationship

$$T_C \times M^{1/2} = \text{constant}$$

This general effect has been noted also for cadmium, palladium, tin, thallium, and zinc. The implication is that superconductivity is largely due to a strong interaction between the electrons and the lattice. Not all elements obey the above equation, but a number follow the general relationship of

$$T_C \times M^a = \text{constant}$$

with various values of the exponent "a".

The device suggested would utilize this phenomenon by employing many thin ribbons or filaments consisting of reasonably pure isotopes. The filaments would be in thermal contact with the superconducting material for which temperature measurement is desired and, integrated with appropriate electronic circuitry, would comprise a highly-reliable temperature monitor since superconductivity of each isotope would occur at a different specific temperature.

The circuitry could be very simple. A small voltage could be applied to the isotopic sensors, and solid-state circuitry would indicate an "on" condition — the onset of superconductivity with decreasing temperature — or an "off" condition — the departure from superconductivity with increasing temperature. Thus, the superconducting filaments, coupled with relatively simple circuitry, would provide a "temperature vernier" of great simplicity, reliability, and precision.

Because of the many isotopes available, each with a different critical temperature, a very sensitive temperature scale with digital output could be constructed. For example, there are 8 cadmium isotopes (Cd-106, 108, 110, 111, 112, 113, 114, 116) and 10 isotopes for tin (Sn-112, 114, 115, 116, 117, 118, 119, 120, 122, 124). With the proper selection of elements and alloys, the entire range of the more practical cryogenic temperatures, 4 to 20 K, could be finely monitored.

Besides the accuracy and reliability possible with such a device, its usefulness would be greatly enhanced by its ability to track very fast thermal transients, and the simple "on/off" output of the superconducting filaments is readily adaptable to remote sensing and telemetry.

*This work was done by Frederick A. White of Rensselaer Polytechnic Institute for **Langley Research Center**. For further information, Circle 24 on the TSP Request Card.*

Inquiries concerning rights for the commercial use of this invention should be addressed to the Patent Counsel, Langley Research Center [see page A8]. Refer to LAR-12055.

High-Pressure High-Temperature Transducer

Compact instrument needs no internal cooling and can take sensitive pressure measurements for fatigue tests and other applications.

Marshall Space Flight Center, Alabama

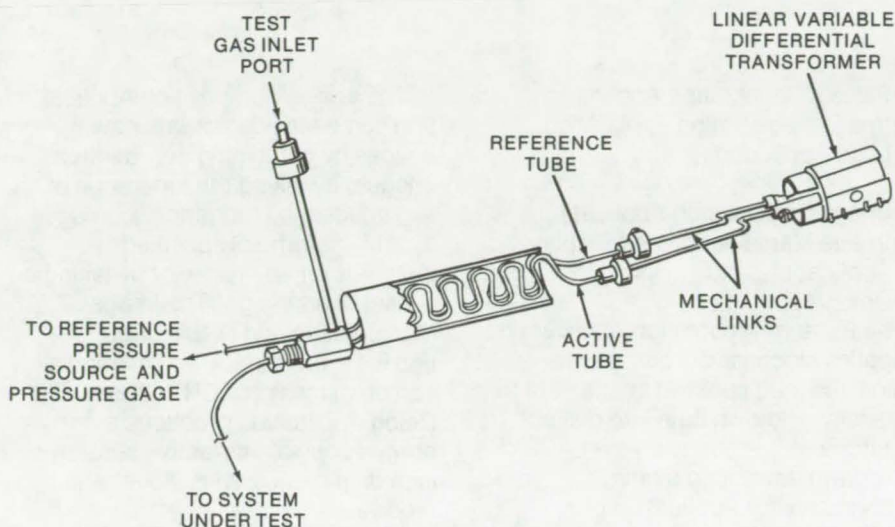
The compact transducer shown in the figure can be placed directly into high-temperature environments and can provide sensitive measurements of high gas pressures. The transducer needs no internal cooling and therefore does not disturb gas equilibrium. This is especially useful when measuring pressures in gases containing saturated steam since it eliminates the problem of condensation droplets forming on cooled surfaces.

The transducer has a pair of parallel, undulating tubes, each similar to several bourdon tubes connected in series, that elongate or contract

parallel to their lengths in response to internal pressure changes. One tube connects to the system under test, and the second leads to a reference pressure source such as a helium gas cylinder. The sealed end of each tube drives a mechanical link connected to a device for measuring relative lateral displacements such as a linear variable differential transformer.

In a typical application, the transducer has been used to determine the pressure at the instant of failure of rocket engine fuel-line conduits that were subjected to high-temperature, high-pressure fatigue testing.

Each conduit was connected directly to the active side of the transducer and was placed inside a quartz-lamp furnace at 1,400° F (760° C) and pressurized to 7,000 psia (48×10^6 N/m²) with a hydrogen steam gas mixture. The reference side was filled to approximately the same pressure with helium gas. The conduit was then subjected to continuous vibratory stress until it failed catastrophically due to a combination of hydrogen embrittlement, heat, and fatigue. This allowed the pressurizing gas to rapidly vent, contracting the active tube of the transducer and displacing it relative



The **High-Pressure High-Temperature Transducer** has active and reference sides consisting of tubes that elongate in response to increasing interior pressures. The relative displacement of the tubes is measured by a linear variable differential transformer to determine the pressure on the active side.

to the reference tube. The displacement was measured by the linear variable differential transformer and was duplicated by venting the reference side to determine the magnitude of pressure that existed within the specimen prior to failure.

*This work was done by John J. Vrolyk of Rockwell International Corp. for **Marshall Space Flight Center**. For further information, Circle 25 on the TSP Request Card.*

Title to this invention, covered by U.S. Patent No. 4,020,696, has been waived under the provisions of the National Aeronautics and Space Act [42 U.S.C. 2457 (f)], to Rockwell International Corp., Canoga Park, CA 91304.

MFS-23765

Books and Reports

These reports, studies, and handbooks are available from NASA as Technical Support Packages (TSP's) when a Request Card number is cited; otherwise they are available from one of NASA's Industrial Application Centers or the National Technical Information Service.

Solar-Cell Array Design Handbook

For the novice and experienced designer

A 12-chapter two-volume compilation of solar-cell design data has been written from industrial, university, and government sources. The volumes, which total about 750 pages, contain tutorial descriptions of analytical methods, solar-cell characteristics, and cell material properties widely used in specifying solar-cell array performance and hardware design, as well as analysis, fabrication, and test methods.

Three levels of design activity are addressed: (1) systems, (2) equip-

ment, and (3) design verification, testing, and review. At the systems level, emphasis is on the overall characteristics of the solar-cell array and its relationship to the system in which it is used. Descriptions are made of available equipment for the implementation of a practical design, as well as for component and material selections and analytical performance prediction and optimization. Design reviewers, by using the handbook, can verify computerized analyses to assure that no major computational errors have occurred. Test methods, also included, are those currently employed to verify performance requirements.

Volume One of the handbook includes brief engineering-level introductions, historical reviews, and current state-of-the-art descriptions of solar-cell arrays. Design details and step-by-step procedures, augmented by actual design examples, permit the novice designer to develop design criteria,

to design and analyze an array, and finally to test it. The volume is concluded by an extensive cross-referencing index.

Volume Two is for the experienced designer and allows for easy access to detailed design and reference data in an appendix-like format. Electrical and mechanical characteristics of solar cells are included, as are the mechanical, electrical, optical, and thermal properties of solar-cell array materials. The volume also contains frequently-used unit conversion factors and physical constants.

*This work was done by Hans S. Rauschenbach of TRW, Inc., for **Caltech/JPL**. Further information may be found in NASA CR-149365 [N77-14193 (Vol. 1) and N77-14194 (Vol. 2)]., "Solar Cell Array Design Handbook" — Volume 1 [\$12.50] and Volume 2 [\$9.00], copies of which may be obtained [prepayment required] from the National Technical Information Service, Springfield, Virginia 22151. NPO-14106*

Computer Programs

These programs may be obtained at very reasonable cost from COSMIC, a facility sponsored by NASA to make new programs available to the public. For information on program price, size, and availability, circle the reference letter on the COSMIC Request Card in this issue.

Earth Resources Interactive Processing System

Data analysis for several remote-sensing programs

The Earth Resources Interactive Processing System (ERIPS) allows interactive processing and analysis of remotely-sensed Earth resources data, including:

- ERTS/LANDSAT satellite (both MSS and RBV data),
- MSC 24-channel multispectral scanner,
- EREP S-192 experiment, and
- Michigan 12-channel scanner.

ERIPS may be modified for other sensors and allows numerous analysis functions on various types of image data.

The primary analysis software packages in the ERIPS system are:

- Pattern Recognition Application,
- Image Registration Application,
- Load Application,

- Image Composition Application,
- Image Manipulation and Display Application, and
- Delog Application.

The Pattern Recognition Application applies stochastic processes to digitized multispectral image data to classify unknown data into distinct materials. It is based on the LARSYS program developed by the Laboratory for Application of Remote Sensing at Purdue University.

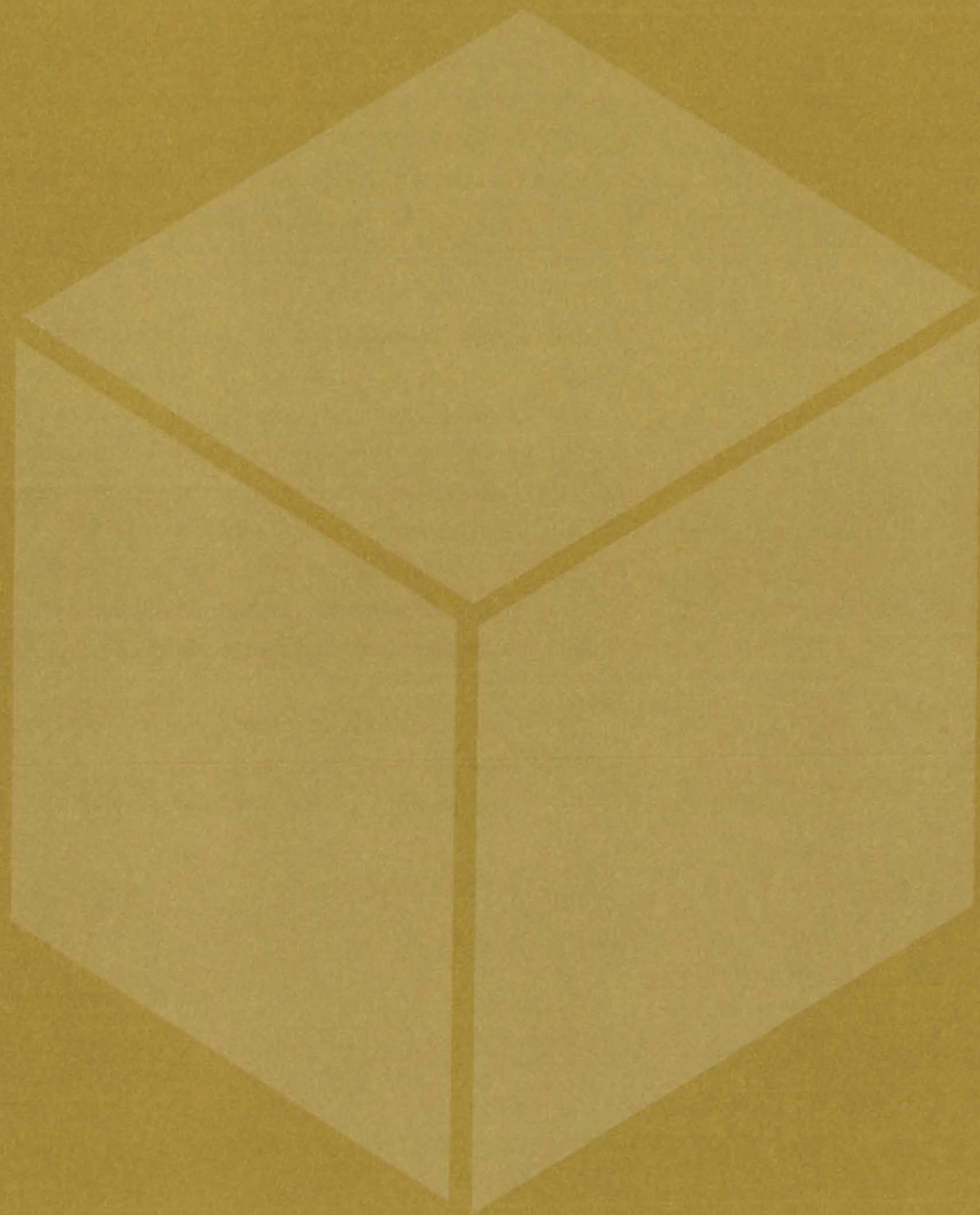
The Image Registration Application allows one to register two images together and to register an image to a longitude-latitude (Universal Transverse Mercator) grid. The Load Application allows image data to be transferred either way between computer-compatible tapes (CCT's) and a system disk pack. It allows the user to view an image directly from tape and to select a portion of the image to be loaded. It also permits the user to view header information for any image.

The Image Composition Application can be used to create new images by combining two identical images, by taking the difference of two images, by merging two images, by taking a ratio of specified channels on an image, or by taking a subset of an image. The Image Manipulation and Display Application is for the display and manipulation of images on a CRT screen. The Delog Application produces a printed copy of interactive session, including menus, messages, and reports.

ERIPS is an interactive system developed to execute on an IBM 360/75 operating under RTOS. The minimum system configuration requirement includes 300K bytes of central memory, 500K bytes of large-capacity storage (LCS), three 2314 disk drives, three 9-track tape drives, and one cluster of Hazeltine digital image interactive display terminals.

This work was done by International Business Machines Corp. for Johnson Space Center. For further information, Circle A on the COSMIC Request Card. MSC-16004

Materials



Hardware, Techniques, and Processes

- 221 Impact-Resistant Boron/Aluminum Composites
- 222 Preparation of Organosiloxy-Molybdenum Monomer
- 223 Preparation of Zinc Orthotitanate
- 224 Thermochemical-Photolytic Production of H₂ and O₂ From Water
- 225 Ni-Cu-Zr Alloy for Catalytic Reactors
- 226 Radiation-Resistant, Electrically Insulating Cermet
- 227 Oxidation-Resistant Cermet
- 228 Stress, Corrosion, and Heat Resistant Cermet
- 229 Liquid-Oxygen-Compatible, Flame-Resistant Coating
- 230 Soluble, Thermally-Stable Aromatic Polyimides
- 231 A New Polyimide Laminating Resin
- 232 Pretreatment for Strong Aluminum/Epoxy/Aluminum Bonds
- 232 Gold Recovery Process From Polyimide Film
- 233 Tensile Viscosities of Non-Newtonian Fluids
- 234 Resilient Thermal Barrier for High Temperatures
- 234 Obtaining Ultradry Crystalline Solids

Books and Reports

- 235 Controlling Stress-Corrosion Cracking
- 235 Anodic Growth of Niobium Oxide
- 236 Properties of Doped Cesium Iodide Crystals

Impact-Resistant Boron/Aluminum Composites

Proper choice of materials and processing conditions results in impact strengths up to 10 times greater than titanium alloys.

Lewis Research Center, Cleveland, Ohio

Most development of boron/aluminum (B/Al) composites has been directed toward structural applications, where the tensile strength of the composite is most important. Usually, in these applications, foreign-object damage problems are not a primary failure mode, and impact strength has not been used as a major factor in the choice of materials selection and processing parameters.

Recently, B/Al composites have been considered as a replacement for titanium, the conventional construction material for fan blades in aircraft-turbine engines. For this application, B/Al offers the advantage of lower weight, better engine performance, and more economical operation. However, collisions with birds are a major flight safety hazard for turbine-engine aircraft operations. Present engines can "swallow" most bird strikes and are not otherwise protected with inlet devices. Designers have not used B/Al composites as fan blades in aircraft engines because their impact strength has been considered to be too low, up to now.

B/Al composites, which normally use a 4- to 5.0-mil (0.10- to 0.13-mm) boron fiber in a 2024 or 6061 aluminum matrix, produce Charpy impact strengths less than those of titanium alloys. Significant improvement in standard notched Charpy impact energy for B/Al composites can be achieved with the proper combination of material variables (fiber diameter, matrix ductility) and processing variables (bonding time and temperature) to produce an optimum fiber/matrix interface. In fact, by the proper choice of materials and processing conditions during the diffusion bonding of B/Al composites, it is possible to increase the impact strength of the composites by as much as a factor of 10 to values higher than for titanium alloys and

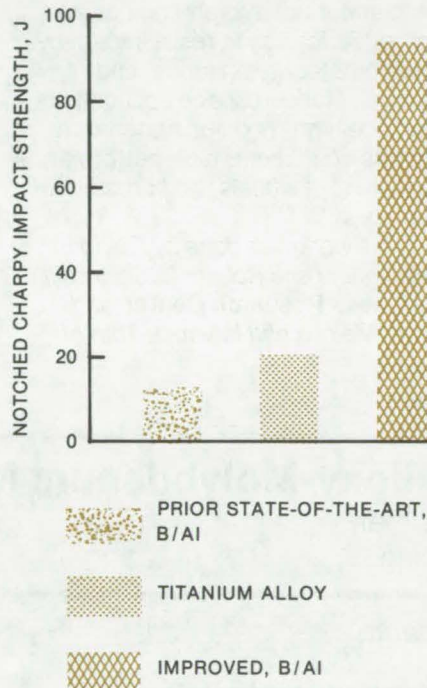


Figure 1. The **Improved Impact Resistance** achievable in B/Al composites, coupled with their light weight, makes them ideal candidates for the fabrication of aircraft-turbine fan blades.

thus make B/Al composites capable of withstanding bird strikes in fan-blade applications (see Figure 1). Their consideration for application to fan and compressor blades in aircraft gas turbines now appears reasonable.

The effects of the proper combination of material and processing variables on the impact strength of B/Al composites can be readily analyzed. For example, making composites with a more ductile matrix, 1100 Al, allows the matrix to undergo greater deformation and matrix shear upon impact, thus making a considerable additional contribution to the impact energy absorption of the composites. The use of larger-diameter boron fibers, such as 8-mil (0.20-mm), allows greater distances between the fibers for a given fiber content. Boron fibers restrain the matrix from deforming under load, thus embrittling the composite. However, the greater the distances between fibers, the less the effect of this restraint, and the more the matrix can deform.

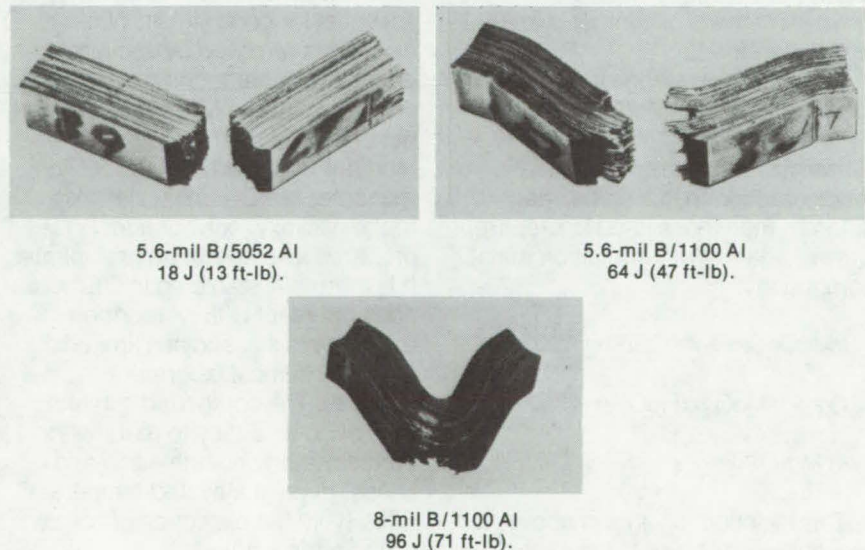


Figure 2. **Failed Charpy Impact Test Specimens** show the effects of fiber diameter and matrix alloy on impact strength and failure ductility.

(continued on next page)

The additional deformation possible by the larger interfiber spacings also allows the fibers to undergo multiple fiber fracture, where each individual fiber can fracture several times. Each separate fracture contributes additional energy absorption to the composite (see Figure 2). The weaker, more ductile 1100 Al matrix results in a composite with over 95 percent of the tensile strength and 10 times the Charpy impact strength of conventional B/Al composites.

Also, impact strength of B/Al composites can be increased by proper choice of fabrication temperatures. Processing at below-optimum temperatures caused impact strength to be reduced by delamination. Processing at above-

optimum temperatures caused impact strength to be reduced by excessive reaction at the fiber/matrix interface.

Additional aerospace applications for improved impact-resistant B/Al composites are for lightweight compressor blades, guide vanes, and stators of aircraft engines and other structures to resist impact by micrometeorites, stones, and gravel. Nonaerospace applications include high-modulus materials for sports equipment, high-performance automotive wheels, and prosthetic devices.

This work was done by David L. McDanel and Robert A. Signorelli of Lewis Research Center and Paul Melnyk and Istvan J. Toth of

TRW, Inc. Further information may be found in:

NASA CR-134770 [N75-24747], "Development of Impact-Resistant Boron/Aluminum Composites for Turbojet Engine Fan Blades," NASA TN-D-8204 [N77-11118], "Effect of Fiber Diameter and Matrix Alloys on Impact-Resistant Boron/Aluminum Composites," and NASA TM-X-71875 [N76-18236], "Improved Impact-Resistant Boron/Aluminum Composites for Use as Turbine Engine Fan Blades."

Copies of these reports may be obtained at cost from the New England Research Application Center [see page A7]. LEW-12472

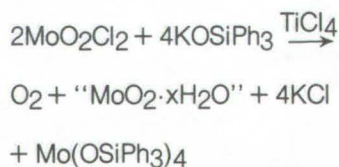
Preparation of Organosiloxy-Molybdenum Monomer

New compound may serve as monomer for thermally-stable polymeric coating.

Marshall Space Flight Center, Alabama

It has been known that organosiloxy polymers can be made more thermally stable by incorporating a transition metal into the backbone of the polymer chain. Several compounds that incorporate silicon-oxygen-transition metal linkages are known; but reaction details and general methods of synthesis are not well understood.

To further knowledge in this area, a new compound, Mo(OSiPh₃)₄ (where Ph is C₆H₅), has been synthesized. It is prepared via a redox reaction that is somewhat different than those used to prepare known organosiloxy-transition metal compounds:

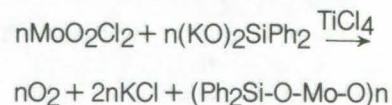


This reaction, as shown above, is thought to explain best the experi-

mental observations. The redox involves the reduction of Mo⁺⁶ to Mo⁺⁵ and the oxidation of O⁻² to O₂. The MoO₂Cl₂ acts as both the oxidant and reductant.

TiCl₄ (or one of its hydrolysis products) appears to act as a catalyst. Small amounts of water are essential for good yields. When water was removed by vacuum drying and other techniques, the blue precipitate "MoO₂·xH₂O" was not observed, and the yields of Mo(OSiPh₃)₄ were very poor. The monomer Mo(OSiPh₃)₄ (tetrakis triphenylsiloxy molybdenum IV) is prepared as a fine white precipitate. It is thermally stable up to 230° C, does not react with water or on exposure to air, and has limited solubility in most laboratory solvents. The compound exhibits little or no tendency to react with concentrated or dilute acids and bases, even at elevated temperatures (with the exception of concentrated nitric acid).

It is expected that it will be possible to polymerize this monomer to produce a species of the type (Ph₂Si-O-Mo-O)_n. A promising approach is to follow a redox reaction similar to that used to produce the monomer:



It remains to be determined whether the polymer will retain the useful properties of the monomer and be suitable for applications such as protective coatings, lubricants, or electrical semiconductors.

This work was done by Gerald A. Marano of Kentucky State University for Marshall Space Flight Center. For further information, including a description of experimental procedures and compound identification, Circle 26 on the TSP Request Card. MFS-23704

Preparation of Zinc Orthotitanate

Pigment for thermal-control paints produced under less stringent conditions

Marshall Space Flight Center, Alabama

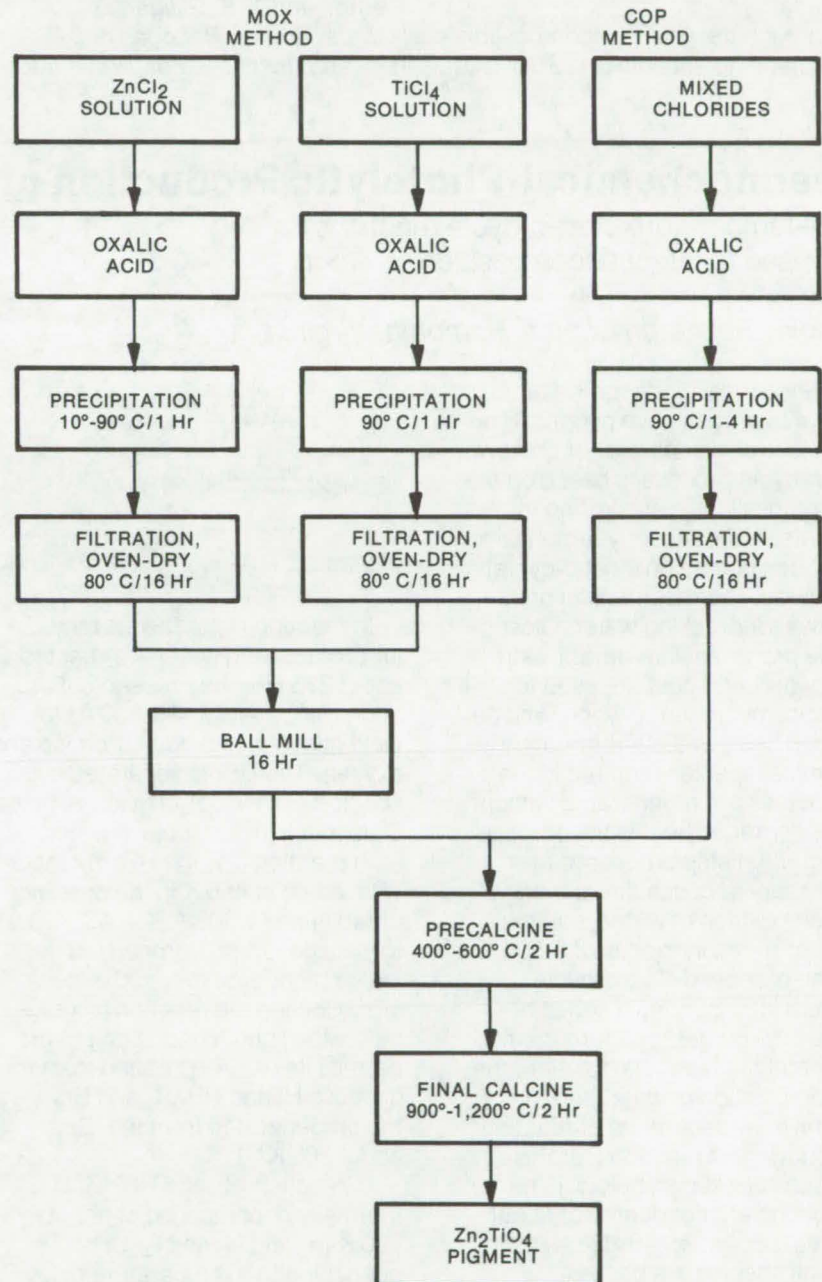
Zinc orthotitanate (Zn_2TiO_4), a pigment for thermal-control paints, has been conventionally prepared by reacting zinc oxide with titanium dioxide. In a new process the pigment is prepared from decomposable precursors as sources for the $ZnO-TiO_2$ reaction. This allows rapid conversion to Zn_2TiO_4 under modest temperatures. The resulting powder is fine enough (submicron to 5 microns) for direct incorporation into a paint, and results in good optical properties.

The first step (see figure) is the preparation of chloride and oxalic acid solutions. The $ZnCl_2$ and $TiCl_4$ solutions can be reacted with oxalic acid solution either individually (MOX method) or as a mixed chloride solution (COP method) having the desired Zn-to-Ti ratio.

The zinc chloride/oxalic acid reaction occurs at 10° to 90° C and produces $ZnC_2O_4 \cdot 2H_2O$. The titanium chloride/oxalic acid reaction is conducted at 90° C and produces a compound with a molecular weight of about 150. Although full characterization of this product has not yet been made, X-ray studies show it to be orthorhombic with a distinctive powder pattern that is not recorded in the literature. Repeated experiments have shown that this new titanium compound is reproducible in terms of crystal structure and molecular weight.

In the COP method, the powder is ready for calcination after washing, filtration, and drying. In the MOX method, the zinc oxalate and the titanium compound are mixed in the desired stoichiometry by dry ball milling.

The firing process is carried out in two steps: a precalcination to remove volatiles formed on decomposition of the precursor compounds and a final calcination to form Zn_2TiO_4 . All firings are conducted by direct insertion of the loose powder mixture into a preheated furnace.



Two Methods of Producing Zinc Orthotitanate for paint pigments are the MOX (metal oxalate) and COP (combined oxalate process) approaches. In the first, the Zn and Ti oxalates are prepared separately and then ball milled in the desired proportions. In the COP method, Zn and Ti chlorides are mixed in the desired ratios and then processed together.

(continued on next page)

The powder is also removed while the furnace is at its working temperature to reduce heating and cooling times. It is this rapid firing that makes the precalcination necessary, since volatile removal at 900° to 1,200° C would be quite violent and result in the loss of material.

Through the use of decomposable precursors to enhance the ZnO-TiO₂

reaction and by the rapid firing, a Zn₂TiO₄ powder pigment is prepared rapidly. The elimination of powder grinding in any of the steps also results in a purer product that is less susceptible to color degradation.

This work was done by D. W. Gates of **Marshall Space Flight Center** and J. E. Gilligan, Y. Harada, and W. R. Logan of **IIT Research Institute**. For further infor-

mation, Circle 27 on the TSP Request Card.

This invention is owned by NASA, and a patent application has been filed. Inquiries concerning non-exclusive or exclusive license for its commercial development should be addressed to the Patent Counsel, Marshall Space Flight Center [see page A8]. Refer to MFS-23345.

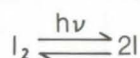
Thermochemical-Photolytic Production of H₂ and O₂ From Water

Low-temperature closed-cycle reactions are used to effect decomposition of water.

Langley Research Center, Hampton, Virginia

Previous methods for the production of hydrogen have depended on the electrolysis of water or on newer open-cycle processes based on the use of fossil fuels as starting reactants. More recently, emphasis has been placed on closed-cycle, multistep, thermochemical processes for cracking water. Closed-cycle processes are attractive in that water and heat are used to produce hydrogen, oxygen, and degraded heat. Since intermediate chemical species required in the processes are regenerated without loss, degraded heat is the only pollutant. Multistep processes are necessary because direct thermal decomposition of water requires temperatures in excess of 2,500 K.

The proposed closed-cycle system incorporates a series of relatively-low-temperature thermal or photolytic reactions to effect the decomposition of water and to permit easy separation of reaction products. The reactions for this process are shown below: [The reactions are conducted at about 0.4 atmospheres (40×10³ N/m²), and all species are gases.]



In reaction (1), gaseous molecular bromine and water are reacted at about 333 K in the presence of radiation (3,650 Å ≤ λ ≤ 5,350 Å) to yield gaseous hydrogen bromide and oxygen. The HBr is separated by solution in a HBr-H₂O mixture, since O₂ is much less soluble in water.

In reaction (2), the HBr is reacted with iodine at 456 K in the presence of radiation (4,300 Å ≤ λ ≤ 7,400 Å) to yield gaseous hydrogen iodide, iodine monobromide, and excess HBr. Cooling the reaction mixture below the liquefaction point of IBr permits its easy separation from the gaseous HI and HBr. I₂ and Br₂ are then regenerated from the IBr at about 700 K.

In reaction (3), the HI-HBr is thermally decomposed at about 700 K to yield H₂ and I₂. Upon quenching to a temperature below 456 K, the I₂ is liquefied and separated. Finally, the solubility of

HBr in H₂O is used to effect the separation of H₂ and HBr.

An alternate approach is also suggested by using silver in place of iodine after the photolytic production of HBr from Br₂ and H₂O.

The validity of the proposed scheme has been partially substantiated by various equilibrium and pseudoequilibrium calculations. Possible radiation sources for the requisite wavelengths in the reactions are solar insolation and the plasma core reactor. In the future, component analysis and kinetic and equilibrium studies are planned to further develop this concept of utilization of solar energy or plasma core reactor for low-temperature reactions in the production of hydrogen from water.

This work was done by N. L. Krascella of **United Technologies Corp.** for **Langley Research Center**. For further information, Circle 28 on the TSP Request Card.

Title to this invention has been waived under the provisions of the **National Aeronautics and Space Act [42 U.S.C. 2457(f)]**, to the **United Technologies Corp.**, East Hartford, Conn. 06108. LAR-12118

Ni-Cu-Zr Alloy for Catalytic Reactors

Potential catalysts for removal of nitrogen oxides from internal-combustion engines

Lewis Research Center, Cleveland, Ohio

Monel alloy 400, nominally nickel with 30 weight-percent copper (Ni-30Cu), has been identified as a suitable catalyst for the reduction of nitrogen oxides (NO_x) from internal-combustion engines. However, this alloy has not shown long-term durability in this application due to the high operating temperatures from 1,300° to 1,700° F (975 to 1,200 K) and active participation of the Monel alloy in the NO_x reduction process. These factors lead to grain-boundary degradation and subsequent loss in strength. Thus a high-strength Ni-30Cu-type alloy with improved grain-boundary strength and stability is desirable. Since the oxidation behavior of the alloy is important in this catalytic application, any attempt to strengthen the base alloy must not affect the overall surface oxidation characteristics.

A minor alloy modification plus appropriate thermal mechanical processing (TMP) were found to satisfy these requirements. Specifically, the addition of 0.2 weight-percent Zr to Ni-30Cu and TMP, consisting of a solution heat treatment of 1/2 hour at 2,000° F (1,365 K) and precipitation aging of approx-

imately 1 hour at 1,381° to 1,745° F (1,025 to 1,225 K), produced a distribution of precipitate, tentatively identified as Ni₅Zr. A TMP schedule, involving a light cold-roll pass (10 percent) after the solution treatment and followed by a precipitation age at 1,560° F (1,125 K), was found to produce a finer, more evenly distributed precipitate than the TMP schedule without cold work.

A preliminary investigation of the properties of the Ni-30Cu-0.2Zr alloy subjected to the TMP schedule with cold work indicates that the goal of improved strength without affecting the oxidation behavior was met. The Ni-30Cu-0.2Zr alloy possessed both higher tensile strength and better tensile ductility than the base Ni-30Cu alloy between 980° and 1,700° F (800 and 1,200 K). Between 980° and 1,520° F (800 and 1,100 K), the stress rupture life of the Ni-30Cu-0.2Zr alloy exceeded that of the base alloy by at least a factor of four. In addition to improved overall strength, metallography revealed that the grain boundaries in the Ni-30Cu-0.2Zr alloy were considerably strengthened in comparison to those in the base

Ni-30Cu alloy, as the onset of grain-boundary cracking was delayed to higher test temperatures. Finally, analysis of the oxides formed during stress rupture testing at 980° and 1,520° F (800 and 1,100 K) indicated that the oxide scales formed on Ni-30Cu-0.2Zr and Ni-30Cu were identical.

The new alloy retains the catalytic properties, and the improved mechanical properties indicate it has potential for use as a catalyst for the reduction of nitrogen oxide from internal-combustion engines.

This work was done by John D. Whittenberger of Lewis Research Center. Further information may be found in the article "An Exploratory Study of Zirconium-Modified, Precipitation-Strengthened Nickel-30 Copper Alloy" by John D. Whittenberger, Metallurgical Transactions, Vol. 5, November 1974, pp. 2359-64.

This invention is owned by NASA, and a patent application has been filed. Inquiries concerning nonexclusive or exclusive license for its commercial development should be addressed to the Patent Counsel, Lewis Research Center [see page A8]. Refer to LEW-12245.



Density Measurements of Trace Gases

The density and thus the concentration of trace components in a gas mixture can be measured with high sensitivity, using a new nondispersive infrared absorption analyzer. Infrared radiation is transmitted through the sample gas and through a reference gas of known density. Both gases are subjected to controlled pressure variations of the same frequency but 180° out of phase. When the absorptions are made to cancel, the ratio of the densities of the sample and reference gases is equal to the ratio of the relative pressure variations. (See page 201.)

Mass Spectrometry Chemi-ionization

A new apparatus allows chemi-ionization to be used for sample fragmentation in mass spectrometry. This method results in simpler fragmentation and greater sensitivity than does electron impact and produces larger molecular ion peaks for compounds having stable parent ions. Electronically ionized metastables of a chemi-ionization reagent are magnetically focused and used to bombard the sample gas. The resulting ions are focused in a quadrupole mass spectrometer and then detected. (See page 204.)

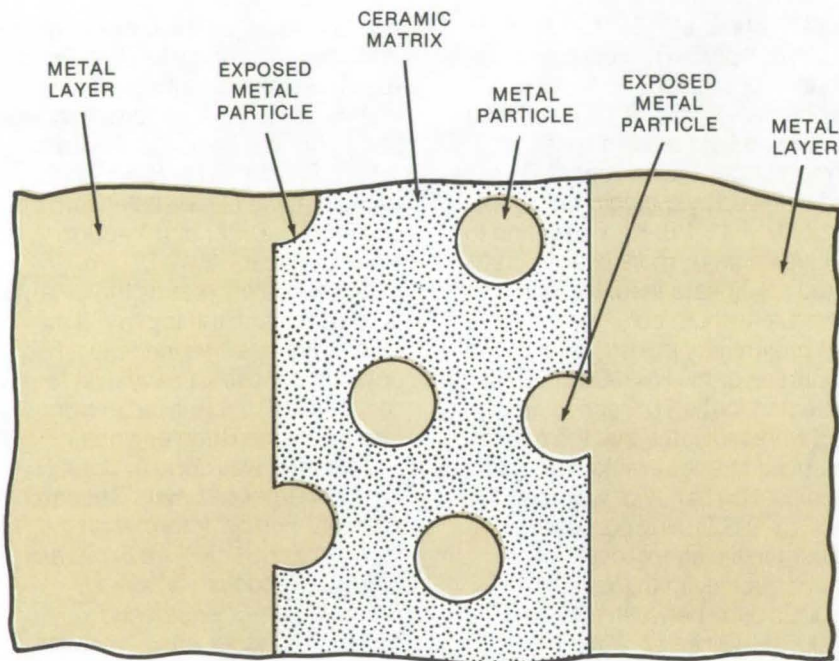
Radioactive-Gas Separation Technique

Cryogenic separation is used to conserve radioactive krypton-85 when this gas is one component of a gaseous mixture. Liquid nitrogen at its normal boiling point of 77 K is used as a cryogen to freeze the krypton-85 to the walls of a coiled copper tube in the gas recovery system. Oxygen and nitrogen remain in their liquid and gaseous forms, respectively, and are drawn off to an external storage tank. When separation is complete, the refrigerant is removed; the krypton then heats to a gas and is pumped to a separate storage tank. (See page 202.)

Radiation-Resistant, Electrically Insulating Cermet

Ceramic-coated metal spheres are sintered into a strong cermet for high-temperature applications such as nuclear reactors.

Caltech/JPL, Pasadena, California



A Trilayer Assembly of Cermet and Metal can be used in thermionic seals. The cermet is very effectively joined to the metal by bonding of the exposed metal particles of the cermet body to the adjacent metal layers. This significantly increases the mechanical strength at the interfaces.

A new cermet, composed of spheres of high-temperature metal coated with a ceramic oxide, offers increased strength for seals in thermionic diodes and other high-temperature environments. Similar materials have been made conventionally by dispersing a ceramic, such as alumina, in a matrix of a metal such as aluminum. Here, the strength of the cermet is increased by reversing this approach, the ceramic oxide being used as the matrix. Materials used are selected for their strength at high temperature, high electrical resistivity, resistance to radiation, and processibility with powder metallurgical techniques.

The cermet is made from ceramic oxides, such as a mixture of 97 percent yttria and 3 percent zirconia, and spherical particles of a high-temperature metal alloy, such as 99 percent niobium and 1 percent zirconium. The metal and ceramic particles of uniform size and shape are mixed until homogeneous and are compacted into the desired shape under a pressure of 5,000 to 100,000 psi (35×10^6 to 690×10^6 N/m²). The pressed cermet body is then sintered under pressures between 2,000 and 15,000 psi (14×10^6 to 105×10^6 N/m²) in a high-temperature (1,000° to 2,000° C) autoclave so that the metal alloy particles are dispersed in and bonded to a continuous matrix of the ceramic oxide.

It is desirable that the ceramic particles be considerably smaller in size than the metal particles. A binder, preferably wax, can be added to the metal alloy particles prior to the addition of the ceramic powder to aid in forming a homogeneous mixture. The binder is removed before compacting and sintering. Particles of other metals or metal alloys can be used to match the coefficients of expansion of the particular ceramic oxide chosen and to achieve the characteristics necessary for the particular cermet application. The proportion of ceramic to metal also depends on the desired characteristics of the resulting cermet.

During the sintering operation, diffusion bonding occurs between the metal particles and the ceramic oxide matrix. (Also, diffusion bonding of exposed metal spheres can be used to join the cermet to other structures; see figure.) The resulting interfacial bond between the particles produces a cermet of high mechanical strength. The cermet can be used at temperatures up to 1,500° C, and electrical resistivity at 1,000° C ranges from 1 to 100 megohm-centimeter.

Two related techniques are described in "Oxidation-Resistant Cermet" (NPO-13666) and "Stress, Corrosion, and Heat Resistant Cermet" (NPO-13690), both of which appear in this issue.

This work was done by Wayne M. Phillips of Caltech/JPL. For further information, Circle 29 on the TSP Request Card.

This invention has been patented by NASA [U.S. Patent No. 3,926,567]. Inquiries concerning nonexclusive or exclusive license for its commercial development should be addressed to the Patent Counsel, NASA Resident Legal Office-JPL [see page A8]. Refer to NPO-13120

Oxidation-Resistant Cermet

Chromium metal alloy and a chromium oxide ceramic are combined for oxidation resistance.

Caltech/JPL, Pasadena, California

Highly oxidation-resistant cermets may be of interest for coal gasification, turbine blades, and other applications requiring a strong material in a hot and corrosive environment. Such oxidation resistance in a new cermet is achieved by using an oxidation-resistant alloy as metal particles in an oxidation-resistant matrix or Cr_2O_3 ceramic.

The cermet is prepared from particles of a chromium-containing alloy such as Type 466 stainless steel. These are coated with beeswax and mixed with particles of Cr_2O_3 or a mixture of Cr_2O_3 and Al_2O_3 . As the mixture is pressed and sintered into a cermet, an impervious layer of chromium oxide forms around each particle, to further enhance oxidation resistance.

The resulting ceramic (see photograph) resists thermal shocks and is highly resistant to oxidation. The incorporation of aluminum oxide into the ceramic matrix lends substantial resistance to corrosion.

Two similar cermets are described in "Radiation-Resistant, Electrically Insulating Cermet" (NPO-13120) and "Stress, Corrosion, and Heat Resistant Cermet" (NPO-13690), both of which appear in this issue.



The **Oxidation-Resistant Cermet** shown in the 100X photograph contains metallic particles in a matrix of ceramic. The metal particles (white areas) are surrounded by a layer of chromium oxide and do not touch, giving the cermet the high electrical resistivity of the ceramic.

*This work was done by Wayne M. Phillips of **Caltech/JPL**. For further information, Circle 30 on the TSP Request Card.*

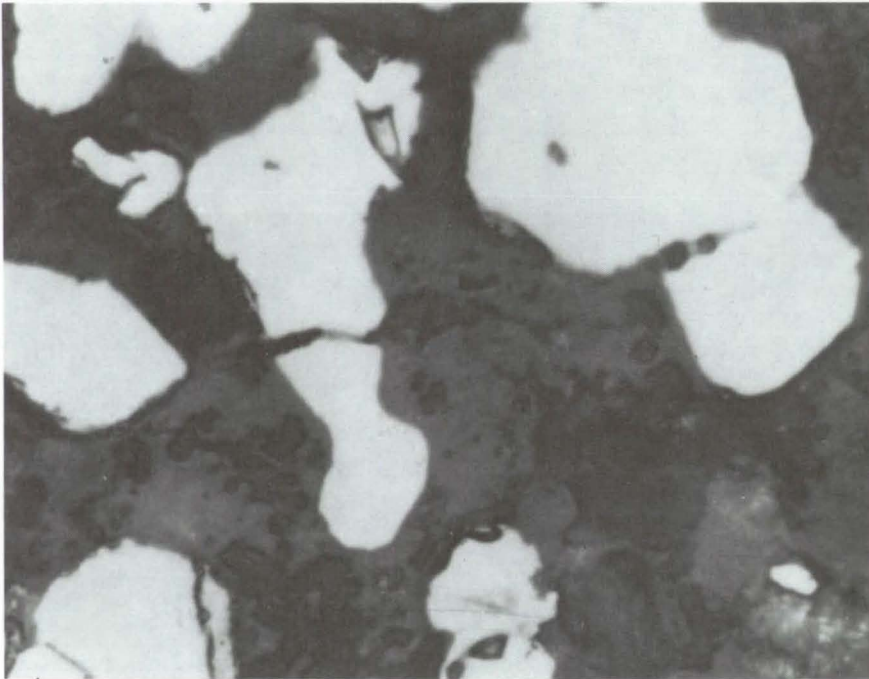
This invention has been patented by NASA [U.S. Patent No.

3,990,860]. Inquiries concerning nonexclusive or exclusive license for its commercial development should be addressed to the Patent Counsel, NASA Resident Legal Office-JPL [see page A8]. Refer to NPO-13666.

Stress, Corrosion, and Heat Resistant Cermet

A combination of a refractory metal and a ceramic substance forms a stable and highly-resistant crystalline alloy.

Caltech/JPL, Pasadena, California



The **Sialon Cermet** shown in the 500X photomicrograph above was prepared as described in the text. The specimen shown was exposed to air at 1,800° F (980° C) for 500 hours. The metallic grains (white areas) show no oxidation.

There is a constant need for cermets (ceramic/metal composites) with superior durability and stress resistance. They are conventionally used as seals for thermionic converters, linings for special combustion or reaction chambers, coatings for high-speed gas-turbine blades, and for other industrial and research applications. Such coatings require considerable resistance to high temperature, oxidation, abrasion, and corrosion.

A cermet (see photograph) with these characteristics has been made by compacting and sintering a mixture of aluminum oxide (Al_2O_3) and silicon nitride (Si_3N_4). This mixture forms a very stable solid solution (a sialon) during processing. In this state, the Si_3N_4 cannot react with the refractory metal to form a silicide, and the cermet retains its structural integrity. Further, the solid solution retains the crystal structure of the Si_3N_4 , so that

the cermet is able to withstand a high degree of abrasion. It also retains its strength and durability at high temperatures, as well as exhibiting a high resistance to thermal shock and oxidation.

To prepare the composition, metallic particles are initially sieved to a uniform size. These are washed twice and coated with a solution of benzene that has been saturated with beeswax. The ceramic particles are also sieved and are then mixed with the wax-coated metallic particles. The mixture is tumbled so that the ceramic particles adhere to the beeswax binder. The mixture is then hot-pressed (compacted and sintered) to obtain the cermet with the desired properties.

Two similar cermets are described in "Radiation-Resistant, Electrically Insulating Cermet" (NPO-13120) and "Oxidation-Resistant Cermet" (NPO-13666), both of which appear in this issue.

This work was done by Wayne M. Phillips of Caltech/JPL. For further information, Circle 31 on the TSP Request Card.

This invention is owned by NASA, and a patent application has been filed. Inquiries concerning nonexclusive or exclusive license for its commercial development should be addressed to the Patent Counsel, NASA Resident Legal Office-JPL [see page A8]. Refer to NPO-13690.

Liquid-Oxygen-Compatible, Flame-Resistant Coating

A polychloroprene rubber composition exhibits superior extrusion and durability and is highly flame and corrosion resistant.

John F. Kennedy Space Center, Florida

Polychloroprene is superior to natural rubber in its resistance to the effects of organic solvents, air oxidation, and chemicals. In combination with magnesium and zinc oxide, carbon black, aluminum oxide hydrate, chlorinated paraffin wax, and other organics, this combination sealant/coating performs well during liquid oxygen compatibility testing. A material exhibiting such qualities has major applications in the fields of aeronautics and safety. The composition of the basic formulation is shown in the table.

•The preferred polychloroprene elastomers are those that offer excellent crystallization resistance, fast extrusion with low nerve and die swell, and firmness. These properties eliminate mill sticking and extrusion profile collapse when large amounts of plasticizers are

used. Any neoprene that has a Mooney viscosity of 75 to 85 and yields a vulcanizate that will pass MIL R-6855B, service at -55° C, can be used in the composition.

- Magnesium oxide is used to influence the processing safety, cure rate, and vulcanizing quality. Oxide particles range from 1 to 12 microns in size and average 5 microns.
- Zinc oxide particles are lead free and average 0.10 to 0.30 micron in size. Generally, any zinc oxide that contains less than 0.01 percent by weight of lead oxide and has a specific surface of 5.0 to 6.0 meters²/gram and a specific gravity of 5.0 to 6.0 can be used.
- Carbon blacks that can be used include furnace black (particle diameter 30 to 100 millimicrons). A blend of two different carbon

blacks in a ratio near 1:1 by weight will give the optimal results. Each particle should range 30 to 40 millimicrons in diameter and should have an iodide number of 40 to 45 mg/g, a pour density of 20 to 25 pounds/foot³ (32 to 40 kg/m³) and a specific gravity of 1.80 to 1.82.

- Alumina hydrate is silica free, and 99 to 100 percent of the particles used in the composition are less than 2 microns in diameter.
- A mixture of antizonants is used. The first antizonant, an antioxidant is an aromatic amine. It is a 1:1 mixture of phenyl-B-naphthylamine and hindered diaryl-p-phenylene-diamine.
- The second antizonant is a wax antizonant. It is a blend of petroleum waxes with specific gravities of 0.88 to 0.92 and melting points of 70° to 80° C.
- Chlorinated paraffin waxes that can be used have 10 to 30 carbon atoms and are 20 to 70 percent chlorinated. Liquid waxes are preferred to aid neoprene plastication.
- Trialkylthioureas are process accelerators with up to four carbon alkyls.
- The bisphenol A diglycidyl ether has an epoxide equivalent of 185 to 192 and a molecular weight of approximately 380.

All components of this coating are commercially available.

This work was done by Charles W. Bright of Kennedy Space Center. For further information, Circle 32 on the TSP Request Card. KSC-11020



BASIC FORMULATION

100	Polychloroprene
3-5	Magnesium Oxide
4-6	Zinc Oxide
40-45	Carbon Black
9-11	Aluminum Oxide Hydrate
3-5	Aromatic Amine Antioxidant/Antizonant
0.75-1.25	Wax Antizonant
7-8	Chlorinated Paraffin Wax
0.75-1.25	Stearic Acid
1-2	Trialkylthiourea
0.1-0.5	Bisphenol A Diglycidyl Ether

The **Polychloroprene Composition** is cured for 15 to 30 minutes at 300° to 310° F. The percentage of each reactant in the formulation can be varied along with the time and temperature of the curing cycle. With each variation there is a corresponding variation in the characteristics of the product.

Soluble, Thermally-Stable Aromatic Polyimides

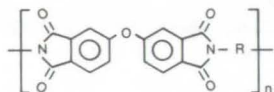
Incorporation of dianhydride monomers and *o,p'*-substituted diamines into polyimides increases solubility of the polymers in organic solvents.

Langley Research Center, Hampton, Virginia

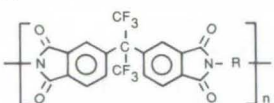
Aromatic polyimides, a very important class of polymers displaying excellent thermal stability, have been somewhat limited in use by their insolubility in organic solvents. A study was made wherein four novel dianhydride monomers with bridging groups intended to impart solubility were incorporated into the polymer chain and where the isomeric points of attachment of the bridging groups in the diamine monomers were varied to further enhance solubility.

The four dianhydrides form polymers with aromatic diamines as shown (where "R" represents an aromatic group):

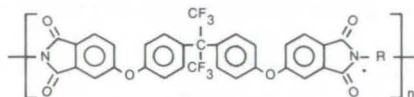
4,4'-oxydiphthalic anhydride (ODPA) forms:



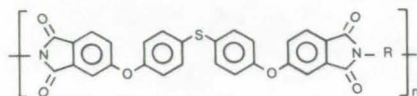
2,2-bis(3,4-dicarboxyphenyl)hexafluoropropane dianhydride (6F) forms:



2,2-bis[4-(3,4-dicarboxyphenoxy)phenyl] hexafluoropropane dianhydride (BFDA) forms:



4,4'-bis(3,4-dicarboxyphenoxy)diphenylsulfide dianhydride (BDSDA) forms:



The dianhydrides were reacted with isomeric variations of diamino-diphenylmethane (MDA), diamino-benzophenone (DABP), diamino-diphenyl ether (ODA), and phenylenediamine (PDA) to form polyamic acids that were spread into films and thermally converted, in air and in some cases nitrogen, to the polyimides.

The solubilities of films heated at 300° C were tested at 2 percent solids (w/w) at room temperature in N-methylpyrrolidone (NMP), dimethylacetamide (DMAc), N,N-dimethylformamide (DMF), and *m*-cresol. The tests showed that the use of ODPA, 6F, and BDSDA anhydrides led to polyimides with improved solubility properties. All BFDA polyimides, however, were insoluble in the solvents used, as well as in chloroform.

The positions at which amino groups attach to aromatic rings relative to bridging groups were also varied in these polyimides. The most widespread solubilities were

obtained by those polymers containing *o,p'*-diamines. Ortho substitution consistently effected the best solubility. Air-cured polymers containing MDA diamines were generally insoluble, but proved to be soluble when imidized in nitrogen instead of air.

Because of the unique enhanced solubility of the ortho-linked polymers, films of 6F-*o,p'*-ODA, BDSDA-*o,p'*-ODA, and ODPA-*o,p'*-ODA were further tested for solubility at higher concentrations in DMF at room temperature. Polyimide films of 6F-*o,p'*-ODA and BDSDA-*o,p'*-ODA were found to be completely soluble at 15 percent solids (w/w); and ODPA-*o,p'*-ODA was readily soluble to at least 40 percent solids (w/w).

The exploitation of these methods for producing soluble, high-molecular-weight polyimides is expected to increase the potential value of polyimides by significantly improving their processability.

This work was done by Terry L. St. Clair of Langley Research Center, A. K. St. Clair of Virginia Polytechnic Institute and State University, and E. N. Smith of Howard University. For further information, Circle 33 on the TSP Request Card.
LAR-12092

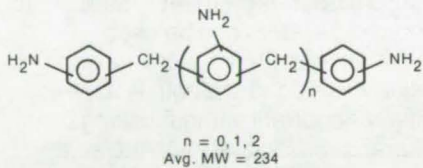
A New Polyimide Laminating Resin

Essentially solventless prepreg has improved drape and tack.

Langley Research Center, Hampton, Virginia

A new addition polyimide for composite materials is based on liquid monomers and has significant advantages over most existing high-temperature resins.

Most current polyimides for composites lack good drape and tack after the prepreg solvent is lost in the fabrication process. In high-

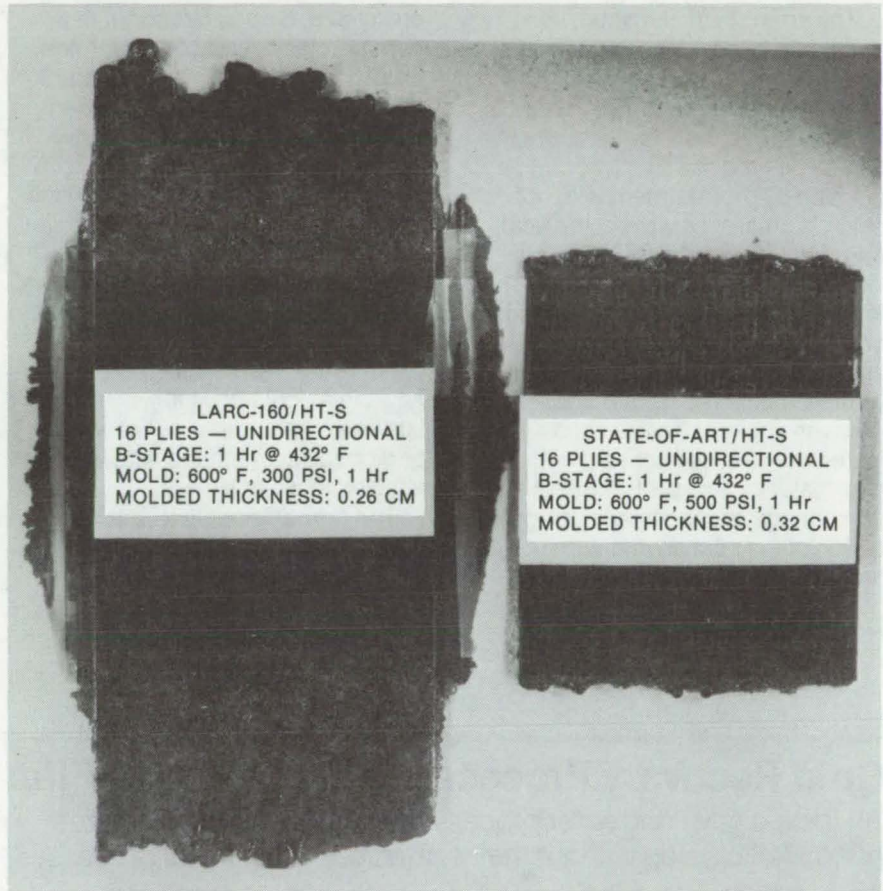


molecular-weight resin systems using the polyamic acid approach to polymerization, the loss of solvent in the prepreg leaves a stiff, "boardy" material that is difficult to work. In low-molecular-weight systems utilizing aromatic amine monomers, some solvent must be retained to prevent a loosely-held grainy deposit of monomeric solids on the reinforcing material.

The new polymer, designated LaRC-160, is a relatively-low-cost polyimide composite-matrix resin that retains its properties at 500° to 550° F (260° to 288° C). It has good drape, tack, and formability after the prepreg solvent is lost, and it is more easily processed than most high-temperature resins. These factors and the use of a nontoxic low-boiling solvent to produce an essentially solventless prepreg make LaRC-160 an attractive resin system.

LaRC-160 was prepared in ethanol, using 0.335 mole of the diethylester of benzophenone tetracarboxylic acid (BTDE), 0.610 mole of the ethylester of norbornene dicarboxylic acid (NE), and 0.539 mole of the polyamine shown below, where n may be 1, 2, or 3 and the average molecular weight is 234.

The LaRC-160 varnish had an average molecular weight of about 1,600, selected after the evaluation of various polymers in the 600-to-2,000 molecular weight range.



Comparison of Resin Flow for state-of-the-art composite (right) and LaRC-160 (left)

Criteria for selection were a combination of glass transition temperatures, flow characteristics, and mechanical properties.

The varnish was applied to drum-wound graphite fiber and was air-dried to produce an essentially solventless prepreg that displayed good drape, tack, and formability. Press molding produced composite laminates that were tested to determine flexural strengths and moduli and short-beam shear strengths. Excellent retention of the mechanical properties of the laminates was realized after prolonged exposure to high temperatures.

Flow characteristics, which generally present a serious problem

in the processing of polyimides, were excellent. Comparisons of LaRC-160/graphite fiber press-molded panels and state-of-the-art nadimide/graphite fiber press-molded panels are shown in the photograph. Processing conditions were not optimized for either resin system, but the B-staging and molding parameters used are reasonable for processing either addition-type polyimide. The imidized LaRC-160 flowed readily when heated above 500° F (260° C).

This work was done by John D. W. Barrick, Robert A. Jewell, and Terry L. St. Clair of **Langley Research Center**. For further information, Circle 34 on the TSP Request Card. LAR-12211

Pretreatment for Strong Aluminum/Epoxy/Aluminum Bonds

A new epoxy-compatible surface primer system permits room-temperature cure of high-strength aluminum-to-aluminum bonds without using corrosive chromate.

Goddard Space Flight Center, Greenbelt, Maryland

The strength of aluminum-to-aluminum bonds depends not only on the adhesive used but also on the surface pretreatment. For instance, the bond lap-shear tensile strength, using one type of adhesive, can be doubled by pretreatment with hot acid chromate. However, the acid chromate is very corrosive and is likely to damage adjacent parts. An improved epoxy-polyamide surface primer system produces bonds as strong as those following chromate pretreatment. The primer is compatible with epoxy adhesives and eliminates the need for hot acid chromate surface pretreatment and the damage caused by the corrosive action of the acid on nonaluminum parts.

The formulation is prepared by combining 5 parts by weight of

epoxy 828, 5 parts by weight of a commercially available polyamide, and 10 parts by weight of absolute methanol. The mixture is blended thoroughly and is kept tightly covered.

Aluminum surfaces to be bonded are cleaned with a slurry of alumina oxide having a particle size of 22 microns. The slurry is applied with a clean cloth and is rubbed repeatedly into the surfaces. The aluminum is clean when fresh distilled water flows in a continuous film over the surface. The surface is then wiped or dipped into methanol and is allowed to air-dry.

The primer is applied with a camel's-hair brush and is allowed to dry in a vacuum chamber at room temperature and at a pressure of 1×10^{-1} torr (13 N/m^2) for 10

minutes. It then is cured in an oven at a temperature of 100°C for 15 minutes.

The epoxy adhesive can be applied within the hour. The lap-shear tensile strength of such a bond is $2,565 \text{ lb/in.}^2$ ($17.69 \times 10^6 \text{ N/m}^2$) compared to $2,684 \text{ lb/in.}^2$ ($18.51 \times 10^6 \text{ N/m}^2$) when the acid chromate pretreatment is used. This nonacid system can be used whenever optimum aluminum-to-aluminum bond strength is especially important without risking the hazards associated with the acid system.

This work was done by Hossein Bahiman, Carroll Clatterbuck, and Aaron Fisher of Goddard Space Flight Center. For further information, Circle 35 on the TSP Request Card.
GSC-12232

Gold Recovery Process From Polyimide Film

An inexpensive and safer process recovers gold from goldized nonmetallic scrap without the hazards of conventional processes.

Lyndon B. Johnson Space Center, Houston, Texas

A process has been developed that economically separates gold from goldized polyimide film and other nonmetallic scrap. Conventionally, mercury or cyanide were used to remove the gold. In the new process, nitric acid is used to destroy the nonmetallic material and leave the gold intact.

The process can be summarized as follows:

1. Cut the polymer scrap into pieces suitable in size for boiling.
2. Place the cut pieces of polymer into an acid-resistant kettle, and fill with concentrated nitric acid. Heat slowly until the polymer scrap is dissolved completely (approximately 2 to 3 hours). The

usual cautions for working with boiling nitric acid should be taken.

3. Filter the solution through an acid-resistant/aspiration filter while the nitric acid solution is hot.
4. Wash the gold flakes in the filter several times with boiling nitric acid to remove residual polymer, then wash several times with hot water to rinse away the nitric acid.
5. Collect the gold flakes in a graphite crucible, and heat to 100°C to burn off all residual polymer and to dry the flakes. In conventional methods, mercury or cyanide (both highly toxic sub-

stances) are used. Although concentrated nitric acid must be handled cautiously, if proper safety measures are taken, the hazards are minimal. In addition, the process eliminates the additional separation process that is necessary in conventional methods to obtain a usable gold end product.

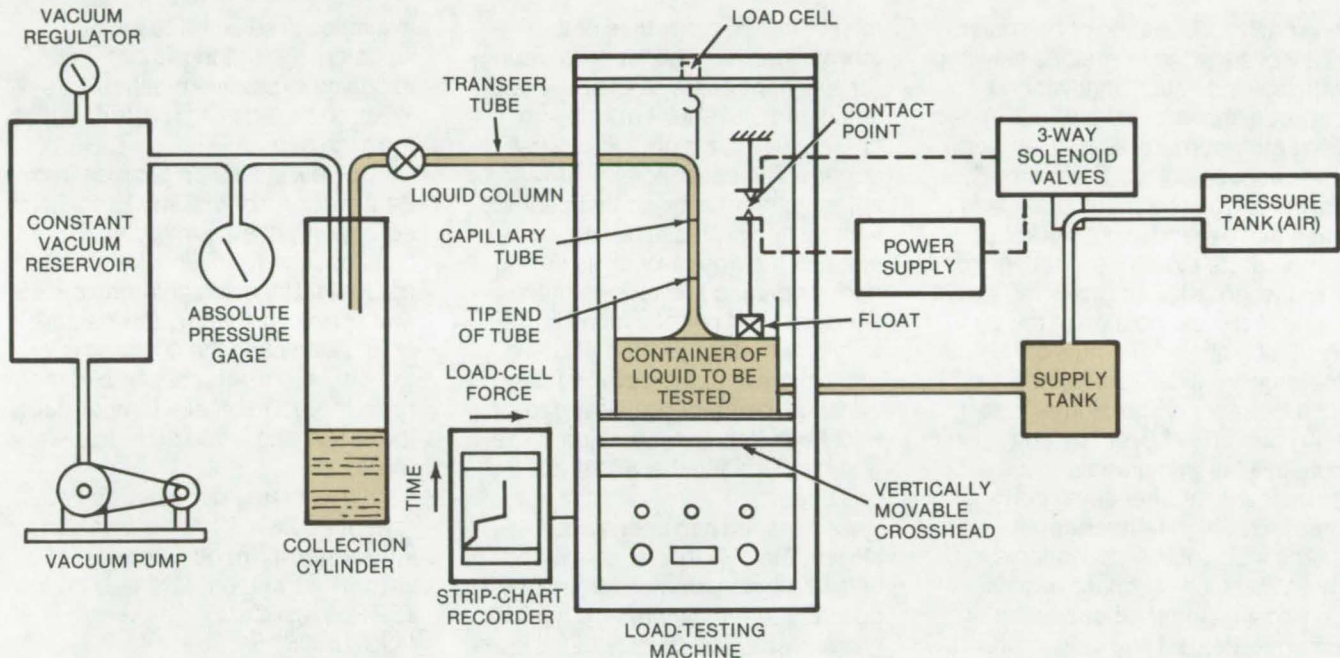
This work was done by Donald W. Houston and George Okamoto of Rockwell International Corp. for Johnson Space Center. No further documentation is available.

Inquiries concerning rights for the commercial use of this invention should be addressed to the Patent Counsel, Johnson Space Center [see page A8]. Refer to MSC-16650.

Tensile Viscosities of Non-Newtonian Fluids

A tubeless siphon technique allows accurate measurements of non-Newtonian liquids.

Caltech/JPL, Pasadena, California



Apparatus for Determining Tensile Viscosities: The load cell is zeroed while the tip of the capillary tube is resting on the liquid surface. This allows the force applied to the liquid column to be measured directly for any flow rate.

A tubeless siphon technique offers a practical means for accurately determining the tensile viscosity of a non-Newtonian liquid. This viscosity parameter, which measures the fluid resistance to extension or compression, may be compared with the more familiar shear viscosity, which characterizes its resistance to shear forces. When the viscosities are constants, independent of the deformation rate, the liquid is called "Newtonian," and there is a simple relationship between the coefficients, given by $\eta_t = 1/3 \eta_s$, where η_t and η_s are the tensile and shear viscosities respectively. For many viscoelastic liquids, such as polymer solutions, pseudo-plastic fluids, and slurries, neither viscosity is constant, and this relationship no longer holds. Preliminary measurements on dilute polymer solutions, using the new apparatus, have shown a very strong

dependence of the tensile viscosity on deformation rate and have yielded values for η_t that are on the order of 10^3 times that of the shear component extrapolated to zero shear rate.

With the apparatus shown in the accompanying figure, liquid is continuously drawn into a capillary from a reservoir container, by means of the partial vacuum maintained in a collection cylinder. The liquid continues to flow as the vertically-moving support crosshead is lowered, displacing the reservoir surface from the tip of the capillary. When the optimum separation has been established for a given flow rate, a symmetric, cylindrical liquid stream, known as a Fano column, is formed. Once stable flow has developed, the displacement D is held constant by adding liquid to the reservoir from a pressurized supply tank. The supply is regulated by

means of the float, electrical contacts, and solenoid valve arrangement shown.

A series of timed, sequential photographs record the varying liquid height in the collection cylinder and give the flow rate. Photographs are also taken of the liquid column profile. The force required to maintain a stable column at a given flow rate is measured, after zeroing, directly from the load cell, and is plotted on a strip-chart recorder. These data allow a determination of the tensile viscosity, using standard analytical techniques of continuum mechanics.

This work was done by Robert F. Landel and Steven T. J. Peng of Caltech/JPL and Robert T. S. Lin of Lockheed Aircraft Co. For further information, Circle 36 on the TSP Request Card.
NPO-13973

Resilient Thermal Barrier for High Temperatures

Bulk insulant exhibits
springback up to 982° C.

Lyndon B. Johnson Space Center, Houston, Texas

A barrier consisting of two layers of a woven fabric or braided sleeving with bulk insulation sandwiched between shows excellent resilience, even after compression at temperatures above 980° C. The thermal barrier provides a method of filling gaps that expand and contract at temperature extremes in an environment where a lack of covering would result in the destruction of the bulk insulation fibers. The new barrier material (a silicate cloth known as Irish Refrasil) is abrasion resistant, an improvement over currently-used bulk-insulation materials that exhibit permanent set after being compressed at high temperatures.

The insulant is also available in a more abrasion-resistant version. A composite alumina-boria-silica chromia-treated covering improves

the emittance properties of the thermal barrier. The fabric covering (or sleeving) contains the bulk insulation and prevents it from being blown away in a high-velocity gas stream. The covering also provides abrasion resistance so that contact with mating surfaces during vibration and rubbing (as well as flexing during opening and closing of the filled gap) will not cause the barrier to fail prematurely. The thickness and tightness of the covering may be adjusted to compensate for gap thickness, material abrasion, vibration, flexing, and the velocity of the gas stream.

As the filled gap opens and closes, the bulk insulation expands or is compressed, thus forcing the covering to remain pressed against the gap wall. The density of the bulk

insulation is selected to provide sufficient insulation without imposing excessive mechanical loads on the adjacent materials that form the gap.

The bulk insulation is made from Saffil alumina or of Saffil zirconia (or equivalent) fibers formed as a blanket or mat. The insulation is made rigid by using an organic resin that assists in shaping the insulation or in assembling the covering over the insulation. After assembly, the resin is burned off at a temperature lower than the final-use temperature.

This work was done by John A. Frye of Rockwell International Corp. for Johnson Space Center. For further information, Circle 37 on the TSP Request Card. MSC-16338

Obtaining Ultradry Crystalline Solids

Drying, cryogenic cooling, and then drying
reduce moisture to less than 0.01 percent.

Caltech/JPL, Pasadena, California

A new process for obtaining ultradry crystalline solids consists of:

- Evaporating the water on the surface of the crystals by conventional high-temperature and vacuum techniques,
- Cooling the solid with liquid nitrogen,
- Evaporating the coolant, and
- Redrying the crystals by conventional high-temperature and vacuum techniques.

The process is effective because, when cooled, almost all solids shrink; whereas, water expands as its temperature goes below 4° C. When a crystalline substance is cooled, the forces that develop within crystal regions surrounding trapped water break the crystal. Thus the trapped water is exposed, and a second drying step results in an ultradry solid.

The process has been successfully demonstrated with ammonium perchlorate (AP) crystals. This compound is used as an oxidizer in solid rocket propellants. One commercial technique is to dry the AP in ovens and store it in the desert for months in barrels with a desiccant. The moisture content after such a treatment is approximately 0.05 percent by weight. When required, only extensive drying of this material in high-temperature ovens lowers the water content below 0.01 percent.

AP from a wet crystallizer is dried faster, and more thoroughly as follows:

- Filter off as much water as possible by centrifugation or by vacuum filtration, wash the crystals with a nonsolvent
- Place the crystals in a vacuum oven (5 mm Hg/0.7×10³ N/m²) at

70° C for 4 hours. In this step the surface water is dried. Higher temperatures could be used for solids that decompose at higher temperatures than AP.

- Cool the crystals to room temperature, and dump them into liquid nitrogen for 15 minutes. (Different liquid coolants could be used.)
 - Decant the liquid nitrogen. Dry the crystals in a vacuum oven (5 mm Hg) at 70° C for 4 hours.
- This process dries the crystals to less than 0.01 percent water by weight (the limit of the apparatus used to measure the moisture) in less than 9 hours.

This work was done by Amir Attar of Caltech/JPL. No further documentation is available. NPO-13618

Books and Reports

These reports, studies, and handbooks are available from NASA as Technical Support Packages (TSP's) when a Request Card number is cited; otherwise they are available from one of NASA's Industrial Application Centers or the National Technical Information Service.

Controlling Stress-Corrosion Cracking

Design criteria help select alloys.

Stress corrosion of metals occurs more easily under the combined influence of sustained tensile stress and exposure to a corrosive environment. Even slight corrosion can lead to failure at a stress that a material would otherwise be expected to withstand; such failure is known as stress-corrosion cracking. To help designers of aerospace equipment, a brief report has been written outlining the characteristics of stress corrosion and the relative resistance of several alloys to this type of failure.

This published information could also be of interest to designers of bridges, pressure vessels, and other structures. Materials were tested at ambient temperatures under exposure to salt water, which is a common corrosive environment; and many commonly used materials were evaluated.

For instance, 300-series stainless steel, 1000-series aluminum alloys, and M1A magnesium alloys were found to be highly resistant to stress-corrosion cracking when formed under all common tempers. On the other hand, 440 stainless steel and 2014 aluminum were found to be quite susceptible to stress-corrosion cracking. In all, about 125 alloys and

tempers are rated as having high, moderate, or low resistance.

Also discussed are the effects of grain orientations in standard wrought forms, weldments, and stress induced by assembly tolerances and other often overlooked sources.

This work was done by D. B. Franklin, H. W. Herring, T. S. Humphries, E. C. McKannan, E. E. Nelson, and James G. Williamson of Marshall Space Flight Center. To learn how to obtain a copy of the report, Circle 38 on the TSP Request Card.

MFS-23416

Anodic Growth of Niobium Oxide

Growth kinetics studied using the current transient technique

The kinetics of metal-oxide growth on anodes have been studied extensively for several years. The two models most commonly used to explain the growth are the Frenkel defect model and the dielectric relaxation model. The growth kinetics of niobium oxide have now been examined experimentally, and the results related to these two models.

The Frenkel defect model assumes the generation of mobile ions within the oxide film by field-assisted thermal activation. The rate of mobile-ion creation is a function of the field alone, since the number of ions is much less than the number of possible creation sites. In the steady state, the ionic growth current can be related to the electric field and is equal to the external current. Transient effects occur when the system is subjected to a discontinuity in applied current; a certain time is required for the mobile-ion current to reach equilibrium.

In the dielectric relaxation model, the ionic growth current takes the same form as for the Frenkel defect model. However, formation of mobile ions depends on an effective electric field rather than the actual field. In this case, the transient effects are the result of a polarization field that must adjust to a new equilibrium level. Thus the two models are essentially the same under steady-state conditions, and the transient behavior must be studied to determine which one best explains the oxide growth.

Transient behavior can be observed by "instantaneously" increasing the current. The cell voltage then increases rapidly, reaches a maximum, decreases, and finally behaves as a steady-state linear function of time. Both models predict that the maximum change in cell voltage will depend linearly on both the film thickness and the log of the ratio of transient currents (initial to final).

Experiments, in which parameters were measured to within 1 percent, produced results that did not reconcile with either model. The maximum change in cell potential was found to be proportional to the log of the final-to-initial current ratio and the cell potential.

It is suggested that a more appropriate theory would be based on the variation of ionic mobility during a transient, rather than on carrier density or effective field. There may be more than one controlling mechanism, possibly one at the metal-oxide interface and one within the oxide itself.

This work was done by M. C. Davidson of Marshall Space Flight Center. For further information, Circle 39 on the TSP Request Card.

MFS-23150



Properties of Doped Cesium Iodide Crystals

Mechanical and thermal properties of sodium and thallium doped cesium iodide crystals

The radiation response and optical properties of undoped cesium iodide are readily available in the literature. However, the soft, ductile, and hygroscopic nature of cesium iodide makes it difficult to handle in large sizes (up to 1 meter diameter). On the other hand, cesium iodide that is doped with sodium or thallium is an excellent scintillator material for high-energy charged-particle detection, primarily because of its high density and scintillation efficiency. For this reason, a study has been conducted on the physical properties of doped cesium iodide crystals.

Large single crystals of cesium iodide doped with sodium and thallium were obtained from several commercial sources and were subjected to ultrasonic, tension, compression, and temperature-dependent tests. Young's modulus, bulk modulus, shear modulus, Poisson's ratio, the thermal expansion, and the thermal conductivity of each sample were determined. Since the crystals

varied in dopant concentration from the upper part to the lower part, test samples were cut parallel to the major axis of the crystal as well as parallel to the other axes. Testing was conducted in temperature-controlled rooms at a relative humidity below 50 percent.

The floating beam resonant technique was used to determine the elastic properties of the crystals. The resonant frequency of a uniform rod of the sample material was determined by suspending the sample at its nodal points on adjustable cross wires. Mechanical vibration was transmitted to the rod from a piezoelectric transducer and a fine coupling wire. A similar system received the mechanical vibration from the specimen. The signal increased sharply in amplitude as the signal from the oscillator approached the resonant frequency of the specimen.

Longitudinal and shear-wave ultrasonic velocity measurements were made by adjusting a calibrated acoustic path length through distilled water until sound propagation times through the sample and the water were equal. This technique was used to substantiate the Young's modulus values and to accurately determine bulk modulus, shear modulus, and Poisson's ratio.

Other physical testing included applying loads of tension and

compression at a constant rate of displacement. Measurements in tension were made by clamping the samples securely at each end. Strain measurements were made with bonded-resistance strain gages. The displacement of the clamps (0.005 cm/min for all measurements) and the load applied were measured simultaneously to yield the required stress/strain curves. The creep of different crystal samples under tension was also determined.

Thermal conductivity measurements of doped cesium iodide at three different temperatures showed little variation from those of undoped crystals. Thermal expansion coefficients were determined with a quartz-tube dilatometer. Measurements made at intervals of 20° F (11° C) from 0° to 300° F (-18° to 149° C) were linear within ±5 percent and accurate within ±2 percent.

This work was done by Robert Snyder of Marshall Space Flight Center. Further information may be found in NASA TM-X-64898 [N75-14908], "Physical Property Measurements of Doped Cesium Iodide Crystals" [\$4]. A copy may be purchased [prepayment required] from the National Technical Information Service, Springfield, Virginia 22151. MFS-23148

Life Sciences



**Hardware,
Techniques, and
Processes**

- 239 Virus Detection System
- 241 Bacteria/Virus Filter Membrane
- 241 Single-Donor Leukophoretic Technique
- 242 Aspirin/Metiamide Reduces Stomach Ulceration
- 244 Ultrasonic-Mammography Apparatus
- 245 Biological-Activity Monitor
- 246 Acquisition System for Biomedical Data
- 247 Drug-Dosage Indicator
- 248 Compact Reliable Multiaxis Pivot

Virus Detection System

A marker virus, monitored by a compact automatic system, is used to determine water-purification efficiency.

Lyndon B. Johnson Space Center, Houston, Texas

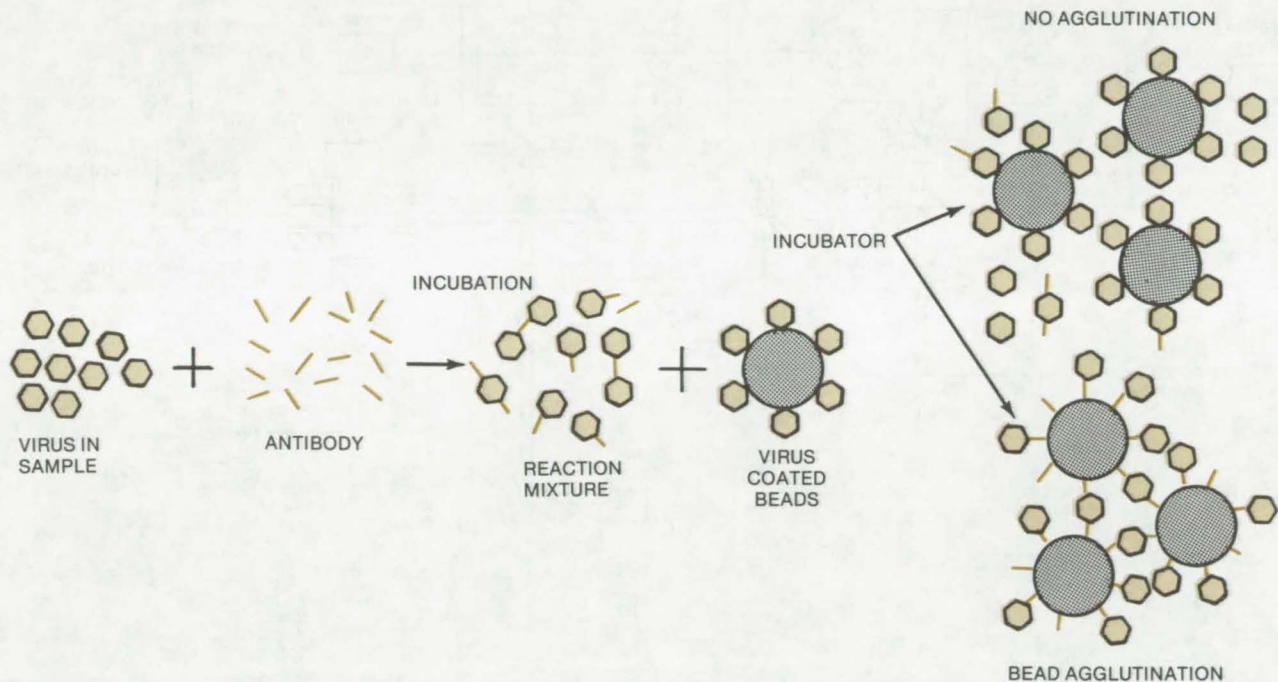


Figure 1. The **Indirect Passive Immune Reaction Sequence** is performed as follows: A sample test fluid is incubated with a predetermined concentration of antibody. Following incubation, antigen-coated latex beads are added for a second incubation. If free antibody is present at the end of the first incubation, bead clumping occurs during the second incubation. However, if the added antibody is completely bound by the presence of antigen in the test sample, then no bead clumping occurs.



A nonpathogenic marker virus is used to determine the ability of a water-reclamation system to reject the passage of viruses into potable water. The marker virus, bacteriophage F_2 , is introduced into the water-processing plant upstream from the recovery unit; downstream from the unit the reclaimed water is monitored by an automatic virus-detection system. The marker virus is especially chosen for its detectability. Acting as a tracer, the virus, by its presence or absence indicates whether other, more toxic, viruses have survived the purification process.

The virus monitoring system operates in two stages: concentration and detection. To concentrate the marker, the virus is adsorbed in cellulose acetate filters in the pre-

sence of trivalent cations and low pH ($AlCl_3$). Subsequent viral desorption uses small volumes of high-pH buffer.

Viral detection is performed via a passive immune agglutination (PIA) test (see Figure 1) that uses specially-prepared polystyrene particles to which either an antigen or an antibody is bound.

In the detection system, either a direct or an indirect PIA technique can be used. When testing via the direct method, an antibody is bound to latex beads. For assay, the beads are incubated with a test sample. The presence of an antigen in the test sample results in cross-linking between the beads and aggregation. When testing via the indirect method, an antigen is bound to the beads.

The waste-water detection system can concentrate a 400-ml sample to 3 ml in approximately 20 minutes with nearly 100 percent recovery of the bacteriophage. As shown in Figure 2, it consists of a reagent pump and metering system, reagent-storage containers, a filter concentrator, an incubation/detector system, and an electronic readout and control system. Using this arrangement and the PIA viral detection, marker virus can be detected at a concentration of 1×10^9 plaque-forming units (PFU)/ml.

The reagent pump/metering system uses peristaltic pumps to control the flow sequence of reagents and sample. Reagents are stored in collapsible, flexible-diaphragm containers. The

(continued on next page)

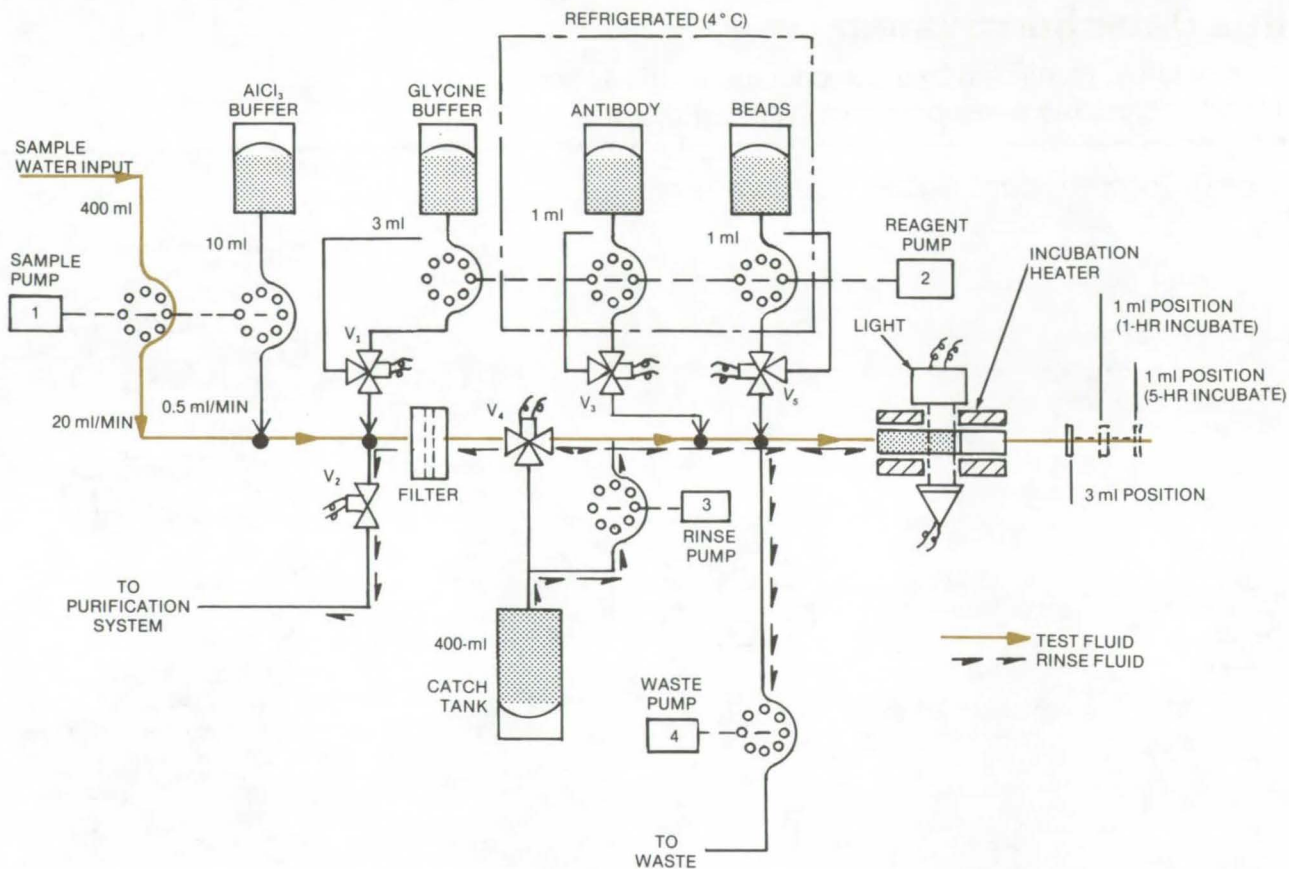


Figure 2. The **Peristaltic Pump Metering System** has two main steps: concentration and detection. The marker virus introduced via the sample-water input port is concentrated from 400 to 3 ml. This system uses a cellulose acetate filter to adsorb viral samples in the presence of $AlCl_3$ and low pH, with subsequent desorption from the filter at high pH. Before passing through the filter, the $AlCl_3$ buffer is added to lower the sample pH to 2.5 to 3.0. Following the treated sample, an additional 10-ml sample of untreated sample is reverse pumped via the catch tank through the filter to remove residual $AlCl_3$. To remove the adsorbed virus, 11.5-pH glycine buffer is pumped through the filter in two timed stages. Next a 1.0-ml sample of a pre-determined dilution of anti-marker-virus antibody is added and the mixture is incubated for a half hour at 45° C. Following this, a predetermined dilution of marker-virus-coated latex beads is added; a spectrophotometric reading is taken to determine the light transmission of the suspension. The mixture is then incubated for 5 hours, and the light transmission is again checked and compared to the original reading.

incubator/detector cell is a syringe such as those used with gas chromatographs. A transmitted-light photometer detects the amount of light varying directly with particle agglutination. A heater blanket keeps the reaction cell at the desired temperature.

If bead agglutination occurs as a result of free antibody interacting with the marker-virus-coated beads, an increase in light transmission results. The test is thus considered

negative for marker virus in the concentrate. If no (or partial) agglutination occurs, the test is positive, indicating complete or partial inactivation of the antibody by the presence of marker virus.

This work was done by Alan S. Fraser, Harold J. Tenoso, Arthur F. Wells, and Carl B. Linnecke of Organon Diagnostics for **Johnson Space Center**. Further information may be found in NASA CR-147491 [N76-19782], "Water System Virus

Detection," [\$6.75]. A copy may be purchased [prepayment required] from the National Technical Information Service, Springfield, Virginia 22151.

This invention is owned by NASA, and a patent application has been filed. Inquiries concerning non-exclusive or exclusive license for its commercial development should be addressed to the Patent Counsel, Johnson Space Center [see page A8]. Refer to MSC-16098.

Bacteria/Virus Filter Membrane

Hollow acrylate fiber membranes that filter bacterial and viral organisms have multiple applications.

Lyndon B. Johnson Space Center, Houston, Texas

An improved hollow acrylate fiber membrane that filters bacterial and viral organisms can be used with closed-cycle life-support systems for underwater habitations or laboratories. The membrane also has applications in the fields of medicine, gnotobiotics, pharmaceutical production, and industries and research facilities that require sterile water.

Hollow-fiber membranes are thin separative barriers that are tubular in shape. Bundles of loosely-packed, uniformly-distributed tubular membranes can be headered at each end and encapsulated to form an ultrafiltration cartridge that collects the pressurized fluid that passes through the membrane walls. Water that is contaminated with bacterial and viral agents passes through the ultrafiltration cartridge and is collec-

ted in the housing for removal from the unit. The liquid flows through the pores in the membrane wall by bulk flow. Bacterial/viral contamination will not pass through the membrane wall and is retained within the hollow-fiber membrane. Membranes withstand challenges of 10^6 bacterial organisms and 10^4 viral organisms per cubic centimeter.

This device should prove simpler and more efficient than most conventional filtration techniques. It eliminates the need for strong chemicals or sterilizing agents and therefore should significantly reduce the operation cost. The device also has the advantage of being smaller than commercially-available bacterial filters and can substitute for them in almost any application. Further study and analysis will more accurately determine long-life capabilities and economic benefits.

Testing and a feasibility study for applications of hollow-fiber membranes are described in a report, "Hollow Fiber Membrane Systems for Advanced Life Support Systems." Also discussed are breadboard development of three specific applications: heat rejection, deaeration, and bacteria filtration.

This work was done by Michael S. Lysaght of Amicon Corp. and Frederick Goodwin and George Roebelen of United Technologies for Johnson Space Center. Further information may be found in NASA CR-151149 [N77-15643], "Hollow Fiber Membrane Systems for Advanced Life Support Systems" [\$9.00]. A copy may be purchased [prepayment required] from the National Technical Information Service, Springfield, Virginia 22151. MSC-16388

Single-Donor Leukophoretic Technique

A fast and efficient granulocyte and monocyte separation-and-retrieval technique has applications in biological and chemical processing, and veterinary research and clinical care.

Lyndon B. Johnson Space Center, Houston, Texas

A new leukocyte separation-and-retrieval device utilizes the granulocyte and monocyte property of leukoadhesion to glass surfaces as the basis of their separation from whole blood. The separator is used with a single-donor technique. Rather than collecting large amounts of blood from several donors to extract a desired quantity of white blood cells, blood from a single donor is processed with a continuous-flow device. The donor's blood is circulated through a separator, for several hours, to remove only the white blood cells. Originally, nylon wool was used as the extracting medium; but the cell

recovery was unpredictable and there was significant loss of viability and damage to the cells.

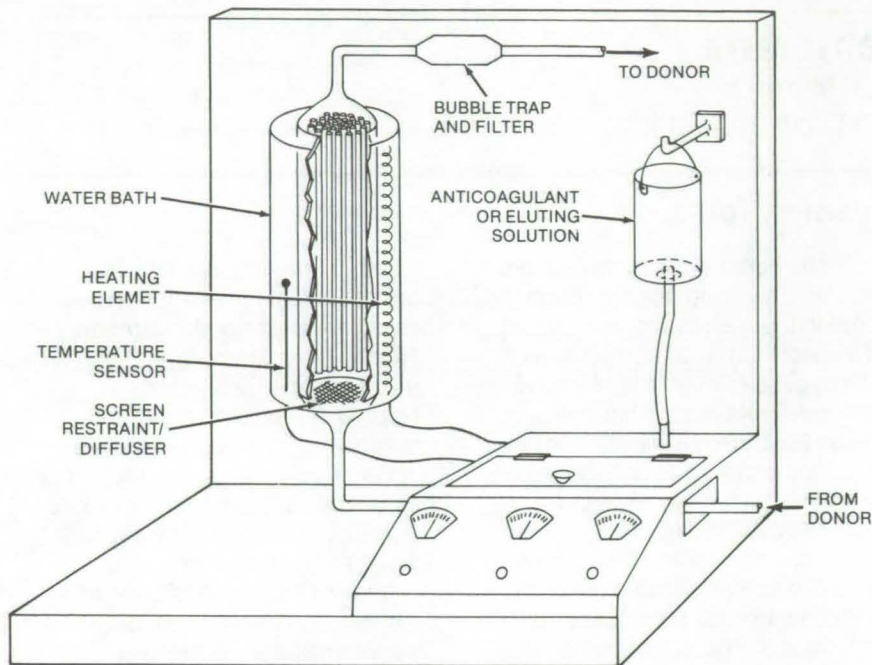
Initial tests indicate that a new glass-capillary technique yields efficiencies from 60 to 70 percent (compared to 50 percent for nylon wool) and that all viability was approximately 90 percent. Commercially-available glass capillary tubes, with an internal diameter of 0.30 cm and a length of 40 cm, are packed inside a large-diameter glass column that is siliconized and sterilized. They are held in place by a 100-mesh stainless-steel screen restraint/diffuser that prevents the tubes from slipping down into the

inlet tube, and spreads the flow of whole blood evenly across the cross-sectional flow area of the capillary tube network. Temperature control is maintained by a water bath that surrounds the glass column. The velocity of the whole blood is regulated at an optimum 10.9 cm/min. A 20-percent heparinized plasma in Hank's balanced salt solution (HBSS) flows through the column at a prescribed rate to condition the glass surface for optimum cell adhesion.

As the whole blood flows from the bottom to the top of the column, granulocytes and monocytes

(continued on next page)





The **Capillary-Tube Separator** for white blood cells is designed to circulate blood from a single donor to obtain large quantities of white blood cells. White cells adhere to the walls of the glass capillaries more efficiently and with less damage than occurred with previous nylon wool separators.

migrate and adhere to both the inner and outer capillary tube walls, while the stream containing the red cells, platelets, and lymphocytes passes through the column, is debubbled, and is returned to the donor. A 20-percent homologous ACD (Formula A) plasma in normal saline solution is used to wash the cells from the column wall.

The flow of blood through the small-diameter tubes closely approximates the flow of blood through the human body, and the flow resist-

ance remains constant with time when the system is operated in a continuous-flow loop with the donor. As a result, the nonadherent red blood cells, platelets, and lymphocytes are subjected to far less trauma before reinfusion into the donor. Dye-exclusion and phagocytosis of latex particles indicate that approximately 90 percent of the recovered granulocytes remain viable. Recovered monocytes also retain their capability to stimulate bone-marrow colony growth.

The new device recovers approximately 10^{11} (absolute count) white blood cells in a 3-hour to 4-hour period of time when run in a continuous-flow loop. A single donor provides a quantity of cells that ordinarily requires multiple donors, using more conventional separation and recovery techniques; and at no time is more than 1 liter of blood removed from the donor. In addition, the donor can be more closely cross-matched with the patient undergoing testing for, or treatment of, leukemia or other blood disorders, thereby decreasing transfusion risk.

A subscale model of the separator has been built and tested, and the results have been published in a report: "Separation of Granulocytes from Whole Blood by Leuko-adhesion." This report includes in-vitro studies of factors affecting leuko-adhesion and a detailed analysis of the separator flow system.

This work was done by Ralph N. Eberhard of Martin Marietta Corp. for Johnson Space Center.

Further information may be found in NASA CR-147883 [N76-31894], "Separation of Granulocytes from Whole Blood by Leuko-adhesion," [\$4.50]. A copy may be obtained [prepayment required] from the National Technical Information Service, Springfield, Virginia 22151.

Inquiries concerning rights for the commercial use of this invention should be addressed to the Patent Counsel, Johnson Space Center [see page A8]. Refer to MSC-16297.

Aspirin/Metiamide Reduces Stomach Ulceration

Stomach ulceration accompanying aspirin use and stress is reduced by a recently developed antihistamine.

Ames Research Center, Moffett Field, California

A new combination of aspirin and metiamide reduces gastric erosion or ulceration that can occur under stress when aspirin is taken alone. Metiamide, a recently-synthesized antihistamine specific to H₂ receptors, has been tested on rats and

shown effective in inhibiting stress-induced ulceration with and without aspirin.

The metiamide appears to inhibit the secretion of gastric acid by blocking the H₂ histamine receptors. Pyrilamine, which specif-

ically blocks H₁ histamine receptors, does not provide the same relief. It is expected that cimetidine, another H₂ specific antihistamine, would be as effective as the metiamide.

Animal tests were performed by

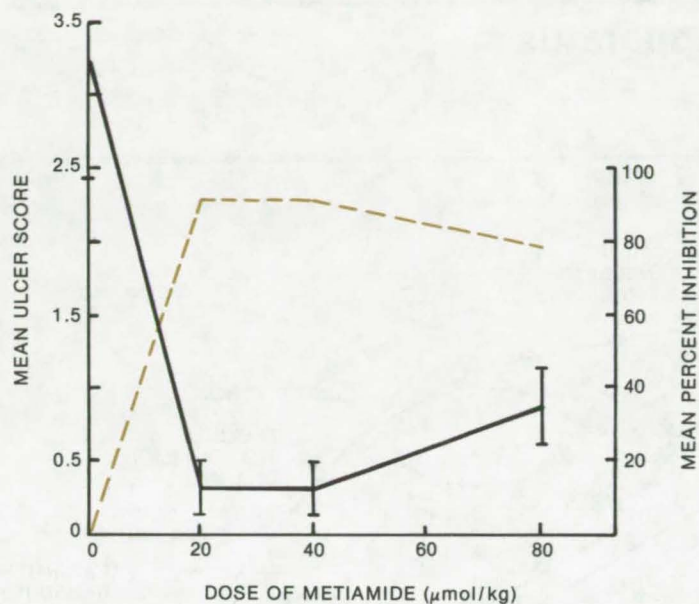


Figure 1. **Metiamide Tests Without Aspirin** were conducted by subjecting animals to stress. Those receiving no drug had a mean ulcer (MU) score of 3.3 (the sum of maximum continuous lengths (in mm) of ulcers observed). Animals receiving the lowest dose of metiamide (20 μmol/kg) had a MU score of 0.3, a reduction of 90 percent from the no drug condition. At higher dosages, fewer than half the animals had ulcers. In the figures, the solid lines show the mean ulcer scores, while the broken lines indicate the mean percent ulcer inhibition.

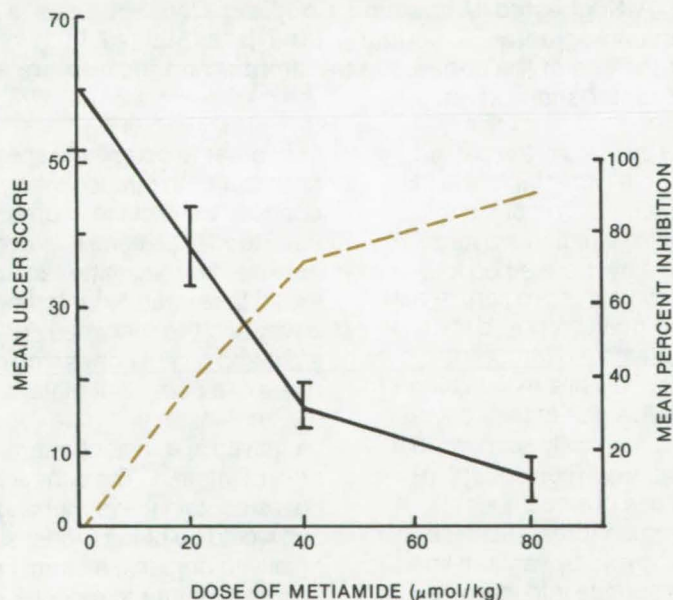


Figure 2. **Metiamide Tests With Aspirin** were also conducted while subjecting the animals to stress. The MU score of those not receiving metiamide was 61.3, a level much higher than that observed for stress alone (3.3). At the lowest dosage of metiamide, a decrease of 39 percent to an MU score of 37.1 was noted. At 80 μmol/kg, the MU score was reduced by 90 percent to 6.3. At this level, most of the animals ulcerated, but the ulcers were quite small. Metiamide was found to have no significant effect on plasma corticosterone levels, thus probably eliminating the adrenal cortex as a factor in this process.

depriving rats of food for 24 hours and restraining them in a chamber at 5° C to produce ulcers. Thirty minutes before they were subjected to these stresses, each rat was given doses of metiamide from 0 to 80 μmol/kg, and one-half of them were simultaneously given 440 μmol/kg of aspirin. After 2 hours of the cold restraint, each animal was sacrificed, and its stomach was examined for ulceration (Figures 1 and 2). Blood was collected, and plasma corticosterone determinations were made.

The successful results indicate that this new formulation could help relieve gastric distress in patients who take large doses of aspirin for diseases such as rheumatoid arthritis.

This work was done by Joan Vernikos-Danellis of Ames Research Center and Patricia A. Brown of San Jose State University. For further information, Circle 40 on the TSP Request Card.

This invention is owned by NASA, and a patent application has been filed. Inquiries concerning nonexclusive or exclusive license for its commercial development should be addressed to the Patent Counsel, Ames Research Center [see page A8]. Refer to ARC-11038.



Ultrasonic-Mammography Apparatus

Improved transmitter/tissue/receiver coupling could enhance sensitivity of tests.

Caltech/JPL, Pasadena, California

One of the major problems in applying ultrasonic analysis for the detection of tumors in breasts and other tissues lies in effectively coupling the ultrasonic signal to the tissue being examined. Ultrasonic signals, because of their relatively low energy, are much more complicated by air and other boundaries than are X-rays.

In routine ultrasonic diagnosis by reflection or transmission, the transducer is moved over the surface of the object (skin) in a raster manner. These movements are coupled and translated to the X-Y coordinates of a CRT or other display, which records the amplitude or other properties of the reflected or transmitted signal as modified by the object under study.

An alternate method in common use is to immerse the object in a liquid that generally matches the ultrasonic properties of the object being explored. If the properties of the immersing medium match those of the specimen, the sound energy will be effectively coupled into the object with minimum loss and a minimum disturbing reflection and refraction at the immersed boundary.

The transmitter and receiver operate best if the path between them produces a uniform delay base. In this condition, the nonuniformities in the intervening tissue result in an optimum signal that makes distinguishable subtle differences in tissue properties. This condition can be met by immersing the body portion in water. For body parts such as arms and legs this would not be restrictive, but would impose some protocols for contamination control.

In the case of diagnosis of the breast for lesions, however, the positioning of the patient may become difficult. Tumors in the lower portion of the breast are

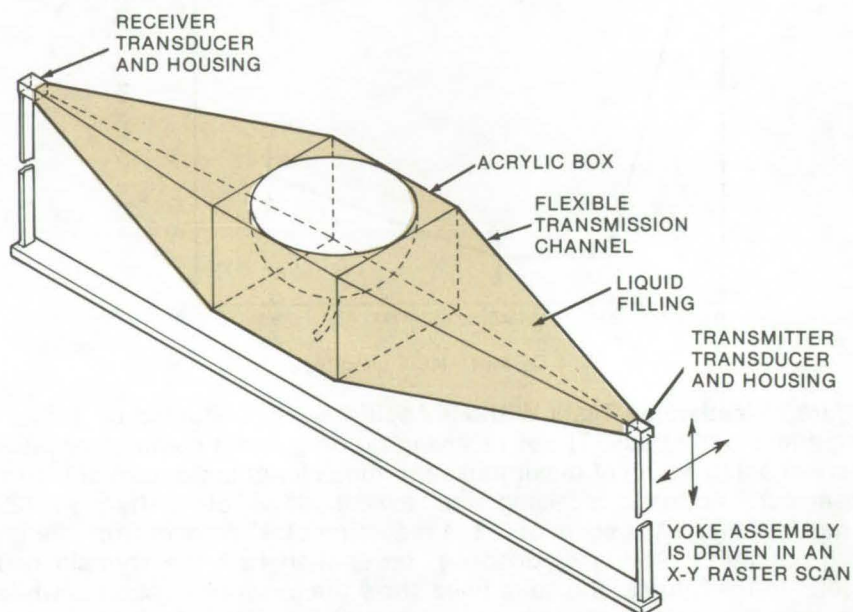


Figure 1. A Suggested Ultrasound Coupling Concept uses a shaped well for mammography. A coupling fluid is contained in two flexible cones. At the end of the cones, the transmitter and receiver are attached to an X-Y raster-scan driver.

accessible by placing the patient prone over the water tank with the breast immersed. Tumors in the critical pectoral region are largely inaccessible by this method.

To overcome this problem, a new method has been proposed for directing ultrasound through a sample volume while maintaining coupling with a pair of transducers that are mechanically scanned in a raster geometry. The concept involves the use of a chamber into which the organ (breast) can be inserted or drawn by vacuum so as to bring its surface into intimate contact with the walls of the cavity. The mating surfaces may be lubricated with a liquid or gel, if necessary, to facilitate entry and ensure good uniform contact. The cavity may be a rigid material with properties that match the specimen, or it may be a compliant material supported by a reinforcing wall.

In the approach shown in Figure

1, in order to couple the specimen chamber to the transducers, two opposite walls of the chamber would be extended as cones. In conical apices, the transmitter and receiver would face each other through the cavity and the specimen. These input and output cones would be made of a compliant material so that the transmitter and receiver could be moved in a raster pattern over the area of interest. The compliant cones contain the immersing liquid and would be of the proper size and rigidity to preserve a direct path from transmitter to receiver, regardless of any flexure imposed by the mechanical drive.

This system has the added advantage that an organ is constrained against random movement that would blur or obscure small details. Another major advantage is that the patient may be in a comfortable position, either sitting or prone with the anterior surface up.

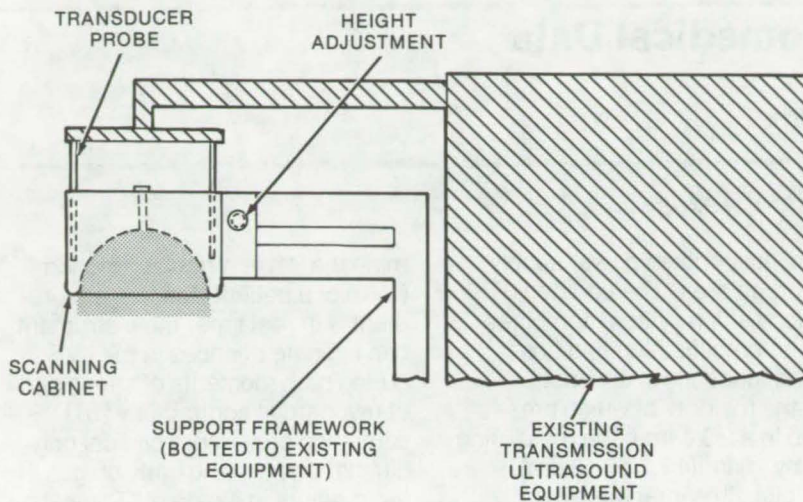


Figure 2. A **Second Coupling Approach** is similar to that proposed in Figure 1. A shaped well would be attached to existing ultrasonic equipment, with the transducer probes immersed within the coupling liquid surrounding the well.

A slightly different approach has been suggested as shown in Figure 2. A patient is placed prone with the anterior side up on a wheeled cot or gurney having a slightly tilted surface and is moved to a position under the scanning cabinet. The

scanning cabinet is mounted on a support framework bolted to the ultrasound transmitter and receiver cabinet, and is free to move along a vertical axis. The height adjustment, in combination with the movable gurney, allows the scanning cabinet

to be centered over the breast, and the raster scan can be taken over a significant area of the pectoral region. The breast is drawn by a vacuum so as to be contiguous with an acrylic cavity centered in the scanning cabinet and forming the interface between the transmission medium and the breast tissue. The transmission media include a liquid contained by the walls of the scanning cabinet and the acrylic walls of the cavity. The transducer probes are immersed in the liquid on either side of the acrylic cavity so as to form a path through the cavity from one probe to the other.

This work was done by Owen C. Buchea and Robert E. Frazer of Caltech/JPL. For further information, Circle 41 on the TSP Request Card.

Inquiries concerning rights for the commercial use of this invention should be addressed to the Patent Counsel, NASA Resident Legal Office-JPL [see page A8]. Refer to NPO-13935.

Biological-Activity Monitor

Ingested fluorescent precursors could be tracked after excretion as fluorescent compounds to monitor activities ranging from metabolism to migration.



Caltech/JPL, Pasadena, California

In a proposed technique for detecting and tracking biological activity, fluorescent precursors are introduced into specimens. These will be modified by metabolic processes to produce fluorescent components that can be detected with known instruments for exciting and detecting specific wavelengths of fluorescent radiation.

The precursors could be delivered to the living subject through ingestion, inhalation, or skin contact. Once in the metabolic pathway, the precursors would be altered by the action of enzymes, and a resulting fluorochrome would be excreted. The precursors could be chosen to

result in fluorochromes that do not occur naturally. Thus their detection would be a specific indication of the movement of the particular subject of interest.

There are a number of possible applications for this concept. For example, a nontoxic precursor could be sprayed over a grassland area to observe the patterns of migrating birds. If a way were found to bind precursors with foods, the excretion of fluorochromes might be used as an indicator of metabolic rates, and it might be possible to note enzyme deficiencies indicative of certain diseases by the failure of a subject to metabolize precursors properly.

The detection of the fluorescence requires excitation, which might best be done with a UV laser. Portable xenon and mercury spotlights could also be used. Detection is possible with a system as simple as a pair of eyeglasses with a narrow-band filter at the emission wavelength of interest. More sophisticated systems could be designed based on existing UV fluorescence spectrometers, and a number of intermediate approaches are possible.

This work was done by Robert E. Frazer and Marylou Ingram of Caltech/JPL. For further information, Circle 42 on the TSP Request Card. NPO-14089

Acquisition System for Biomedical Data

Systolic time intervals are fed to (and conditioned by) one instrument in real time.

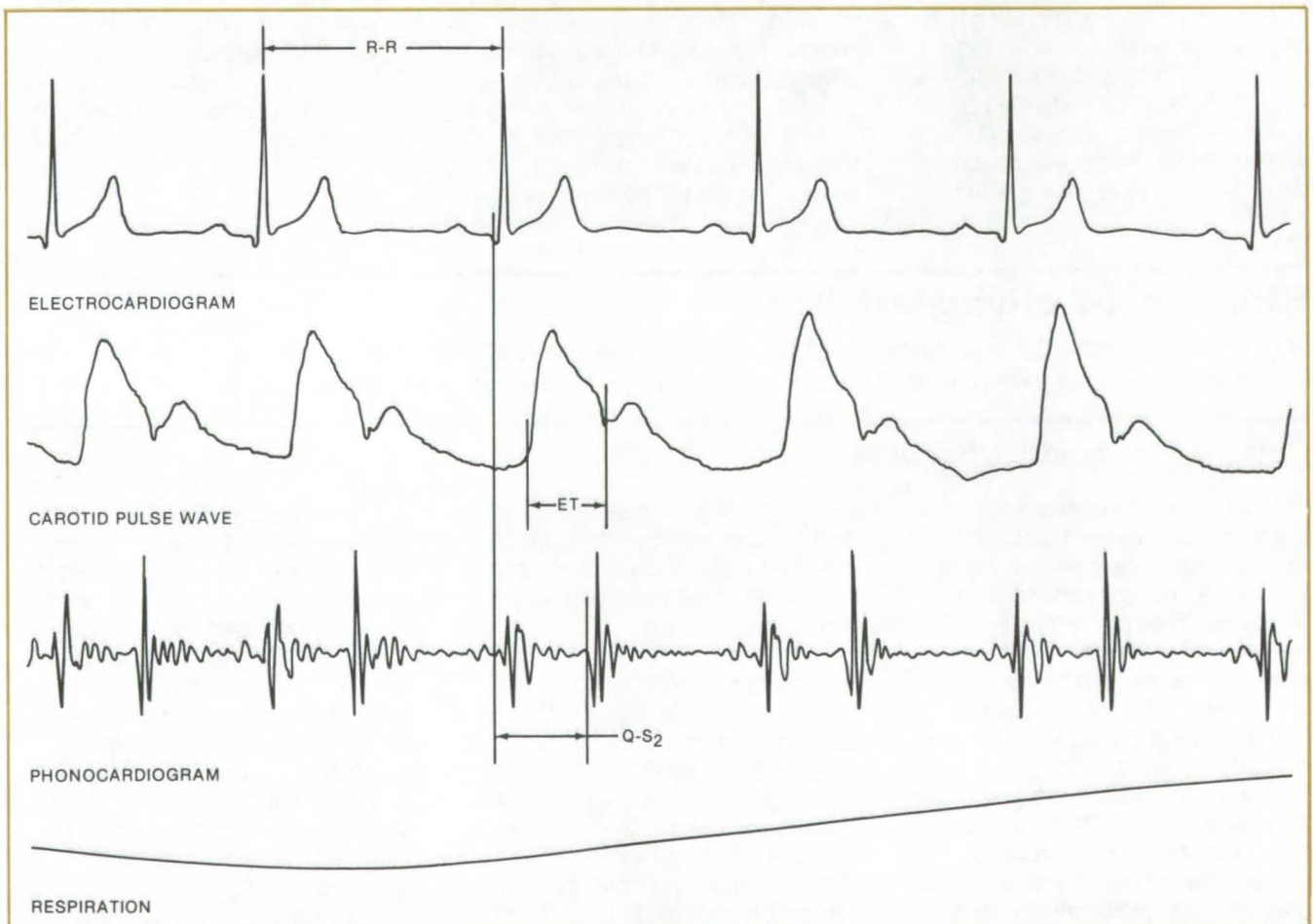
Lyndon B. Johnson Space Center, Houston, Texas

A multifunction biomedical data-acquisition system monitors the cardiovascular and pulmonary performance of a patient in real time. The instrument gathers data from four noninvasive sensors that, with suitable signal conditioning, enable systolic time interval (STI) evaluation. After the data are conditioned, they are fed to a strip-chart recorder, a tape recorder, or a computer for analysis. Previously, STI evaluation was made by using several instruments, each requiring

its own independent power supply and storage area. The updated STI data-acquisition system combines all signal-amplification and conditioning functions in one instrument, the majority of which are located in a PC card cage measuring 5-1/4 by 10 in. (13.5 by 48 cm).

Systolic time intervals are a group of measurements taken within a time domain made from both the electrical and mechanical events present in the cardiopulmonary cycle. STI testing is used to deter-

mine the left ventricular function (LVF) of a patient. Since measurement is in real time, the instrument can indicate changes in the LVF during both moments of stress and of myocardial contractility. STI screening can, under clinical conditions, pinpoint the early stages of heart failure in a patient. The instrument also can be made portable; in the ruggedized version, it could be used onsite during emergencies such as floods and earthquakes.



The **Systolic Time Interval** is determined from calculations based on the parameters displayed. The R-R interval indicates instantaneous heart rate prior to the measured beat. Total electromechanical systole (Q-S₂) is measured from the onset of the electrocardiogram Q-wave to that of the second (S₂) heart sound. Ejection time (ET) is measured from carotid upstroke to the incisure. The preejection period (PEP) is computed by subtracting ET from Q-S₂; the PEP/ET ratio is thus directly established.

The four parameters used to evaluate STI are:

- Electrocardiogram — the Q-wave is used for timing;
- Carotid pulse — obtained via a strain-gage transducer placed over either carotid artery;
- Phonocardiogram — obtained via a microphone transducer located on the chest and used to record the first (S₁) heart sound and the second (S₂) heart sound; and
- Respiration — recorded via a temperature-sensitive transducer as the patient exhales.

The systolic-time-interval data-acquisition system is assembled in two units connected by a cable. One

contains the signal conditioners and dc power supply. The second contains the controls accessible to the operator, such as gain and offset adjustments that allow optimization of the transducer signals (typical waveforms of each are shown). The carotid pulse sensor is a force transducer held to the carotid artery, using a strap. Phonocardiogram signals are transduced, using a piezoelectric accelerometer-type microphone. The low weight of the sensor applied to the chest wall, using double-backed adhesive tape, matches the mechanical impedance of the wall. Respiration is taken via a strain-gage pneumogram taped to

the chest or by a temperature-sensitive pneumogram located in the airstream just outside the nostrils. Transducer type depends upon the condition of the patient.

This work was done by Stuart A. Bergman, Jr., and George W. Hoffer of Johnson Space Center and Joseph T. Baker, William G. Crosier, and John A. Donaldson of Technology Inc. Further information may be found in NASA CR-151213 [N77-18725], "Systolic Time Interval Data Acquisition System." A copy may be obtained for \$4.00 [prepayment required] from the National Technical Information Service, Springfield, Virginia 22151. MSC-16144

Drug-Dosage Indicator

Indicator on containers allows patients to keep track of medication intake.

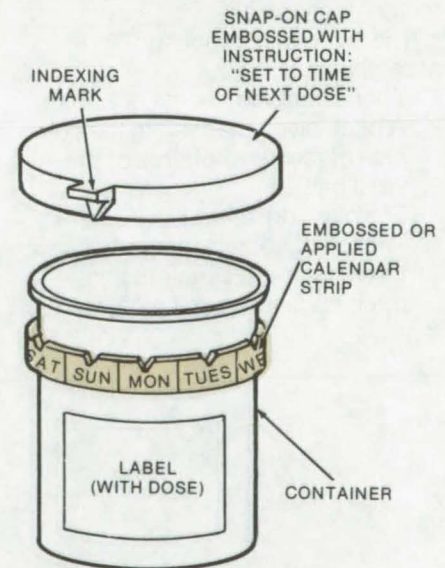
Goddard Space Flight Center, Greenbelt, Maryland

A simple indicator that can be made part of a typical drug container serves as a reminder of the time the next dose of medication is due and the time that the last dose was taken. The indicator is set manually by the patient and can be used to help dispense either loose tablets or liquids.

Inexpensive to manufacture, the indicator is merely a pointer and a "calendar." As shown in the illustration, the pointer is part of a snap-on cap; and the days of the week, hours of the day, or other dosage

periods are marked on a ring that is embossed on the container or vial that holds the medication. In practice, after dispensing a dosage of medication, the patient replaces and rotates the snap-on cap so that the pointer indicates the next dosage period that appears on the sequential dosage "calendar." This is done each time a dose is taken.

This work was done by Werner M. Neupert of Goddard Space Flight Center. No further documentation is available. GSC-12139



Snap-On Cap can be embossed with the instruction "Set to Time of Next Dose," and the "calendar" of sequential dosage times can be subdivided if more than one dose per day is indicated.

Compact Reliable Multiaxis Pivot

Manipulator-arm pivot wrist could be used with prosthetics.

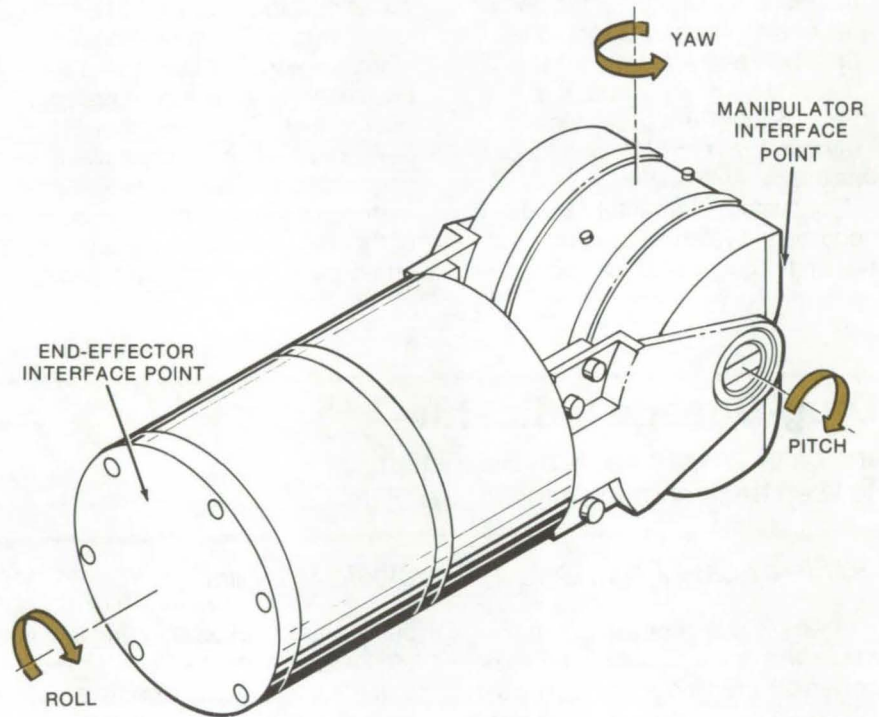
Marshall Space Flight Center, Alabama

A triple-axis pivot-arm wrist developed for the wrist joint of a remote-manipulator arm allows three degrees of freedom in the wrist joint: roll (continuous), yaw ($\pm 45^\circ$), and pitch ($\pm 90^\circ$). It also contains power-chain components sufficient for a torque of 15 ft-lb (20J). It could serve as a compact and highly-reliable multiaxis pivot for prosthetics.

The assembly can supply full torque on each axis, and it overcomes the "weak-wrist" problem common in the design of remote manipulators. The number of vectors required to control wrist position are three less than for previous models. The joint is quite compact, and it could be made triply redundant by clustering three motors for each axis.

There are four major sub-assemblies:

1. A wrist ball with 14 major parts,
2. A pitch pivot attached to the outside of the hemispheres of the wrist ball,
3. The pitch drive, and
4. The roll drive, which also houses three pitch-drive motors and three continuous-roll motors.

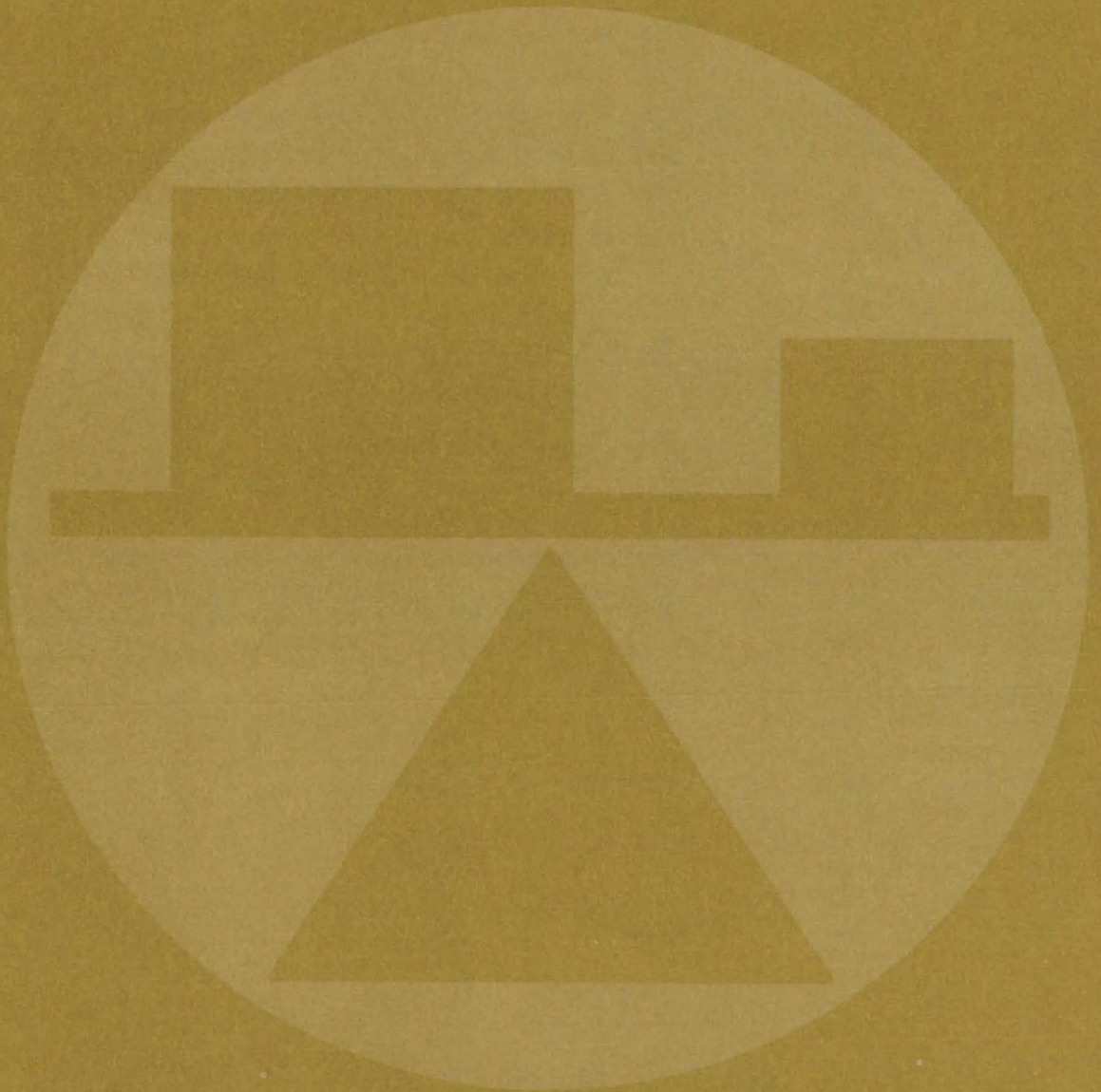


The Triple-Axis Common-Pivot Arm Wrist has three degrees of freedom: continuous roll, $\pm 90^\circ$ pitch, $\pm 45^\circ$ yaw. It weighs 15 lbs (6.7 kg) and can apply a torque of 15 ft-lbs (20 J).

*This work was done by J. Dwight Johnston of **Marshall Space Flight Center** and Leendert Kersten of the University of Nebraska. For further information, Circle 43 on the TSP Request Card.*

This invention is owned by NASA, and a patent application has been filed. Inquiries concerning nonexclusive or exclusive license for its commercial development should be addressed to the Patent Counsel, Marshall Space Flight Center [see page A8]. Refer to MFS-23311.

Mechanics



Hardware, Techniques, and Processes

- 251 Improved Accuracy With Phase-Change Paints
- 251 Fatigue-Failure Load Indicator
- 253 Improved Load-Cell Compensation
- 254 Detecting Gas Leaks in Propellant Lines
- 255 Record Dielectric Breakdown Automatically
- 256 Quantitative Measurement of Surface Contamination
- 257 Fuel Burner With Low Nitrogen Oxide Formation
- 258 Protection Against Explosive Blasts
- 259 Controlling Fires in Silver/Zinc Batteries

Books and Reports

- 260 Pressurization Systems
- 260 Engine Injectors
- 261 Fluid-Line Math Model

Computer Programs

- 262 Multispectral Data Analysis
- 262 Aircraft Aerodynamics at High Angles of Attack
- 263 Crack-Propagation Predictions

Improved Accuracy With Phase-Change Paints

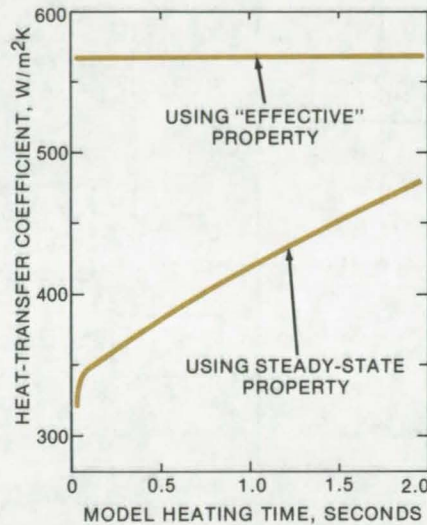
New technique reduces error in phase-change coating method of estimating heat-transfer coefficients.

Langley Research Center, Hampton, Virginia

A new approach significantly improves accuracy when phase-change paints are used to determine the heat-transfer rate over the surface of small complex models. Significant error had been noted with the conventional calculational procedure. In the new approach, a readily-obtained "effective thermophysical property" is substituted for the steady-state properties that are currently used. The remainder of the phase-change technique is the same as before.

The phase-change paint technique involves coating the surface of a model with a paint that changes from a solid to a liquid at a precisely known temperature. When the model is heated, the paint melts across well-defined surface locations as the phase-change temperature is reached. Using the time required to reach the phase-change temperature, the aerodynamic heat-transfer coefficient can be accurately calculated from the appropriate thermophysical property of the model.

Model thermophysical properties have been determined until now by using steady-state techniques applied in one step over the entire thickness of the model. In reality, however, conditions can be far from steady-state, and the models are



A Comparison of Methods shows that the use of an "effective thermophysical property" allows heat-transfer coefficients of inhomogeneous materials to be measured more accurately.

often spatially inhomogeneous because of filler materials added to withstand high temperatures. These discrepancies are eliminated with the new technique by determining an effective thermophysical property that accounts for the transient environment, inhomogeneity, and temperature dependency of the model.

The determination of the effective thermophysical property of a model is quick and straightforward. It has already been determined successfully for a number of model materials, using both a numerical and an experimental approach. The numerical results as illustrated for a highly-inhomogeneous model material show significant differences in the convective heat-transfer coefficient between the old steady-state and the new effective property approaches.

An electronic apparatus is now being developed that allows measurement of the thermophysical property directly from the model surface, using principles identical to the numerical approach. Preliminary work indicates that dynamic measurements can be obtained significantly faster than the currently-used steady-state technique allowed. In light of this potential improvement in accuracy and the increase in speed, the use of an effective thermophysical property to reduce phase-change paint data appears to offer significant advantages.

This work was done by J. Philip Drummond of Langley Research Center. For further information, Circle 44 on the TSP Request Card. LAR-12025

Fatigue-Failure Load Indicator

New device easily and economically records load at instant of failure.

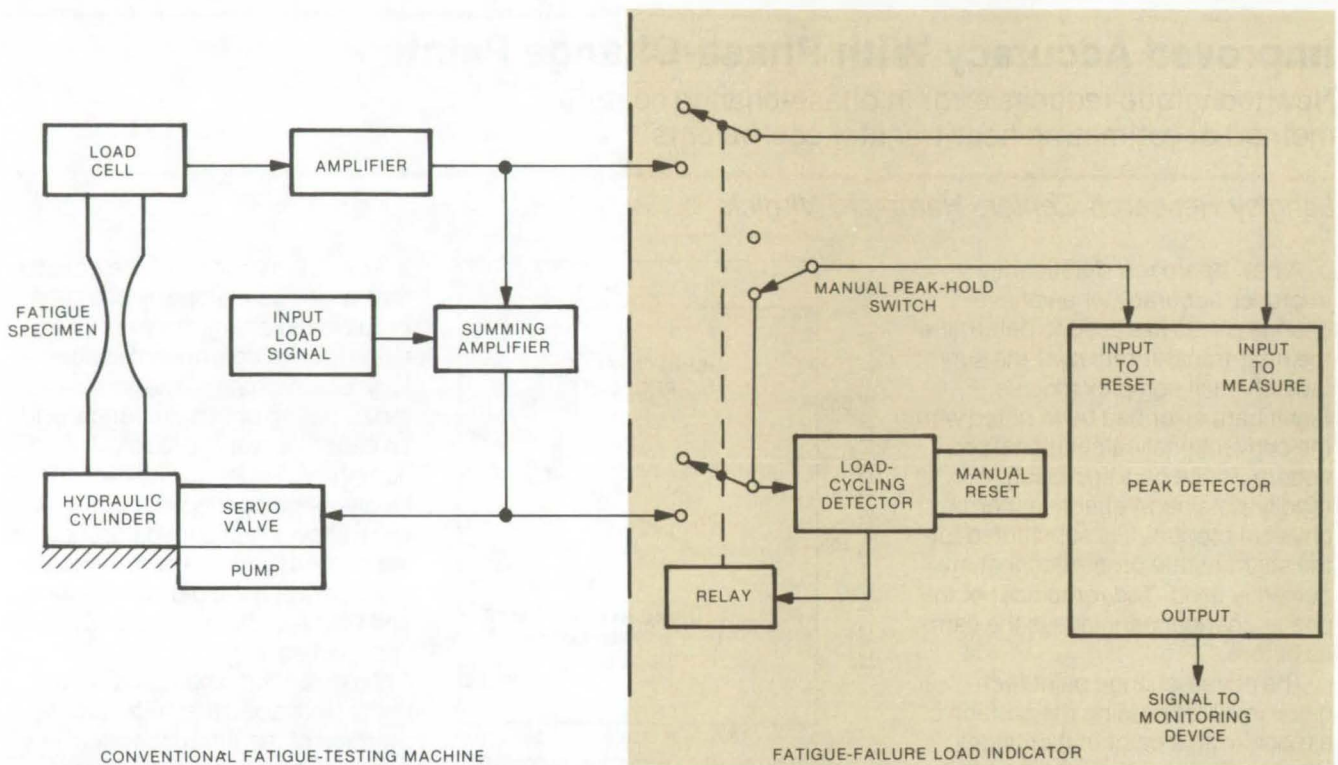
Langley Research Center, Hampton, Virginia

In material fatigue tests, specimens are subjected to a series of loads of either the same or of varying magnitude. When the specimen breaks, the load usually recorded is that which the fatigue

test machine is attempting to apply to the specimen, not the actual load at which the failure occurs. The actual load at failure can be determined by making continuous strip-chart records of test loads, using an

oscillograph or a similar instrument. In practice, however, actual breaking loads are not usually determined because of the extra expense of the required auxiliary equipment.

(continued on next page)



The **Fatigue-Failure Load Indicator**, with built-in cyclic reset capability, can be readily employed with any conventional fatigue-testing machine to permit researchers to determine easily and economically the exact load at which each test specimen fails.

Now a fatigue-failure load indicator has been developed to monitor and retain the value of the exact load that causes a specimen to break. The indicator can be used with conventional fatigue-testing machines. It monitors the load carried by the specimen during each cycle of the fatigue test. After the applied load passes through its maximum value in each cycle (when the direction of the load reverses), the indicator resets itself to monitor the rising applied load during the next cycle. If the specimen breaks, i.e., the load sought by the load detector is not achieved, the indicator does not reset but instead retains an electrical measure of the load at the instant of failure.

In a conventional fatigue-testing machine, as shown in the left half of the illustration, an electrical signal proportional to the amplitude of the applied load is produced by an amplifier connected to the load cell.

In the new indicator, this signal is transmitted to a commercially-available peak detector through a relay contact. This signal is fed, along with the input load signal, to a summing amplifier, which produces alternate positive and negative voltage pulses in phase with the loads applied to the test specimen. The output of the peak detector is reset to zero when a positive voltage pulse is applied to its reset terminal. When the loading rate becomes negative (each time a maximum load is achieved), a positive voltage pulse is transmitted from the summing amplifier through a second relay contact to the reset terminal of the peak detector. This causes the peak detector to reset and to remain in the reset mode until the loading rate again becomes positive. Thus, for each cycle, the peak detector monitors increasing load and resets during decreasing load. The peak-hold switch allows the operator to

check the value contained in the peak detector at any time.

The two relay contacts are closed by the relay when alternating voltages are received at the load-cycling detector from the summing amplifier. If the test specimen fails, or if the cyclic loading is interrupted in any way, the relay contacts open, isolating the peak detector from spurious electrical signals. Thus, upon specimen failure, the load value contained in the peak detector is protected from changing and can be obtained at the convenience of the operator.

This work was done by David C. Davis, William T. Davis, and Leland A. Imig of Langley Research Center. No further documentation is available.

Inquiries concerning rights for the commercial use of this invention should be addressed to the Patent Counsel, Langley Research Center [see page A8]. Refer to LAR-12027.

Improved Load-Cell Compensation

Major time savings when balancing strain-gage-bridge outputs of load cells

Lyndon B. Johnson Space Center, Houston, Texas

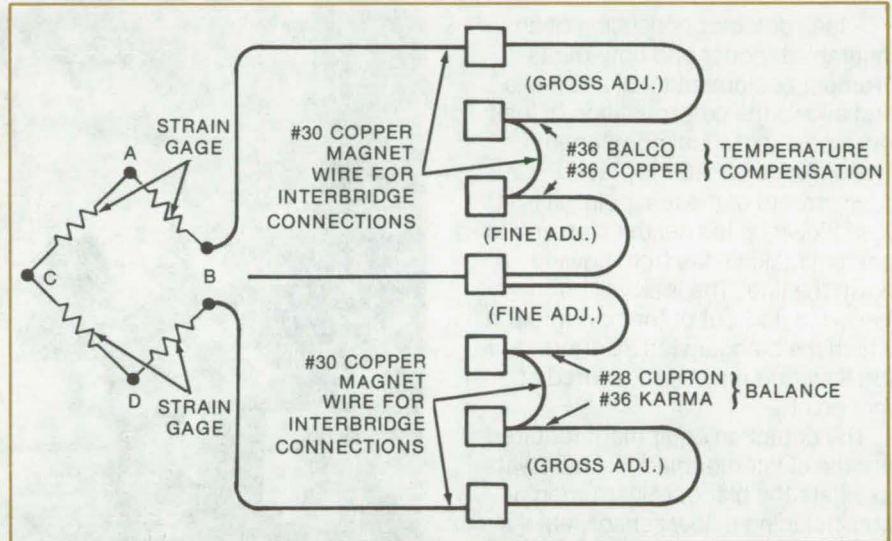
Strain gages used in load cells are electrically connected in a Wheatstone bridge configuration. In precision load cells, the bridge outputs are balance-compensated under a no-load condition to minimize the output changes with variations in temperature. The usual compensation technique is to temporarily complete the bridge connection, to measure the no-load output, and to subject the cell to a baseline temperature cycle. One then determines the size, type, and length of resistance wires that must be used for balance and temperature compensation.

The selected resistances are then tested under another temperature cycle to verify the degree of compensation. When, as is usually the case, the verification cycle does not produce the desired results, the procedure is repeated.

Normally, a single resistive wire with a very high temperature-resistance coefficient is used for temperature compensation, and a second resistive wire, with a very low temperature-resistance coefficient, is used for bridge balance. In one application with load cells having a large thermal mass and a fairly wide temperature-cycle range, this procedure was quite time consuming. There were from 6 to 10 bridges on each of six load cells, each requiring considerable compensation. Six verification cycles were required to compensate the first six-bridge cell, and even then the results were not entirely satisfactory.

In order to speed up the compensation process, the improved bridge-compensation circuit shown in the diagram was used, and several variations were made in the procedure.

An initial determination is made of where large bridge-balance compensation resistances are required,



The **Improved Bridge-Compensation Circuit** saves considerable time in balancing the bridge and wiring it for temperature compensation. Large bridge-balance compensation is made before temperature cycling, and small adjustments are made with a different type of wire.

and a nominal balance resistance is installed before the baseline temperature cycle. This step of including the less-than-perfect temperature characteristics of the large balance-compensating wires in the baseline temperature-cycle data allows the succeeding temperature-compensation determinations to include the temperature effects of the less-than-perfect balance-compensating wire.

Next, make provisions to add [rather than to replace] compensation wires to make small adjustments during repeated verification temperature cycles. The addition of a small amount of wire to make a small compensating-resistance adjustment affords a fine tuning. This contrasts with the conventional approach wherein small resistance adjustments are made in large resistances.

Finally, when adding compensation wires for small adjustments, use a different type and size of wire to

facilitate the resistance adjustment and installation. This technique takes advantage of the fact that the optimum size and type of resistance wires for large compensations are different than the characteristics of wires best for small compensations.

This approach was followed in the application described earlier. After the problems encountered with the needed six verification cycles to compensate the first bridge (each cycle required about 30 man-hours), the new procedure was used with the remaining five load cells. Even though some of the cells had as many as 10 bridges, only two to four verification cycles were required to complete the task. The total man-hour savings were estimated at 975 man-hours.

This work was done by Richard L. Egger of The Boeing Co. for Johnson Space Center. No further documentation is available. MSC-16466

Detecting Gas Leaks in Propellant Lines

Simple leak detector
fits many pipe sizes.

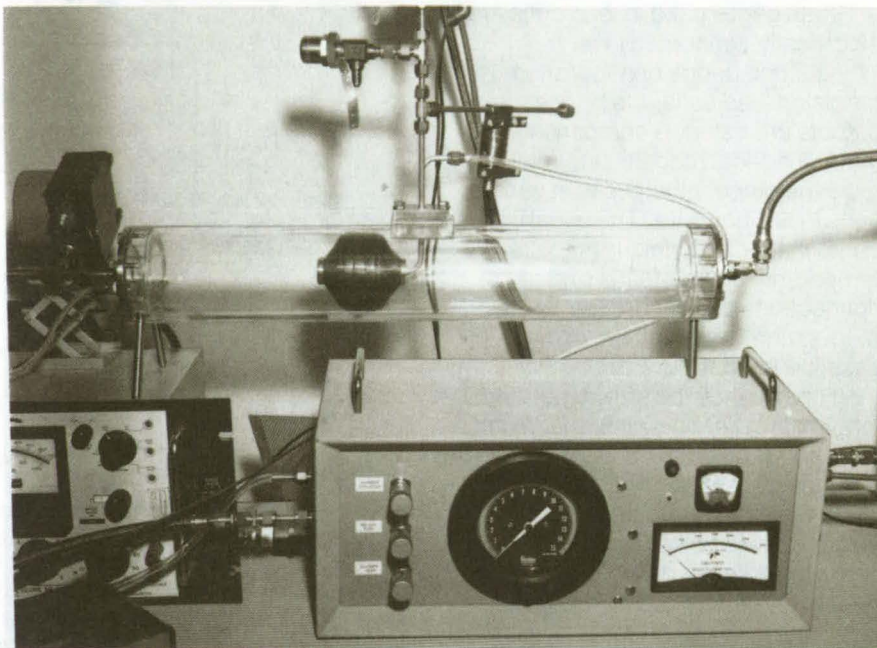
Marshall Space Flight Center, Alabama

A leak detector consisting of an inflatable bladder and flow-measurement equipment localizes leaks and allows the determination of leak rates past individual components. The deflated bladder is placed downstream of the test point; it is then blown up to seal the pipe and to prevent leaking gas from flowing down the line. The leak will be forced to flow out of the port through which the bladder was inserted, and the flow rate may be measured at that point.

The detection equipment required are the elastomer bladder; hardware to inflate the bladder; instrumentation including a flow sensor, electronic circuitry and a readout meter; and fail-safe components. The system can be packaged in a console about 20 by 40 by 50 cm. Power requirements are 115 Vac at 60 Hz or 28 Vdc.

Fail-safe systems prevent the bladder from being overpressurized in the line. A differential pressure sensor on the bladder-inflation line detects a pressure over 5 psi ($35 \times 10^3 \text{ N/m}^2$) and opens the line to a negative pressure pump that immediately deflates the bladder. In addition, a pressure-relief valve, set at 7 psi ($50 \times 10^3 \text{ N/m}^2$), vents the bladder to the atmosphere if the first system fails.

All operations are controlled from the console, which may be placed



Inflatable Bladder Leak Detector is shown in a test setup. The bladder is placed downstream from the test point and is inflated to block the pipe. Any leak at the test point will flow out the port through which the bladder was inserted. Flow rate is measured with a standard flow sensor.

up to 3 meters away from the line. The detectable flow range depends on the flow sensor used. Suitable available models range from 5 to 28,000 standard cm^3 per min. The system has been used with a calibrated leak source and was found to agree within ± 1.0 percent. Sensitivity was measured at 0.1 standard in.^3 per min. (1.6 standard cm^3 per min.), and repeatability was found to

be excellent over the range 0.1 to 300 standard in.^3 per min. (1.6 to 4,900 standard cm^3 per min.).

This work was done by William T. Escue, Harry K. Feagley, and Thaddeus I. Sokolowski of Sperry Rand Corp. for Marshall Space Flight Center. For further information, Circle 45 on the TSP Request Card.
MFS-23404

Thermal-Impedance Test for Hybrid Power Devices

The thermal impedance of a hybrid structure may be verified from its power dissipation and the change in its junction temperature and used to evaluate device quality. The junction temperature can be determined from measurements of VCE(SAT). The method can provide a convenient in-process test to evaluate device performance. (See page 178.)

Modular Test System for Solar Collectors

A modular test system can be used with a solar simulator or direct Sunlight to evaluate solar-collector components. The system can be used to study the effects of vacuum insulation, flow rate, inlet temperature, and reflectors on heat gain and is suitable for interface with a small computer. (See page 207.)

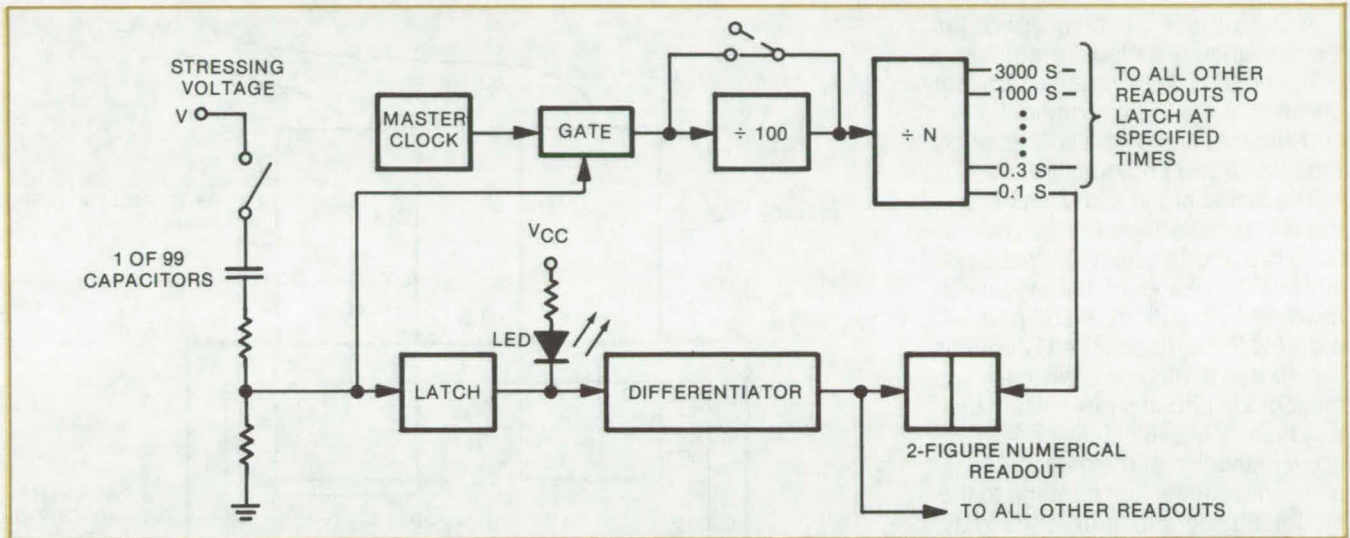
Alignment Tolerant Schlieren System

A simplified schlieren photography system can view gas flows with relaxed optical-precision requirements. The system has two mountings that are not rigidly fastened to each other. One mounting contains the light source, optics, and screen; the other carries only a porro prism. The new design may be suitable for construction as a portable model. (See page 214.)

Record Dielectric Breakdown Automatically

Time-dependent dielectric breakdown in MOS capacitors is determined for 99 samples in one run.

Caltech/JPL, Pasadena, California



Automatic Monitoring System for time-dependent dielectric breakdown can be used to test 99 MOS capacitors simultaneously. Each breakdown generates a voltage spike, which is registered on the readouts and indicated by an LED. A latching circuit prevents the recording of possible subsequent breakdowns in the same capacitor. In addition to research use, this system could also be adapted for quality control.

An automated test system for monitoring dielectric breakdowns in metal-oxide semiconductors (MOS) considerably simplifies data recording and the analysis of failure rates in these devices. The apparatus has found immediate application in research aimed at understanding the mechanisms responsible for time-dependent breakdown in the oxide layer and will ultimately lead to improved predictions of the reliability of MOS-based integrated circuits.

Dielectric failure of the SiO_2 layer may occur abruptly when an applied field exceeds the intrinsic breakdown value of 9×10^6 V/cm. It has also been discovered that a time-dependent failure probability exists for lower fields; however, efforts to obtain reliable information relating this failure rate to parameters such as temperature, field strength, and chip area have been complicated by the nonreproducibility, by several orders of magnitude, of data from

samples fabricated on different wafers. This problem is diminished by depositing arrays of test devices in a single wafer, but to recognize meaningful trends, it is still necessary to work with sample subgroups of 90 to 100 units so that the standard error is reduced sufficiently. The large number of devices involved, coupled with the fact that characteristic times for test runs are in the neighborhood of 50 minutes, has meant that considerable man-hours are consumed in this work.

With the new system, counting, timing, and recording are performed automatically by the combination of logic and display circuitry shown in the accompanying block diagram. A test system consisting of an array of identical MOS capacitors is fabricated on a silicon wafer. Each capacitor occupies an area of 2.2×10^{-3} cm^2 . These are tested for failure, 99 at a time, by means of a composite integrated-circuit probe card, with

three rows of 33 contacts that match the capacitor sites on the sample array. Simultaneous application of a stressing voltage in the range 25 to 70 volts to all devices opens the master clock gate and initiates the test. Each capacitor breakdown generates a voltage spike that closes a latch circuit and produces a pulse, which advances a counter by one unit.

Ten timing intervals, in steps from 0.1 to 3,000 seconds, are provided. At the end of each interval, a separate two-digit display is latched, storing the number of device failures that have been counted to that point. Thus by the end of the run, the displays have stored the time dependence of the number of failures that have occurred.

This work was done by Eugene T. Bates, Jr., and Seung P. Li of Caltech/JPL. For further information, Circle 46 on the TSP Request Card.
NPO-13599

Quantitative Measurement of Surface Contamination

A portable and highly sensitive system permits quantitative determinations of organic contaminants on test surfaces.

Lyndon B. Johnson Space Center, Houston, Texas

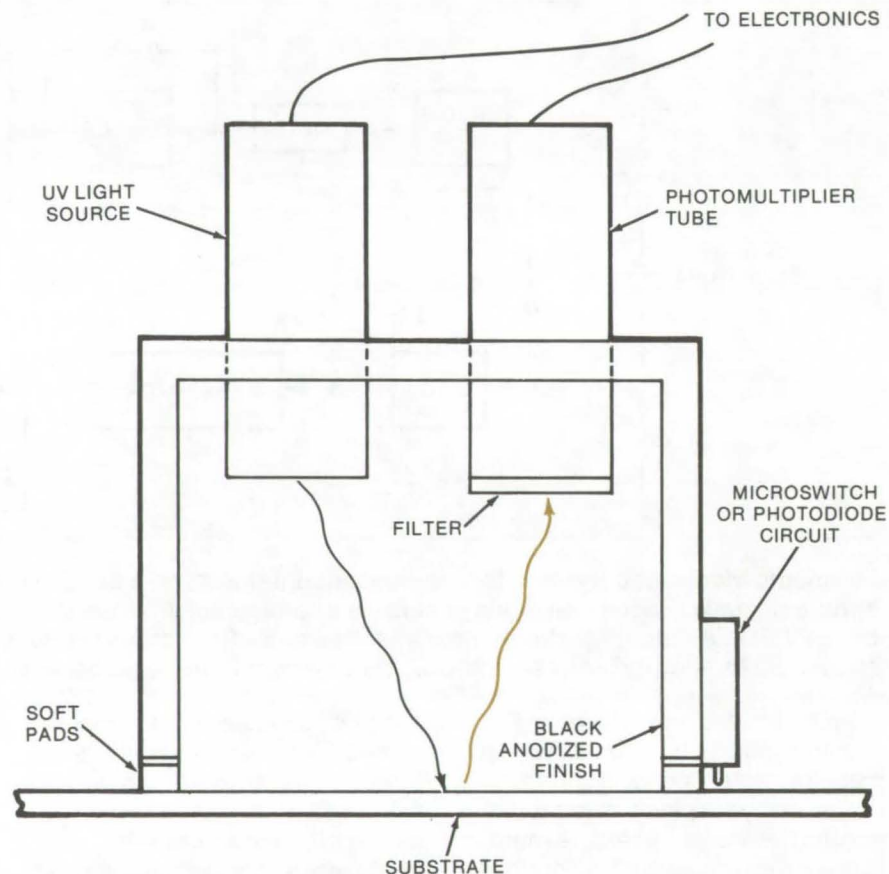
A test surface can be scanned for the presence of molecular organic contaminants by using a system that consists of a portable lighttight housing that contains a source of UV radiation and a photomultiplier.

The inside of the sampling head has a black anodized finish. The head is placed against the test surface firmly enough to make the head cavity lighttight. A soft pad protects the surface. The UV source is powered at all times, while a photodiode circuit senses when the head cavity is sufficiently dark to allow activation of the photomultiplier, thus preventing damage to the photomultiplier ordinarily caused by extraneous room light.

The UV source energizes organic contaminants present on the test surface, and they respond by giving off radiation (fluorescing) at a wavelength slightly longer than that used for activation. The fluorescing radiation, even if extremely dim, can be detected by means of the photomultiplier. The signal can be quantified if desired.

The system uses a sealed hydrogen lamp as a source of short-wavelength UV radiation having a peak at about 2,500 Å and prominent emissions at 1,216 and 1,608 Å. These shorter wavelengths are extremely effective in inducing fluorescence (high fluorescent yield).

The excited fluorescence spectra range from 3,500 Å to a peak of 4,500 Å. To insure the measurement of fluorescence rather than UV reflectance generally caused by scratches or a highly-reflective surface material, a suitable filter placed in front of the photomultiplier cuts off wavelengths below 3,500 Å.



The **UV Excitation Fluorescence Sensor** requires that the user place the sensor head firmly against the subject surface to form a lighttight seal. Small parts can be inspected by placing them on a table and covering them with the sensor head.

Preliminary testing suggests that the photomultiplier is at least 10^4 times as sensitive as standard UV lamp inspection processes. Output from the photomultiplier is either pulse-counted (if the fluorescence quantity is low) or digitized by means of standard nuclear instrumentation electronics.

The system boasts several advantages over conventional detection techniques. It is truly portable. The sensor head may be operated

several hundred feet from the electronic module. It may be used in normal room light and permits the detection of significantly smaller (thinner) samples (under 1,000 Å). In addition, digitation of the output permits easy evaluation of contamination cleanup techniques.

*This work was done by Robert G. Richmond of **Johnson Space Center**. No further documentation is available. MSC-16679*

Fuel Burner With Low Nitrogen Oxide Formation

A concentric-tube burner controls combustion temperature to maintain efficiency, while lowering the formation of nitrogen oxides.

Caltech/JPL, Pasadena, California

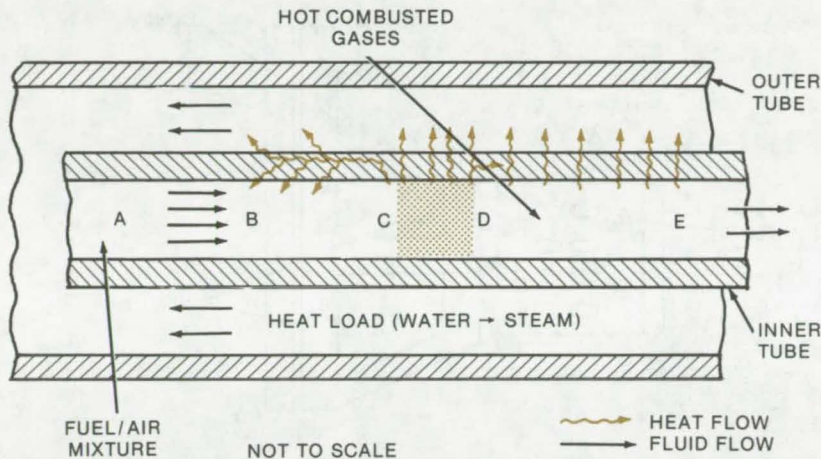


Figure 1. In the **Load-Coupled Combustor**, a fuel/air mixture enters at point A at ambient temperature; temperature begins to increase until combustion occurs in the zone from C to D. Heat is transferred along the load until point E, where design considerations indicate that the combustion products will have dropped to a temperature at which heat transfer is no longer practical. Figures 2 and 3 compare the temperature and the rate of heat generation of this arrangement to one without load coupling.

Utility boilers, water and space heaters, and other combustors operate most efficiently when the combustion temperature is as high as possible. One of the reasons for this is that heat is transferred to the working fluid or load more efficiently at higher temperature gradients. However, as temperature gets higher, the formation of polluting nitrogen oxides by the oxidation of nitrogen in the air also becomes more efficient.

A method of maintaining efficient combustion while reducing the formation of nitrogen oxides is now under investigation. The core of the approach is the use of a "load-coupled combustor": a furnace in which the load and the combustion zone share a common wall and are relatively close together. This arrangement transfers heat efficiently and, at the same time, keeps the combustion temperature well below free-flame temperatures.

The combustor as shown in Figure 1 consists of two concentric tubes. The inner tube contains fuel and air

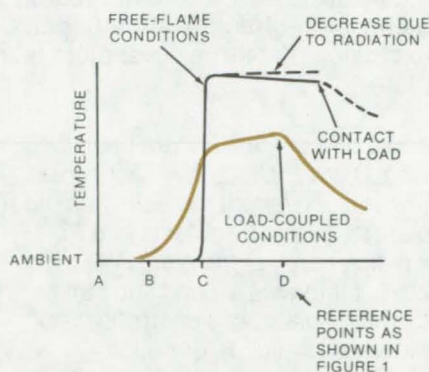


Figure 2. The **Temperature Profile** across a free-flame combustion zone is compared with that across the system shown in Figure 1. Temperature is plotted against the A-through-D reference points shown in Figure 1.

and is the combustion chamber. The space between the inner and outer tubes is occupied by the load or working fluid, which absorbs the heat of combustion along the length of the tubes. Because the combustion chamber is completely surrounded by a vaporizing fluid or other heat sink, its temperature never reaches that of free flame. This low temperature prevents the formation of appreciable amounts of nitrogen oxides; yet the close coupling between the burning gases and the load insures efficient heat transfer.

In three series of tests, using a prototype load-coupled combustor, each of the key features of this system has been verified: nitrogen oxide suppression, combustor stability, and complete combustion. Testing is now underway to verify all three conditions simultaneously.

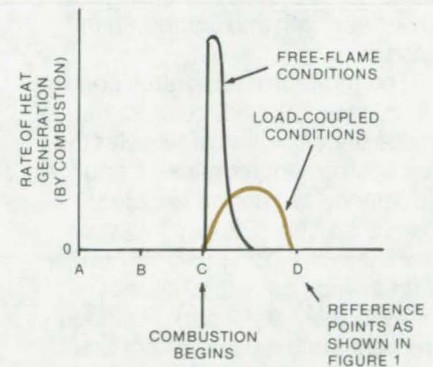


Figure 3. The **Heat Generated** by free-flame combustion is compared to that for a load-coupled system. Heat generation is plotted against the A-through-D reference points shown in Figure 1.

This work was done by Richard A. McKay of Caltech/JPL. For further information, Circle 47 on the TSP Request Card.

Inquiries concerning rights for the commercial use of this invention should be addressed to the Patent Counsel, NASA Resident Legal Office-JPL [see page A8]. Refer to NPO-13958.

Protection Against Explosive Blasts

Simple, hinged cover plate is effective against high explosive blasts.

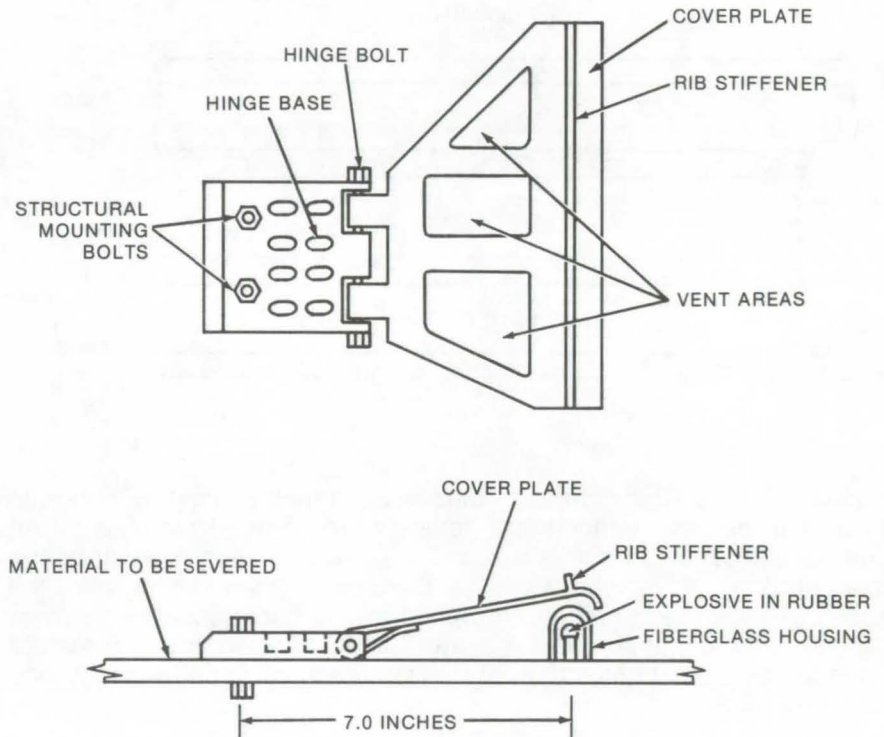
Langley Research Center, Hampton, Virginia

A prototype of the protective shield shown in the illustrations has been used successfully to shield against blasts, created by the detonation of high-explosive charges. The design of the apparatus resulted from a requirement in a material-severance application to protect a surface that was parallel to the material to be severed and only 15 cm away from it.

The high explosive used was an 8-in. (20-cm) length of 94% RDX/6% wax at 125 grains/foot (0.266 g/cm totaling 5.4 g). The lead-sheathed, flexible, linear-shaped charge was contained in a rubber extrusion inside a fiberglass housing. The protection problem was compounded by the fact that the only available structural mounting-bolt attachments in this application were located 18 cm from the center-line of the explosive. A lesser distance would have allowed a lower-strength and lighter hinge base.

The protective apparatus consists of a simple, hinged, cover plate made of cold-rolled steel selected for its strength, toughness, and resistance to fracture under dynamic loading. The cover plate thickness is 0.125 in. (0.317 cm) with a hinge base thickness of 0.3875 in. (0.9842 cm). Rounded corners are used in the vent areas to help minimize stress concentrations and tearing. The lap areas of the hinge and the rib stiffener are continuous, 100-percent electric-arc fusion welds. High-strength aircraft steel bolts were used.

This apparatus protects from blasts by converting the dynamic energy of the blast wave and the resultant housing fragmentation into kinetic energy of the cover plate and into heat, which is generated by metal deformation. The blast wave



A Hinged Cover Plate used for protection from explosive blasts is made from cold-rolled steel. The cover plate is 0.125 in. thick, and the hinge is 0.3875 in. thick. It is mounted on a piece to be severed explosively by using high-strength aircraft bolts. Much of the blast energy from an explosion under the cover plate is transformed into kinetic energy of the plate.

and the fragments impact upon the hinged cover plate, driving it into an arc and converting the energy in the blast wave and fragments into kinetic energy of the plate. When the cover plate arcs around and strikes the hinge plate, this energy is dissipated as heat of deformation created on the impact of both the cover plate and hinge base and as kinetic energy in the cover plate rebound.

Experiments with vertically-oriented witness plates (cover plate hanging downward) showed that this device effectively stopped the explosive blast wave as well as the

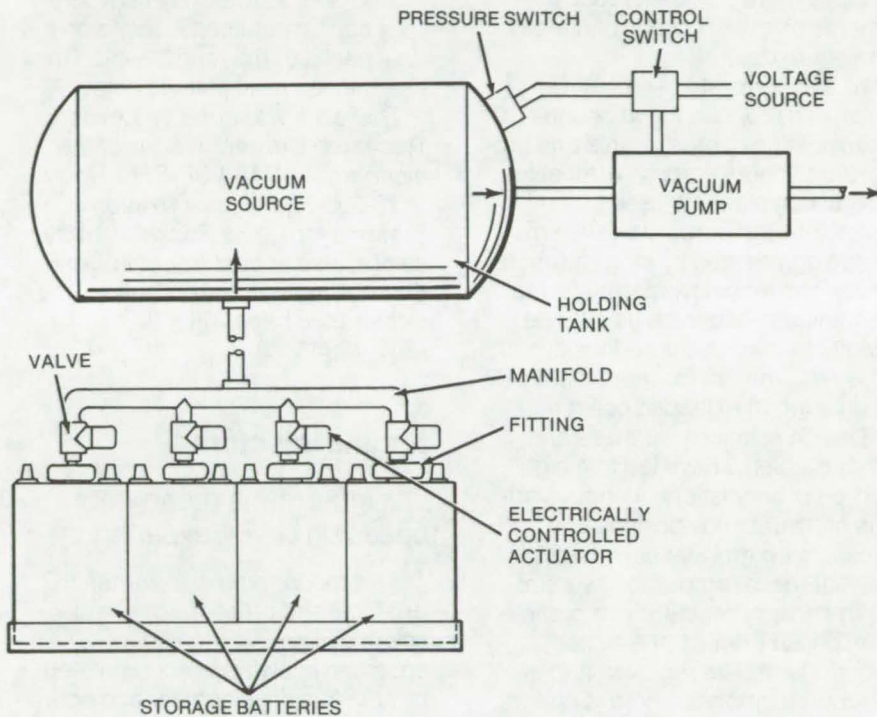
high-velocity fragments of the explosive housing assembly. Without the apparatus, the wood-frame aluminum witness plates were horizontally displaced, imparting a total of 72 foot-pounds (97 joules) of energy and exhibited deformation, severe indentation, and surface scoring. Using the protective apparatus, identical witness plates exhibited no displacement, deformation or scoring.

This work was done by Laurence J. Bement of Langley Research Center. No further documentation is available.
LAR-12014

Controlling Fires in Silver/Zinc Batteries

Combustion-supporting gases are vented from the cells, using a vacuum system.

Marshall Space Flight Center, Alabama



A Fire Extinguisher for Sealed Secondary Batteries is shown in the schematic view. Combustion gases are admitted to a collection manifold and are drawn to a holding tank. The vacuum pump is connected to a voltage source through a control switch. A pressure switch, located at the tank and connected to the control switch, continuously monitors the pressure within the holding tank. It, in turn, operates the control switch. The pump is used to maintain a constant pressure of under 1 atmosphere in the holding tank. Each of the electrically controlled actuators is wired to a voltage source via a temperature-sensing switch (not shown) mounted on the battery housings. In response to the temperature of the battery housing, a bimetallic element in the switch closes the circuit at a predetermined housing temperature, thus admitting combustion-supporting gases to the manifold where they are drawn via a vacuum to the holding tank.

Considerable difficulty is often encountered in extinguishing fires that occur in a silver/zinc (and similar) storage battery. The battery plates, formed of chemicals containing oxides, supply oxygen to the fire as it burns. One method used to extinguish the flames has been to remove the battery from the equipment bay, place it in a drum, seal the drum, and wait for the oxygen to be depleted. The method is obviously extremely hazardous for the people involved.

An improved technique for extinguishing a fire in a silver/zinc battery uses a manifold connected to a central evacuation chamber to vent rapidly the combustion-supporting gases generated by the oxides of the battery plates. In a multiple-cell battery bank, a system of manifolds is connected from each battery cell to the evacuation chamber. The manifolds are located adjacent to the battery cells and are connected to each by electrically-actuated solenoid valves. The valves are separately powered and are actuated via series-connected thermal-sensing switches mounted on the cells.

The multiple-cell fire-extinguisher system, as shown, is connected to the cells via a venting orifice formed in each battery housing. The manifold connects the orifices through a conduit to a vacuum holding tank and vacuum pump. A fitting, seated in each orifice, is connected with the manifold through a valve that is located between the fitting and the manifold. A nipple connects each of the valves with the manifold.

This work was done by William A. Boshers and William J. Britz of Marshall Space Flight Center. For further information, Circle 48 on the TSP Request Card.
MFS-22952



Books and Reports

These reports, studies, and handbooks are available from NASA as Technical Support Packages (TSP's) when a Request Card number is cited; otherwise they are available from one of NASA's Industrial Application Centers or the National Technical Information Service.

Pressurization Systems

Design-criteria monograph

The significant experience and knowledge with pressurization systems accumulated by NASA in development and operational programs has been organized and presented in a monograph for effective use in design. It reviews and assesses current design practices and from them establishes firm guidance for achieving greater consistency in design, increased reliability in the end product, and greater efficiency in the design effort.

The pressurization system in a liquid rocket propulsion system provides a controlled gas pressure in the ullage space of the vehicle propellant tanks. In a rocket with a "pressure-fed" propellant-feed system, the ullage pressure is directly responsible for forcing the propellant through the feed-system lines and into the rocket-engine combustion chamber at the proper flow rate and pressure; in a "pump-fed" system, the ullage pressure supplies propellant to the engine pumps at the proper pump inlet conditions, and the pump delivers the propellant to the engine at specified rates and pressures.

Pressurization system designers have developed many innovations in response to the challenge of advanced propulsion systems and an increasing diversity of mission requirements. For example:

- The use of hydrogen as a high-energy fuel in pump-fed propulsion systems introduced the need to incorporate variable pressurization to compensate for the vapor pressure increase resulting from in-flight temperature stratification of the

propellant.

- The use of pressure-supported monocoque tank structures and common bulkheads between tanks to minimize stage hardware weight places more stringent requirements on the accuracy of ullage pressure control.
- The problems of absorption of gases in propellant and counter permeation of pressurants and propellant vapors across permeable expulsion bladders used in pressure-fed propulsion systems were aggravated by long-duration missions, and new materials and techniques had to be developed.
- Multiple-start missions introduced the requirement for repressurization after an extended coast period.

Design solutions for these and other problems have led to a high degree of sophistication in the various pressurization designs and pressure control systems used in current rocket propulsion systems.

The design begins with a preliminary phase in which the system requirements are received and evaluated; the emphasis here is on the major factors that influence the selection of system type and initial design. Next comes a detail-design and integration phase in which the controls and the hardware components that make up the system are determined. The final phase, design evaluation, provides an analysis of problems that may arise at any point in the design when components are combined and considered for operation as a system.

The monograph comprises two major sections: "State of the Art" and "Design Criteria and Recommended Practices." References complement the text.

Both major sections are divided into three subject categories: "Preliminary Design" (basic design parameters, selection of system type, initial system design); "Detail Design and Integration" (pressure control systems, system components); and "Design Evaluation" (heat-transfer effects, mass-transfer effects, system dynamics).

This monograph is one of a series being published on chemical propulsion covering the areas of environment, structures, guidance, and control. A list of all monographs issued prior to this one and where they can be obtained is found on the final pages of the report, which may be obtained as explained below.

This work was done by Lewis Research Center. A copy of the monograph, NASA SP-8112 [N76-22300], "Pressurization Systems for Liquid Rockets," may be obtained at cost from the New England Research Application Center [see page A7]. LEW-12845

Engine Injectors

Design-criteria monograph based on NASA experience

This monograph was written to organize and present, for effective use in design, the significant experience and knowledge accumulated by NASA in development and operational programs. It reviews and assesses current design practices and from them establishes firm guidance for achieving greater consistency in design, increased reliability in the end product, and greater efficiency in the design effort.

The injector in a liquid rocket engine atomizes and mixes the fuel with the oxidizer to produce efficient and stable combustion that will provide the required thrust without damaging the engine. Injectors usually take the form of a perforated disk at the head of the rocket-engine combustion chamber and have varied from a few centimeters (inches) to more than a meter (yard) in diameter. This monograph treats specifically bipropellant injectors, emphasis being placed on the liquid/liquid and liquid/gas injectors that have been developed for and used in flight-proved engines. The information provided has limited application to monopropellant

injectors and gas/gas propellant systems.

In the past, the design of injectors has been primarily an art that depended for success on the experience and intuition of the injector design team. This design approach led to expensive, time-consuming development programs and often to marginal final designs. More recently, injector design capability has been improved considerably by the use of computer programs that characterize the combustion field and by cold-flow techniques that are used to determine the mass, mixture-ratio, and drop-size distribution characteristics. In addition, a long history of practical experience has pinpointed numerous problem areas in injector design and operation.

The first and foremost step in injector design is to establish the injector flow-system geometry. This system geometry is the flow-controlling aspect of the injector and is composed of the total injector element pattern, the individual orifice geometry used in the total pattern, and the flow-system geometry or manifolding upstream of the orifices. The second step is to develop the injector assembly; this step involves handling the structural and material aspects of the proposed injector and includes the design of the auxiliary components. These steps, accomplished systematically with careful attention to detail, result in a successful rocket-engine injector.

The monograph comprises two major sections: "State of the Art" and "Design Criteria and Recommended Practices." References complement the text.

Both major sections are divided into two subject categories: "Injector Flow-System Geometry" (total element pattern, individual orifice geometry, flow-system

geometry upstream) and "Injector Assembly" (general structure, injector face, baffles and acoustic absorbers, auxiliary components).

This monograph is one of a series being published on chemical propulsion covering the areas of environment, structures, guidance, and control. A list of all monographs issued prior to this one and where they can be obtained is found on the final pages of the report, which may be obtained as explained below.

This work was done by Lewis Research Center. A copy of the monograph, NASA SP-8089 [N76-30284], "Liquid Rocket Engine Injectors," may be obtained at cost from the New England Research Application Center [see page A7]. LEW-12846

Fluid-Line Math Model

Simplified, but accurate, model for study of pipelines and circulator-system dynamics

A simplified mathematical model can be used to simulate very large hydraulic systems on either analog or digital computers. Models of pumps, servoactuators, reservoirs, accumulators, and valves can be connected together with a line model generating systems containing typically 600 elements.

The model is a simplification and extension of one developed earlier by D'Souza and Oldenburger (D'Souza, A. F., and Oldenburger, R., "Dynamic Response of Fluid Lines," *Journal of Basic Engineering*, Trans. ASME, Series D, Vol. 86, No. 3, Sept. 1964, pp. 589-598). This earlier model employed Laplace transforms for viscous lines, yielding transcendental transfer functions. Although it provides excellent results in the frequency domain, this

technique has been unwieldy for time-response situations.

The model of D'Souza and Oldenburger has been simplified by using infinite product expansions of the transcendental transfer functions. The expansions are simplified by eliminating higher order terms and replacing them with correcting constants. The lines are then divided into series of lumped segments. By reversing the boundary conditions, two pairs of flow and pressure equations are generated.

The resulting model employs a two-port, four-terminal network approach that has proved to be a powerful tool for integrating various individual-element models in a systematic manner. The model can be analyzed by classical system-analysis techniques for stability (open-loop frequency response and root locus) and for performance (closed-loop frequency response and transient response). This facilitates the use of generally-available simulation language programs (CSMP and CSSL) and linear system-analysis programs.

The new line model has been reduced to practice in both FORTRAN and CSMP. It has been refined over the last 3 years for hydraulic-subsystem dynamic analysis. Simulation runs have been made generating pressure-transient data at the Space Shuttle main-engine hydraulic interface. The study led to successful design changes in the thrust-vector-control isolation valve and to the addition of return-line accumulators in order to meet interface-control-document pressure-level requirements.

This work was done by Allen Kandelman and Desmond J. Nelson of Rockwell International Corp. for Johnson Space Center. For further information, including discussions of theory and experimental verification, Circle 49 on the TSP Request Card. MSC-16230



Computer Programs

These programs may be obtained at very reasonable cost from COSMIC, a facility sponsored by NASA to make new programs available to the public. For information on program price, size, and availability, circle the reference letter on the COSMIC Request Card in this issue.

Multispectral Data Analysis

LARSYS III.1 extends availability of major data-analysis program.

The Multispectral Data-Analysis program, LARSYS, is designed for remote-sensing research and applications. Pattern recognition and interactive data-handling techniques are used to analyze remotely-sensed multispectral and multitemporal data. The primary inputs are multispectral data in image orientation. These data may be obtained from multispectral scanners on high-altitude aircraft, spacecraft, satellites such as LANDSAT, or from digitized photographs. These images of the Earth's surface are either recorded in or converted to digital data and are stored on multispectral image storage tapes (MIST).

An area of the Earth's surface is represented on the MIST tape by a run of data consisting of an identification record, many data records, and an end-of-file record. Each data record contains one scan line of data from each of the recorded wavelength bands. The end-of-file record represents the end of a run. It allows several runs to be stored on one tape. A run represents all of the multispectral data from a single image in terms of scan lines, columns (samples within scan lines), and channels (spectral bands).

The basic analysis concept of LARSYS consists of locating data points, contained on the MIST tape, which are believed to represent classes (clusters) of interest. Typical classes of interest are crops, beaches, woods, and geological features. Gaussian statistics of

these data points (a key assumption made in several LARSYS algorithms is that distributions are Gaussian) are calculated. When one or more classes have been statistically defined, any area of the image may be classified by spectral similarity.

There are two machine versions of LARSYS III.1 available. LARSYS was developed at the Laboratory for Applied Remote Sensing (LARS) at Purdue. The Purdue LARSYS was developed as a total system, an integration of hardware and software. COSMIC distributes only the software part of the system. The hardware required consists of:

- An IBM 360 having 512K bytes of main storage under Control Program-67 using the Cambridge Monitoring System (for virtual machine operation);
- An OS G-level FORTRAN IV Compiler and an OS/360 Assembler;
- Two 9-track tape drives; and
- Four 2314 disk drives.

For interactive graphics processing, an IBM 4507 Digital Image Display System is required. (The IBM 4507 was developed for LARSYS and is available only at LARS.) Implementation of this version on a system other than that described above could require extensive modification. In particular, the time-sharing aspect of Control Program-67 and the virtual machine operation concept of the Cambridge Monitoring System are very important to the logical structure of the Purdue version of LARSYS III.1.

Due to the stringent operating environment required by the Purdue LARSYS, Texas A. & M. University (TAMU) was contracted to modify the LARSYS software for use on the IBM 370. The TAMU LARSYS should run on any IBM 360 or 370 operating under OS with at least 400K bytes available for user application programs. The TAMU LARSYS is basically a batch-oriented system with interactive control card entry via TSO available. The only additional hardware requirements are two 9-track tape drives and some

direct access (the amount depends on the type and complexity of usage). The TAMU LARSYS III.1 has most of the capabilities (excluding the interactive graphics) of the Purdue LARSYS III.1 plus two programs written by TAMU to support LARSYS processing. The first is an ERTS-to-MIST conversion program used to convert multispectral-scanner (MSS) computer-compatible tapes (CCT) (LANDSAT tapes that are available from the EROS Data Center) to the LARSYS input form, the MIST tape. The second is a System Runtape code that maintains tape/file location information for the MIST data sets.

This program was written by Texas A. & M. University for Johnson Space Center. For further information, Circle B [Purdue LARSYS III.1, MSC-14823] or G [TAMU LARSYS III.1, MSC-16322] on the COSMIC Request Card. MSC-16322/MS-14823

Aircraft Aerodynamics at High Angles of Attack

Estimate transonic aerodynamics at angles up to 60°

The AEROX computer program can be used to estimate aircraft aerodynamics to high angles of attack (up to 60°). It estimates the coefficients of lift, induced drag, and pitching moment for wings and for wing-body combinations with or without an aft horizontal tail. Both trimmed and untrimmed characteristics are calculated.

AEROX is based on new, non-linear formulations of compressible wing theory extended to cover transonic and supersonic flows, including shock waves and attendant rotational flows. Estimates of longitudinal aerodynamics are possible through maximum lift at all Mach

numbers above those where low-speed, viscous stall predominates. The separate or combined estimated characteristics of wings, bodies, and tails can be calculated. The program has been validated by comparison with experimental results for nine different aircraft configurations over a broad flight envelope. Because of its versatility and its parameterization capability, AEROX is a valuable tool for estimating, correlating, augmenting, and validating aerodynamic characteristics and is ideally suited to computerized design, instruction, and research.

In the past, rigorous methods for calculating three-dimensional aerodynamics to high angles of attack were unavailable. The primary obstacle cited was the inability to define the overall influence of viscosity. The AEROX approach postulates that transonic and supersonic flows past airfoils are dominated by shock waves and that the primary effects of viscosity are in determining the skin friction and in influencing the chordwise location of transonic shock waves. These shock locations are not extracted by AEROX as solutions, but are entered as an input parameter. Then the effects of varying the shock location can be studied.

The onset of nonpotential transonic flow around conventional blunt airfoils is assumed to occur when the Laitone limit for local Mach numbers or certain loadings are attained on the airfoil. After this onset, the lift no longer conforms to potential theory, and AEROX solves lift and induced-drag equations based on the integration of the downwash momentum in the plane passing through the airfoil trailing edge and normal to the flight direction. The aerodynamic normal force on the body is estimated by an equation summing the slender-body contribution and the viscous cross-flow drag.

The formulations in the program constitute an analytical method for estimating transonic aircraft aerodynamics to maximum lift. No estimates are included for the effects of the propulsion system, such as the inlets, nacelles, nozzles, or power-induced effects. Approximations are included for the contributions of the nose, afterbody, horizontal tail, and wing leading-edge chord extensions or strakes.

AEROX is written to execute in the batch mode. Input consists of planform parameters, aerodynamic geometry, and data on the flight environment. Output consists of the estimated coefficients in printed format or as plotted output. The program is written in FORTRAN IV and has been implemented on an IBM 360 and a CDC 7600. On the IBM the program has a central memory requirement of approximately 124K 8-bit bytes.

This program was written by John A. Axelson of Ames Research Center. For further information, Circle C on the COSMIC Request Card.
ARC-11133

Crack-Propagation Predictions

Growth of subcritical cracks predicted for anticipated loads

A new program, FLAGRO-III, aids in the predictive analysis of preexisting subcritical flaws or cracks. Structural failures may result when flaws grow to a critical size under fatigue loadings, even at load levels well below the ultimate capability of the structure. FLAGRO provides an analytical procedure for predicting the growth rate of fatigue cracks. Fracture mechanics are applied as a tool to predict the growth of fatigue cracks and to evaluate the tolerance of a given structural design to

damage. FLAGRO should find wide applications in the design phase (or failure analysis) to check safe-life capabilities of structural components.

To predict crack growth for a given structural component, the following must be known:

- Anticipated load history;
- Material crack-propagation rate;
- Stress intensity relationship, which describes the local stress field, crack size, crack morphology, and component geometry; and
- An appropriate initial crack size, which can be determined by proof testing of the structure or by non-destructive evaluation.

With this information as input, the program can be used as an analysis tool in several ways:

- To describe crack growth by three methods: (1) Collipriest growth-rate equation, (2) Paris growth-rate equation, or (3) the interpolation of tabulated growth-rate data;
- To develop a two-dimensional crack-growth model that predicts flaw growth in two directions independently;
- To account for variations in material properties due to environmental changes during a life history profile;
- To vary the load-stress relationship within a given spectrum;
- To "continue" crack growth while other data change; and
- To "grow" cracks under complex stress distributions.

Part-through, and corner cracks can be analyzed when they occur on panels, at open holes, at pin-loaded holes, at pin-loaded circular or rectangular lugs, and on the surface of tubes or bars. The specific inputs required include the dimensions of the initial crack, solution type, flaw type, material properties, and the load spectrum. Output consists of printed output, a step-by-step

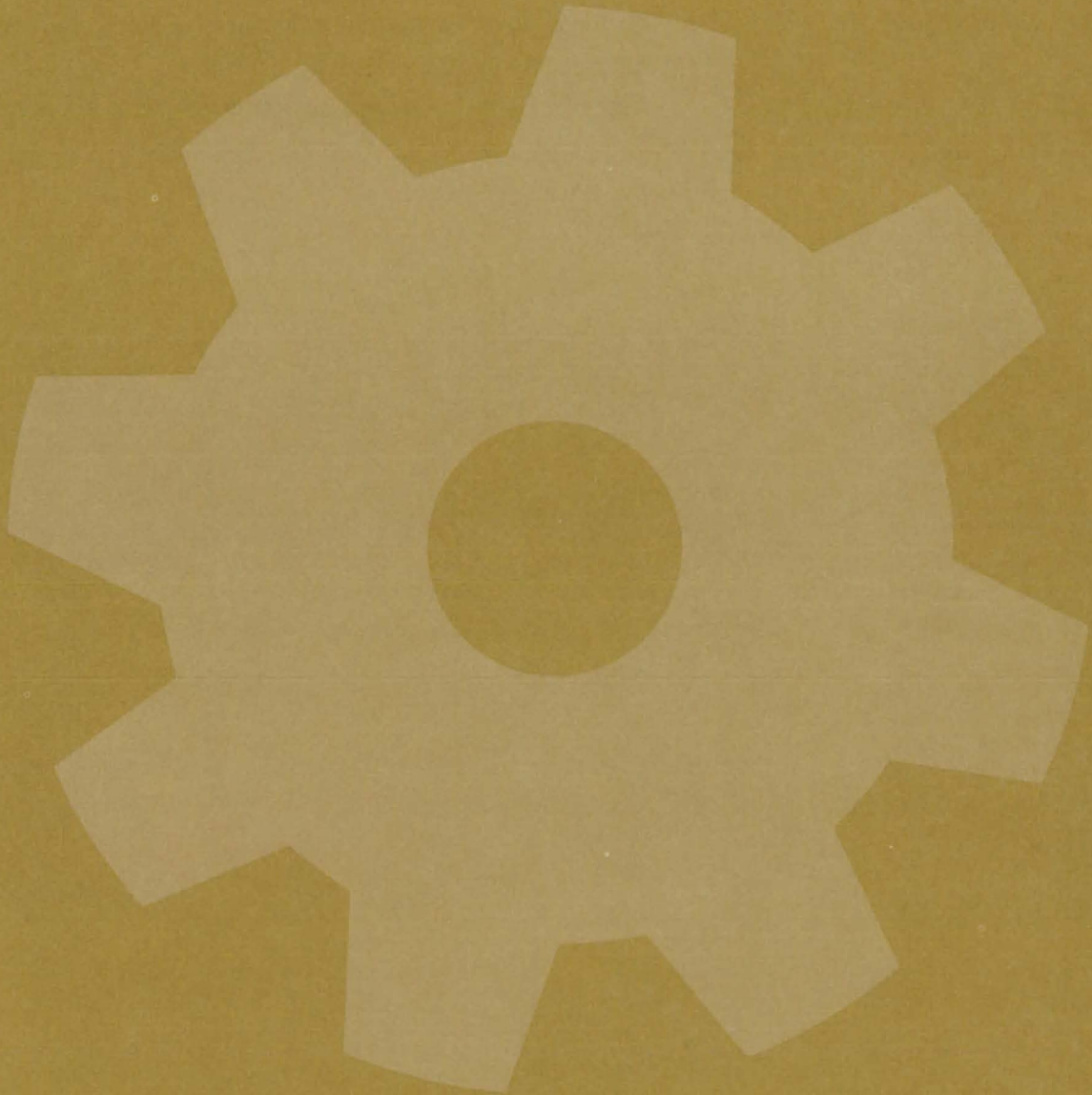


history of flaw size, growth rate, maximum stress intensity, and applicable correction factors. FLAGRO also contains an extensive error-checking capability and provides informative diagnostics when difficulties are encountered during execution.

This program is written in FORTRAN IV to be executed in the batch mode and has been implemented on an IBM 370 computer with a central memory requirement of approximately 140K 8-bit bytes.

*This program was written by Han P. Kan, Alan F. Liu, and Herbert L. Reed of Rockwell International Corp. for **Johnson Space Center**. For further information, Circle D on the COSMIC Request Card. MSC-16436*

Machinery



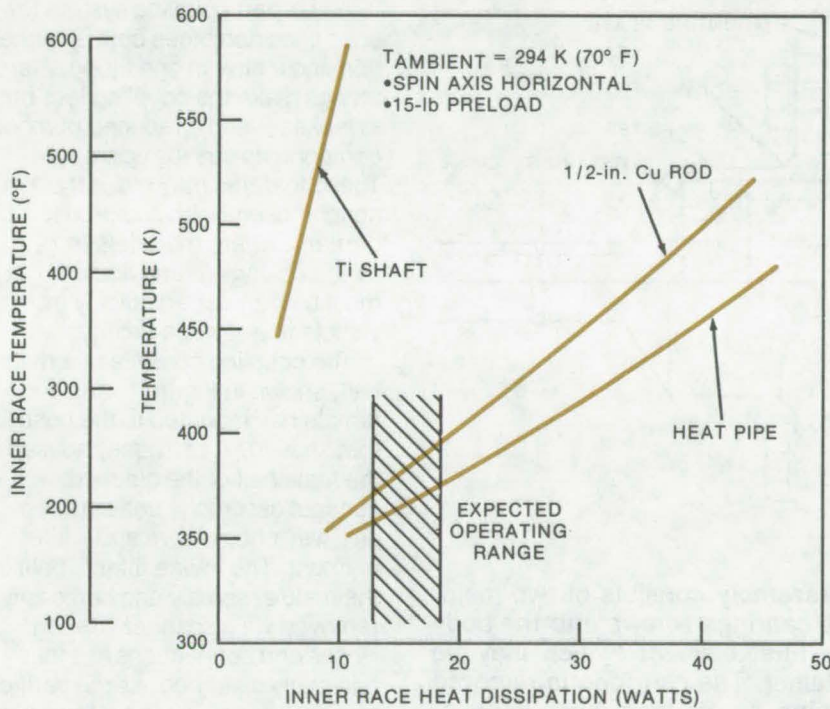
**Hardware,
Techniques, and
Processes**

- 267 Heat Pipe Controls Bearing Temperature
- 268 Quick-Disconnect Coupling/Filter
- 269 Integrated Temperature Sensor
- 270 Cartridge Getter for Vacuum Jacketing
- 271 Magnetically-Controlled Bearing Lubrication
- 272 Fuel Injector for Jet-Stirred Combustors

Heat Pipe Controls Bearing Temperature

Centerline heat pipe minimizes rotating-assembly bearing temperatures.

Langley Research Center, Hampton, Virginia



Heat Dissipation Approaches were compared by estimating the temperature difference from the bearing inner race to the rotor root, using a 50-node computer program with conductive series and parallel thermal circuits for three cases: the titanium bearing support only; a copper conductive rod; and a heat pipe. Results are shown in the graph.

One of the major design problems in the Integrated Power/Attitude Control System (IPACS) is an effective method for transporting heat from the bearing inner race of the rotating assembly in order to minimize inner-race temperatures and the temperature differential across the bearing. The high-speed rotating assembly in this application is essentially a device for storing energy in an electrically-driven rotating flywheel.

The IPACS has three significant heat-generating areas: bearing inner race, bearing outer race, and motor-generator stator. These areas require thermal-control design integration to ensure unit operation

within allowable temperature limits. The heat generated at these locations must be transported to the IPACS case where it can be dissipated to the environment. The IPACS rotor operates in a vacuum with minimal heat transport across the bearing. The bearing-outer-race heat and the stator heat can be transported to the case primarily by conduction. However, preliminary thermal analyses indicated that the structural heat-transport path is not sufficient to carry heat away from the bearing inner race without resulting in excessive bearing-race temperatures and bearing-temperature gradient. Increasing the heat path effectiveness from the bearing

inner race to the main rotor body, from which the heat is radiated to the housing, is the most direct method of reducing bearing temperatures.

An increase in the support-wall thickness for this application is limited in effectiveness because of the low thermal conductivity of the wall material, in this case titanium, and because of the maximum wall thickness imposed by the system design. The most feasible approach, the incorporation of a high-conduction rod or a heat pipe at the shaft center, was analyzed to determine the effect on system temperatures.

The results are shown in the graph. Both the heat pipe and the copper rod greatly reduce bearing temperature compared with the titanium support alone, but the minimum race temperature is clearly obtained with the heat pipe. The heat pipe would utilize water as a working fluid, with or without an internal wick. It would operate essentially as a centrifugal pump with a temperature-dependent vapor return path.

As a result, the IPACS rotating assembly has been designed by using passive thermal-control techniques, including judicious material selection and parts design and the use of rotating heat pipes in the rotor shaft. The centerline heat pipe is the most effective thermal design for minimizing rotating-assembly bearing temperatures.

This work was done by Alexander Cormack III and John E. Notti, Jr., of Rockwell International Corp. for Langley Research Center. For further information, Circle 50 on the TSP Request Card.
LAR-11846



Quick-Disconnect Coupling/Filter

A filter cartridge housed in the coupler speeds servicing and turnaround time.

Marshall Space Flight Center, Alabama

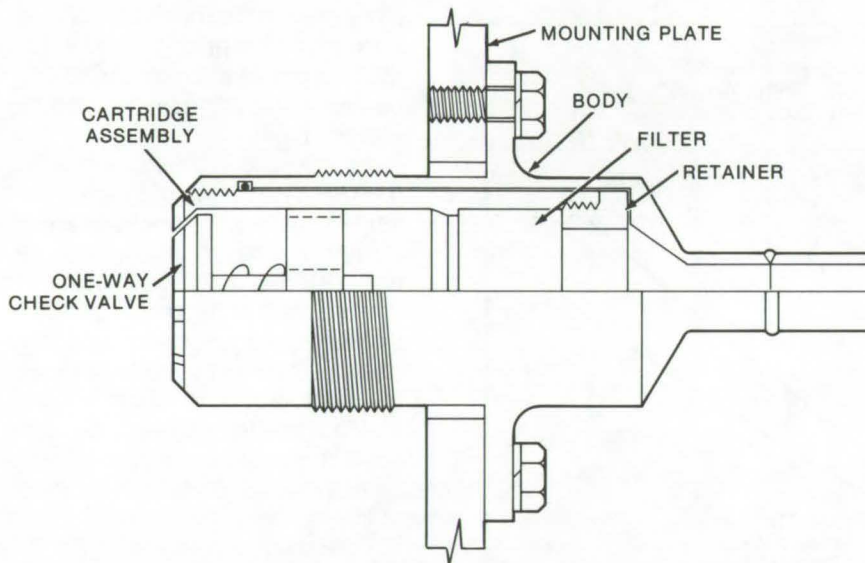


Figure 1. The **Quick-Disconnect Male Assembly** consists of two major assemblies: a cartridge and a body. The cartridge screws into the body and houses a one-way check valve, a filter element (which may be disposable or reusable), and a filter retainer. The cartridge is removed with a spanner wrench without disturbing downstream hose connections, thus aiding servicing turnaround time.

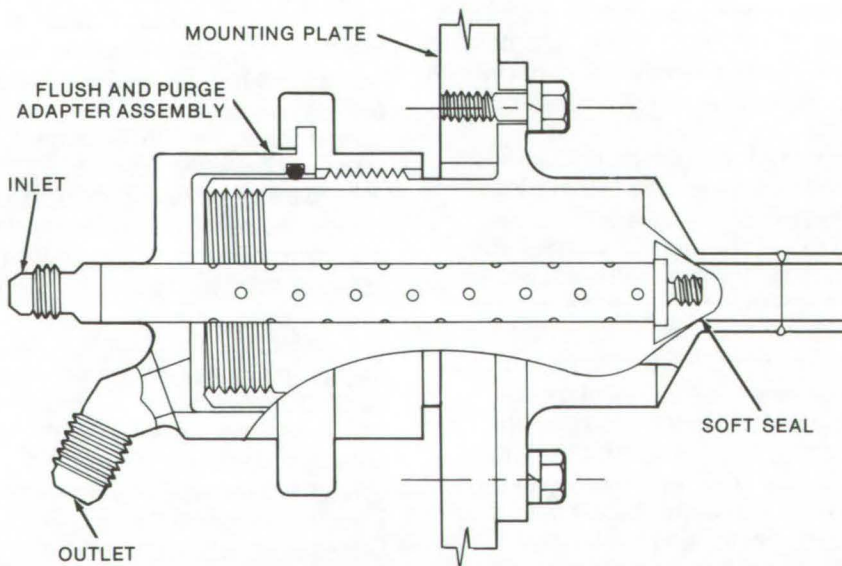


Figure 2. A **Flush Adapter** is used to purge the male half of the coupler. Cleaning fluid flows through the inlet under pressure, onto the coupler surfaces, and exits via the purge adapter outlet. The filter-cartridge assembly is removed, prior to use. A soft seal blocks the downstream end of the coupler and prevents cleaning fluid from entering it.

A two-part coupling system for hose lines combines both a connection and a filter in one fitting. Flared fittings make the coupling less prone to leakage, and a reduced number of components speeds operation. These features may make the coupler useful with liquid-bulk carriers, where materials (e.g., milk, cooking oil, and liquid sugar) must be transferred quickly from a vehicle to a storage facility.

The coupling consists of a male half, shown in Figure 1, and a female half mounted to the hose line (not shown). A cartridge, housed in the male half of the quick-disconnect assembly, consists of a one-way check valve and a filter element. The in-line filter is built into the male assembly and can easily be removed via a spanner wrench. Hoses and connections are thus minimally disturbed, as the verification of connections is performed at only the attachment site.

One of the chief advantages of this fixture is the ease of cleaning it. The male half of the coupling is cleaned by removing the filter-cartridge assembly and placing a flush-and-purge assembly, shown in Figure 2, over the male coupling. The purge assembly has a soft seal that blocks cleaning fluid from entering the downstream end of the male coupler. Cleaning fluid enters the unit under pressure, spraying the internal surfaces, and returns through the outlet to the fluid supply.

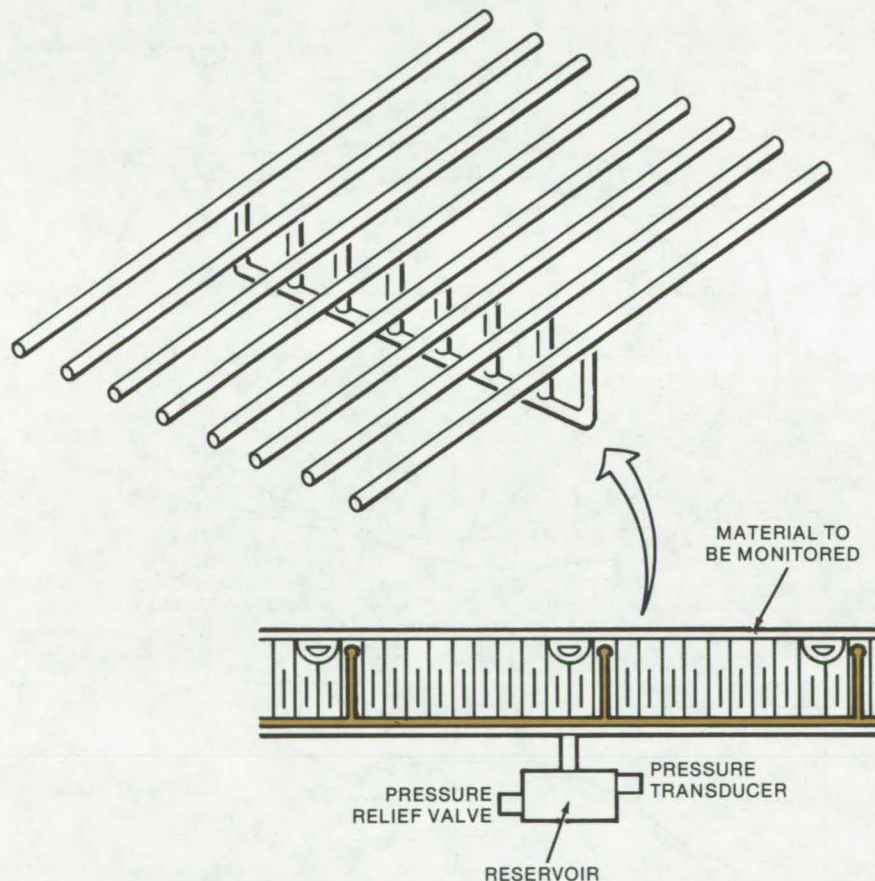
This work was done by Fred Jankowski of Marshall Space Flight Center. For further information, Circle 51 on the TSP Request Card.

This invention has been patented by NASA [U.S. Patent No. 3,910,307]. Inquiries concerning nonexclusive or exclusive license for its commercial development should be addressed to the Patent Counsel, Marshall Space Flight Center [see page A8]. Refer to MFS-22323.

Integrated Temperature Sensor

Liquid-filled temperature sensors are integral part of monitored surface.

Langley Research Center, Hampton, Virginia



The **Phase-Change Temperature Sensor** is a network of tubes manifolded together and filled with a liquid that boils at the temperature of interest. The tubes are connected to a pressure transducer, which indicates a temperature increase sufficient to boil the liquid by sensing the resultant pressure increase.

The success of using lightweight materials such as aluminum for the primary structure of hypersonic aircraft depends upon a reliable structural cooling system, monitored by a lightweight and dependable temperature-sensor/failure-detection system. An undetected loss of cooling could result in catastrophic failure of such an aircraft structure.

A proposed temperature-sensor/failure-detection system utilizes liquid-filled sensors attached as a matrix to the monitored surface. The fluid passages could be made an

integral part of the monitored surface or could be small-diameter tubing in good thermal contact with the monitored surface.

The system which was designed (see figure) utilizes a freon refrigerating liquid in the fluid passages at pressure levels above the vapor pressures associated with the normal operating temperatures of the monitored surface. Changes in liquid volume, due to either thermal expansion or contraction, generate pressure signals via pressure transducers. Thus, continuous tempera-

ture monitoring through pressure measurements is provided for normal operation.

In case of cooling-system failure and the resultant overheating of the monitored surface, a phase change, or local boiling of the contained liquid, occurs, creating a sudden increase in pressure in the fluid passage network. This sudden increase, transmitted as a pulse via the pressure transducers, signals the overtemperature failure condition.

Conversely, a loss in pressure below normal operating range, caused by loss of liquid in the fluid passage network if designed as an integral part of the monitored surface, signals a crack in the monitored surface. No temperature-sensor system now in use has this capability.

This temperature-sensor/failure-detection system offers other significant advantages over discrete sensors — thermocouples and thermistors — in terms of simplicity, reliability, cost, ease of installation, maintainability, and weight. For example, this system required only 1 temperature sensor/failure detector per 100 square feet of panel used, whereas it would have taken up to 10,000 discrete sensors to provide similar coverage.

In addition to the proposed aircraft structural usage, this integrated temperature-sensor/failure-detection system could be adapted for use in other critical applications, such as temperature monitoring of cryogenic containers.

This work was done by Ralph L. Herring and LaVerne L. Pagel of McDonnell Douglas Corp. for Langley Research Center. For further information, Circle 52 on the TSP Request Card.
LAR-12056



Cartridge Getter for Vacuum Jacketing

Threaded getter can be replaced without cutting the jacket.

Lyndon B. Johnson Space Center, Houston, Texas

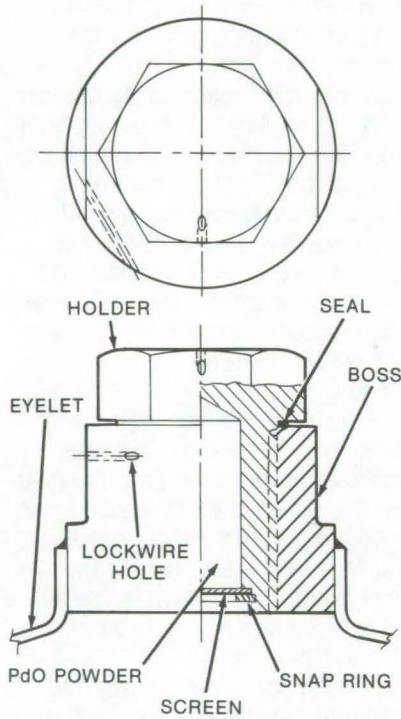


Figure 1. A **Getter Cartridge** for vacuum apparatus can be machined to hold PdO powder. A screen physically retains the PdO, and the cartridge is screwed into a boss attached to the vacuum jacket.

An inexpensively-manufactured getter cartridge can save users considerable time in vacuum system maintenance and will allow most anyone to carry out a replacement procedure that formerly required a skilled welder. Potential manufacturers of this device will find a wide market among the many who use vacuum apparatus.

Vacuum jacketed assemblies frequently include a getter, such as palladium oxide (PdO). In most cases, the getter is installed before the last welding and sealing of the apparatus. For instance, capsules of

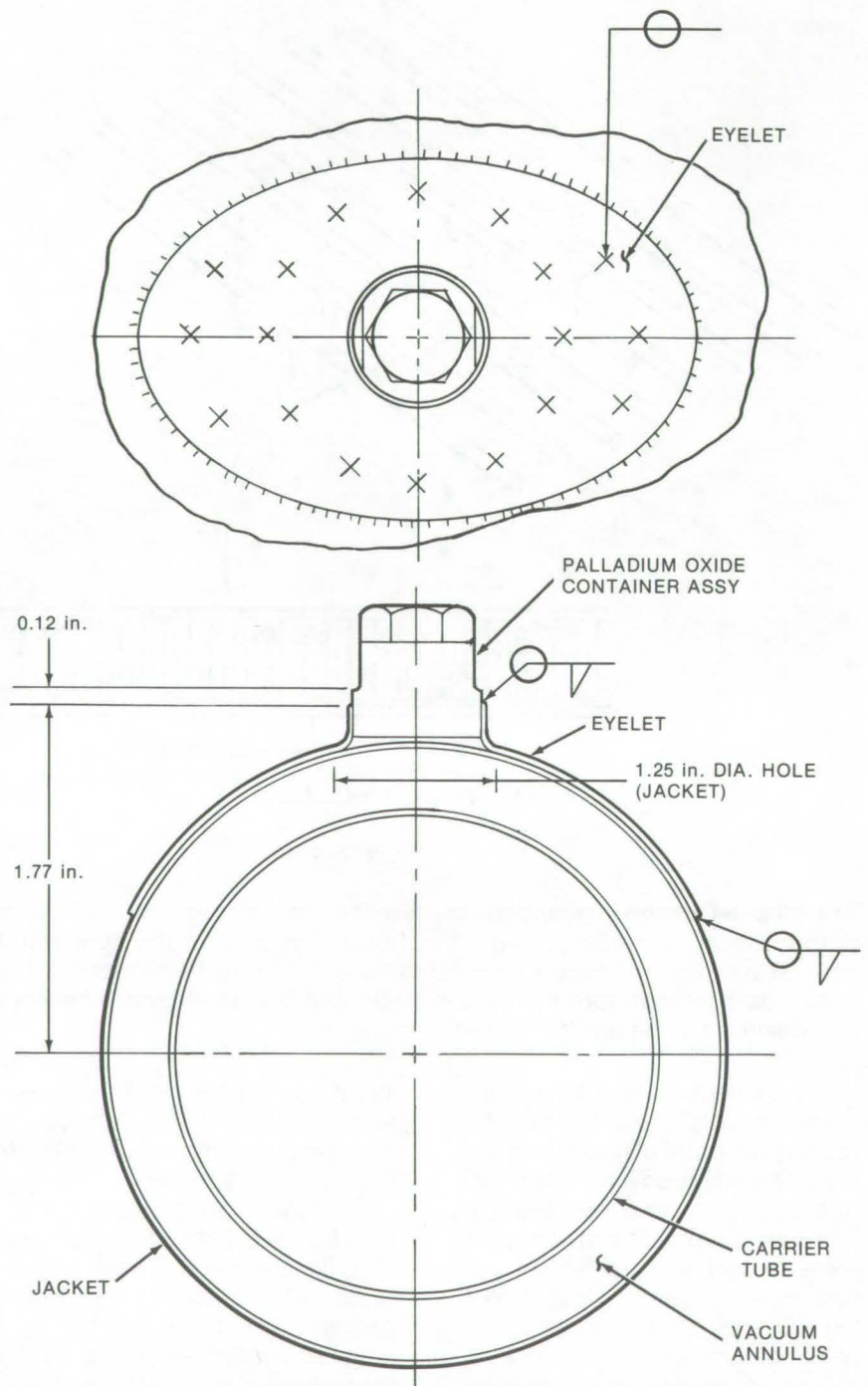


Figure 2. The **Cartridge is Installed in the Vacuum Apparatus** through a port attached to the outer vacuum jacket.

palladium oxide would be placed in the vacuum annulus; then, any remaining components would be installed, and the assembly would be welded shut. This procedure meant that the vacuum apparatus must be disassembled, cut, and later re-welded to replace the getter.

This situation can be simplified considerably by using a replaceable cartridge, as illustrated in Figure 1, to hold the palladium oxide. This cartridge is screwed into a port in the outer wall of a vacuum jacket as shown in Figure 2. The getter may be replaced by simply unscrewing

the cartridge rather than cutting and rewelding.

This work was done by Charles J. Luebbers of AMETEK for Johnson Space Center. No further documentation is available.
MSC-16610

Magnetically-Controlled Bearing Lubrication

Magnetic force is used to retain and supply lubricant to bearing.

Marshall Space Flight Center, Alabama

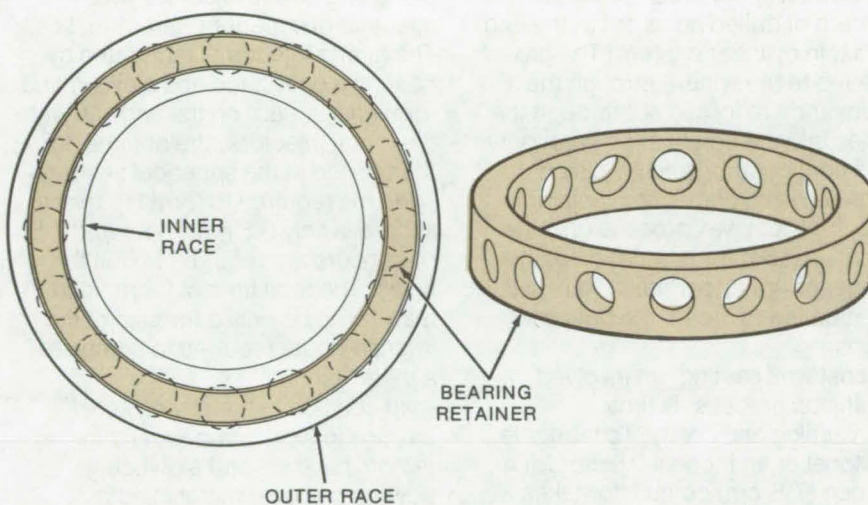
In a bearing system under development, magnetic forces are being used to retain and supply a ferrolubricant. The ferrolubricant can be one of several types that consist of particles of ferrite, or magnetite suspended in a carrier fluid.

The low-viscosity ferrolubricant is held on a permanently magnetized bearing retainer, which may be made of one of several types of materials:

- a magnetic metal
- a phenolic filled with magnetic component
- a porous magnetic metal, or
- a material filled with a porous magnetic metal

Such materials can be prepared by casting, sintering, or other common methods. The porous materials have the added feature of acting as a lubricant reservoir. They may be machined into ribbons or solid cages and subjected to a strong magnetic field. An example of a ball-bearing assembly of this type is illustrated.

In addition to ball bearings, this technique could be applied to other



A Proposed Magnetic-Lubricant Ball-Bearing Assembly has a permanently-magnetized bearing retainer fabricated of a porous material. The pores of the retainer are filled with a ferrolubricant. Surface tension causes the retainer to deliver sufficient lubricant to the nonmagnetic ball bearings.

types of bearings. For instance, the shaft of a journal could be made of a magnetized porous material and the sleeve could be made of a nonmagnetic material.

This work was done by Ann F. Whitaker of Marshall Space Flight Center. For further information, Circle 53 on the TSP Request Card.
MFS-23009



Fuel Injector for Jet-Stirred Combustors

Easily-fabricated quartz injector has long operating life.

Langley Research Center, Hampton, Virginia

Jet-stirred combustors, used for pollution, combustion, and energy studies, have been under development for over 20 years. All have employed metal fuel injectors, typically Monel, Inconel, or the equivalent, to supply and diffuse gases in the combustion chamber. A typical injector is fabricated in one piece as a spherical shell with a pattern of drilled holes set at the end of a thin cylinder or stem. The gases are fed to the sphere through the stem and are forced out through the holes into the combustion chamber. The configuration and precision requirements of the metal injectors require a lost wax process (investment casting) for fabrication of the stem and spherical shell. The shell is then drilled to create the orifice holes.

Lost wax casting, an involved multistep process, is time consuming and costly. To fabricate a Monel or an Inconel injector for a 3-inch (7.6-cm) combustor takes 32 man-hours for casting and 8 man-

hours to drill the holes. In addition, only about 50 percent of the casts are usable, the rest being rejects; the metal injectors are not efficient with liquid fuels, and combustion temperatures are limited by the properties of the metal.

A simple and inexpensive method of making quartz injectors yields injectors of superior characteristics. The quartz injector is fabricated by heating a quartz rod and blowing and forming a sphere on the end. As with the metal injectors, the orifices are then drilled in the spherical shell. The time required to form the quartz sphere is only 0.5 man-hour and 7.5 man-hours are required to drill the holes. The total time of fabrication, 8 man-hours, is only a fraction of the 40 man-hours required to complete a metal injector.

In addition to the obvious cost savings in fabrication, quartz injectors have several significant advantages over metal injectors.

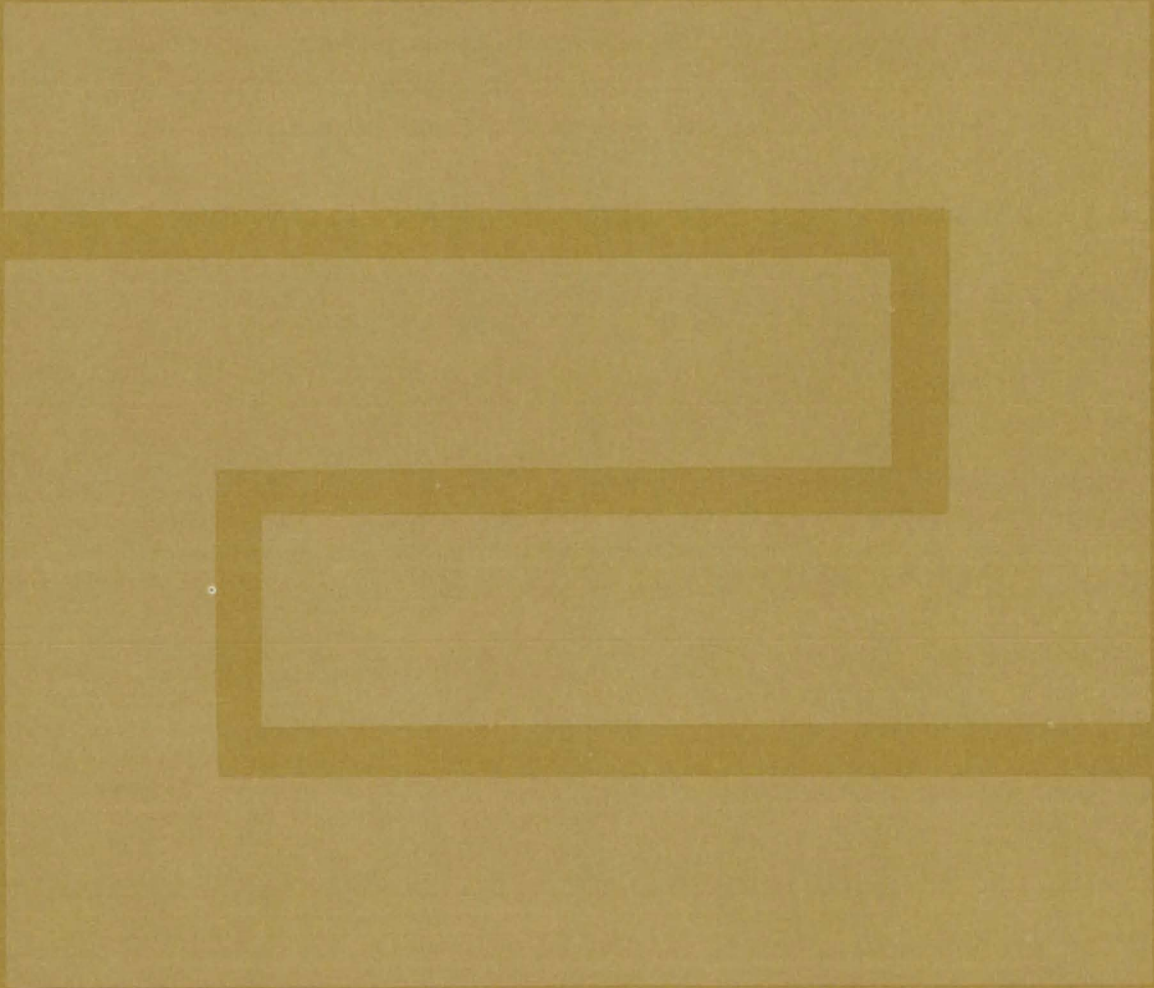
The quartz injector is capable of operating with liquid fuel. It can withstand a temperature 400° F (220° C) greater than can the Inconel injector, and it does not oxidize at high temperature to create a problem with plugged holes, as does the Monel injector. A further advantage is that test results have shown a seemingly-indefinite life expectancy for the quartz unit compared with an average operating life of 40 hours for Inconel.

Success with this technique and material is such that further substitutions for other related components are being contemplated.

*This work was done by Swen G. Anderson of **Langley Research Center**. No further documentation is available.*

Inquiries concerning rights for the commercial use of this invention should be addressed to the Patent Counsel, Langley Research Center [see page A8]. Refer to LAR-12146.

Fabrication Technology



**Hardware,
Techniques, and
Processes**

- 275 Semiautomatic Labeling of Small Wires
- 276 Vibration-Resistant PC Board Feedthrough
- 277 Inspection Tool for Butt-Welded Tubing
- 278 Molding Cork Sheets to Complex Shapes
- 279 Honeycomb Chassis for Electronic Components
- 280 Extruded Edge Members for Honeycombs
- 280 Polyimide Thin-Film Dielectrics on Ferroelectrics

Books and Reports

- 282 The Processing of Materials in Outer Space

Semiautomatic Labeling of Small Wires

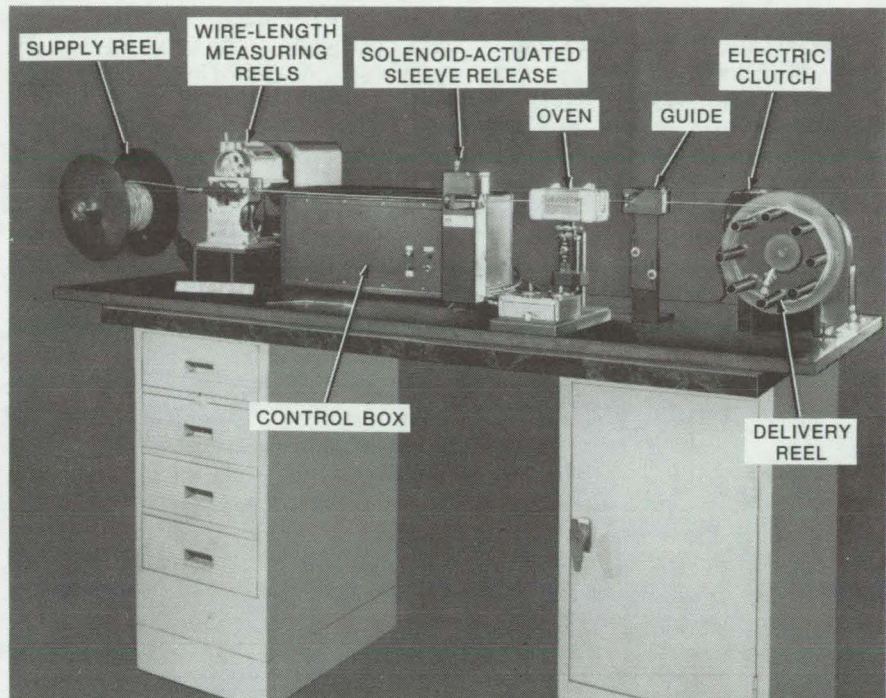
Labeling with heat-shrink sleeves is made effective for small production runs.

Lyndon B. Johnson Space Center, Houston, Texas

Modern wiring systems often incorporate small polyimide-insulated wires that are difficult to label with conventional hot-stamping methods. A quick new procedure is to label the wires with heat-shrink identification sleeves semiautomatically by modifying equipment available in most production shops.

The wires are labeled with a tabletop motor-driven unit normally used for measuring small quantities of different lengths of 26- to 10-gage wire. This unit is modified and combined with controls and additional devices to space and install heat-shrink identification sleeves semiautomatically at required intervals along the wire.

The equipment (see figure) consists of a supply reel, wire-length measuring rolls, a solenoid-actuated sleeve release, a manually operated oven, and a takeup reel. An economical bandoleer-type system is used separately to mark the heat-shrink sleeves with programmed typewriters using identification numbers. The wire from the supply reel is threaded through the properly marked bandoleer of sleeves and is fed through the solenoid-actuated sleeve release. As each sleeve is released at the selected wire length, it is heat shrunk in a manually-operated infrared tube-shrinker oven. The labeled wire then is fed into the takeup reel.



The **Semiautomatic-Wire Labeling Equipment** is used to install heat-shrink identification sleeves on small-diameter wires for moderate-size production runs. The supply reel contains wire of the desired diameter, is cut into lengths as set on the measuring rolls. The required number of identification sleeves are slipped over the wire, which is then placed through the sleeve-releasing mechanism. The sleeves are shrunk at 350° F in an infrared oven.

The wire reeling speed is approximately 10.5 m/min (35 ft/min). The sleeves are shrunk within 3 to 10 seconds, depending on the wire size. This new unit is suitable for relatively small-quantity production runs.

This work was done by Lewis P. David, Robert M. Heisman, and Andrew R. Keir of Rockwell International Corp. for Johnson Space Center. For further information, Circle 54 on the TSP Request Card. MSC-16233



Vibration-Resistant PC Board Feedthrough

Inexpensive ribbon interface cuts vibration-induced failure between coaxial cable and printed-wiring board.

Lyndon B. Johnson Space Center, Houston, Texas

A new fabrication method uses an annealed-nickel ribbon loop to interface a coaxial input (or output) connector to a printed-wiring board. The method is particularly useful in

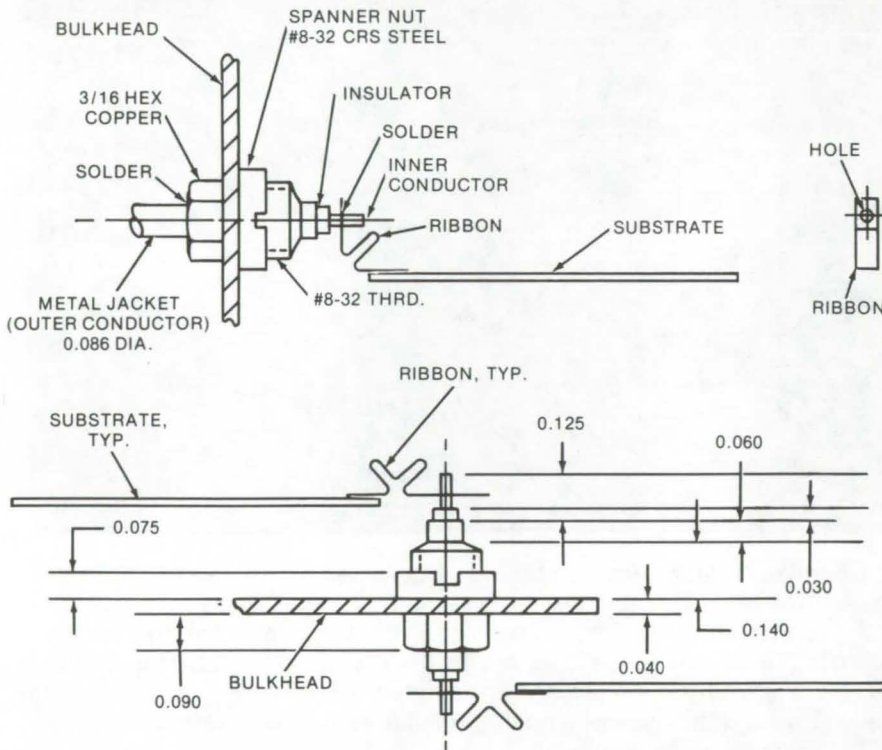
equipment plagued by vibration-induced failure at the cable-to-printed-wiring-board interface. The loop, in mechanically and electrically coupling cable to the board,

lowers fabrication costs by reducing the number of parts needed, a primary goal of low-cost portable electronics equipment designers.

Two applications of the loop are shown. In both, the ribbon has a hole drilled in one end. The blank end is soldered to the appropriate printed-wiring board land. The inner conductor of the cable (top view) or of the feedthrough (bottom) is slipped through the loop hole and is soldered, using a low-temperature solder (Sn 63).

Previously the cable connector was bolted to one side of the bulkhead, and the inner conductor was exposed. The connector shell (ground-plane conductor) was soldered to the bulkhead, using a high-melting-point solder, and the inner conductor was soldered, using a low-melting-point solder. In the new method, only the latter solder is required at both sites. A similarly shaped loop is used to interface wiring boards on either side of a coaxial feedthrough. As before, a hole is drilled on one end of the ribbon to ease fastening to the feedthrough conductor.

This work was done by Harold Mandel and Jesus R. Muniz of TRW, Inc., for Johnson Space Center. No further documentation is available.
MSC-16371



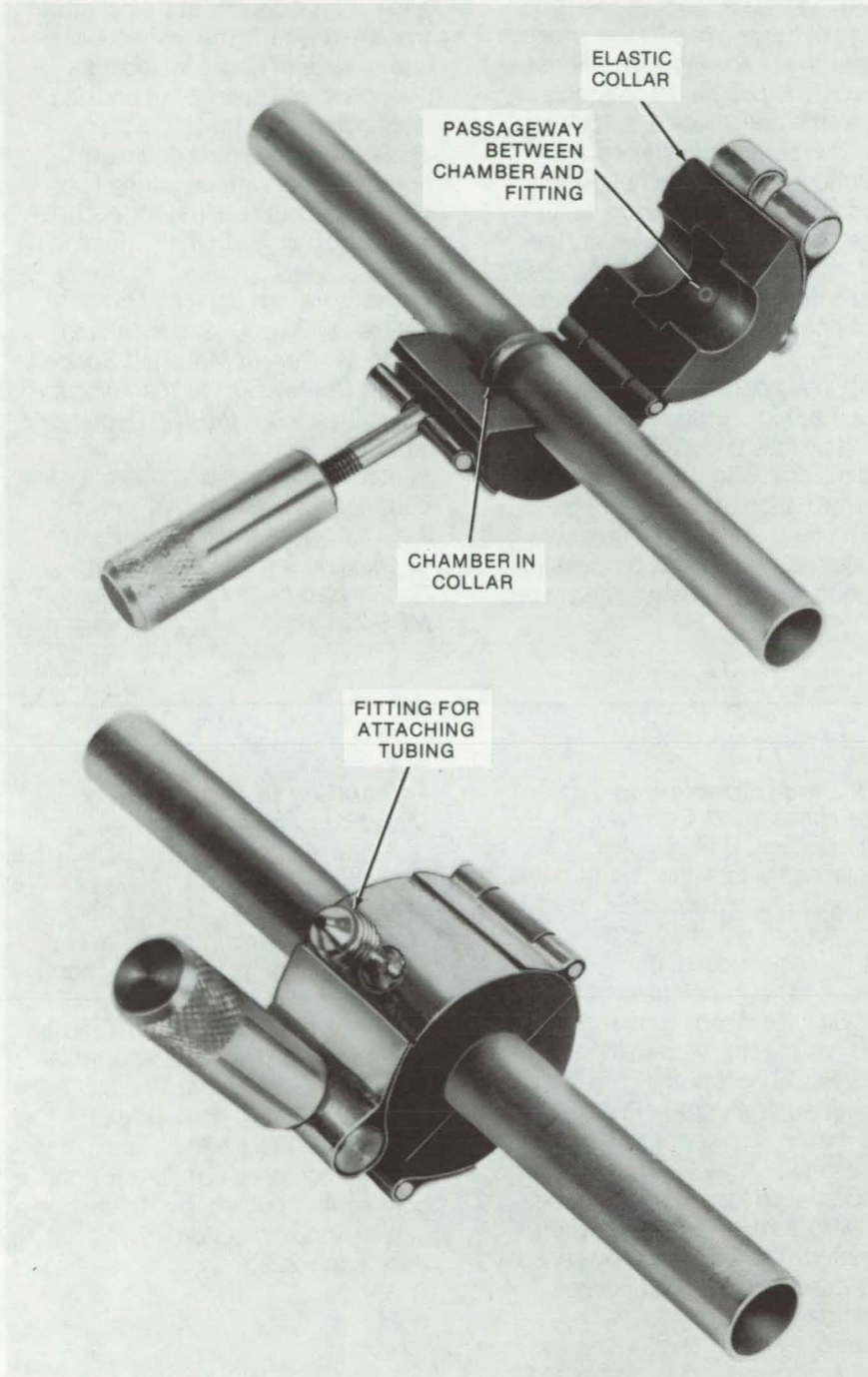
NOTE: ALL DIMENSIONS ARE IN INCHES.

The **Hard-Wiring Loop** is used to interface a coaxial cable (top) or a feedthrough (bottom) to a printed-wiring board. The loop, a strip of annealed-nickel ribbon bent as shown, absorbs vibration that may cause joint failure. In the version shown, the ribbon width is 0.05 in. (0.013 cm); the coax inner conductor diameter is 0.02 in. (0.005 cm). The loop can eliminate much of the cable-to-board interface hardware used, particularly in low-cost portable electronics equipment.

Inspection Tool for Butt-Welded Tubing

A leaking joint is more readily tested, even at an inaccessible weld site.

Caltech/JPL, Pasadena, California



An inspection tool tests the cohesion of butt-welded joints that are difficult to reach with conventional weld-seam testers. The tool, particularly useful in detecting leakage in joints that are close to one another, consists of a small elastic collar that surrounds the butt joint. Any leakage through the weld is contained in the collar; then it is bled to a suitable detection device.

The leak inspection tool collar, as illustrated, is surrounded by a metal casing held tightly about the weld via a screw clamp. Leakage flows through the passageway between the chamber and the tubing and exits via a fitting. As originally designed, the tool is slipped over tubing typically having an outside diameter of 3/16 to 1/2 in. (0.5 to 1.3 cm).

This work was done by Douglas P. Horman of Caltech/JPL. No further documentation is available. NPO-13975

The **Inspection Tool for Tubing** consists of a metal casing that houses an elastic collar. The collar, shown in the open position (above), is clamped around the weld site under test. Any leakage through the weld is contained within a chamber and is bled to the detector via tubing attached to a fitting (below). The tool, originally designed to detect fluid leakage in tubing, can also be used to detect gas leaks.

Molding Cork Sheets to Complex Shapes

Partially-cured cork sheet could be easily formed to complex shapes and then final-cured.

Marshall Space Flight Center, Alabama

Cork sheet produced by conventional techniques is a composite material made of chopped or ground cork bound together with a fully-cured heat-resistant phenolic resin. It is generally produced in a block and sliced into sheets of the desired thickness. These sheets can be shaped readily for bonding onto flat surfaces, but the cork composite retains a memory of its flat shape and is difficult to bond to complex shapes without cracking or breaking.

A proposed technique would allow large sheets of cork to be draped over the contour of a complex surface and bonded in place without introducing undue stresses or folding in the sheet. The curing process would be interrupted when

the resin binder reaches the "B" stage of the polymerization process, rather than allowing it to become completely polymerized. At this point, the cork block is sufficiently cured to be cut into sheets of the desired thickness and handled in much the same way as the fully-cured cork sheets. However, the "B"-stage material readily drapes over a complex shape and, under heat and pressure, conforms closely to the supporting surfaces. Under continued application of heat and vacuum-bag pressure, the sheet could be fully cured, while eliminating the cracking, tearing, bridging, and formation of residual stresses.

The temperature and pressure levels required for this process will depend upon the resin system used

and the final density and strength that are desired. The resin could be one of several types, including phenolics, melamines, or epoxies. Depending upon the particular application, the sheet could be bonded to the surface during final cure, or it could be first-formed in a mold and bonded to the surface in a separate step.

This work was done by Max H. Sharpe, William G. Simpson, and Hill M. Walker, of Marshall Space Flight Center. For further information, Circle 55 on the TSP Request Card.

Inquiries concerning rights for the commercial use of this invention should be addressed to the Patent Counsel, Marshall Space Flight Center [see page A8]. Refer to MFS-23626.

Pretreatment for Strong Aluminum/Epoxy/Aluminum Bonds

An improved epoxy-polyamide surface primer system produces aluminum/aluminum bonds as strong as those following chromate pretreatment. The primer is compatible with epoxy adhesives and eliminates the need for hot acid-chromate surface pretreatment. The formulation is prepared by combining 5 parts by weight of epoxy 828, 5 parts by weight of a commercially available polyamide, and 10 parts by weight of absolute methanol. It is applied to precleaned aluminum surfaces with a camel's-hair brush, is allowed to dry, and is cured in an oven for 15 minutes. The epoxy adhesive can be applied within the hour.

(See page 232.)

MIS Diode Structure in As⁺-Implanted CdS

Undoped CdS boules can be implanted with As ions and overlaid with platinum electrodes to form a structure that behaves as a metal-insulator-semiconductor (MIS) diode. The implanted structures exhibit increased turnover voltages that rise with increasing current. Analysis suggests that this behavior is characteristic of a Pt-CdS potential barrier in series with a high-resistance layer. The implanted diodes also show a decrease in forward turnover voltage when illuminated. This is caused by optically-activated tunneling processes.

(See page 185.)

Preparation of Organosiloxy-Molybdenum Monomer

A new compound may serve as a monomer for a thermally stable polymer suitable for lubricants, electrical semiconductors, and protective coatings. The monomer, Mo(OSiPh₃)₄, is stable to 230° C, does not react with water, and has limited solubility. It is prepared via a redox reaction in which MoO₂Cl₂ acts as both the oxidant and reductant. TiCl₄ serves as a catalyst. It should be possible to form a polymeric species by following a similar redox reaction.

(See page 222.)

Honeycomb Chassis for Electronic Components

Component-support plates provide load sharing, reduce weight, and lower costs.

Caltech/JPL, Pasadena, California

In a new electronic chassis support, machined honeycomb members are used to change the basic relationship between the chassis and the support structure itself. Until now, thermal loads generated by components on the chassis and the mechanical weight of the chassis

were considered separately from the thermal dissipation and support requirements of the structure within which the chassis was mounted. The improved chassis combines internal and external support and heat dissipation by altering the chassis internal geometry. Honeycomb

materials allow mechanical support and thermal load sharing to be combined at a lower weight and at a lower cost than in previous equipment.

As illustrated in Figure 1, the redesigned chassis utilizes several component-support plates, fabricated from honeycomb core and sheet metal. Components are mounted on these support plates with mechanical fasteners that isolate them from external structural and acoustical loads.

The support plates are mounted between two aluminum shear plates. In addition to supporting the component-support boards, these shear plates were designed to be an integral part of a spacecraft bus structure, and they share external loads. As such, the concept could be particularly useful for equipment mounted on the frame or other structural members of a moving vehicle. This is especially true when the equipment must be mounted near a heat source, such as an engine, because the aluminum support plates will disperse uneven external heat loads and help to eliminate hotspots within the chassis.

The completed assembly is installed into a framework (see Figure 2) with mechanical fasteners. Brackets are used to conduct heat directly to the front shear plate. Thermal control louvers, if needed, are attached to it. Aluminum channels and fastener inserts are attached to the core and panel sandwich assembly. A notched bracket on one side of the panel provides a mounting surface for electrical connectors.

This work was done by William S. Read and Bill W. Stebbins of Caltech/JPL. For further information, Circle 56 on the TSP Request Card.

NPO-13891

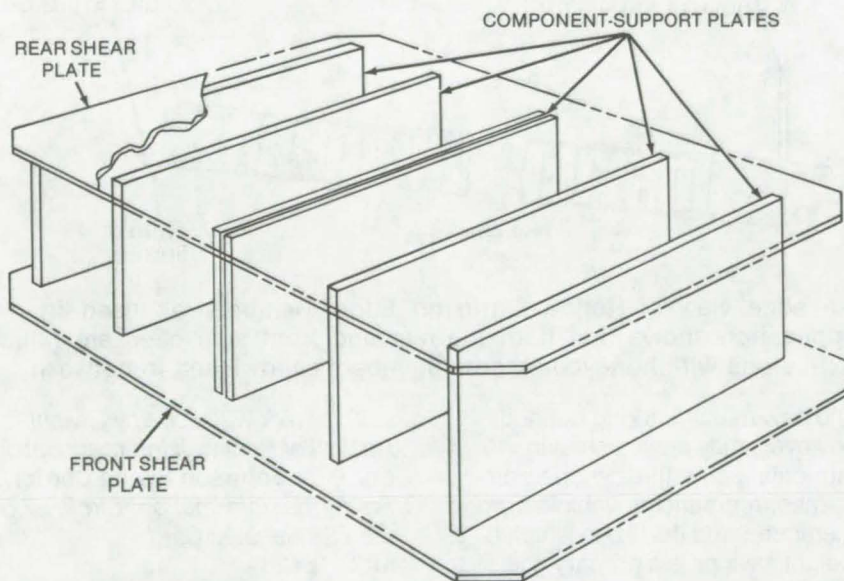


Figure 1. Honeycomb Structure Component-Support Members are mounted between front and rear shear plates. The modular structure comprises a subchassis having a load-sharing function. The shear plates also serve as radiators for thermal dissipation. The subchassis serves as a beam spanning the width and length of a larger structure. In one application, brackets are used to conduct heat to the front shear plate. Thermal control louvers are attached to this plate.

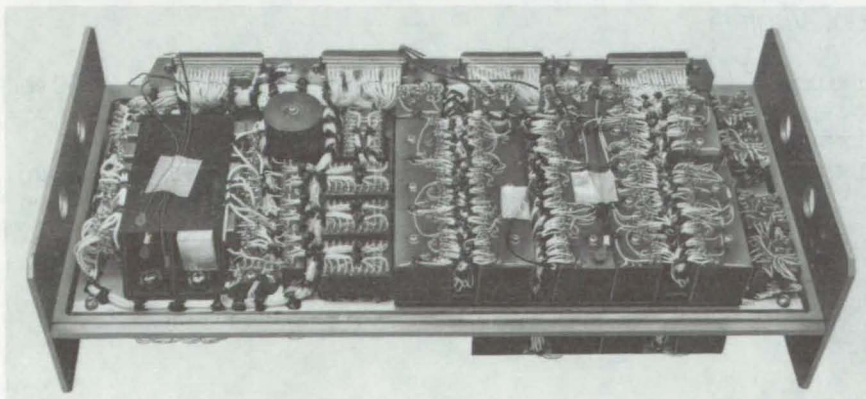


Figure 2. A Support Plate After Installation shows the notched brackets on one side of the plate. The notched brackets are for mounting electrical connectors that fit within the notches.

Extruded Edge Members for Honeycombs

Hollow edge members are made from bonded aluminum extrusions that don't require stuffing.

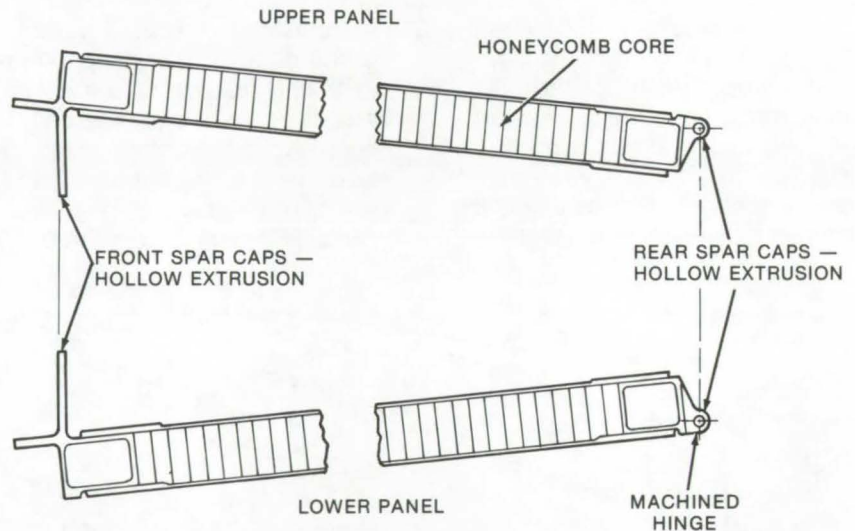
Lyndon B. Johnson Space Center, Houston, Texas

Edge members in bonded honeycomb panel structures are conventionally made by machining channels in aluminum bars. The open ends are stuffed with honeycomb core, using an intumescent adhesive. A less expensive technique for manufacturing these hollow extrusion-edge members eliminates the need for stuffing. Furthermore, the extruded edges are more reliable, lighter, and easier to install.

The advantages of the hollow members are:

- Core splicing and attendant time-consuming steps are no longer required.
- A two-stage bond sequence is used instead of the more costly three-stage sequence.
- Material and machining costs are reduced.

Hollow complex shapes of this type had not been used previously as edge members in primary structures because of the small circum-scribing-hole diameter, complex shape, and relatively small hollow.



An edge view of **Hollow-Extrusion Edge Members** as used in one application shows that both the rear and front spar caps are hollow extrusions with honeycomb core members sandwiched in between.

The new manufacturing method, however, may prove useful in fabricating structures such as airframes, recreational-vehicle frame members, and the like in which a weight savings is a primary goal.

*This work was done by Dwight R. Haskell of Rockwell International Corp. for **Johnson Space Center**. For further information, Circle 57 on the TSP Request Card. MSC-16428*

Polyimide Thin-Film Dielectrics on Ferroelectrics

Liquid polymer is applied in desired thickness on photoresist spinner.

Langley Research Center, Hampton, Virginia

The conducting layers of a multilayered thin-film ferroelectric device, such as is used in a liquid crystal/ferroelectric display, can be electrically isolated using a thin-film layer of polyimide. The thickness of

the polyimide dielectric is controlled by applying the polyimide in liquid form to the substrate and spinning the substrate at a specific rate.

A commercially-available liquid polyimide with an electrical break-

down strength exceeding 3,000 volts per mil was successfully used for this application. The polyimide adheres well to glass, gold, ceramic materials composed of lead zirconate and lead titanate (PZT), and PZT

doped with lanthanum (PLZT). Insulating layers from less than 1 and up to 5 microns thick, with electrical breakdown strengths of up to 300 volts, have been applied on a variety of substrates, using a photoresist spinner, the spin rate determining the thickness of the film.

The recommended curing temperature for the commercially available polyimide used is 300° C. However, lower temperatures can be employed, using longer curing cycles.

The polyimide insulating layer can be applied as a continuous insulation between two conducting layers or may be formed with crossovers or

vias (feedthrough holes). Vias can be formed at any place in the thin film after substrate coating, using standard photolithographic techniques. Using positive photoresist, the areas of photoresist exposed to UV light and the polyimide are simultaneously developed in alkaline developer. During developing, the polyimide is simultaneously removed in areas where the photoresist is not polymerized. Edge definitions of ± 0.1 mil tolerance have been achieved with this technique.

The polyimide thin-film dielectric on ferroelectrics proved to be superior to other thin-film dielectrics, such as oxides on silicon. The

fabrication of multilayered ferroelectric circuits is greatly simplified by the incorporation of this material applied by the spinning technique. The use of polyimide as a dielectric is not restricted to ferroelectric devices. Its ease of application and high electrical breakdown strength allow a dependable and economical means of providing a dielectric for other thin-film microelectronic devices.

This work was done by Rodney V. Galiardi of Rockwell International Corp. for Langley Research Center. No further documentation is available.
LAR-11996

Gold Recovery Process From Polyimide Film

A new process economically separates gold from goldized polyimide film and other nonmetallic scrap. The process uses nitric acid to destroy the nonmetallic material and to leave the gold intact. After the polymer scrap is cut into pieces suitable for boiling, it is slowly heated in an acid-resistant kettle for approximately 2 to 3 hours. The solution is filtered, and the gold flakes are washed and then baked at 100° C to burn off all residual polymer and to dry the flakes. No additional separation step is necessary.

(See page 232.)

Thermal-Impedance Test for Hybrid Power Devices

An in-process test of the quality and performance of a hybrid structure can be made by measuring its thermal impedance. In the case of a Darlington power semiconductor, this measurement was used to evaluate the eutectic bond quality between the BeO substrate and the Kovar case. The thermal impedance may be verified from the device power dissipation and the change in its junction temperature. The latter can be determined from measurements of the collector-to-emitter saturation voltage.

(See page 178.)

Ni-Cu-Zr Alloy for Catalytic Reactors

An improved Ni-Cu-Zr alloy is potentially superior material for use in catalytic reactors. The new material is a minor alloy modification of Monel alloy 400, a known catalyst, but has better mechanical properties at elevated temperatures and essentially-identical catalytic behavior. The new alloy is prepared by adding 0.2 weight-percent Zr to Ni-30Cu, solution heat treating at 2,000° F, and precipitation aging at 1,381° to 1,745° F. A light cold-roll pass after the solution heat treatment produces a finer, more evenly distributed precipitate.

(See page 225.)

Books and Reports

These reports, studies, and handbooks are available from NASA as Technical Support Packages (TSP's) when a Request Card number is cited; otherwise they are available from one of NASA's Industrial Application Centers or the National Technical Information Service.

The Processing of Materials in Outer Space

Zero-gravity environment may lead to the fabrication of new and improved materials.

The properties of many materials may be substantially improved when processed in the microgravity environment of outer space. According to a comprehensive study of the application of this promising technology to superconducting and electrical contact materials, outer space

processing could improve the microstructure and homogeneity of many single and multicomponent systems that are formed from the solidification of fluid phases. New structures that are impossible to form terrestrially may also be accessible in the space environment.

The unique conditions of zero gravity offer the possibility that solid billets could be produced from liquid melts without the need for a container. If so, contamination would be

(continued on next page)

reduced; and since the number of nucleation sites would also be diminished, large undercoolings may be possible leading to a finer, more uniform microstructure in the solidified material. Zero gravity would also retard segregation and agglomeration processes that are encouraged by convective currents resulting from density variations and thermal gradients.

In the fabrication of superconductors, these unique characteristics could improve the quality of superconducting normal metal systems such as the Tseui alloys (Cu-Nb-Sn for example) by yielding a more homogeneous distribution of superconducting dendrites within the normal matrix. Improved samples of the A15 compounds and metallic sulfides are also possible, and new materials with high critical currents and fields may be formed since these properties are known to be

strongly dependent on microstructure. The possibility that superconducting wires could be cast directly from liquid melts has also been suggested.

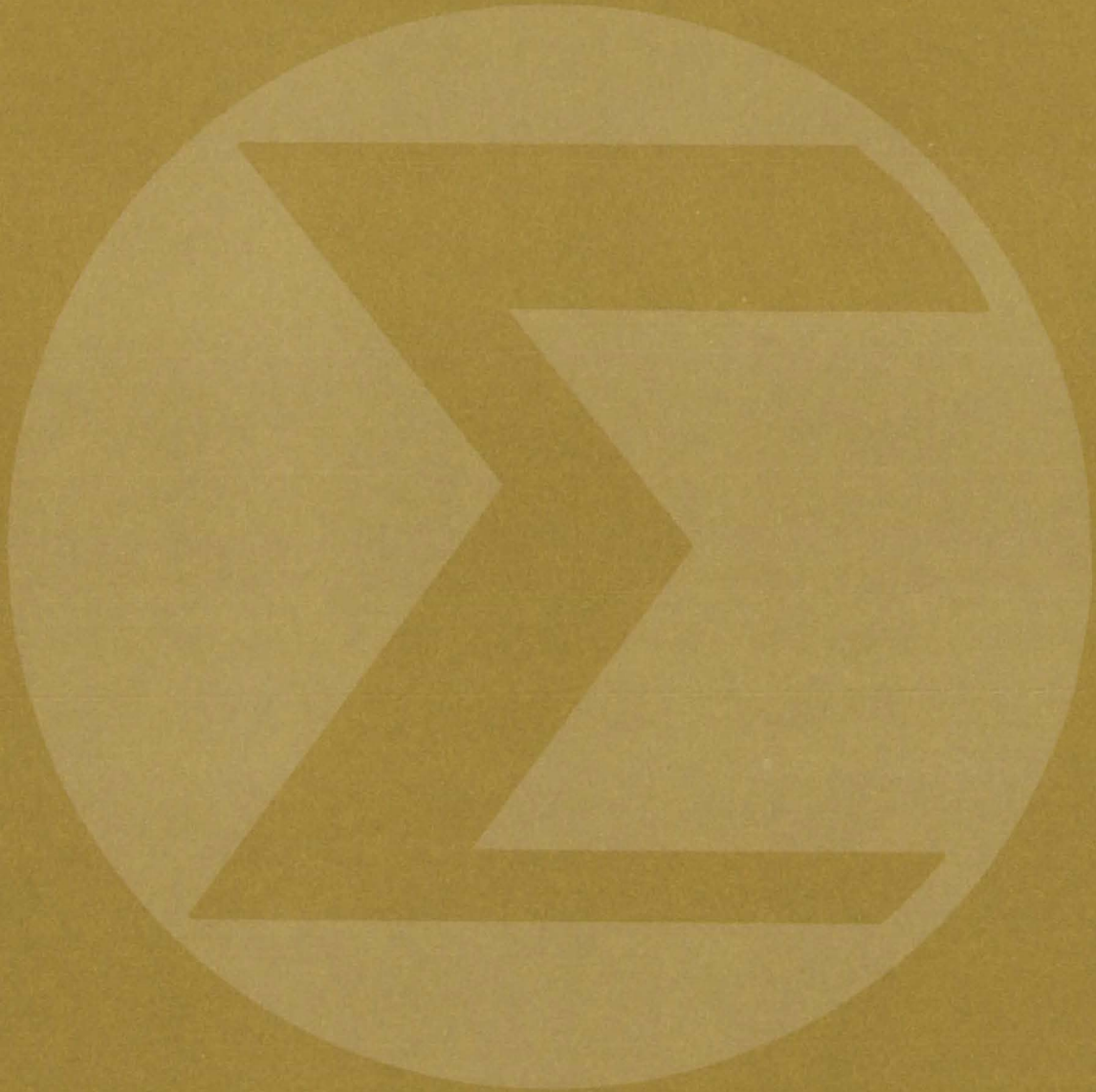
The application of space processing to the fabrication of electrical contact materials such as Ag-W and Ag-CdO may lead to improved properties since electrical contact performance is known to be dependent on microstructural features, such as the concentration of the dispersed phase, porosity, and particle size and distribution. Special techniques such as powder blending and internal oxidation of the dispersed phase, which are difficult to carry out when gravity-induced disturbances are present, may be carried out in space to produce new and better materials. Outer space may also serve as the ideal laboratory for the preparation of research specimens to study the properties of

these materials.

A preliminary terrestrial experimental effort was carried out to produce and evaluate rapidly-cooled Pb-Zn and Cu-Nb-Sn alloys in order to understand the relationship between microstructure and superconducting properties and to simulate the fine structure potentially achievable by space processing.

*This work was done by S. H. Gelles and E. W. Colling of Battelle Columbus Laboratories for **Marshall Space Flight Center**. Further information may be found in NASA CR-150156 [N77-16075], "Analytical Study of Space Processing of Immiscible Materials for Superconductors and Electrical Contacts" [\$4.50]. A copy may be purchased [prepayment required] from the National Technical Information Service, Springfield, Virginia 22151. MFS-23695*

Mathematics and Information Sciences



Computer Programs

285 Shuttle Avionics Visual Display

285 Flexible Data-Management System

Computer Programs

These programs may be obtained at very reasonable cost from COSMIC, a facility sponsored by NASA to make new programs available to the public. For information on program price, size, and availability, circle the reference letter on the COSMIC Request Card in this issue.

Shuttle Avionics Visual Display

SAV-D support system helps to develop displays.

The SAV-D system is composed of a display description language (DDL) and its language processor. The language provides for the description of displays in terms of static and variable references for text, special symbols, lines, and circles. Graphic displays have previously been hand-coded, using macro capabilities supplied by the manufacturer. SAV-D permits the use of a high-order English-like language to describe complete displays with increased speed and ease of coding, debugging, and modification. It also allows one to specify static and variable attributes, such as location, flash, dash, character size, and intensity.

With direct communication of computers via CRT terminals and the general use of graphic displays becoming widespread, a system such as SAV-D should find many commercial applications. Although SAV-D was adapted specifically for Shuttle displays, its principles and logic could be modified for other equipment. In conjunction with appropriate CRT's, SAV-D could be used directly to develop, test, and generate end-use graphics.

The SAV-D DDL simplifies the construction of displays for the display unit (DU) CRT's used on the Space Shuttle vehicle. The language processor translates a display description written in DDL to an object program that, when executed by the display electronics unit

(DEU), produces the desired display. The object program consists of a sequence of binary format control words (FCW's) and a control interface block (CIB). The FCW's are DEU instructions for display generation. The CIB contains information required to update the generated FCW's with values that are functions of dynamic data available at the time the FCW's are loaded or being executed in the DEU memory.

Inputs to the SAV-D language processor are a source program written in DDL and an optional DEU character-set reassignment file. The source program may contain two types of DDL statements. Normal SAV-D statements permit the programmer to describe a display symbolically, without concern for the instruction set available on the DEU. Symbolic FCW statements permit direct programming of the hardware by providing a facility to express FCW's to be executed by the DEU. SAV-D assigns a CRT symbol and symbol name to each hexadecimal DEU code. The programmer may override these assignments, either selectively or completely, by supplying his own reassignments. The reassignment consists of a symbol name and single character code representation (if one exists) for each hexadecimal DEU code to be reassigned.

The language processor outputs an executable object program, directives for real-time modification of the program, and listings that help to resolve problems with unsatisfactory displays. The object program is loaded in the DEU memory, is updated with real-time values, and is executed to produce the desired display. The DEU in the Space Shuttle system interfaces the IBM AP101 with the Multifunctional CRT Display System (MCDS).

The SAV-D program is written in FORTRAN IV for execution in the batch mode and has been implemented on an IBM 370/165 with a

central memory requirement of approximately 500K (decimal) of 8-bit bytes.

This program was written by Arthur A. Yoshimura of Rockwell International Corp. for Johnson Space Center. For further information, Circle E on the COSMIC Request Card.
MSC-16591

Flexible Data-Management System

Management and analysis of large data bases

The NASA Aerospace Safety Research and Data Institute (ASRDI) has developed a computerized data-management and data-analysis system called CADMAT (Combined ASRDI Data-Management and Analysis Technique). CADMAT is a system of computer programs and procedures that can be used to conduct data-management tasks. The CADMAT system was developed specifically for use by scientists and engineers who are confronted with the task of management and analysis of large quantities of data that are organized into records of events (up to 32,750 "rows" through the data) and parametric fields (up to 60 "columns" through the data). Each data element or value is represented to the system as either a single four-byte floating-point number or a four-byte "fact" (an alphanumeric character string).

CADMAT is particularly useful when the data are continually being accumulated, such as the results of a test program, and when the need for retrieval and analysis is ongoing. CADMAT can accommodate only one user at a time and is not suitable for situations requiring simultaneous multiple-user access. In order to use the CADMAT system, an understanding of Boolean algebra and set theory is necessary.



Several unique features exist in the CADMAT system. They include:

- The accommodation of raw data in virtually any FORTRAN readable format. Preparatory data manipulations such as field inversions are not necessary. Data can be added by simply inserting them beneath the previous data.
- An administrative authority, accessed by a code word, that provides for the joining and quitting of data files and users, controls user time and page rations, and determines user access to particular files.
- A second access level within each data file that partitions "sensitive" fields and "sensitive" activities.
- A system self-performance evaluation feature that is a data file in itself in the form of a usage log (a record of activities on the system), which is automatically updated by

the system after each user session and is definable to the system as a data file for retrieval and analysis. This provides a complete historical accounting of the use of the system.

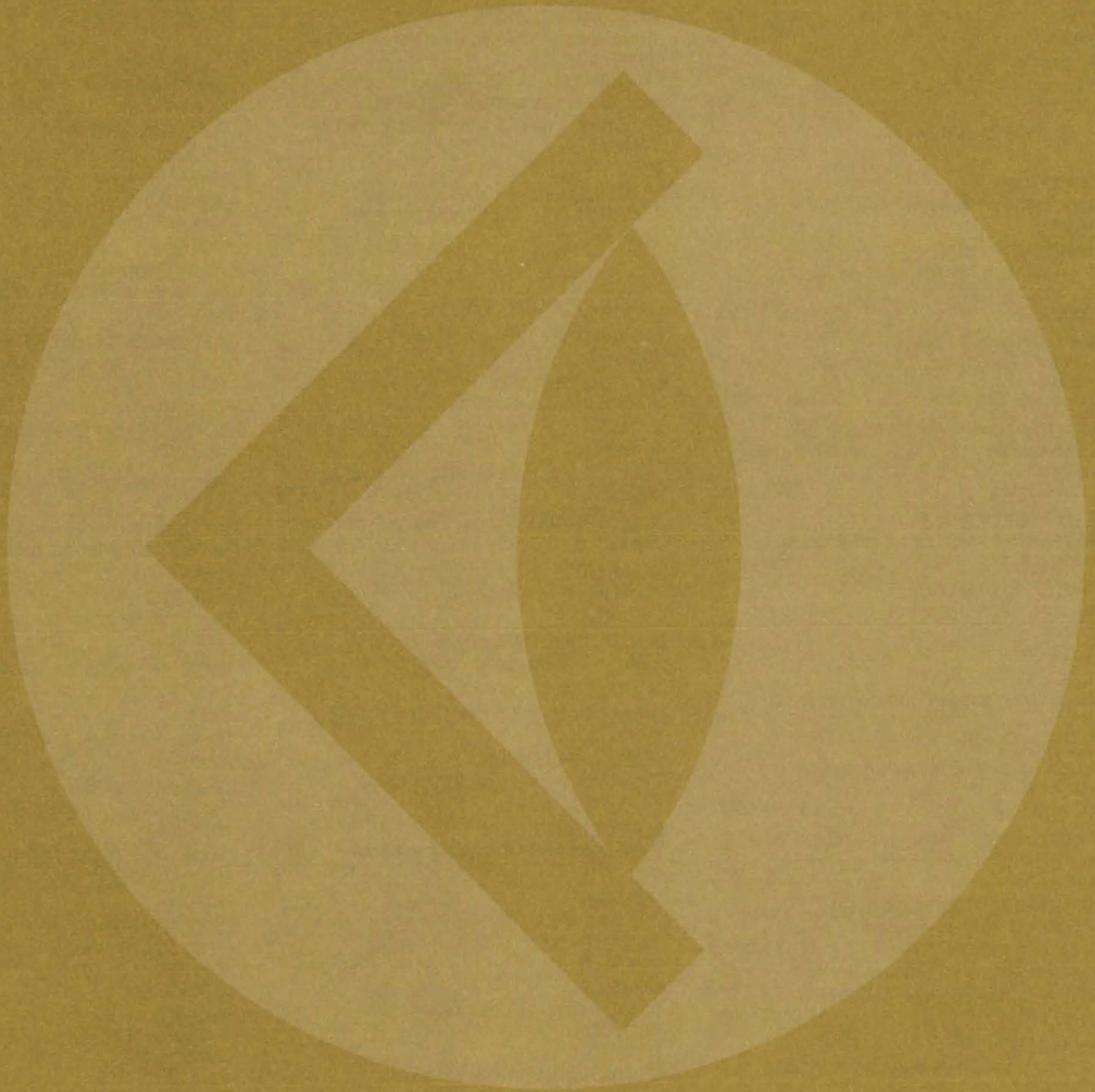
- The capability to search on any or all of up to 60 fields.
- Online or offline operations, using either interactively formulated strategies or previously formulated strategies.
- Automatic restart of user sessions after interruptions due to machine problems.
- A selection of many data-analysis features directly accessible by the user that allow him to perform a variety of diagnostic manipulations of the data. These features include: the generation of graphs and histograms, alphabetical and numerical sorting, the calculation of means and variances, statistical and

mathematical modeling, the preparation of data outlines, raw data output to external data set locations, and raw data entry from the user's terminal.

- A feature in the software that allows further analytic capabilities to be added without extensive re-programming of the CADMAT code.
- The CADMAT system is written in FORTRAN IV for the IBM FORTRAN (H) compiler. CADMAT has been implemented on an IBM TSS/360 with a central memory requirement of approximately 1,000K 8-bit bytes. Though tailored to the TSS environment, the program could be modified for use on other operating systems.

*This work was done by James J. Pelouch, Jr., of **Lewis Research Center**. For further information, Circle F on the COSMIC Request Card.*
LEW-12570

SUBJECT INDEX



ABSORBERS [MATERIALS]

Electromagnetic power absorber
page 208 NPO-13830

Modular test system for solar collector
page 207 MFS-23701

ACETYSALICYLIC ACID

Aspirin/metiamide reduces stomach
ulceration
page 242 ARC-11038

ACOUSTIC MEASUREMENTS

Ultrasonic-mammography apparatus
page 244 NPO-13935

ACTIVATION

Carbon-chlorine-carbon sewage treatment
page 200 NPO-13972

ACTIVITY [BIOLOGY]

Biological-activity monitor
page 245 NPO-14089

Virus Detection System
page 239 MSC-16098

ADHESION

Single-donor leukophoretic technique
page 241 MSC-16297

ADHESIVE BONDING

Pretreatment for strong aluminum/epoxy/
aluminum bonds
page 232 GSC-12232

AERODYNAMIC DRAG

Aircraft aerodynamics at high angles of
attack
page 262 ARC-11133

AERODYNAMIC HEAT TRANSFER

Improved accuracy with phase-change
paints
page 251 LAR-12025

AIR CONDITIONING

Modular test system for solar collector
page 207 MFS-23701

AIRCRAFT DESIGN

Aircraft aerodynamics at high angles of
attack
page 262 ARC-11133

ALLOYS

Controlling stress-corrosion cracking
page 235 MFS-23416

ALUMINUM

Impact-resistant boron/aluminum
composites
page 221 LEW-12472

Pretreatment for strong aluminum/epoxy/
aluminum bonds
page 232 GSC-12232

AMMONIUM PERCHLORATES

Obtaining ultradry crystalline solids
page 234 NPO-13618

AMPLIFIERS

Bidirectional amplifier
page 175 KSC-10856

ANALGESIA

Aspirin/metiamide reduces stomach
ulceration
page 242 ARC-11038

ANALOG DATA

Bidirectional amplifier
page 175 KSC-10856

ANGULAR RESOLUTION

Mass spectrometer has wide angular
acceptance
page 203 NPO-14111

ANODES

Anodic growth of niobium oxide
page 235 MFS-23150

ANODIC COATINGS

Anodic growth of niobium oxide
page 235 MFS-23150

ANTIHISTAMINICS

Aspirin/metiamide reduces stomach
ulceration
page 242 ARC-11038

ARSENIC

MIS diode structure in As⁺-implanted CdS
page 185 LAR-12156

AUTOCORRELATION

Three-level signal sampler has automatic
threshold
page 182 NPO-14042

AUTOMATIC CONTROL VALVES

Automatic channel trimming for control
systems
page 189 MSC-16027

AUTOMOBILE ENGINES

Ni-Cu-Zr alloy for catalytic reactors
page 225 LEW-12245

BACTERIA

Bacteria/virus filter membrane
page 241 MSC-16388

BACTERIOPHAGES

Virus detection system
page 239 MSC-16098

BEARINGS

Heat pipe controls bearing temperature
page 267 LAR-11846

Magnetically-Controlled Bearing Lubrication
page 271 MFS-23009

BIOMETRICS

Acquisition system for biomedical data
page 246 MSC-16144

BLACK BODY RADIATION

Electromagnetic power absorber
page 208 NPO-13830

Active-cavity radiometer/pyrheliometer
page 211 NPO-13819

BLAST DEFLECTORS

Protection against explosive blasts
page 258 LAR-12014

BLAST LOADS

Protection against explosive blasts
page 258 LAR-12014

BONDING

Pretreatment for strong aluminum/epoxy/
aluminum bonds
page 232 GSC-12232

BORON

Impact-resistant boron/aluminum
composites
page 221 LEW-12472

BORON REINFORCED MATERIALS

Impact-resistant boron/aluminum
composites
page 221 LEW-12472

BOTTLES

Drug-dosage indicator
page 247 GSC-12139

BOURDON TUBES

High-pressure high-temperature transducer
page 216 MFS-23765

BREWSTER ANGLE

Electromagnetic power absorber
page 208 NPO-13830

BURNERS

Fuel burner with low nitrogen oxide
formation
page 257 NPO-13958

BUTT JOINTS

Inspection tool for butt-welded tubing
page 277 NPO-13975

CADMIUM SULFIDES

MIS diode structure in As⁺-implanted CdS
page 185 LAR-12156

CAPACITORS

Record dielectric breakdown automatically
page 255 NPO-13599

CAPILLARY TUBES

Single-donor leukophoretic technique
page 241 MSC-16297

CARBON

Carbon-chlorine-carbon sewage treatment
page 200 NPO-13972

CARDIOGRAPHY

Acquisition system for biomedical data
page 246 MSC-16144

CARDIOVASCULAR SYSTEM

Acquisition system for biomedical data
page 246 MSC-16144

CARTRIDGES

Cartridge getter for vacuum jacketing
page 270 MSC-16610

Quick-disconnect coupling/filter
page 268 MFS-22323

CATALYSTS

Ni-Cu-Zr alloy for catalytic reactors
page 225 LEW-12245

CERMETS

Oxidation-resistant cermet
page 227 NPO-13666

Radiation-resistant, electrically insulating
cermet
page 226 NPO-13120

Stress, corrosion, and heat-resistant cermet
page 228 NPO-13690

CESIUM IODIDES

Properties of doped cesium iodide crystals
page 236 MFS-23148

CHANNELS [DATA TRANSMISSION]

Multiplexed fiber-optic transmission system
page 193 KSC-11047

CHARGED PARTICLES

Mass spectrometer has wide angular
acceptance
page 203 NPO-14111

CHASSIS

Honeycomb chassis for electronic
components
page 279 NPO-13891

CHEMICAL BONDS

Mass spectrometry by chemi-ionization
page 204 NPO-13857

CHEMICAL REACTORS

Ni-Cu-Zr alloy for catalytic reactors
page 225 LEW-12245

CHLORIDES

Low-temperature coal desulfurization
page 199 NPO-13937

CHLORINATION

Carbon-chlorine-carbon sewage treatment
page 200 NPO-13972

CHLOROPRENE RESINS

Liquid-oxygen-compatible, flame-resistant
coating
page 229 KSC-11020

CIRCUIT BOARDS

Honeycomb chassis for electronic
components
page 279 NPO-13891

COAL

Low-temperature coal desulfurization
page 199 NPO-13937

COATINGS

Improved accuracy with phase-change
paints
page 251 LAR-12025

Preparation of organosiloxo-molybdenum
monomer
page 222 MFS-23704

Pretreatment for strong aluminum/epoxy/
aluminum
page 232 GSC-12232

CODING

Secure communications system
page 190 MSC-16462

COLD TRAPS

Radioactive-gas separation technique
page 202 GSC-12019

COMBUSTION CHAMBERS

Engine injectors
page 260 LEW-12846

Fuel injector for jet-stirred combustors
page 272 LAR-12146

COMBUSTION TEMPERATURE

Fuel burner with low nitrogen oxide
formation
page 257 NPO-13958

COMPARATORS

Three-level signal sampler has automatic
threshold
page 182 NPO-14042

COMPENSATORY TRACKING

Inexpensive high-temperature solar collector
page 213 NPO-13979

COMPOSITE MATERIALS

Impact-resistant boron/aluminum
composites
page 221 LEW-12472

COMPOSITE STRUCTURES

Extruded edge members for honeycombs
page 280 MSC-16428

COMPUTER GRAPHICS

Shuttle avionics visual display
page 285 MSC-16591

COMPUTERIZED SIMULATION

Fluid-line math model
page 260 MSC-16230

CONCENTRATORS

Inexpensive high-temperature solar collector
page 213 NPO-13979

Solar-power mountain concept
page 212 NPO-13861

CONDUCTIVE HEAT TRANSFER

Resilient thermal barrier for high
temperatures
page 234 MSC-16338

CONNECTORS

Quick-disconnect coupling/filter
page 268 MFS-22323

CONTAINERLESS MELTS

The processing of materials in outer space
page 282 MFS-23695

CONTAMINANTS

Quantitative measurement of surface
contamination
page 256 MSC-16679

CONTROL EQUIPMENT

Automatic channel trimming for control
systems
page 189 MSC-16027

Compact reliable multiaxis pivot
page 248 MFS-23311

COOLING SYSTEMS

Heat pipe controls bearing temperature
page 267 LAR-11846

Integrated temperature sensor
page 269 LAR-12056

CORK [MATERIALS]

Molding cork sheets to complex shapes
page 278 MFS-23626

CORROSION PREVENTION

Liquid-oxygen-compatible, flame-resistant
coating
page 229 KSC-11020

CORROSION RESISTANCE

Oxidation-resistant cermet
page 227 NPO-13666

Stress, corrosion, and heat-resistant cermet
page 228 NPO-13690

COUNTING CIRCUITS

Record dielectric breakdown automatically
page 255 NPO-13599

COUPLINGS

Quick-disconnect coupling/filter
page 268 MFS-22323

CRACKING [FRACTURING]

Controlling stress-corrosion cracking
page 235 MFS-23416

Crack-propagation predictions
page 263 MSC-16436

CRACK PROPAGATION

Crack-propagation predictions
page 263 MSC-16436

CROP IDENTIFICATION

Multispectral image processor
page 206 MSC-16253

CRYOGENICS

Radioactive-gas separation technique
page 202 GSC-12019

Superconducting thermometer for
cryogenics
page 215 LAR-12055

CRYOPUMPING

Radioactive-gas separation technique
page 202 GSC-12019

CRYSTALS

Obtaining ultradry crystalline solids
page 234 NPO-13618

Properties of doped cesium iodide crystals
page 236 MFS-23148

CURRENT REGULATORS

Pulse-width-modulated high-current power
supply
page 184 MSC-14668

CURVED PANELS

Molding cork sheets to complex shapes
page 278 MFS-23626

DATA BASES

Flexible data-management system
page 285 LEW-12570

DATA CONVERTERS

"Exclusive-OR" frequency multiplier
page 181 MSC-16677

High speed DAC
page 191 NPO-13805

DATA MANAGEMENT

Flexible data-management system
page 285 LEW-12570

DATA PROCESSING

Advanced general-purpose computer
page 195 MFS-23531

Multispectral data analysis
page 275 MSC-16322/14823

DATA RECORDERS

Record dielectric breakdown automatically
page 255 NPO-13599

DATA REDUCTION

Flexible data-management system
page 285 LEW-12570

Multispectral data analysis
page 275 MSC-16322/14823

DATA SAMPLING

Three-level signal sampler has automatic
threshold
page 182 NPO-14042

DATA SYSTEMS

Earth resources interactive processing
system
page 218 MSC-16004

Flexible data-management system
page 285 LEW-12570

DATA TRANSMISSION

Advanced general-purpose computer
page 195 MFS-23531

Bidirectional amplifier
page 175 KSC-10856

High speed DAC
page 191 NPO-13805

Multiplexed fiber-optic transmission system
page 193 KSC-11047

DECODING

Secure communications system
page 190 MSC-16462

DEHYDRATION

Obtaining ultradry crystalline solids
page 234 NPO-13618

DENSITY MEASUREMENTS

Density measurements of trace gases
page 201 ARC-10760

DESICCATORS

Obtaining ultradry crystalline solids
page 234 NPO-13618

DESULFURIZING

Low-temperature coal desulfurization
page 199 NPO-13937

DIAMINES

Soluble, thermally-stable aromatic
polyimides
page 230 LAR-12092

DIELECTRICS

Polyimide thin-film dielectrics on
ferroelectrics
page 280 LAR-11996

Record dielectric breakdown automatically
page 255 NPO-13599



DIGITAL COMPUTERS Advanced general-purpose computer page 195	MFS-23531	ELECTRIC POWER PLANTS Solar-power mountain concept page 212	NPO-13861	ENERGY DISSIPATION Save power in ac induction motors page 179	MFS-23280
DIGITAL FILTERS "Exclusive-OR" frequency multiplier page 181	MSC-16677	ELECTRIC POWER SUPPLIES Pulse-width-modulated high-current power supply page 184	MSC-14668	ENERGY REQUIREMENTS Power switch/filter for digital circuits page 181	MSC-16442
DIGITAL TO ANALOG CONVERTERS High speed DAC page 191	NPO-13805	ELECTRIC WIRING Semiautomatic labeling of small wires page 267	MSC-16233	ENGINE DESIGN Ni-Cu-Zr alloy for catalytic reactors page 225	LEW-12245
Three-level signal sampler has automatic threshold page 182	NPO-14042	ELECTRICAL INSULATION Polyimide thin-film dielectrics on ferroelectrics page 280	LAR-11996	ENZYME ACTIVITY Biological-activity monitor page 245	NPO-14089
DIODES MIS diode structure in As ⁺ -implanted CdS page 185	LAR-12156	ELECTRICAL RESISTANCE Improved load-cell compensation page 253	MSC-16466	EPOXY RESINS Pretreatment for strong aluminum/epoxy/ aluminum bonds page 232	GSC-12232
DISCONNECT DEVICES Quick-disconnect coupling/filter page 268	MFS-22323	ELECTROCATALYSTS Hollow-fiber H ₂ /O ₂ fuel cell page 210	NPO-13732	EQUALIZERS [CIRCUITS] Bidirectional amplifier page 175	KSC-10856
DISPENSERS Drug-dosage indicator page 247	GSC-12139	ELECTROCHEMICAL CELLS Controlling fires in silver/zinc batteries page 259	MFS-22952	EVAPORATION Obtaining ultradry crystalline solids page 234	NPO-13618
DISPLAY DEVICES Multispectral image processor page 206	MSC-16253	ELECTRODEPOSITION Anodic growth of niobium oxide page 235	MFS-23150	EXCRETION Biological-activity monitor page 245	NPO-14089
Record dielectric breakdown automatically page 255	NPO-13599	ELECTRODES Hollow-fiber H ₂ /O ₂ fuel cell page 210	NPO-13732	EXHAUST SYSTEMS Ni-Cu-Zr alloy for catalytic reactors page 225	LEW-12245
Shuttle avionics visual display page 285	MSC-16591	ELECTROENCEPHALOGRAPHY Acquisition system for biomedical data page 246	MSC-16144	EXPLOSIVES Protection against explosive blasts page 258	LAR-12014
DOSAGE Drug-dosage indicator page 247	GSC-12139	ELECTROLYSIS Thermochemical-photolytic production of hydrogen and oxygen from water page 224	LAR-12118	EXPULSION BLADDERS Detecting gas leaks in propellant lines page 254	MFS-23404
DRUGS Drug-dosage indicator page 247	GSC-12139	ELECTROMAGNETIC ABSORPTION Electromagnetic power absorber page 208	NPO-13830	EXTRACTION Single-donor leukophoretic technique page 241	MSC-16297
DRYING Obtaining ultradry crystalline solids page 234	NPO-13618	ELECTRONIC EQUIPMENT TESTS Thermal-impedance test for hybrid power devices page 178	MSC-16643	FAIL-SAFE SYSTEMS Detecting gas leaks in propellant lines page 254	MFS-23404
DYNAMIC CONTROL Automatic channel trimming for control systems page 189	MSC-16027	ELECTRONIC FILTERS Noise reduction in photomultiplier circuits page 186	LAR-12091	FAILURE Controlling stress-corrosion cracking page 235	MFS-23416
DYNAMIC RESPONSE Wide-dynamic-range detector page 175	GSC-12149	Power switch/filter for digital circuits page 181	MSC-16442	Fatigue-failure load indicator page 251	LAR-12027
EARTH RESOURCES Earth resources interactive processing system page 218	MSC-16004	ELECTRONIC PACKAGING Honeycomb chassis for electronic components page 279	NPO-13891	Integrated temperature sensor page 269	LAR-12056
EFFLUENTS Carbon-chlorine-carbon sewage treatment page 200	NPO-13972	Semiautomatic labeling of small wires page 267	MSC-16233	FAILURE ANALYSIS Crack-propagation predictions page 263	MSC-16436
ELECTRIC BATTERIES Power switch/filter for digital circuits page 181	MSC-16442	ELECTRON IMPACT Mass spectrometry by chemi-ionization page 204	NPO-13857	Record dielectric breakdown automatically page 255	NPO-13599
ELECTRIC BRIDGES Improved load-cell compensation page 253	MSC-16466	ELECTROPLATING Anodic growth of niobium oxide page 235	MFS-23150	FASTENERS Vibration-resistant PC board feedthrough page 276	MSC-16371
ELECTRIC CELLS Solar-cell array design handbook page 217	NPO-14106	ENCODING Secure communications system page 190	MSC-16462	FATIGUE [MATERIALS] Crack-propagation predictions page 263	MSC-16436
ELECTRIC GENERATORS Solar-power mountain concept page 212	NPO-13861	ENERGY ABSORPTION Electromagnetic power absorber page 208	NPO-13830	Fatigue-failure load indicator page 251	LAR-12027
ELECTRIC MOTORS Save power in ac induction motors page 179	MFS-23280	ENERGY CONVERSION Power switch/filter for digital circuits page 181	MSC-16442	FATIGUE TESTS High-pressure high-temperature transducer page 216	MFS-23765
				FEEDBACK CONTROL Automatic channel trimming for control systems page 189	MSC-16027

FERROELECTRICITY Polyimide thin-film dielectrics on ferroelectrics page 280	LAR-11996	FUEL INJECTION Engine injectors page 260	LEW-12846	HONEYCOMB CORES Extruded edge members for honeycombs page 280	MSC-16428
FERROFLUIDS Magnetically-controlled bearing lubrication page 271	MFS-23009	Fuel injector for jet-stirred combustors page 272	LAR-12146	HONEYCOMB STRUCTURES Extruded edge members for honeycombs page 280	MSC-16428
FIBER OPTICS Multiplexed fiber-optic transmission system page 193	KSC-11047	FUELS Low-temperature coal desulfurization page 199	NPO-13937	Honeycomb chassis for electronic components page 279	NPO-13891
FIELD STRENGTH Record dielectric breakdown automatically page 255	NPO-13599	FUEL TANK PRESSURIZATION Pressurization systems page 261	LEW-12845	HYBRID CIRCUITS Thermal-impedance test for hybrid power devices page 178	MSC-16643
FILTRATION Bacteria/virus filter membrane page 241	MSC-16388	GAS DENSITY Density measurements of trace gases page 201	ARC-10760	HYBRID COMPUTERS Advanced general-purpose computer page 195	MFS-23531
FINISHES Pretreatment for strong aluminum/epoxy/aluminum bonds page 232	GSC-12232	Alignment tolerant schlieren system page 214	ARC-10971	HYDRAULIC ANALOGIES Fluid-line math model page 260	MSC-16230
FIRE PREVENTION Controlling fires in silver/zinc batteries page 259	MFS-22952	GAS DETECTORS Density measurements of trace gases page 201	ARC-10760	HYDRAULIC CONTROL Automatic channel trimming for control systems page 189	MSC-16027
FLAME RETARDANTS Liquid-oxygen-compatible, flame-resistant coating page 229	KSC-11020	Detecting gas leaks in propellant lines page 254	MFS-23404	HYDRAULIC EQUIPMENT Fluid-line math model page 260	MSC-16230
FLOW MEASUREMENT Detecting gas leaks in propellant lines page 254	MFS-23404	GAS FLOW Detecting gas leaks in propellant lines page 254	MFS-23404	HYDROGEN Thermochemical-photolytic production of hydrogen and oxygen from water page 224	LAR-12118
FLOW VISUALIZATION Alignment tolerant schlieren system page 214	ARC-10971	Alignment tolerant schlieren system page 214	ARC-10971	HYDROGEN OXYGEN FUEL CELLS Hollow-fiber H ₂ /O ₂ fuel cell page 210	NPO-13732
FLUID FILTERS Bacteria/virus filter membrane page 241	MSC-16388	GAS MIXTURES Density measurements of trace gases page 201	ARC-10760	HYPERSONIC AIRCRAFT Integrated temperature sensor page 269	LAR-12056
Quick-disconnect coupling/filter page 268	MFS-22323	Radioactive-gas separation technique page 202	GSC-12019	IDENTIFYING Semiautomatic labeling of small wires page 267	MSC-16233
FLUIDIC CIRCUITS Fluid-line math model page 260	MSC-16230	GAS RECOVERY Radioactive-gas separation technique page 202	GSC-12019	IMAGE CORRELATORS Earth resources interactive processing system page 218	MSC-16004
FLUORESCENCE Biological-activity monitor page 245	NPO-14089	GETTERS Cartridge getter for vacuum jacketing page 270	MSC-16610	Multispectral data analysis page 275	MSC-16322/14823
Quantitative measurement of surface contamination page 256	MSC-16679	GOLD Gold recovery process from polyimide film page 232	MSC-16650	Multispectral image processor page 206	MSC-16253
FRENKEL DEFECTS Anodic growth of niobium oxide page 235	MFS-23150	HEART RATE Acquisition system for biomedical data page 246	MSC-16144	IMAGERY Shuttle avionics visual display page 285	MSC-16591
FREON Integrated temperature sensor page 269	LAR-12056	HEAT GENERATION Fuel burner with low nitrogen oxide formation page 257	NPO-13958	IMAGING TECHNIQUES Multispectral image processor page 206	MSC-16253
FREQUENCY CONTROL Digital frequency-offset detector page 177	MSC-16358	HEAT PIPES Heat pipe controls bearing temperature page 267	LAR-11846	IMPACT STRENGTH Impact-resistant boron/aluminum composites page 221	LEW-12472
FREQUENCY DIVISION MULTIPLEXING Multiplexed fiber-optic transmission system page 193	KSC-11047	HEAT SHIELDING Resilient thermal barrier for high temperatures page 234	MSC-16338	IMPURITIES Quantitative measurement of surface contamination page 256	MSC-16679
FREQUENCY MEASUREMENT Digital frequency-offset detector page 177	MSC-16358	HEAT TRANSFER Fuel burner with low nitrogen oxide formation page 257	NPO-13958	INDICATING INSTRUMENTS Drug-dosage indicator page 247	GSC-12139
FREQUENCY MULTIPLIERS "Exclusive-OR" frequency multiplier page 181	MSC-16677	HEAT TRANSFER COEFFICIENTS Improved accuracy with phase-change paints page 251	LAR-12025	INDUCTION MOTORS Save power in ac induction motors page 179	MFS-23280
FRICTION REDUCTION Magnetically-controlled bearing lubrication page 271	MFS-23009	HIGH RESOLUTION Mass spectrometer has wide angular acceptance page 203	NPO-14111	INFRARED ADSORPTION Density measurements of trace gases page 201	ARC-10760



INGESTION [BIOLOGY] Biological-activity monitor page 245	NPO-14089	LIFT Aircraft aerodynamics at high angles of attack page 262	ARC-11133	MECHANICAL PROPERTIES Controlling stress-corrosion cracking page 235	MFS-23416
INJECTORS Engine injectors page 260	LEW-12846	LIGHT EMITTING DIODES MIS diode structure in As ⁺ -implanted CdS page 185	LAR-12156	Properties of doped cesium iodide crystals page 236	MFS-23148
Fuel injector for jet-stirred combustors page 272	LAR-12146	LINEARITY Wide-dynamic-range detector page 175	GSC-12149	MECHANICAL SHOCK Vibration-resistant PC board feedthrough page 276	MSC-16371
INSPECTION Inspection tool for butt-welded tubing page 277	NPO-13975	LINEAR RECEIVERS Wide-dynamic-range detector page 175	GSC-12149	METABOLISM Biological-activity monitor page 245	NPO-14089
INSTRUMENT COMPENSATION Improved load-cell compensation page 253	MSC-16466	LIQUID OXYGEN Liquid-oxygen-compatible, flame-resistant coating page 229	KSC-11020	METAL FATIGUE Controlling stress-corrosion cracking page 235	MFS-23416
INTERNAL COMBUSTION ENGINES Ni-Cu-Zr alloy for catalytic reactors page 225	LEW-12245	LIQUID PROPELLANT ROCKET ENGINES Engine injectors page 260	LEW-12846	Fatigue-failure load indicator page 251	LAR-12027
ION BEAMS Mass spectrometry by chemi-ionization page 204	NPO-13857	LIQUID ROCKET PROPELLANTS Engine injectors page 260	LEW-12846	METAL-METAL BONDING Pretreatment for strong aluminum/epoxy/ aluminum bonds page 232	GSC-12232
Mass spectrometer has wide angular acceptance page 203	NPO-14111	LIQUID-GAS MIXTURES Integrated temperature sensor page 269	LAR-12056	METAL OXIDE SEMICONDUCTORS Record dielectric breakdown automatically page 255	NPO-13599
ION EXCHANGE MEMBRANE ELECTROLYTES Hollow-fiber H ₂ /O ₂ fuel cell page 210	NPO-13732	LOADS [FORCES] Fatigue-failure load indicator page 251	LAR-12027	METAL SURFACES Pretreatment for strong aluminum/epoxy/ aluminum bonds page 232	GSC-12232
ION IMPLANTATION MIS diode structure in As ⁺ -implanted CdS page 185	LAR-12156	LOGIC CIRCUITS Record dielectric breakdown automatically page 255	NPO-13599	METASTABLE STATE Mass spectrometry by chemi-ionization page 204	NPO-13857
IONIZATION Mass spectrometry by chemi-ionization page 204	NPO-13857	LOW GRAVITY MANUFACTURING The processing of materials in outer space page 282	MFS-23695	METIAMIDE Aspirin/metiamide reduces stomach ulceration page 242	ARC-11038
ISOTOPE EFFECT Superconducting thermometer for cryogenics page 215	LAR-12055	LUBRICANTS Magnetically-controlled bearing lubrication page 271	MFS-23009	MICROPHONES Density measurements of trace gases page 201	ARC-10760
JET ENGINES Fuel injector for jet-stirred combustors page 272	LAR-12146	MAMMARY GLANDS Ultrasonic-mammography apparatus page 244	NPO-13935	MICROWAVES Electromagnetic power absorber page 208	NPO-13830
JUMPERS Vibration-resistant PC board feedthrough page 276	MSC-16371	MANIPULATORS Automatic channel trimming for control systems page 189	MSC-16027	MIS [SEMICONDUCTORS] MIS diode structure in As ⁺ -implanted CdS page 185	LAR-12156
JUNCTION DIODES MIS diode structure in As ⁺ -implanted CdS page 185	LAR-12156	MAN MACHINE SYSTEMS Multispectral image processor page 206	MSC-16253	MOLDS Molding cork sheets to complex shapes page 278	MFS-23626
KRYPTON 85 Radioactive-gas separation technique page 202	GSC-12019	MARKING Semiautomatic labeling of small wires page 267	MSC-16233	MOLECULAR SPECTROSCOPY Mass spectrometry by chemi-ionization page 204	NPO-13857
LAMINAR FLOW Alinement tolerant schlieren system page 214	ARC-10971	MASS SPECTROMETERS Mass spectrometer has wide angular acceptance page 203	NPO-14111	MOLYBDENUM Preparation of organosiloxy-molybdenum monomer page 222	MFS-23704
LAMINATES A new polyimide laminating resin page 231	LAR-12211	MASS SPECTROSCOPY Mass spectrometry by chemi-ionization page 204	NPO-13857	MONITORS Biological-activity monitor page 245	NPO-14089
Extruded edge members for honeycombs page 280	MSC-16428	MATERIALS RECOVERY Gold recovery process from polyimide film page 232	MSC-16650	MONOMERS Preparation of organosiloxy-molybdenum monomer page 222	MFS-23704
LENSES Inexpensive high-temperature solar collector page 213	NPO-13979			Soluble, thermally-stable aromatic polyimides page 230	LAR-12092
LEUKOCYTES Single-donor leukophoretic technique page 241	MSC-16297			MOTORS Save power in ac induction motors page 179	MFS-23280
				MOUNTAINS Solar-power mountain concept page 212	NPO-13861

- MTBF**
Vibration-resistant PC board feedthrough
page 276 MSC-16371
- MULTIPLEXING**
Bidirectional amplifier
page 175 KSC-10856
Multiplexed fiber-optic transmission system
page 193 KSC-11047
Advanced general-purpose computer
page 195 MFS-23531
- MULTIPROCESSING (COMPUTERS)**
Advanced general-purpose computer
page 195 MFS-23531
- MULTISPECTRAL BAND SCANNERS**
Multispectral data analysis
page 275 MSC-16322/14823
Multispectral image processor
page 206 MSC-16253
- NIObIUM OXIDES**
Anodic growth of niobium oxide
page 235 MFS-23150
- NITROGEN OXIDES**
Fuel burner with low nitrogen oxide
formation
page 257 NPO-13958
- NOISE MEASUREMENT**
Three-level signal sampler has automatic
threshold
page 182 NPO-14042
- NOISE REDUCTION**
Noise reduction in photomultiplier circuits
page 186 LAR-12091
- NONDESTRUCTIVE TESTS**
Inspection tool for butt-welded tubing
page 277 NPO-13975
Thermal-impedance test for hybrid power
devices
page 178 MSC-16643
- NONNEWTONIAN FLUIDS**
Tensile viscosities of non-Newtonian fluids
page 233 NPO-13973
- OPTICAL DENSITY**
Alignment tolerant schlieren system
page 214 ARC-10971
- OPTICAL PROPERTIES**
Properties of doped cesium iodide crystals
page 236 MFS-23148
- OXIDATION RESISTANCE**
Oxidation-resistant cermet
page 227 NPO-13666
Stress, corrosion, and heat-resistant cermet
page 228 NPO-13690
- OXYGEN**
Thermochemical-photolytic production of
hydrogen and oxygen from water
page 224 LAR-12118
- PAINTS**
Improved accuracy with phase-change
paints
page 251 LAR-12025
Preparation of zinc orthotitanate
page 223 MFS-23345
- PALLADIUM COMPOUNDS**
Cartridge getter for vacuum jacketing
page 270 MSC-16610
- PATHOGENS**
Virus detection system
page 239 MSC-16098
- PATTERN RECOGNITION**
Earth resources interactive processing
system
page 218 MSC-16004
Multispectral data analysis
page 275 MSC-16322/14823
- PATTERN REGISTRATION**
Multispectral image processor
page 206 MSC-16253
- PHASE TRANSFORMATIONS**
The processing of materials in outer space
page 282 MFS-23695
- PHENOLIC RESINS**
Molding cork sheets to complex shapes
page 278 MFS-23626
- PHONOCARDIOGRAPHY**
Acquisition system for biomedical data
page 246 MSC-16144
- PHOTOCHEMICAL REACTIONS**
Thermochemical-photolytic production of
hydrogen and oxygen from water
page 224 LAR-12118
- PHOTODECOMPOSITION**
Thermochemical-photolytic production of
hydrogen and oxygen from water
page 224 LAR-12118
- PHOTODIODES**
Solar-cell array design handbook
page 217 NPO-14106
- PHOTOLYSIS**
Thermochemical-photolytic production of
hydrogen and oxygen from water
page 224 LAR-12118
- PHOTOMULTIPLIER TUBES**
Noise reduction in photomultiplier circuits
page 186 LAR-12091
- PHOTORECONNAISSANCE**
Multispectral data analysis
page 275 MSC-16322/14823
- PIPES (TUBES)**
Inspection tool for butt-welded tubing
page 277 NPO-13975
- PITCH (INCLINATION)**
Aircraft aerodynamics at high angles of
attack
page 262 ARC-11133
- PIVOTS**
Compact reliable multiaxis pivot
page 248 MFS-23311
- POLARIZATION CHARACTERISTICS**
Electromagnetic power absorber
page 208 NPO-13830
- POLLUTION CONTROL**
Low-temperature coal desulfurization
page 199 NPO-13937
- POLYIMIDES**
A new polyimide laminating resin
page 231 LAR-12211
Gold recovery process from polyimide film
page 232 MSC-16650
Polyimide thin-film dielectrics on
ferroelectrics
page 280 LAR-11996
Soluble, thermally-stable aromatic
polyimides
page 230 LAR-12092
- POLYMER CHEMISTRY**
Tensile viscosities of non-Newtonian fluids
page 233 NPO-13973
- POLYMERIZATION**
A new polyimide laminating resin
page 231 LAR-12211
- POTABLE WATER**
Virus detection system
page 239 MSC-16098
- POWDER METALLURGY**
Radiation-resistant, electrically insulating
cermet
page 226 NPO-13120
- POWER CONDITIONING**
Power switch/filter for digital circuits
page 181 MSC-16442
- POWER EFFICIENCY**
Save power in ac induction motors
page 179 MFS-23280
- POWER SUPPLIES**
Power switch/filter for digital circuits
page 181 MSC-16442
Pulse-width-modulated high-current power
supply
page 184 MSC-14668
- POWER SUPPLY CIRCUITS**
Noise reduction in photomultiplier circuits
page 186 LAR-12091
- PRESSURE MEASUREMENTS**
High-pressure high-temperature transducer
page 216 MFS-23765
- PRESSURE SENSORS**
Detecting gas leaks in propellant lines
page 254 MFS-23404
High-pressure high-temperature transducer
page 216 MFS-23765
- PRESSURE VESSEL DESIGN**
Pressurization systems
page 261 LEW-12845
- PRESSURIZING**
Pressurization systems
page 261 LEW-12845
- PROPELLANT SPRAYS**
Fuel injector for jet-stirred combustors
page 272 LAR-12146
- PROPELLANT TANKS**
Pressurization systems
page 261 LEW-12845
- PROPELLANT TRANSFER**
Pressurization systems
page 261 LEW-12845
- PROPULSION**
Pressurization systems
page 261 LEW-12845



PROSTHETIC DEVICES			
Compact reliable multiaxis pivot			
page 248	MFS-23311		
PROTECTIVE COATINGS			
Liquid-oxygen-compatible, flame-resistant coating			
page 229	KSC-11020		
PROVING			
Improved load-cell compensation			
page 253	MSC-16466		
PSEUDORANDOM SEQUENCES			
Secure communications system			
page 190	MSC-16462		
PULSE DURATION MODULATION			
Pulse-width-modulated high-current power supply			
page 184	MSC-14668		
PURIFICATION			
Virus detection system			
page 239	MSC-16098		
PYROHELIOMETERS			
Active-cavity radiometer/pyrheliometer			
page 211	NPO-13819		
PYROLYSIS			
Thermochemical-photolytic production of hydrogen and oxygen from water			
page 224	LAR-12118		
QUALITY CONTROL			
Thermal-impedance test for hybrid power devices			
page 178	MSC-16643		
QUARTZ			
Fuel injector for jet-stirred combustors			
page 272	LAR-12146		
RADIATION ABSORPTION			
Active-cavity radiometer ^{1/2} pyrheliometer			
page 211	NPO-13819		
RADIATION COUNTERS			
Properties of doped cesium iodide crystals			
page 236	MFS-23148		
RADIATION TOLERANCE			
Radiation-resistant, electrically insulating cermet			
page 226	NPO-13120		
RADIOACTIVITY			
Radioactive-gas separation technique			
page 202	GSC-12019		
RADIOMETERS			
Active-cavity radiometer/pyrheliometer			
page 211	NPO-13819		
Electromagnetic power absorber			
page 208	NPO-13830		
RANDOM NUMBERS			
Secure communications system			
page 190	MSC-16462		
RANDOM SAMPLING			
Three-level signal sampler has automatic threshold			
page 182	NPO-14042		
REACTOR MATERIALS			
Ni-Cu-Zr alloy for catalytic reactors			
page 225	LEW-12245		
RECLAMATION			
Gold recovery process from polyimide film			
page 232	MSC-16650		
REFRACTIVE INDEX			
Alignment tolerant schlieren system			
page 214	ARC-10971		
REINFORCING FIBERS			
Impact-resistant boron/aluminum composites			
page 221	LEW-12472		
REMOTE HANDLING			
Compact reliable multiaxis pivot			
page 248	MFS-23311		
RESIDUAL GAS			
Cartridge getter for vacuum jacketing			
page 270	MSC-16610		
RESILIENCE			
Resilient thermal barrier for high temperatures			
page 234	MSC-16338		
RESINS			
A new polyimide laminating resin			
page 231	LAR-12211		
RESOLUTION			
Mass spectrometer has wide angular acceptance			
page 203	NPO-14111		
ROCKET ENGINE DESIGN			
Engine injectors			
page 260	LEW-12846		
ROTORS			
Heat pipe controls bearing temperature			
page 267	LAR-11846		
RUBBER COATINGS			
Liquid-oxygen-compatible, flame-resistant coating			
page 229	KSC-11020		
SAFETY DEVICES			
Controlling fires in silver/zinc batteries			
page 259	MFS-22952		
SAFETY MANAGEMENT			
Controlling fires in silver/zinc batteries			
page 259	MFS-22952		
SANDWICH STRUCTURES			
Extruded edge members for honeycombs			
page 280	MSC-16428		
Honeycomb chassis for electronic components			
page 279	NPO-13891		
SATELLITE SOLAR ENERGY CONVERSION			
Solar-cell array design handbook			
page 217	NPO-14106		
SCANNERS			
Ultrasonic-mammography apparatus			
page 244	NPO-13935		
SCHEDULING			
Drug-dosage indicator			
page 247	GSC-12139		
SCHLIEREN PHOTOGRAPHY			
Alignment tolerant schlieren system			
page 214	ARC-10971		
SCINTILLATION COUNTERS			
Properties of doped cesium iodide crystals			
page 236	MFS-23148		
SCRAMBLING [COMMUNICATION]			
Secure communications system			
page 190	MSC-16462		
SCRAP			
Gold recovery process from polyimide film			
page 232	MSC-16650		
SEALERS			
Liquid-oxygen-compatible, flame-resistant coating			
page 229	KSC-11020		
SECURITY			
Secure communications system			
page 190	MSC-16462		
SELF ALIGNMENT			
Automatic channel trimming for control systems			
page 189	MSC-16027		
SEPARATORS			
Bacteria/virus filter membrane			
page 241	MSC-16388		
SERVOCONTROL			
Automatic channel trimming for control systems			
page 189	MSC-16027		
SEWAGE			
Carbon-chlorine-carbon sewage treatment			
page 200	NPO-13972		
SHAPES			
Molding cork sheets to complex shapes			
page 278	MFS-23626		
SHIELDING			
Protection against explosive blasts			
page 258	LAR-12014		
SHOCK WAVES			
Aircraft aerodynamics at high angles of attack			
page 262	ARC-11133		
SIGNAL DETECTION			
Wide-dynamic-range detector			
page 175	GSC-12149		
SIGNAL DISTORTION			
Bidirectional amplifier			
page 175	KSC-10856		
SIGNAL TO NOISE RATIOS			
Noise reduction in photomultiplier circuits			
page 186	LAR-12091		
Three-level signal sampler has automatic threshold			
page 182	NPO-14042		
SILICON POLYMERS			
Preparation of organosiloxy-molybdenum monomer			
page 222	MFS-23704		
SILVER ZINC BATTERIES			
Controlling fires in silver/zinc batteries			
page 259	MFS-22952		
SOLAR CELLS			
Solar-cell array design handbook			
page 217	NPO-14106		
SOLAR COLLECTORS			
Inexpensive high-temperature solar collector			
page 213	NPO-13979		
Modular test system for solar collector			
page 207	MFS-23701		
Solar-power mountain concept			
page 212	NPO-13861		

SOLAR ENERGY			
Solar-cell array design handbook page 217	NPO-14106		
Solar-power mountain concept page 212	NPO-13861		
SOLAR ENERGY CONVERSION			
Modular test system for solar collector page 207	MFS-23701		
SOLAR HEATING			
Inexpensive high-temperature solar collector page 213	NPO-13979		
SOLAR RADIATION			
Active-cavity radiometer/pyrheliometer page 211	NPO-13819		
SOLAR SIMULATION			
Modular test system for solar collector page 207	MFS-23701		
SOLENOIDS			
Density measurements of trace gases page 201	ARC-10760		
SOLID SOLUTIONS			
Stress, corrosion, and heat-resistant cermet page 228	NPO-13690		
SOLUBILITY			
Soluble, thermally-stable aromatic polyimides page 230	LAR-12092		
SOUND TRANSDUCERS			
Ultrasonic-mammography apparatus page 244	NPO-13935		
SPACE MANUFACTURING			
The processing of materials in outer space page 282	MFS-23695		
SPACE SHUTTLE ORBITERS			
Shuttle avionics visual display page 285	MSC-16591		
STATISTICAL ANALYSIS			
Three-level signal sampler has automatic threshold page 182	NPO-14042		
STOMACH			
Aspirin/metiamide reduces stomach ulceration page 242	ARC-11038		
STORAGE BATTERIES			
Controlling fires in silver/zinc batteries page 259	MFS-22952		
STRAIN GAGES			
Improved load-cell compensation page 253	MSC-16466		
STRESS [PSYCHOLOGY]			
Aspirin/metiamide reduces stomach ulceration page 242	ARC-11038		
STRESS CORROSION CRACKING			
Controlling stress-corrosion cracking page 235	MFS-23416		
STRESS CYCLES			
Fatigue-failure load indicator page 251	LAR-12027		
STRUCTURAL DESIGN			
Controlling stress-corrosion cracking page 235	MFS-23416		
STRUCTURAL FAILURE			
Crack-propagation predictions page 263	MSC-16436		
Fatigue-failure load indicator page 251	LAR-12027		
SULFATES			
Low-temperature coal desulfurization page 199	NPO-13937		
SUPERCONDUCTIVITY			
Superconducting thermometer for cryogenics page 215	LAR-12055		
SUPERCONDUCTORS			
The processing of materials in outer space page 282	MFS-23695		
SUPERSONIC FLOW			
Aircraft aerodynamics at high angles of attack page 262	ARC-11133		
SUPPORTS			
Honeycomb chassis for electronic components page 279	NPO-13891		
SUPPRESSORS			
Noise reduction in photomultiplier circuits page 186	LAR-12091		
SURFACE FINISHING			
Pretreatment for strong aluminum/epoxy/ aluminum bonds page 232	GSC-12232		
SURFACE PROPERTIES			
Quantitative measurement of surface contamination page 256	MSC-16679		
SWITCHING CIRCUITS			
Pulse-width-modulated high-current power supply page 184	MSC-14668		
SYNTHETIC RUBBERS			
Liquid-oxygen-compatible, flame-resistant coating page 229	KSC-11020		
SYSTOLIC PRESSURE			
Acquisition system for biomedical data page 246	MSC-16144		
TELEMETRY			
Advanced general-purpose computer page 195	MFS-23531		
Bidirectional amplifier page 175	KSC-10856		
High speed DAC page 191	NPO-13805		
Secure communications system page 190	MSC-16462		
TEMPERATURE COMPENSATION			
Improved load-cell compensation page 253	MSC-16466		
TEMPERATURE CONTROL			
Heat pipe controls bearing temperature page 267	LAR-11846		
Modular test system for solar collector page 207	MFS-23701		
Resilient thermal barrier for high temperatures page 234	MSC-16338		
TEMPERATURE DISTRIBUTION			
Improved accuracy with phase-change paints page 251	LAR-12025		
TEMPERATURE EFFECTS			
High-pressure high-temperature transducer page 216	MFS-23765		
TEMPERATURE GRADIENTS			
Fuel burner with low nitrogen oxide formation page 257	NPO-13958		
TEMPERATURE MEASURING INSTRUMENTS			
Improved load-cell compensation page 253	MSC-16466		
Integrated temperature sensor page 269	LAR-12056		
Superconducting thermometer for cryogenics page 215	LAR-12055		
TEST CHAMBERS			
Ultrasonic-mammography apparatus page 244	NPO-13935		
THERMAL CONTROL COATINGS			
Preparation of zinc orthotitanate page 223	MFS-23345		
Resilient thermal barrier for high temperatures page 234	MSC-16338		
THERMAL CYCLING TESTS			
Thermal-impedance test for hybrid power devices page 178	MSC-16643		
THERMAL ENERGY			
Solar-power mountain concept page 212	NPO-13861		
THERMAL INSULATION			
Resilient thermal barrier for high temperatures page 234	MSC-16338		
THERMAL RESISTANCE			
Oxidation-resistant cermet page 227	NPO-13666		
Stress, corrosion, and heat-resistant cermet page 228	NPO-13690		
THERMAL STABILITY			
Resilient thermal barrier for high temperatures page 234	MSC-16338		
Soluble, thermally-stable aromatic polyimides page 230	LAR-12092		
THERMIONIC DIODES			
Radiation-resistant, electrically insulating cermet page 226	NPO-13120		
THERMODYNAMIC PROPERTIES			
Thermal-impedance test for hybrid power devices page 178	MSC-16643		
THERMOMETERS			
Superconducting thermometer for cryogenics page 215	LAR-12055		
THERMOSETTING RESINS			
A new polyimide laminating resin page 231	LAR-12211		
TISSUES [BIOLOGY]			
Ultrasonic-mammography apparatus page 244	NPO-13935		
TITANIUM OXIDES			
Preparation of zinc orthotitanate page 223	MFS-23345		



TRACE ELEMENTS

Density measurements of trace gases
page 201 ARC-10760

TRACKING [POSITION]

Inexpensive high-temperature solar
collector
page 213 NPO-13979

TRANSDUCERS

High-pressure high-temperature transducer
page 216 MFS-23765

TRANSITION METALS

Preparation of organosiloxy-molybdenum
monomer
page 222 MFS-23704

TRANSITION TEMPERATURE

Superconducting thermometer for
cryogenics
page 215 LAR-12055

TRANSONIC FLOW

Aircraft aerodynamics at high angles of
attack
page 262 ARC-11133

TUMORS

Ultrasonic-mammography apparatus
page 244 NPO-13935

TURBOFANS

Impact-resistant boron/aluminum
composites
page 221 LEW-12472

ULCERS

Aspirin/metiamide reduces stomach
ulceration
page 242 ARC-11038

ULTRASONIC TESTS

Ultrasonic-mammography apparatus
page 244 NPO-13935

ULTRAVIOLET RADIATION

Biological-activity monitor
page 245 NPO-14089

UNIONS [CONNECTORS]

Quick-disconnect coupling/filter
page 268 MFS-22323

VACUUM APPARATUS

Cartridge getter for vacuum jacketing
page 270 MSC-16610

Ultrasonic-mammography apparatus
page 244 NPO-13935

VELOCITY MODULATION

Mass spectrometer has wide angular
acceptance
page 203 NPO-14111

VIBRATION ISOLATORS

Vibration-resistant PC board feedthrough
page 276 MSC-16371

VIDEO DATA

Multispectral image processor
page 206 MSC-16253

Shuttle avionics visual display
page 285 MSC-16591

VIRUSES

Bacteria/virus filter membrane
page 241 MSC-16388

Virus detection system
page 239 MSC-16098

VISCOELASTICITY

Tensile viscosities of non-Newtonian fluids
page 233 NPO-13973

VISCOSITY

Tensile viscosities of non-Newtonian fluids
page 233 NPO-13973

VISCOUS FLOW

Fluid-line math model
page 260 MSC-16230

Tensile viscosities of non-Newtonian fluids
page 233 NPO-13973

VOLTAGE CONVERTERS [DCTODC]

Power switch/filter for digital circuits
page 181 MSC-16442

VOLTAGE REGULATORS

Pulse-width-modulated high-current power
supply
page 184 MSC-14668

WASTE DISPOSAL

Carbon-chlorine-carbon sewage treatment
page 200 NPO-13972

WATER QUALITY

Virus detection system
page 239 MSC-16098

WATER TREATMENT

Carbon-chlorine-carbon sewage treatment
page 200 NPO-13972

Virus detection system
page 239 MSC-16098

WEIGHTLESSNESS

The processing of materials in outer space
page 282 MFS-23695

WELD TESTS

Inspection tool for butt-welded tubing
page 277 NPO-13975

WHITE BLOOD CELLS

Single-donor leukophoretic technique
page 241 MSC-16297

WIRING

Semiautomatic labeling of small wires
page 267 MSC-16233

Vibration-resistant PC board feedthrough
page 276 MSC-16371

ZINC OXIDES

Preparation of zinc orthotitanate
page 223 MFS-23345

National Aeronautics and
Space Administration

Washington, D.C.
20546

Official Business
Penalty for Private Use: \$300

SPECIAL FOURTH CLASS MAIL
BOOK

Postage and Fees Paid
National Aeronautics and
Space Administration
NASA-451



NASA



NASA's Lewis Research Center and the Energy Research and Development Administration are using spacecraft solar cells to develop a Sun-powered refrigerator for campers and work crews in remote areas.



An inexpensive frame, built at Kennedy Space Center, can be used with instant film to make quick copies of pictures without a darkroom.

A sensor developed at Ames Research Center for measuring air pressure in wind-tunnel tests is being used in the development of a pulsed sensor for diagnosing increased cranial pressure.

